

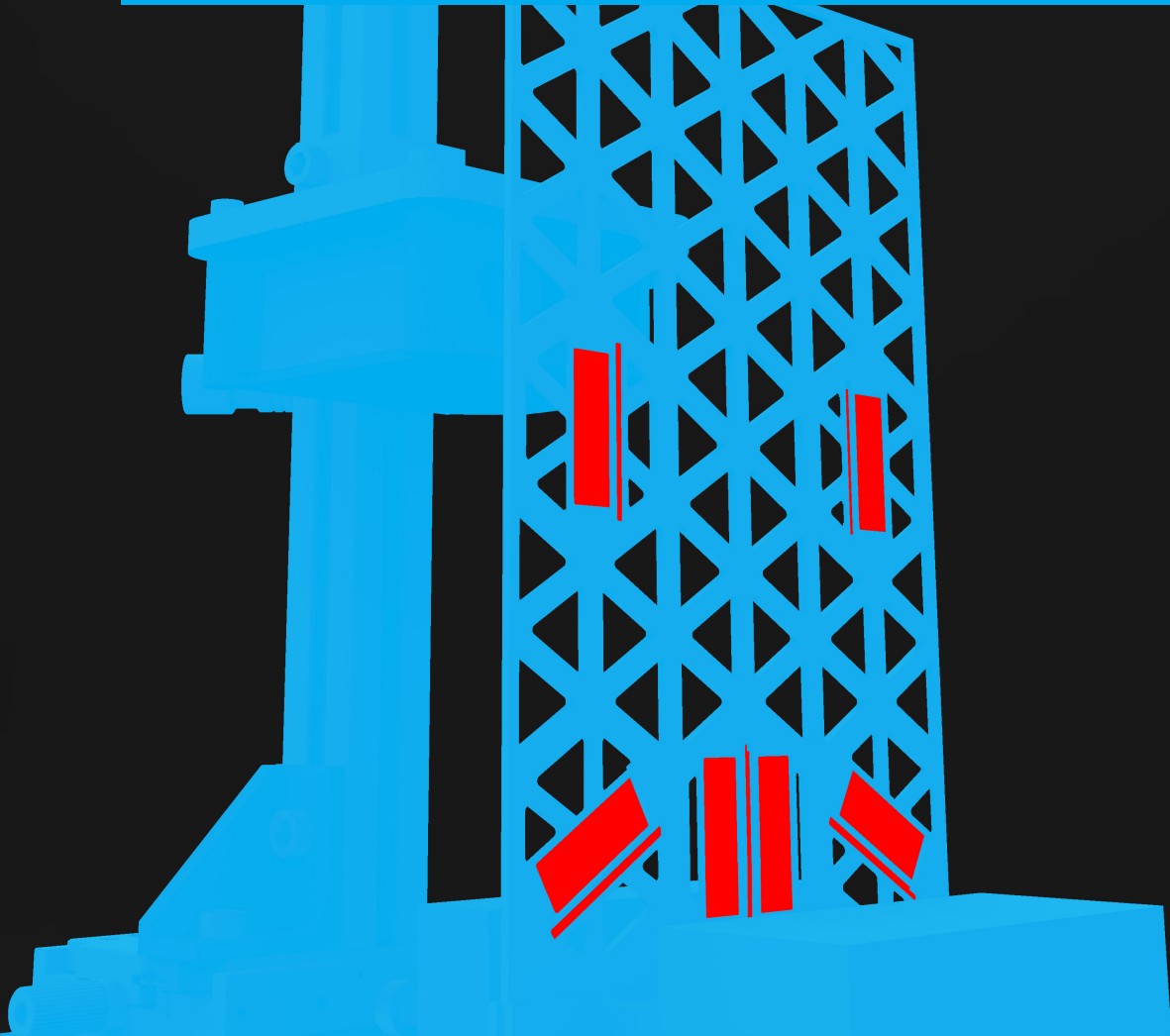
Department of Precision and Microsystems Engineering

Multimode damping with activated metamaterials:

Hexagonal patterned flexure with integrated piezo elements for active damping

Goran Barac

Report no : 2020.051
Coach : Dr.Niranjan Saikumar
Professor : Dr.Hassan HossienNia
Specialisation : Mechatronics System Design
Type of report : MSc Thesis
Date : 27 November 2020



Multimode damping with activated metamaterials

Hexagonal patterned flexure with integrated
piezo elements for active damping

by

G. Barac

to obtain the degree of Master of Science
at the Delft University of Technology,
to be defended publicly on Friday November 27, 2020 at 13:00.

Student number: 4320700
Project duration: November , 2018 – November , 2020
Thesis committee: Dr. ir. N. Saikumar, TU Delft, supervisor
Dr. ir. S. H. HossienNia, TU Delft, supervisor
Dr. ir. A. g. j. Verbiest, TU Delft

An electronic version of this thesis is available at <http://repository.tudelft.nl/>.

Abstract

High Tech industry is looking to push the bounds of what is possible, this requires machines that run with ever increasing speed and precision for longer amount of time under progressively more hostile environments. These requirements necessitate the use of compliant mechanisms instead of traditional rigid body counterparts. However, as these flexures are pushed to operate at ever higher speeds, high frequency modes affect precision and hence require better damping.

Currently active damping relies on a single or small amount of actuators which makes their placement for multimode damping inefficient. To this end, the MetaMech project was created which aims to combine the disciplines of mechatronics and metamaterials to create flexures with integrated cells housing sensors, active and passive dampers in optimal positions and orientations. This will enable more efficient placement and orientation of dampers, reducing the force and thus the size and weight needed to damp the system.

This thesis takes the first step in this direction and is concerned with developing the first prototype demonstrator of a metamaterial flexure with integrated damping using currently available technology. Two demonstrator flexures have been designed, put through Finite Element Analysis, constructed and tested. In both cases successfully damping has been achieved using PPF (Positive Position Feedback).

The first flexure is a small flexure containing two piezo actuator denoted as P1 and P2, which are clamped inside two flexure halves without the use of any adhesives on the piezos themselves. All wire connections are routed through the flexure. A laser sensor was used for sensing. Two sets of damping experiments were done, in the first P1 one provided the disturbance and both piezos damped. In the second P2 provided the disturbance and both piezos damped. In the first experiment, the first mode was damped by 85% and the second by 56%. In the second experiment, the first mode was damped by 87% and the second by 45%

The second flexure was a bigger open flexure containing six actuator piezos and 5 sensor piezos colocated with those actuators all bonded with epoxy adhesives. The flexure had a hexagonal pattern, with some cells containing piezo sensor actuator pairs, or in one case two actuators and a sensor in a single cell. These active cells were placed in topologically optimized positions where they could best observe and damp their assigned modes. One cell with double actuators was used to damp the first mode. Two cells were used to damp the 7th mode. And two cells were used to damp the third mode.

This flexure was a partial success. The plan was to damp the first three modes. But the piezos assigned to damp the second mode, a torsional mode could not observe that mode very well, so it was decided to use them to damp a higher mode, the 7th mode. Damping this 7th mode was a partial success as one cell damped the mode, but the other just added stiffness, this was a problem with the implementation of the damping filter, not the physical design of the flexure. The first mode was damped very well. The third mode was damped well by one cell, whereas the other cell assigned to damping it just added stiffness. This was once again a problem with the implementation of the damping filter and not the physical design of the flexure.

Overall the average gain decrease at the first mode was 76.8%, the average gain decrease at the 7th mode was 80.7%, and the average gain decrease at the third mode was 55.1%. The gain decrease for the 7th and third mode is not just due to damping but also due to adding of stiffness. Still the overall results are impressive.

Apart from the experimentation with the physical flexure the research and Finite Element Analysis provided some useful insights. The research revealed a hexagonal pattern was the most suited for a cellular flexure. It also revealed which type of hexagonal pattern. One pattern has the flat edges facing in the direction of the longest axis of a flexure, and the other has the corners. The piezos can also be oriented to face the edges or the corners. The corners facing pattern with the piezos facing the corner as well is superior as it allows the forming of straight lines of force and more suited diagonal lines of force.

A more advanced flexure design was researched where the hexagons were subdivided in to triangles or diamond shapes, these hexagonal cells could exert force in three different directions. The diamond shape could form the best lines of force. Furthermore researched showed that piezo elements with empty space on the side between the individual elements would be better at directing their force as they did not exert force on the neighbours on either side in the same cell but along the axis they are meant to, and in to adjacent cells.

The Finite Element Analysis of several flexures with piezo elements inside of them simulated revealed that flexures which were symmetrical with respect to their front and back with piezos placed in the center were superior when causing torsional displacement. Which would make them superior at damping torsional modes. It is important that piezo sitting inside a flexure have about as much contact with their frontside as well as their backside.

The lessons form the FEA about symmetrical flexures could not be applied as attempts at symmetrical closed off flexures failed due to bad connections. New types of closed of symmetrical flexures have been proposed in the recommendations sections of Chapter 5 and Chapter 6.

Preface

I have loved the natural sciences my whole life. I still remember graduating high school with a specialization in economics and society and regretting my decision. The truth of the matter is I didn't think I had the aptitude to follow my dreams. Years later I decided to do so anyway, by going back and redoing high school courses I needed, to get into higher education. This thesis is the culmination of years of work. It was a hard and long, but worthwhile journey. Throughout the years I have learned many things about the natural sciences, and I hope to learn many more. I have also learned to make things that work, maybe not perfectly. But I'm getting there. I have also met some remarkable individuals, people I will never forget. The amount of people that deserve a thank you could fill a whole thesis by itself. But I will retrain myself to just those individuals and organization key to my thesis.

Niranjan Saikumar, thank you for being there from the beginning till the very end. You stuck through it even when you left your role at the TU Delft. Your advice and insights have always propelled the thesis forward. I always left our meetings in more positive mood than before. You are quite a remarkable individual, and it seems with you around, there is no problem that cannot be overcome.

Hassan HosseinNia, thank you for making this all possible. You introduced me to the world of mechatronics. You were always there in the most critical parts and always took time to ask how things were going and help out when it was needed. Your enthusiasm and no nonsense attitude helped move things along. And thanks for giving me the time I needed to complete my project.

Andres Hunt, for all intents and purposes you were my second supervisor. I have been to your office more than any other. You were a great help with every aspect of the working of piezo electric actuators, sensors, oscilloscopes, and amplifiers. Things that would have taken me days to figure out were handled in minutes. You have saved me time, prevented injuries and damage to equipment. Thank you.

Madhan Gopal Muruganandam Mallur, help comes from unexpected individuals. As is the case with Madhan, a fellow thesis student who worked on the control side of this project. But was also the first person to talk to when problems arose. His research and experience with amplifiers as well as his knowledge of LabVIEW saved me weeks of work. He is an individual with remarkable intellectual faculties, an eye for detail and amazing powers of deduction. Discussion for almost any topic regarding this project was always fruitful. Thank you.

PME Lab Support staff, **Bradley, Gideon, Patrick, Rob** and **Spiridon**. Thank you, you guys went above and beyond to help all of us.

Holland Shielding Systems, all the effort in the world would have been a waste if I did not have the means to support myself. The fact is that without my job at Holland Shielding Systems I would not have been able to finish my bachelor and master. I'd like to thank all of the staff but these individuals especially: **Jos de Bruin, Jan van Tienhoven, Marc Baaij, Aron Keijzer** and **Frank van 't Hoenderdaal**. I didn't just have a flexible job where I could take time off when needed for my studies or work more days when I needed more money. I also had direct help with my thesis in the form material advice, laser cutting, and supply of materials.

G. Barac
Delft, November 2020

Contents

1	Introduction	1
1.1	The Problem	2
2	State of the Art Damping	3
2.1	Damping Systems Categorization	3
2.2	Passive dampers	4
2.2.1	Double-Shear Lap Joint (DSLJ)	4
2.2.2	Shunted piezo networks	5
2.3	Active Damping	6
2.3.1	Piezo Patches	6
2.4	Control Techniques	8
2.4.1	Lead Control	8
2.4.2	Integral Resonance Control & Positive Position Feedback	8
2.5	Evaluation and utility of damping systems	9
2.6	MetaMech Project	10
3	Research	11
3.1	Flexure Approximations	11
3.2	Material Selection	12
3.2.1	Eigenfrequency and Damping Finite Element Analysis	12
3.2.2	Stiffness Finite Element Analysis	14
3.3	Cell Structures	16
3.4	Piezo Properties	22
3.4.1	Working principles	22
3.4.2	Parameters describing the relationship	22
3.4.3	Advantages and Disadvantages	23
3.5	Amplification Mechanism for Piezo's	24
3.5.1	Internally Leveraged Actuators	24
3.5.2	Externally leveraged Actuators	27
3.5.3	Early concepts and ideas	29
3.5.4	Suitability of the different amplification methods	29
3.6	Commercially available piezo actuators	30
3.7	Reflections	33
4	Design and Finite Element Analysis	35
4.1	Flextensional Design and Finite Element Analysis	35
4.1.1	Displacement and Force testing	37
4.2	Results	38
4.3	Force testing	39
4.4	Design and FEA for patch elements	41
4.4.1	T220-H4BR-1305XB vs Finite Element Analysis	41
4.4.2	Displacement	42
4.4.3	Flexure displacement	44
4.4.4	Second Flexure test	46
4.4.5	Stiffness & Force	48
4.5	Advanced Cell designs	49
4.6	Expectations check	54
4.6.1	Force at the outer end	54
4.6.2	Bender vs Split	55

4.7	Advanced Real design	57
4.8	Reflections	60
5	Practical Design and Experiments	61
5.1	Test Setup	62
5.2	BD300 Dual-Channel 300V encasing	63
5.3	Small flexure	63
5.3.1	Small Flxure Experiments	68
5.4	Octo Flexure	73
5.5	Open Flexure	77
5.5.1	Finite Element Analysis	79
5.5.2	UHU Flexure	79
5.5.3	DP460	81
5.5.4	Bison.	83
5.6	Damping results UHU Flexure	86
5.6.1	P1 Cell	87
5.6.2	P2 Cell	91
5.6.3	P3 Cell	95
5.6.4	P4 Cell	99
5.6.5	P5 Cell	103
5.6.6	Damping Result summarization	107
5.7	Reflections	108
5.8	Recommended future designs	110
5.8.1	PICMA PL Symmetrical Flexure	110
5.8.2	Advanced Real Flexure	111
6	Conclusions & Recommendations	113
6.1	The Research	113
6.2	Finite Element Analysis	114
6.3	Practical design & Experiments	114
6.4	Recommendations	116
	Bibliography	119
	Appendices	123
A		125
A.1	Appendix A (H3 Research)	125
A.2	Damping Figures PLA	131
A.3	Damping Figures Aluminium	132
A.4	Commercial Actuators Appendix	134
B		139
B.1	Appendix B (H4 Designs & Finite Element Analysis).	139
C		141
C.1	Appendix C (H5 Practical Design and Experiments).	141
C.2	Small Flexure Appendix	146
C.3	BA Sensor Spects	154
C.4	Octo Flexure Appendix	156
C.5	Open Small Flexure	161
C.6	UHU Appendix	163
C.7	DP 460 Appendix	166
C.8	Bison Appendix	173

1

Introduction

High Tech industries require machines that run with ever increasing speed and precision for longer amount of time under progressively more hostile environments. These requirements necessitate the use of compliant mechanisms/ flexures instead of traditional rotational joints. Compliant mechanisms exhibit several advantages over classical joints. These include [1][2]:

- Excellent repeatability
 - no friction
 - no backlash
 - low hysteresis
- Low cost manufacturing
 - less parts
 - compatible with injection molding
 - compatible with additive manufacturing
- Low maintenance
 - less parts
 - no lubrication
 - no friction wear
 - not susceptible to contaminants
- Environment compatibility (vacuum, cryogenic, radiation, moisture, dirt, chemical)
 - no lubrication
 - not susceptible to contaminants
 - no particle generation
 - no out-gassing
- Minimization/weight reduction
 - less parts
 - works at micro-scale

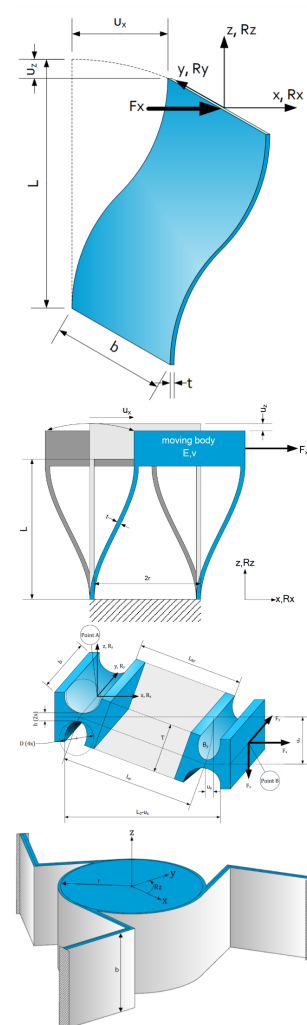


Figure 1.1: Examples of Flexure (source: Jansen Precision Engineering)

1.1. The Problem

The main problems arise when these compliant mechanisms are pushed to operate at ever increasing frequencies. Which necessitates higher damping to attenuate excessive amplitudes of desired frequencies and suppresses undesired ones. This needs to be done with minimal increase in weight, and heat production. High frequencies activate higher order modes that need to be suppressed, which requires damping that can handle a multitude of modes. To complicate matters more, the frequencies of the various modes vary throughout the range of motion as the stiffness of a flexure changes during deformation.

There is a need for damping that can adjust to changes in the modes present and their frequency. The ability to operate in hostile environments is increasingly important as many high tech industry applications require vacuum to increase speed and decrease contamination, or take place in irradiated, low/high temperature environments due to production and sensing needs. Better damping will also increase the operating lifetime of a structure as it decreases the amplitudes of oscillation the structure is exposed to, which is a big factor when the structure is in a hostile hard to reach environment like space. Figure 1.2 visualized these problems.

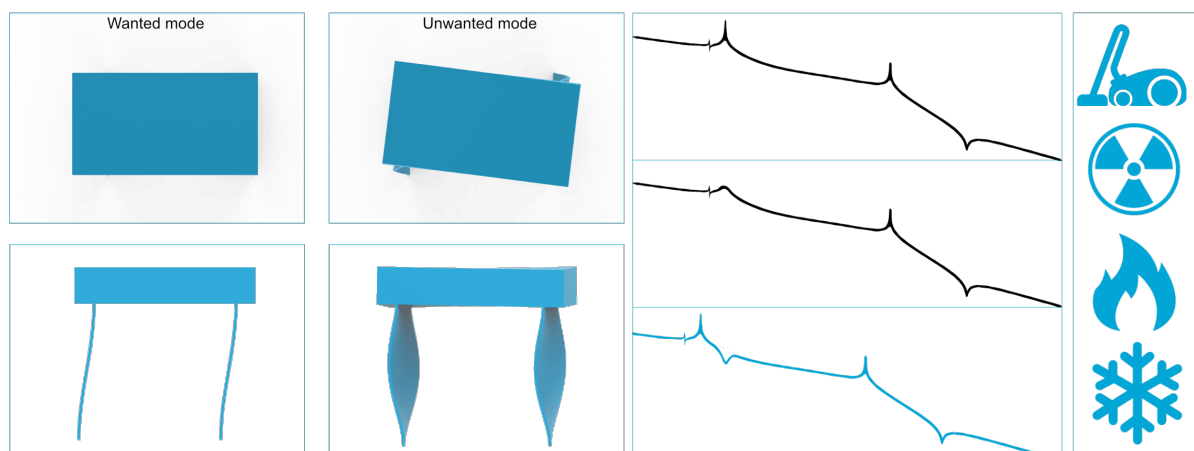


Figure 1.2: Left) Wanted and Unwanted Modes. Middle) Changing mode frequency. Left) Hostile environments

Current passive methods add too much weight, cannot be operated in vacuum due to out-gassing and particle production, and show poor performance when dealing with multiple modes or varying modes. Active damping shows more promise when weight and multiple modes are concerned. Unfortunately current active damping solutions are very limited in their ability to deal with varying modes especially when they vary over a broad range. Additionally current active dampers rely on a single or very few actuators to suppress different modes, this make their positioning and direction inefficient and requires a lot of force for suppression, as shown in the right most image of Figure 1.3.

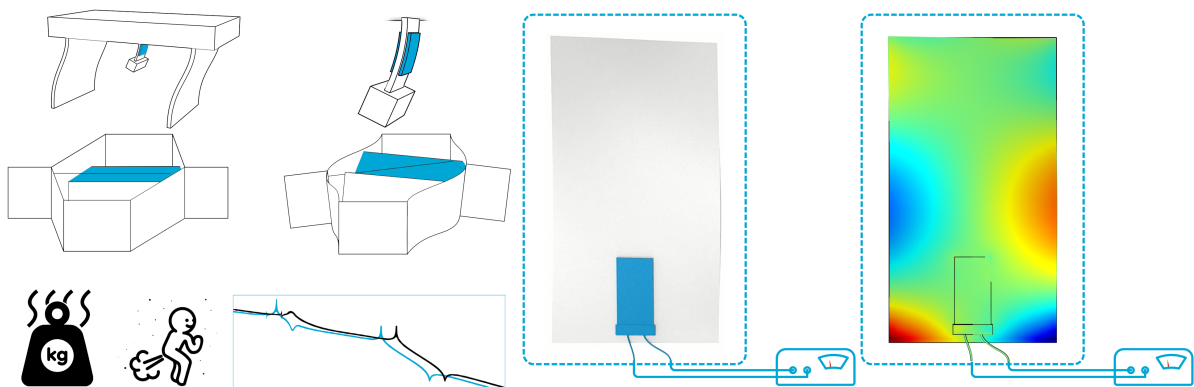


Figure 1.3: Left) Shows a TMD and a novel viscoelastic damper with the problems. Right) Active piezo damper with the problems.

2

State of the Art Damping

The previous chapter gave an overview of the problems associated with the current methods, with this in mind it's important to take a more in depth look at the current methods and how they work. By understanding the current methods it's possible to explore ways in which to improve them or to create better and new alternatives. The study of damping and the systems used for damping is vast. This chapter will only focus on a subset of damping systems used to damp flexures, namely those systems that directly influenced this project. To tackle the subject more effectively it's prudent to understand how damping system can be categorized.

2.1. Damping Systems Categorization

Damping systems can be categorized in three main groups. Passive dampers, active dampers and a hybrid of the two. Passive dampers dissipate energy without the need of an external energy source. They are always damping and cannot be adjusted on the fly to changing conditions Generally the energy is dissipated as heat right inside the dampers. Their damping ability is proportional to their mass. Active dampers use force to damp the vibration, they require an external power source and sensors, energy is generally transported out of the system. Their damping ability is proportional to the power density they possess. Lastly there are the hybrid damping systems, these make use of some type of actuator to enhance passive damping.

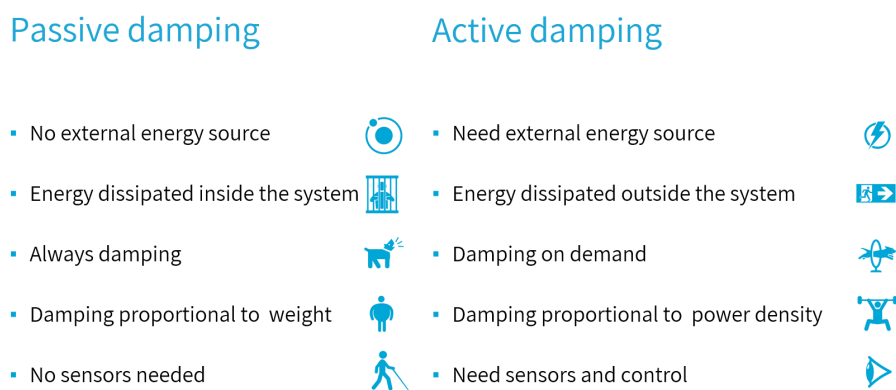


Figure 2.1: Passive vs Active Systems summerized

Hybrid systems were used when the active control schemes were to limited. The idea was to use simple control schemes to enhance the damping of passive systems outside of their normal operating range in terms of frequency and temperature. One of the aims of this project is to develop advanced control systems to maximize the utility of active damping. Therefore hybrid systems are not a very attractive option and will be left out of the discussion.[3][4]

2.2. Passive dampers

Passive damping systems can utilize several different mechanisms of damping, the one relevant here is internal damping.

Several energy dissipation mechanisms play a role in internal damping, among them microstructure defects like grain boundaries and impurities, thermoelastic effects, eddy current effects, dislocation motion, and chain motion in polymers.

Majority of passive dampers utilize viscoelastic materials (VEM) where the main energy dissipation mechanism is the friction between long molecular chains of polymers moving and rubbing against each other is.

2.2.1. Double-Shear Lap Joint (DSLJ)

This design relies on a hexagonal cell based structure. Where cells filled with damping material can be placed and oriented throughout the structure to provide the needed damping for specific modes. These cells are designed in such a way to maximize shearing, and can be placed to maximize their effect for specific modes.

The first thing to focus on is the way the damping inside the cells themselves work. The top of Figure 2.2 shows the traditional constrained layer damping. In constrained layer damping (CLD), the damping layer consisting out of a viscoelastic material is put in between two structures, during the flexing of the structure the damping layer is being sheared. Energy is dissipated as a result of this shearing. The new method shown in the bottom of Figure 2.2 still uses shearing of damping material, but due to the new design the same amount of flexing from the structure produces more shearing, hence more damping.

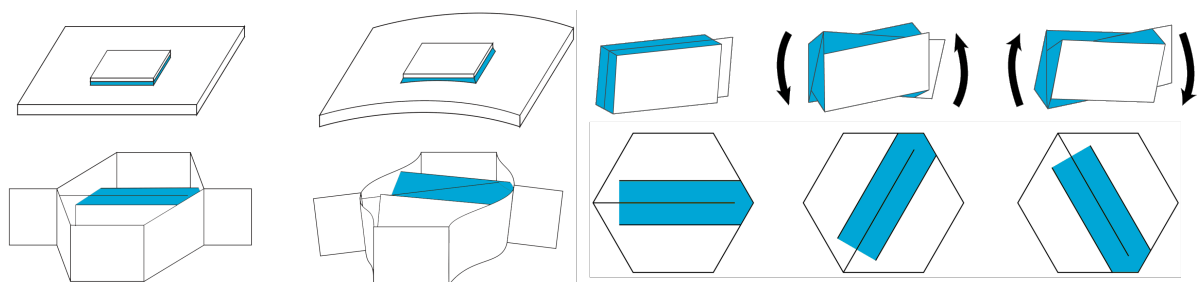


Figure 2.2: Top Left) A traditional Constrained Layer Damping. Bottom Left) the DSLJ. Top Right) clarifies the way the DSLJ shearing works during the deformation of the flexure. Bottom Right) Bottom images shows the cell from top and the way it can be oriented. [5][6]

The cell based design allows for the material to be positioned and oriented in the most efficient way. To find out what the best distribution and orientation is, an optimization algorithm can be used. The result of such an optimization is shown in Figure 2.3

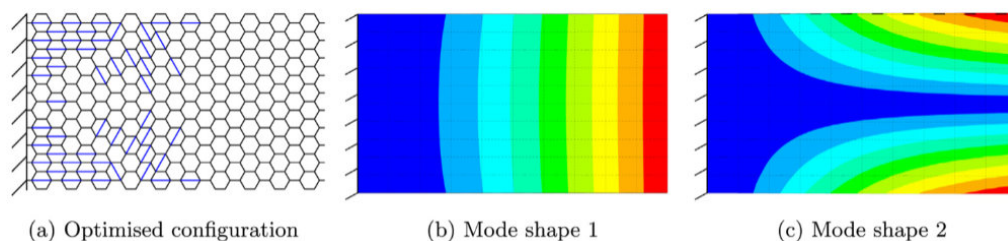


Figure 2.3: Figure shows the topology of dampers optimized for two modes [5][6]

FEA analysis showed this design to be competitive or better than traditional CLD, in some cases even increasing the resonant frequency, implying the ratio of modal stiffness to modal mass was increased by the addition of this damper. [5][6]

2.2.2. Shunted piezo networks

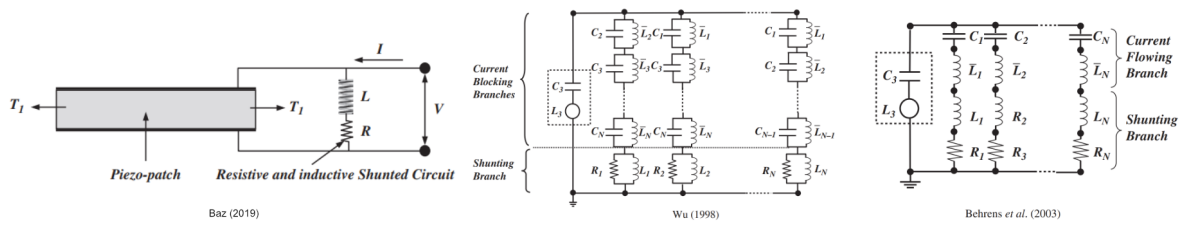


Figure 2.4: Left) a simple shunted network tuned to one mode. Middle) A more complex shunted network designed to suppress multiple eigenmodes by selectively blocking current. Right) A more complex shunted network designed to suppress multiple eigenmodes by selectively passing current. [4].

Figure 2.4 shows examples of a shunted piezo network. The top image shows the basic idea. Where a piezo-electric film is bonded to the structure. During vibration the mechanical energy is converted to electrical energy. This electrical energy is then dissipated in an electric network. This electric network can consist of resistors, inductors, capacitors or a combination. Simple resistor will act like a first order electrical circuit and will act like a light viscoelastic damper with little mechanical damping. If an inductor or capacitor is added the damping can be significantly increased especially if the electrical resonance of the system is equal to that of the mechanical system. These networks can become very complicated if multiple modes need to be suppressed as the bottom image of Figure 2.4 shows. [4][7]

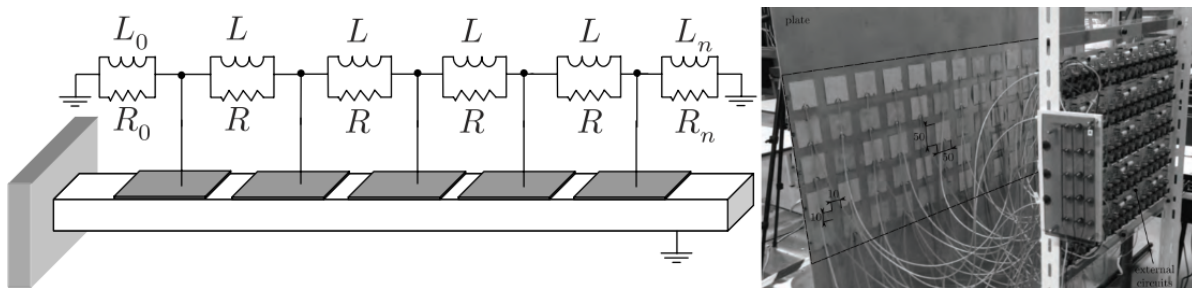


Figure 2.5: Left) Schematic of a shunted network where the piezo patches are connected to individual networks [8]. Right) Experimental version containing 75 piezo patches [9]

The left image in Figure 2.5 shows a more recent development where piezo patches are connect to different networks. In the image each patch is connected to a different network. In practice the situation might call for half of the patches to be connected to one network and the other half to another one. This saves in the amount of elements. As there is no need for extra elements to block or pass current to the right elements when the right frequency has been achieved.

2.3. Active Damping

In active damping the unwanted oscillation are attuned by actively providing force. This type of damping needs sensors and an energy source. Where as most passive dampers dissipate the energy in their own volume inside the structure, active dampers transported the energy in to peripheral systems that store or dissipate the energy. This results in systems with more power density then passive systems. Active systems also only apply damping when needed.

2.3.1. Piezo Patches

Figure 2.6 shows a setup where the piezo actuators and piezo sensors are separate. However Piezo's can be made to self-sense. This achieves true collocated sensor actuator system, and at the same time helps to reduce the weight. Figure 2.7 shows a setup where the piezo actuator self-senses, the two schematics show a the electrical circuit needed to measure the rate of change of piezoelectric voltage (middle), and a circuit setup to measure the piezoelectric voltage.

Multiple active piezo patches have been tried, but the number remains still very small, the placement and size are not optimized. In fact often one patch is used to sense, one to actuate and the last one to create the disturbance. Various control schemes can be used to control the piezo patches, all of them result in the application of force when the flexure is moving away from equilibrium.

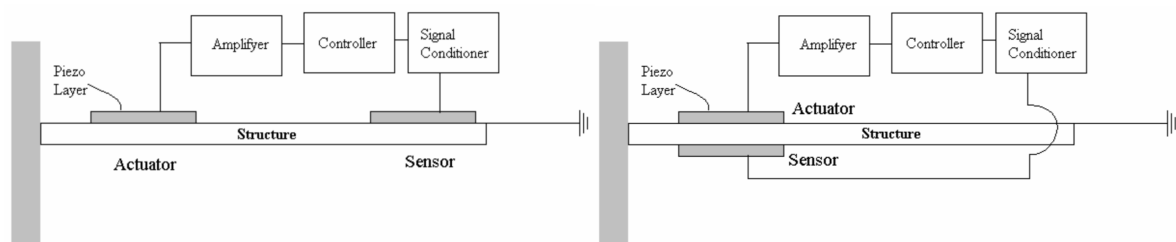


Figure 2.6: Shown are two different ways to have separate piezo actuators and sensors [10]

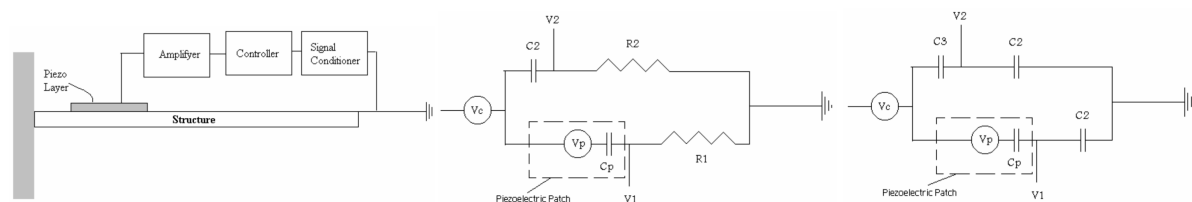


Figure 2.7: Left) Shows a setup where the piezo actuator self-senses. Middle) Circuit setup to measure the rate of change of piezoelectric voltage. Right) Circuit setup to measure the piezo voltage. [10]

Hybrid systems combining active and passive elements also exist. The graph in the middle of Figure 2.8 shows a comparison between a system in only active mode and the same system in hybrid mode. The Y_2 represents the structural vibration amplitude created by the active actuator. Larger Y_2 means the actuator is better able to excite the structure for a given voltage. A larger Y_2 thus means vibrations can be damped better. The hybrid system reduces the maximum value of the peak, but broadens the bandwidth.

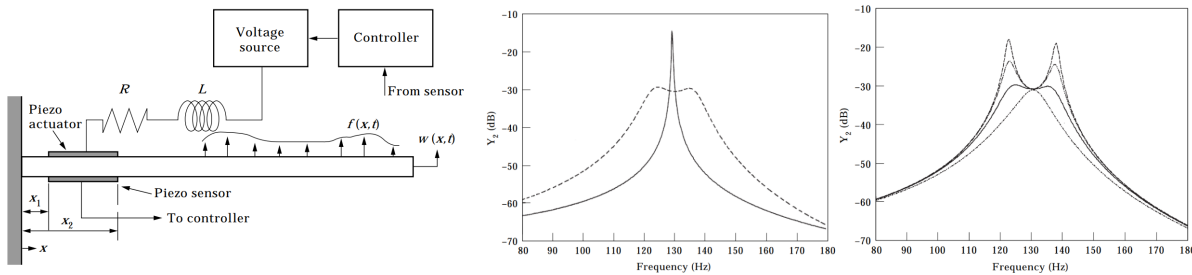


Figure 2.8: Left) Shows a hybrid setup where the passive elements are connected to the voltage source [11]. Middle) a graph by (Tsai [11]) showing a hybrid system(dashed line ---), and a active system alone (solid line). Y_2 is an index for the system's active control authority, the larger it is, the more authority it has and the better. Right) Shows a hybrid system with different values for the resistance as the values of the resistance increase the Y_2 . [11]

The shunt circuit is optimized for passive damping, so having it directly connected to the active elements interfere with their functioning. The passive elements could also be dissipating the control power from the active element. This is supported by the right graph in Figure 2.8, this graph compares different values of resistance to the peak value of Y_2 . The actual numerical values are not important, what is important is the fact that as the value increases the peak and total area beneath the graph reduces. But the shunt circuit can also be separated. It is still a hybrid system, but the active and passive elements do not interact directly. This is shown in Figure 2.9. The right side of Figure 2.9 compares the result of a hybrid system where the passive elements are connected to the voltage source (dashed line ---), and where they are separated (solid line). The system where they are connected is still better. The shunt circuit can increase input voltage going to the piezo patch around the resonant frequency, even when the RL elements are not optimized to enhance the active input.

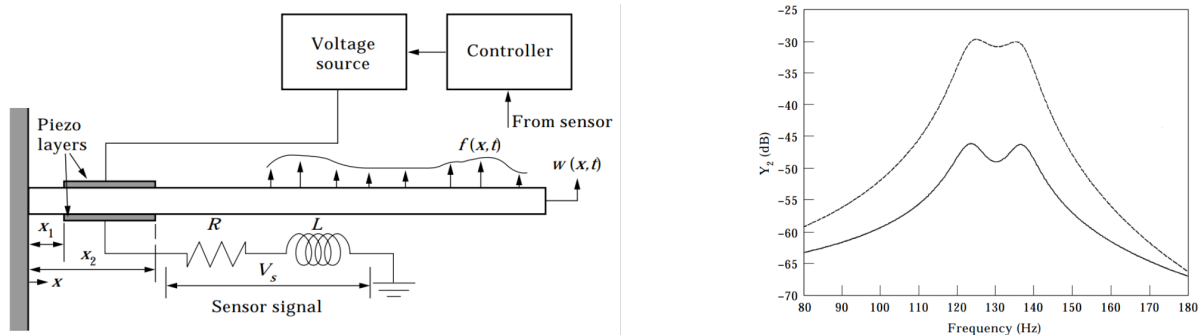


Figure 2.9: Left) Shows a hybrid setup where the passive elements are not connected to the voltage source. [11]. Right) a graph by (Tsai [11]) showing that a hybrid system where the passive elements are connected (dashed line ---), and a system where they are not connected (solid line)

2.4. Control Techniques

2.4.1. Lead Control

This is the most popular method. It's capable of suppressing multiple modes by creating positive phase in a predefined frequency band. It's robust against mode variation. However the noise of sensors is amplified as it adds an extra frequency dependent term in the numerator.

2.4.2. Integral Resonance Control & Positive Position Feedback

These methods utilize positive feedback to create phase and a roll off at higher frequencies. This roll off at higher frequencies makes them less sensitive to noise, as noise is generally a high frequency signal. Their performance deteriorates when faced with varying modes. Additionally designing an integral resonance controller capable of suppressing multiple modes is difficult even with advanced filtering techniques[12]. PPF handles each modes separately, both IRC and PPF suffer from spillover effect of modes at lower frequencies [13], this means that the suppression of one mode changes the amplitude and frequency of the other modes. In worst case scenario this could lead to instability. The biggest drawback of PPF in relation to the precision industry is the reduced closed-loop low-frequency stiffness, as this reduces precision and makes the overall stability dependent on the low frequency behaviour of a varying system [14]

What is really wanted is a controller with the phase addition properties of negative feedback controllers, with the high frequency roll-off of IRC/PPF controllers for noise attenuation and assured stability. The perfect controller needs the phase behaviour of a lead controller with the gain behaviour of IRC/PPF controllers. Bode's gain-phase relationship ensures that this can't be achieved with linear filters.

Recently a non-linear control technique was employed to develop a non linear lead filter with these properties. However this filter has never been adapted for mode suppression. Simulation results have been promising, however the non-linear nature of the controller introduces higher order harmonics in to the system. New tools have been developed to visualize and study these effects on performance. Additionally the results of WP2 which deal with the tracking of varying mods will be used to adapt these novel filters for higher performance gain.

2.5. Evaluation and utility of damping systems

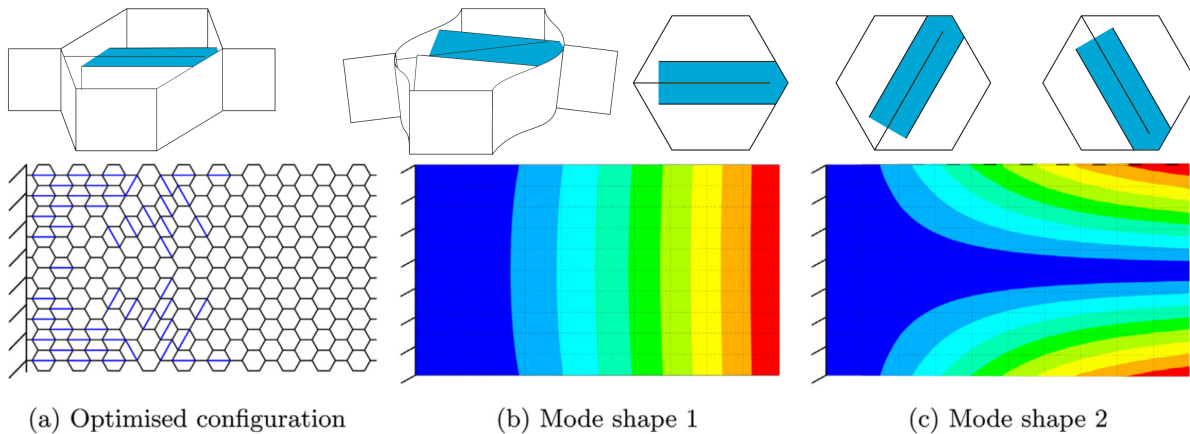


Figure 2.10: Double Shear Lap Joint

The cell based design and optimization of the DSLJ damping system in Figure 2.10 provided a great template to start researching the optimal cell structure for flexures. The optimization done for that project can be directly taken and applied to this project. The biggest disadvantages of their approach is common to most passive system which is out-gassing and particle generation of the VEM, the lack of adaptability, bad low frequency damping and narrow thermal range of operation, thermal effects on damping and heat generation.

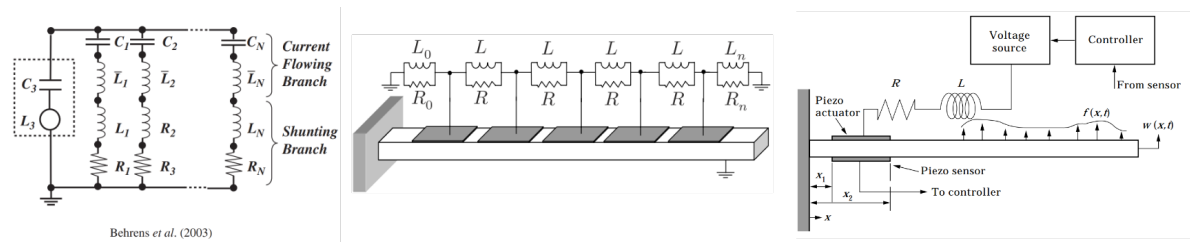


Figure 2.11: Left) Passive current flowing shunt network. Middle) Network where elements are connected to individual elements. Right) A hybrid piezo damper.

The problems pertaining to out gassing, particle generation, bad low frequency performance and narrow thermal range of operation, and heat generation can be dealt with by replacing the VEM with piezo elements connected to a shunted network. The left most shunted network in Figure 2.11 is handy for piezo elements that are involved with the damping of multiple modes, as it is designed to pass current to differently tuned elements depending on the frequency. The middle of Figure 2.11 shows the type of system suited when each element or a group needs to damp only one frequency. It is especially suited to designs with many individual damping elements as it simplifies the shunted network. Piezo elements do not out gas, they do not generate particles, they can be tuned for low frequency, they can operate in much lower and much higher temperatures than VEM and the energy is transported outside to be dissipated in the tuned impedance elements. However a passive network cannot adapt to changing modes.

To achieve the best damping passive damping should be replaced with active or hybrid elements wherever that is possible as shown in Figure 2.11. The active/hybrid elements will provide the best damping per weight, with all the advantages of the passive piezo shunted network. The active part of the network can also adapt to changing conditions. And while piezo material properties change with temperature this can be compensated for by including the necessary changes in to the controller. The ideal damping element would be a hybrid patch where the passive elements are connected to the voltage source thus a combination of the system in Figure 2.7 and Figure 2.8. The passive elements should be tuned for higher frequencies where sensing is hard or impossible.

2.6. MetaMech Project

The Mechatronic Metamaterials for Dynamic Mode Suppression project aims to address the problems mentioned in the previous section. The idea is to combine two disciplines, that of mechatronics and metamaterials to create a mechatronic metamaterial structure and control scheme enabling better and more efficient vibration suppression. Additionally new fabrication methods will be researched allowing for cheaper and faster prototyping and production of structures with integrated cells.

As shown in Figure 2.12 structure in question will be made out of cells capable of housing active, and passive dampers, sensors, or just solid material. This enables the efficient distribution and orientation of dampers, which in turn helps to overcome the mass and force limitation of dampers. Additionally this will permit the development and implementation of new adaptive non-linear vibration suppression methods, to overcome the limitations imposed with known linear damping methods.

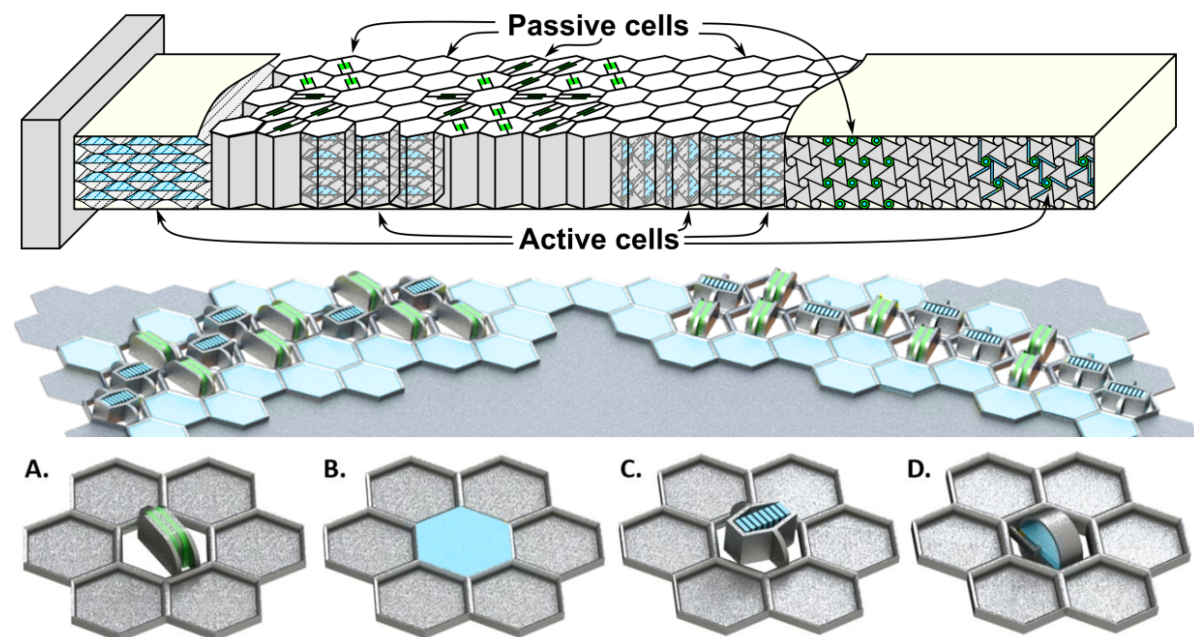


Figure 2.12: Top) General structure of the metamech material . Middle) Render of possible realistic structure. Bottom) Individual Cells (source : MetaMech)

To achieve the final goal of the MetaMech project, it has been divided in to several more manageable sub projects. These sub projects are in turn divided between the Technical University Delft and The University of Twente. WP1 done at the TU Delft encompasses, the design and testing of an individual cell, the integration of

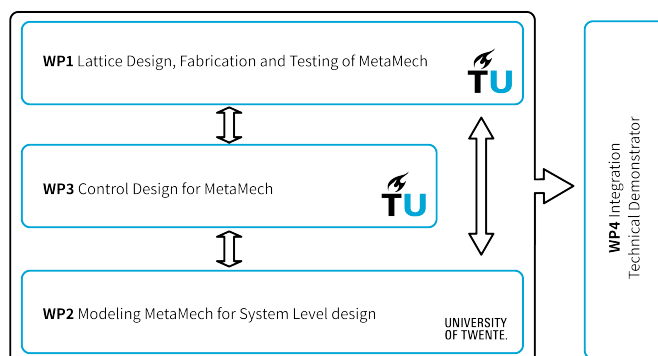


Figure 2.13: The four different sub projects of the Meta-mech Project(source : MetaMech Proposal)

that cell in to the larger structure and the testing of that structure, and finally novel manufacturing techniques for the cells and structures. WP2 done at the University of Twente deals with the development of more efficient modelling techniques. WP3 done at the TU Delft aims to develop new control methods for multimode suppression. In WP4 the previous work is combined in to a working demonstrator. This thesis is part of WP1, it will deal with the designing and testing of both a cell and a flexure with multiple integrated cells.

3

Research

The first part of the research consisted out the familiarization with the State of the Art. Which was detailed in the previous chapter. This chapter will detail the results of the research done to aid the design and testing of a cell based active damping system. The direction of this research was guided by general considerations regarding flexures, the needs of the industry and the idea behind the metamech project.

The following items were researched.

- Flexure Approximations
- Flexure Materials (FEA & Lab Testing)
- Cell Structures
- Piezo properties
- Amplification Mechanism for Piezo's
- Finite Element Analysis

3.1. Flexure Approximations

Flexures need to have certain material properties and dimensional ratios to work. Any solutions needed to stay within the limits imposed by these general criteria.

A rough idea of the relationships between different dimensions can be built up by simple observation. However analytical methods relating the maximum stress to the displacement can be used to construct guidelines about the length, width and thickness a functional flexure should have.

Flexure with finite length must have finite movement as no material can be strained infinitely, it needs to stay below critical stress. This critical stress can be related to the bending moment of the flexure, the bending moment can be related to the applied load, and the load can be related to the displacement through the stiffness. This leads to the following equation [15]

$$\frac{\delta_{max}}{L} \sim \left(\frac{\sigma_{max}}{E} \right) \left(\frac{L}{h} \right) \quad (3.1)$$

δ_{max} is the maximum displacement of the endpoint of the flexure, L is the length of the flexure, σ_{max} is the maximum stress the material can handle, E is the young modulus, h is the half thickness of the flexure.

The derivation is as follows:

$$\sigma_{max} = \frac{Mh}{I} \quad M = FL = K\delta_{max}L \quad K = \frac{3EI}{L^3}$$

$$\sigma_{max} = \frac{3EI\delta_{max}Lh}{IL^3} = \frac{3\delta_{max}Eh}{L^2}$$

$$\delta_{max} = \frac{\sigma_{max}L^2}{3Eh} \quad \rightarrow \quad \frac{\delta_{max}}{L} \sim \left(\frac{\sigma_{max}}{E}\right)\left(\frac{L}{h}\right)$$

Wherein M is the moment, F is the force, I the moment of inertia For most metal $\sigma_{max}/E \sim 10^{-3}$, and for most plastics it is 10^{-2} . The ratio of $\frac{L}{h}$ is usually between 10 and 100. Below 10 simple beam theory approximation do not apply and the flexure can be too stiff. Above 100 buckling can become a problem. The width to half thickness (h) ratio is usually above 10. As the flexure needs to be significantly more stiff in the out of plane direction to work as a flexure.

3.2. Material Selection

Ideally the materials used would have the needed properties to withstand the environmental challenges outlined earlier. However cheaper, easier to shape and manufacture materials can be used to prove the concept as long as the solution can also be applied to a more suited material. The selection criteria were the cost of the raw material, compatibility with cheap manufacturing techniques, non-toxicity, stiffness, resilience to bending, and inherent damping ratio. The last one is important as the flexure should not be damping itself too much.

Four different materials were analysed using Finite Element method and tested in the lab to see if they have the right properties. Those materials were Aluminium (Alu), Polycarbonate (PC), Polyoxymethylene (POM), and Polylactic acid (PLA, as used in 3D printing). All of the materials are fairly cheap, however PC, POM and PLA are much less stiff than aluminium and would allow for thicker flexures. Thicker flexures allow for easier integration of available piezo actuators. Additionally PLA could be 3d printed and would allow for much more complex and three dimensional designs. The other materials are compatible with laser and waterjet cutting. The worry was that PC, POM and PLA would have too much inherent damping.

3.2.1. Eigenfrequency and Damping Finite Element Analysis

The FEA was done on a flexure with the following dimensions 152x96x3 mm. Anticipating that the bottom of the flexure would be clamped some way on the testing setup, rectangular shaped wedges were modelled with the following dimensions 130x20x20. In the Finite Element Analysis the flexure was wedged between those rectangular shapes as shown in Figure 3.1 to simulate the clamping, in turn a fixed constrain boundary condition was applied to the bottom of those rectangular shapes, as indicated by the yellow colour in Figure 3.1. The flexure was analysed with the aforementioned four different materials, while the wedges were always given the PLA material. The flexure is coloured red in Figure 3.1. The visualization also identifies areas that will always show displacement regardless of mode, this makes it possible to use one laser distance measurer to observe multiple modes. Top left and right areas of a flexure are such locations.

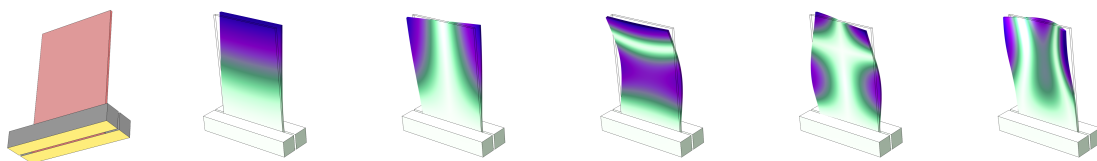


Figure 3.1: Left) shows the setup, with the flexure in red, the rectangular wedges in grey and yellow indicates the fixed constraint boundary condition. Second to left to right) Shows the modes from the first to the fifth.

Figure 3.2 shows the setup used to test out the damping of the flexures. As the figure shows the flexures were placed upright between two 3d printed elements that were held tight by bolts and nuts. All the flexures had the same dimensions. The epoxy used to bond two 3d printed flexure halves was UHU Quickset [16], Figure A.1 in Appendix A.1 shows a picture of this Epoxy. The PLA & Epoxy was made by printing two halves that were 1.4 mm thick and glueing them together using Epoxy, the end flexure turned out to be 2.9mm instead of 3 mm thick. The thickness of the epoxy layer was overestimated. 0.1mm is a very small difference. The laser distance measure device used was the optoNCDT-1420, in combination with the NI-6002 USB data acquisition module [17]. The optoNCDT-1420 measures over a distance of 10 mm. The reproducibility is $0.5 \mu\text{m}$ at 2 kHz. 2kHz was also the rate the measurements were taken at. The full specifications can be found in the manual [18]. The Laser is connected to a 3d printed part, the dimensions of this part can be found in the upper drawing of Figure A.2 in Appendix A.1. The flexure was displaced by pushing or pulling the top end with a finger and letting go. The flexure was pushed 6 times and pulled 6 times for a total of 12 measurements.

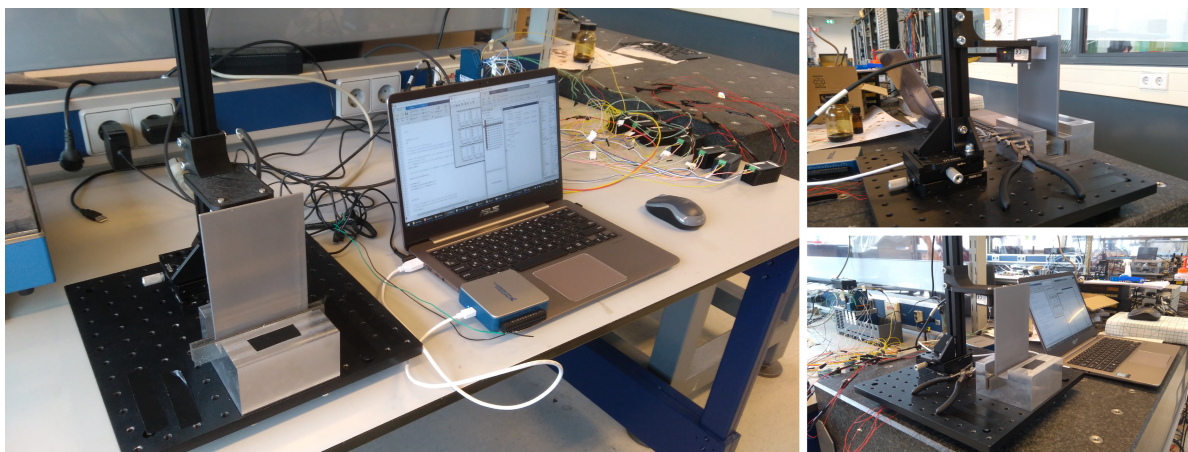


Figure 3.2: The setup to test the damping of flexures made out different materials, a PLA Flexure is shown in the image. The left image also shows the NI-6002 USB data acquisition module used in combination with the sensor.

The damping ratio was calculated by using the logarithmic decrement method. The logarithmic decrement is the natural log of the ratio of any two successive peaks.

$$\delta = \frac{1}{n} \ln \frac{x(t)}{x(t + nt)} \quad (3.2)$$

δ logarithmic decrement, $x(t)$ is the amplitude at time t , $x(t + nt)$ is the amplitude at n time periods away, n are the amount of periods. Using the found logarithmic decrement the damping ratio can be found using the following equation. With ζ being the damping ratio.

$$\zeta = \frac{1}{\sqrt{1 + \left(\frac{2\pi}{\delta}\right)^2}} \quad (3.3)$$

The procedure for calculating the damping ratio is shown in Figure 3.3. The following text will reference images a to e from Figure 3.3 and describe a simplified version of the procedure. First the raw data is plotted as shown in figure a. This is done for all twelve tests at the same time. The plots will show from which point on the data is clear and can be used, in figure a this is from the 1000 mark. Based on the data from this point on the average is calculated and the whole plot is shifted by the average/mean as is shown in figure b, then amplitudes above a certain value and below a certain value are removed which is shown in figure c. The data in c is used to calculate the eigenfrequency and produced images like those in figure e. To calculate the damping ratio only the positive peaks are taken from the data in figure c, figure d shows a plot of these peaks. Then equation 3.2 and equation 3.3 are used to calculate the damping ratio. This is done for all twelve tests.

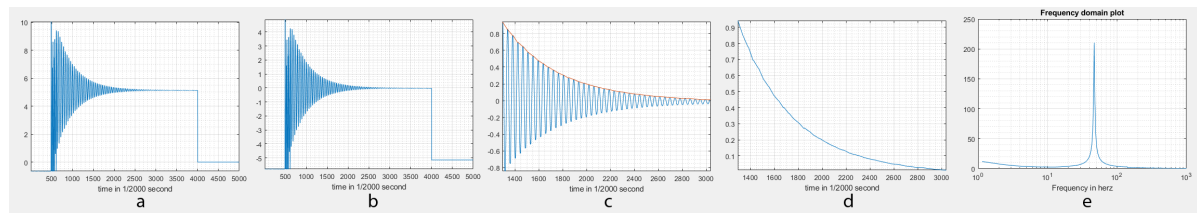


Figure 3.3: Procedure for damping.

More complete Figures for the data corresponding to images a, c, and e of Figure 3.3 can be found in Figures A.3, A.4, and A.5 in Appendix A.1. The graphs for PC and POM are not in the Appendix as they look nearly identical to PLA, Aluminium is different so that will also be shown in the Appendix.

Tables 3.1 and show the FEA and testing results for the eigenfrequency and damping of the materials. Do note that no FEA was done for the Polylactic Acid & Epoxy, as it was not known how to accurately model the epoxy.

Table 3.1: Upper tables shows the comparison between the first eigenmodes calculated using FEA and from the real life experiments. Below that are the damping ratios from real life experiments.

Comparison of Finite Element Analysis and measurements of the first eigenfrequency for different materials.										
Materials	Aluminium		Polycarbonate		Polyoxymethylene		Polylactic Acid		Polylactic Acid & Epoxy	
	FEA	Exp	FEA	Exp	FEA	Exp	FEA	Exp	FEA	Exp
First Mode	139	142 ± 0.21	51	43 ± 0.11	42	45 ± 0.20	47	47 ± 0.057		44 ± 0.15
Second Mode	439		153		129		145			
Third Mode	861		311		259		290			
Fourth Mode	1496		526		441		497			
Fifth Mode	1933		672		559		627			

Damping Ratio for different materials from experiments.					
Materials	Aluminium	Polycarbonate	Polyoxymethylene	Polylactic Acid	Polylactic Acid & Epoxy
Damping ratio	0.0042 ± 0.0066	0.066 ± 0.00087	0.0107 ± 0.0025	0.0105 ± 0.0028	0.0122 ± 0.0029

The testing shows that all the materials have low damping, and show clear peaks when a Fourier analysis is applied. Aluminium however has a pretty high first eigenmode, this could prove problematic if there is any phase lag because of the setup. Aluminium was also noticeably stiffer, it was very hard to bend the aluminium flexure. Often the whole breadboard the setup was sitting on would move. For the Aluminium testing weights were placed on the breadboard to stop it from moving because of the force exerted on the Aluminium flexure by my hand. Appendix A.1 has similar figures for Aluminium corresponding to the raw data, filtered data and frequency domain plot in Figures A.6, A.7, and A.8. They show the plots are pretty jerky, this is why the Aluminium damping ratio has the highest standard deviation. yet the data is still very accurate.

The damping itself was done in two different batches and redone once again. Initially it was thought that 3d printing would not be feasible, especially not with epoxy and no tests were done. So initially PC and POM were selected as the best candidates for material. Later on PLA and PLA with Epoxy was tested and that proved to work just fine.

3.2.2. Stiffness Finite Element Analysis

A finite element analysis was done to see if the disparity between the different materials and piezo was not too great. This is important if patch elements like benders and contractors are used as they need to flex properly with the flexure. If the disparity in stiffness is too great then the piezo elements would not flex properly along with the rest of the flexure and would change the behaviour by introducing inflexible nodes wherever they were integrated. The idea is to compensate for the increased stiffness of the piezo material by reducing the thickness of the flexure material wherever the piezo elements are integrated if possible. As an example suppose a .5mm piezo is integrated in to 2 mm flexure. But the .5 mm piezo is as stiff as a 1mm thick part of the flexure. In that case 1 mm of material would be removed to make space for the piezo, the other

1mm left over would be just as stiff as the piezo and would be able to transmit forced properly to the piezo. The testing was fairly simple. Two models of identical width and length were created but the thickness of the flexure material was a variable, while the thickness of the piezo material was a constant. The same force was applied to both models at the same point. The flexure materials thickness was varied until the displacement of the ends was identical. This was done using the inbuilt optimization algorithm in COMSOL 5.4. Figure 3.4 showcases how this was done.

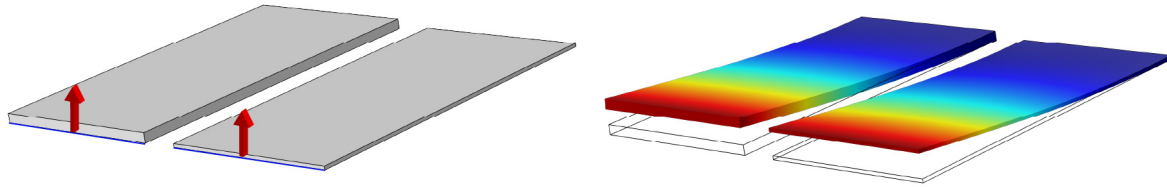


Figure 3.4: Shows the finite element analysis of the stiffness of different material compared to pzt, the materials were Aluminium, Polycarbonate, Polyoxymethylene, and Polylactic Acid. In the left image the blue lines indicate where the forces were applied, and the red arrows point in the direction of the force.

Table 3.2 shows the results of the finite element analysis. It shows how thicker something has to be compared to a PZT material to have the same bending stiffness (Thickness proportion). It also shows how much more or less stiff a material is compared to PZT from the FEA(Stiffness proportion column), and what is expected from the young modulus (Young modulus proportion column). While some materials are significantly less stiff, this is made up by the fact that bending stiffness scales to the power of 3, so thickening up a part quickly compensates. What is notable is that Aluminium has a higher young modulus then PZT, yet seems to be less stiff in bending. This is most likely due to the fact that the Young modulus values are simple averages. The actual young modulus is given by a stiffness matrix.

Table 3.2: Shows the results of the finite element analysis. The stiffness proportion column assumes stiffness for bending scales to the power of 3, so something twice as thick will be 8 times as stiff. The stiffness proportion column shows how much more or less stiff any material would be for the same thickness compared to PZT. Stiffness

Material	Young Modulus (Gpa)	Thickness (mm)	error(mm)	Thickness proportion	Stiffness proportion	Young Modulus proportion
PZT	63	0.2		1	1.00	1.00
Alu	70	0.21	2.24E-06	1.05	0.86	1.11
PC	4	0.55	4.62E-07	2.75	0.05	0.06
PLA	3.5	0.575	3.90E-06	2.875	0.04	0.06
POM	3	0.675	8.14E-06	3.375	0.03	0.05

3.3. Cell Structures

Creating the flexure out of discrete cells simplifies the design and optimization. Individual cells can be modelled, created, tested and the results can be extrapolated to multiple cells working together. The discrete nature makes optimization easier and efficient.

Several criteria were used to judge the different cell shapes, these criteria have a high degree of overlap. For clarity sake they will be listed as separate.

- Mechanical Properties
- Uniformity
- Simplicity
- Rotational symmetry
- Efficiency

Mechanical properties designate the directional stiffness and ability to transfer force to the next shape or outside force to the inner space of the shape. Uniformity designates two aspects. First how many different cells shapes are used to make a pattern, one shape is ideal. The second aspect is the actual shape, a square has four side with the same length, and no other edges to define it, a circle has one edge at one distance, both have high uniformity. Such shapes generally have larger unobstructed internal areas, they are easier to make, work with, and analyse.

Simplicity refers to the shape complexity, all kinds of shapes can be made using edges of the same length, but the simpler a shape the better. This criteria has a very high overlap with uniformity. Rotational symmetry refers to the ability of a shape to be rotated and still look the same, this would allow for a single shape to be made with an actuator in one direction, but with the ability to rotate that shape in different directions at a specific placement. This criteria again has a high overlap with simplicity and uniformity. The last criteria is efficiency, which can be seen as a combination of the previous three criteria, however it also refers to the way various shapes can be tiled, how much gaps and overlap there is. The less the better and more efficient.

Efficient tiling can best be described by the theory of tessellation. Which deals in all the ways shapes can be tiled without any gaps or overlap. Regular tessellation deals with the tessellation of regular shapes. A regular shape is a shape where all the sides and interior angles are the same. Regular shapes thus have high uniformity, and simplicity. Mathematically only three different shapes allow for regular tessellation. These shapes are the Square, the Equilateral Triangle and Hexagon as shown in Figure 3.5.

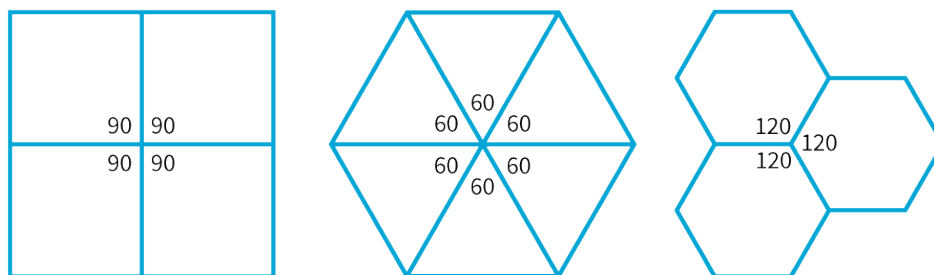


Figure 3.5: Three different basic shapes that can be tessellated[19][20]

In terms of mechanical properties the triangle has the highest stiffness, followed by the Hexagon, and lastly by the Square. The hexagon is the only shape where every neighbour shares at least one edge with another hexagon. Both the square and triangle have neighbours only sharing a vertex/point. Force transference along an edge is greater than through a single vertex.

Both the triangle and hexagon have three useful rotational symmetries, while the square only has two, though these are the principal ones, horizontal and vertical. In terms of inner area, the square and hexagon seem to be easier to work with and incorporate mechanism as they have flat edges parallel to one another. [21][19][20]. A further possibility is a semi-regular tessellation, which is a pattern made out of 2 regular polygons, there are 8 possible semi-regular patterns. These patterns are shown in Figure 3.6. For the sake of simplicity these patterns were left out. In terms of directionality this type of pattern does not add anything new, while being more complex. The mechanical properties haven't been investigated in this project as of yet. In practice most of these patterns will find some use, different types of patterns have different mechanical, conductive, and acoustic properties, Figure 3.7 shows an example of evolution of the basic patterns.

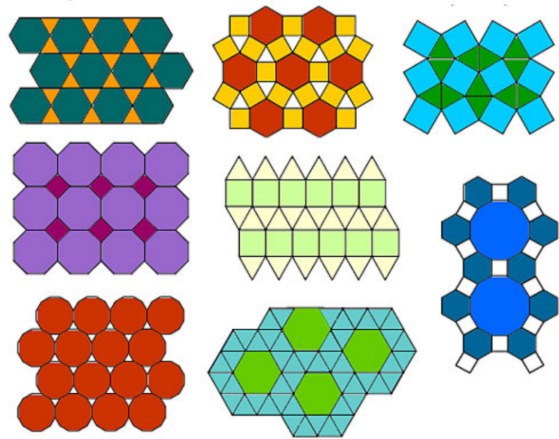


Figure 3.6: Eight different semi-regular tessellation patterns. [21]

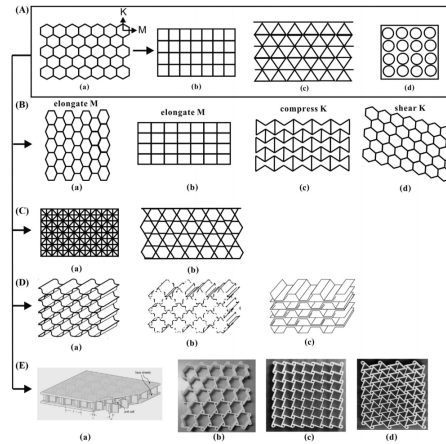


Figure 3.7: Evolution of the basic cell shapes [22]

The triangle and hexagon remained as the two best options. Both shapes were evaluated by looking in which way a rectangle shaped mechanism could be fitted in the cell and how the force is transferred. The reason for using a rectangle shape is that most actuators that can be bought are rectangle shaped. Geometry that can more easily accommodate a rectangle shape and more effectively transfer the force exerted by a rectangular actuator is preferable. Figure 3.8 shows that a hexagon shape will always be smaller for the same size actuator. Thus more cells can be arrayed in the same space, or a smaller flexure can be made with the same size actuators.

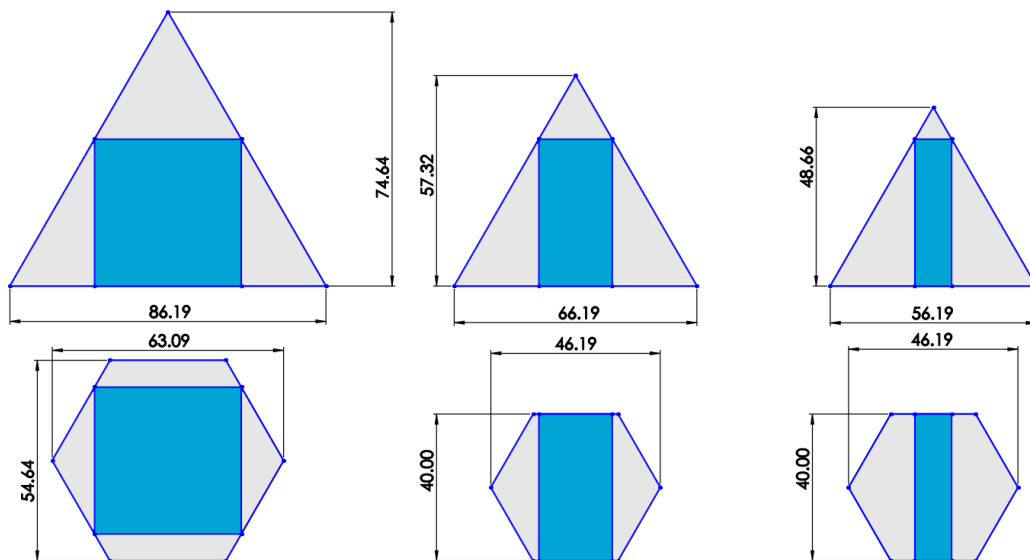


Figure 3.8: Comparison between a triangle and hexagon shape when accommodating the same size actuator. The actuator (in blue) on the left is 40x40mm, in the middle it is 40x20mm, and to the right it is 40x10 mm. In all cases the hexagon shape is smaller, the difference decreases as the rectangular shapes become elongated.

More important are the directions and lines of force a particular cell array can produce. Figure 3.9 shows the stress and thus the strain a flexure undergoes. Particular types of shapes and patterns they form lend themselves better to match the strain curves.

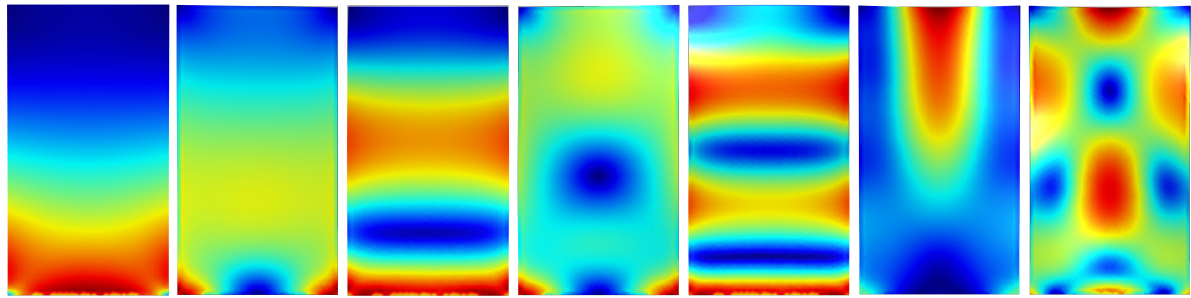


Figure 3.9: Shows the modes a flexure undergoes. Left is the first mode, higher modes are to the right. Next to the first mode is the torsional mode. The red areas indicate areas of high stress and thus strain.

Figure 3.10 shows some possible cell designs and Figures 3.11 and 3.13 explore the type of patterns possible with those cells. Figures 3.11 and 3.13 show that besides the orientation of the piezo within the cell, the orientation of the cell itself within the array creates different possibilities. The blue elements are piezo's and the red elements are piezo that are activated. This way patterns of force can be illustrated.

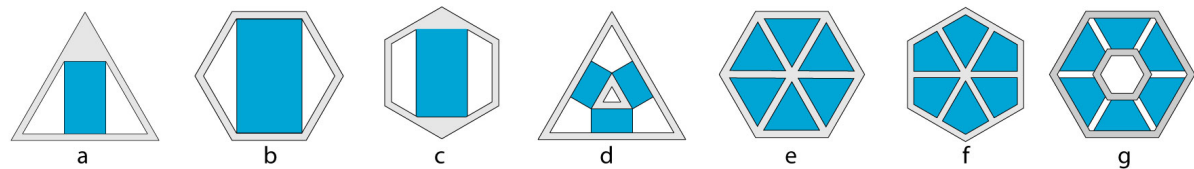


Figure 3.10: Shows a couple of cell designs next to each other. a,b,c are cells with a single actuator that can be bought. d,e,f,g feature custom designed actuators.

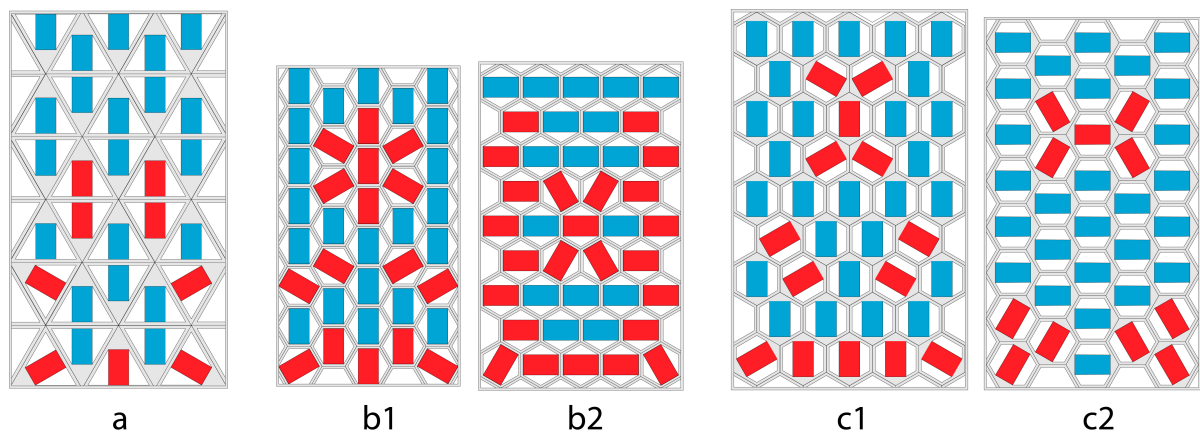


Figure 3.11: Shows the possible force patterns that can be made with the cells. The designations a,b,c correspond to the cells designs in Figure 3.10. The sizes of the internal piezo are the same for all flexures. This showcases how some design are more efficient in packing.

Flexure a in Figure 3.11 shows that the triangle is much less efficient in packing mechanism. Though the flexure is not much bigger then it's rivals it incorporates less cells, and thus will be able to produce less intricate force patterns. The designs in Figure 3.11 that can create the best match to the lines of strain shows in Figure 3.9 are b1 and c1. Flexure c1 allows for a horizontal row of piezo to exert force in the vertical direction, thereby damping the first mode effectively. The first mode is also the one with the most displacement and the most easily exited one, it should be prioritized when damping. b1 would be a bit better at damping the second torsional mode as the angled piezo are closer to the corner. The purpose of these patterns was to showcase what could be done, they do not necessarily have to make sense. Though when creating them some logic was

followed. At the bottom of the flexure the cells are always driven in such a way to damp the first and second mode as best as possible. The visualization show that some flexure designs like b2 and c2 in Figure 3.11 simply don't work very well.

Figure 3.13 shows more advanced designs with custom piezo. These flexures are all the same length as the piezo elements can be cut to a different size to compensate for any packaging differences. However this case the cells can be driven in a simpler or more complex way, which creates differences in patterns that can be created. As the hexagonal cells only have three directions in which to exert force, it is logical to drive piezo's that sit opposite each other as one larger piezo, simplifying the control and wiring. But each of the six piezo's could be driven separately enabling more complex patterns. Figure 3.12 a and b show case this difference. In Figure 3.12 a each pair has a different color, either blue, red or green. In Figure 3.12 b piezo's from two separate cells work together to form a force pattern. In Figure 3.13 the color palettes has been simplified there the red coloured piezo's represent piezo's exerting force, in a system where piezo's are driven in pairs. While the yellow piezo's represent piezo's exerting force in cells where each of the six piezo's is driven separately.

Figure 3.12 c shows the purpose of cell design g in Figure 3.10. In this design the force is directed from the center of the cell to the outer walls as there is space in between the piezo's. Where as in the other cell designs force is exerted in all directions. The design of cell g in Figure 3.10 can be applied to the other designs as well with a little modification. The design is mostly there to showcase the problem has been considered, and the other designs are just even more simplified models, design e is a direct simplification.

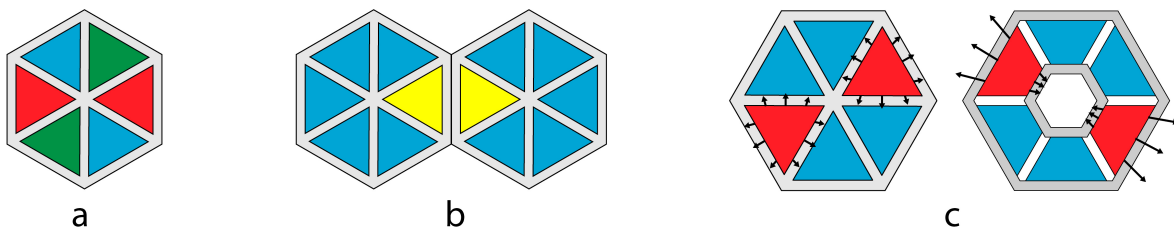


Figure 3.12: a) Showcases piezo pairs in cells, these pairs would be powered at the same time and work as one piezo. b) Showcases the possibility of powering each piezo in a cell separately. In this case piezo from two different cells work in unison. c) shows an improved cell design where the forces are directed from the center to the outward part of the cell instead of in all directions.

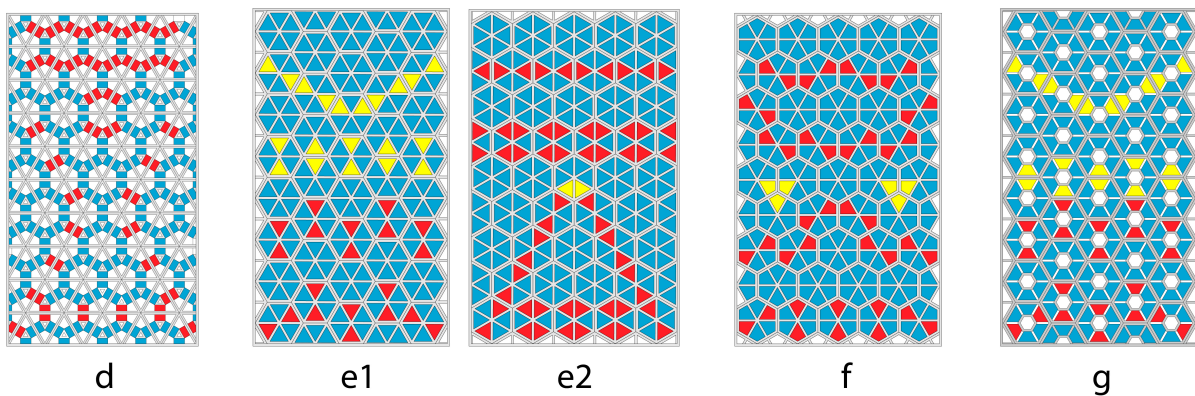


Figure 3.13: Shows more advanced flexure possible with custom actuators. d,e,f,g correspond to the cells designs in Figure 3.10

Flexures e1 and g show how driving the piezo elements individually enables these designs to create less zigzaggy and more clean horizontal lines of piezo's exerting force in the vertical direction.

Cell g and Flexure g are an evolution of cell design e. Leaving space between the piezo's necessitates a hole or solid part in the middle, which makes the cells less capable of creating a horizontal line of force. A more advanced design of f with spaces between the piezo elements would not have this problem as the cells can be lined perfectly next to each other in a horizontal manner. This is shown in Figure 3.14

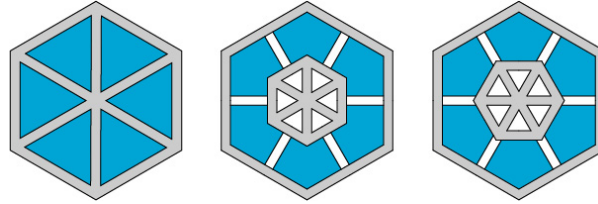


Figure 3.14: Two cell design variations of cell f in Figure 3.8 which improve the directionality of force exerted by leaving space between the piezo elements.

The mechanical properties of a hexagon cell can be altered by changing the internal structure. A simple cell is solid, but it can also have holes. By having a cell with hollow structure, the same in plane stiffness can be created with a thicker cell, and thus thicker flexure. The out of plane stiffness which needs to be high will also suffer, but depending on the structure this loss of stiffness can be reduced. This is handy as a thicker cell can accommodate more mechanisms. The active elements inside a cell can be stiffer than the cell material itself. By making the cell more hollow the total stiffness of the cell can be brought inline with the rest of the flexure. Thus reducing points of discontinuities during flexing.

Different structures are shown in Figure 3.15

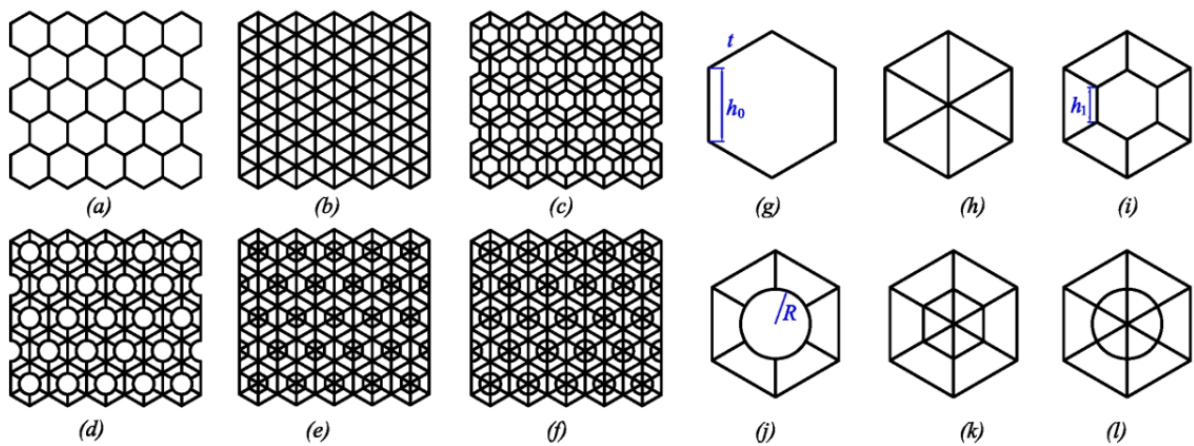


Figure 3.15: Hexagonal honeycomb with different kinds of reinforcements (a) general structure; (b) Triangular; (c) double hexagonal; (d) inside circular; (e) full double hexagonal; (f) full inside circular; (g) cell of hexagonal; (h) cell of full-triangular; (i) cell of double hexagonal; (j) cell of inside circular; (k) cell of full inside hexagonal; (l) cell of full inside circular [23]

Of the shown reinforcements the (k) cell of full inside hexagonal and (l) cell of full inside circular reinforcements perform the best. Figure 3.16 and Figure 3.17 show these two reinforcement have the highest stiffness. Well specifically they show that for the same compression they need to experience higher stress. The stiffness is increased by about 6 times in absolute terms. Though when taking weight in to account the increase is about 1.4

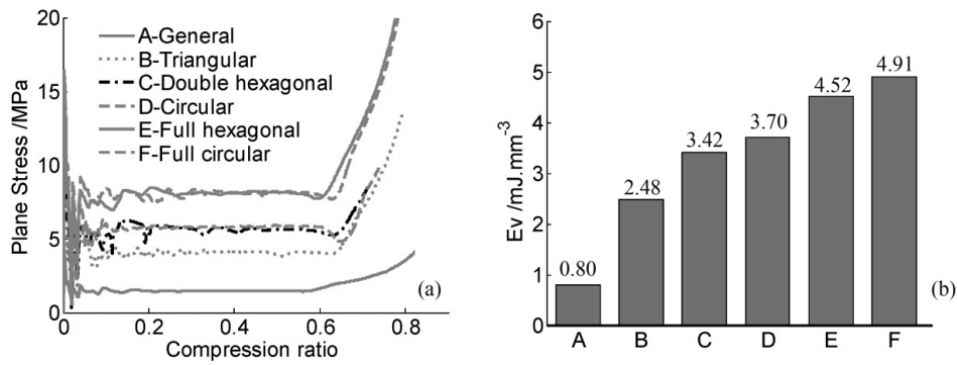


Figure 3.16: Left) Plane Stress vs Compression Ratio. Right) Energy absorption [23]

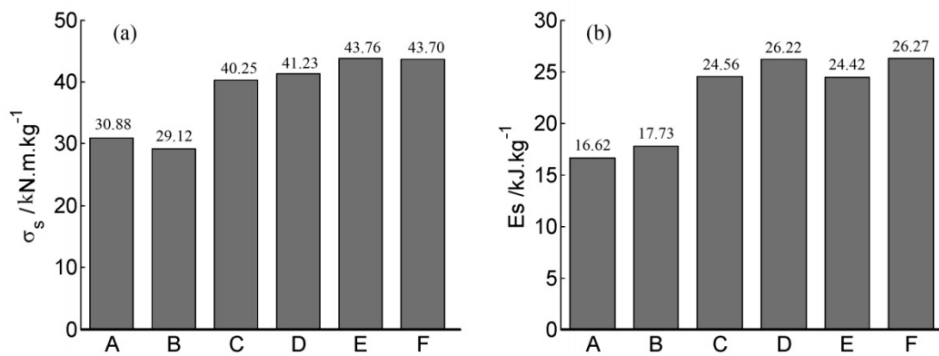


Figure 3.17: Left) Specific mean stress. Right) Specific mean energy absorption.[23]

Finally a finite element analysis was done in Comsol to calculate the difference in stiffness between the in plane and out of plane direction. This was done by applying the same force at the same edges in the in plane and out of plane direction and calculating the displacements. The results are shown in Figure 3.18. dz is the displacement in the out of plane direction, which is down when looking at the page, and dx is the displacement in plane which is in/or out of the page. Bot the solid and fully reinforced cell perform well, but the hollow cell is bad.

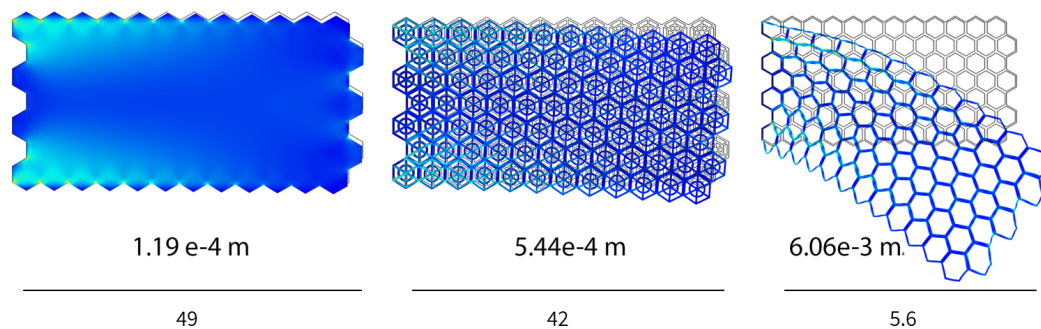


Figure 3.18: shows flexure made out of three different cells undergoing FEA to find out the ratio of stiffness between the out of plane and in plane directions.

3.4. Piezo Properties

3.4.1. Working principles

Piezo materials are transducers, meaning they convert one type of energy in to another. In this case electrical in to mechanical or vice versa.

Piezo electric materials exhibit a dipole moment. This can have natural causes but can also be create by a process known as polling, whereby a strong electric field is applied to a piezo material to orient all the dipoles in the same direction. This is shown in Figure 3.19 in a,b and c.

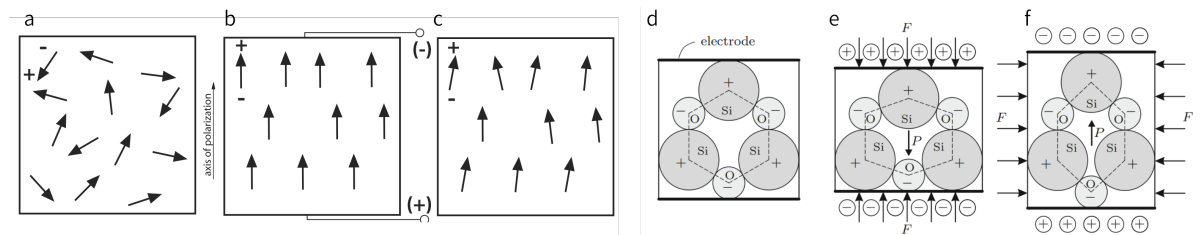


Figure 3.19: (a,b,c) Poling Process. a) polar domains oriented randomly. b) Large DC field is applied above curie temperature. c) After temperature is lowered and DC field removed remanent polarization.[4]. (d,e,f) Show the atomic structure that causes the polarization and the direct piezoelectric effects due to mechanical loads d) undisturbed state. e) When a compressional load is applied f) when a tensional load is applied [24]

Under compression or tension this dipole moment is changed resulting in a voltage. If the materials is compressed along the direction of polarization or in tension perpendicular to the direction of polarization the materials will generate a voltage of the same polarity as the polling voltage as shown in Figure 3.20 b. Tension along the polarization direction or compression perpendicular to that direction will create a voltage opposite to the poling voltage as shown in Figure 3.20 c.

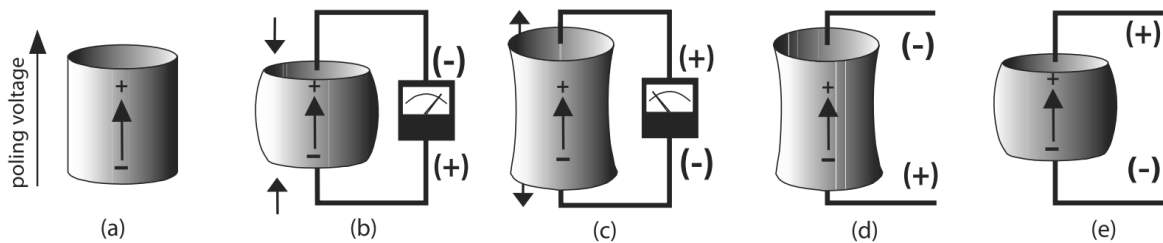


Figure 3.20: a) Piezo in a stress free state. b) piezo under compression. c) Piezo under tensions. d) Voltage applied in the polling direction. e) Voltage applied in the opposite of the poling direction. [4]

If a voltage of the same polarity as the poling voltage is applied in the direction of the polarization the element will lengthen and it's diameter will reduce as shown in Figure 3.20 d. The material will become shorter and expand if a voltage of the opposite polarity is applied in the polarization direction. As shown in figure 3.20 e.

Piezo have an efficiency between 0.3 to .5 when it comes to converting electrical to mechanical energy.[4]

Piezo's have a high power density. Meaning they can release a lot of energy relatively quickly.

3.4.2. Parameters describing the relationship

The piezoelectric coefficient of the material d_{ij} describes the relationship between the voltage and the strain. The d_{33} parameter describes the relationship between the strain and voltage in the direction of the polarization, and the d_{31} parameter describes he relationship between the voltage and strain perpendicular to the

polarization direction. d_{33} is about twice as large as d_{31} , however for most piezo materials the dimensions perpendicular to the polling direction are much larger than parallel to the polarization direction, and the material will contract and expand much more in absolute terms in those directions.

3.4.3. Advantages and Disadvantages

Their main advantage as actuators is their fast response (high operating frequency), ability to produce large forces for their volume, and their high sensitivity. Their main drawback are the small strains produced, typically 0.1 % of the length of the piezo element. Piezo's also exhibit hysteresis, the maximum hysteresis error lies between 10 and 15 % of the stroke. And finally they exhibit drift. After minutes to hours the strain can increase by 1 to 5%

Piezo's are particularly suited as strain sensors. They have higher signal to noise ratios than conventional wire strain gages. [25] Additionally they power themselves when put under strain, hence no external source of power is needed. In fact they can be used for energy harvesting.










Advantages		Disadvantages	
▪ High power density		▪ Small Strain	
▪ Fast response		▪ Hysteresis	
▪ Large Force		▪ Drift	
▪ High sensitivity			
▪ Linear response			
▪ Self sense (no power needed)			

Figure 3.21: Summary of the advantages and disadvantages of piezo's.

3.5. Amplification Mechanism for Piezo's

As mentioned piezo's generally change about 0.1% in length, which is inadequate for many applications. A great deal of effort has been spent to amplify the effective stroke.

3.5.1. Internally Leveraged Actuators

These type of amplifications usually do not result in a reduction of force.

Bender

Figure 3.22 shows a bimorph bender actuator.



Figure 3.22: Left) Bimorph Bender Actuator [26]. Angle-dashed arrows show polarization. Right) shows how the bender works. Blue is extending, and red is contracting piezo.

There are two types of bender actuators, unimorph and bimorph.

Unimorph consist out of 2 layers, one is a piezo layer, the other is an inactive layer. When the piezo layer expands or contracts, the inactive layer resist and the actuator bends to produce a fairly large displacement at the tip.

Bimorph, these actuators utilize two or more piezo layers. One layer is made to extend and the other made to contract, since the layers are connected the structure will bend. The displacement and force of the tip depend on the voltage and length of the bender actuator. The displacement is in two dimensions, when the bending occurs the tip will not just move perpendicular to the main axis but along the axis as the actuator contracts with respect to it rest frame.

Distance between the layers has an inverse relationship with the amplification. Figure 3.23 shows a small Finite Element Analysis. There the blue layer is the expanding piezo, the red layer the contracting piezo and the grey area is plastic. Two small plastic standoff were used instead of a single solid layer as that layer grew thicker the stiffness of the plastic layer would have player a big role in the amount of bending. The graph on the rightside of Figure 3.23 shows the relationship between the distance and displacement of the outer end of the system.

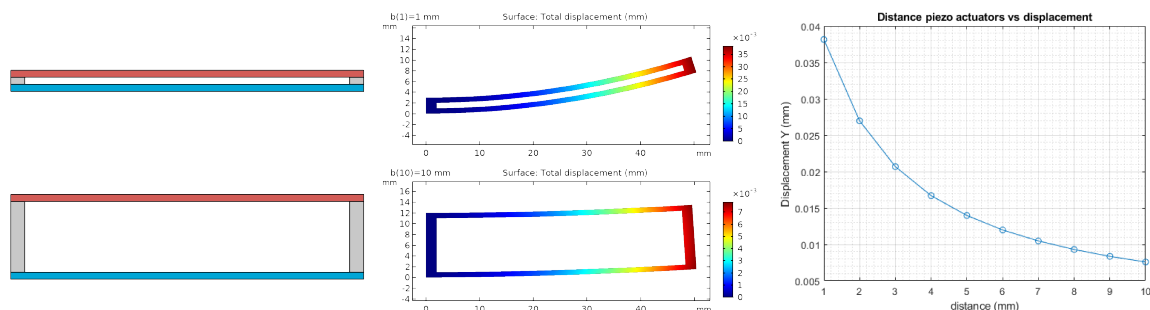


Figure 3.23: Left) the model used for the analysis. Only the two grey plastic layers change in size. The blue expanding and red contracting layer stay the same size. Middle shows the FEA. Right) Shows the relationship between the distance of the two piezo layers and the displacement of the outer end.

Fiber Composites and Interdigital Electrode Actuators

Active Fiber Composites and Macro Fiber Composites try to take advantage of the larger d_{33} displacement of piezo's. As illustrated in Figure 3.24, AFC's and MFC's consist out of long piezo fibers sandwiched between flexible polymers with electrodes attached to their sides at intermittent distances. Even though the electrodes are attached to the sides the voltage difference is in the longitudinal direction of the fibers. This is achieved by making sure that each electrode is preceded and followed by an electrode of the opposite polarity. Along the longitudinal axis of the fiber the electrodes are attached in a +,-,+,- pattern. The fibers are polarized along the longitudinal axis as well, so their expansion is governed by the larger d_{33} parameter.

Interdigital electrode actuators are monolithic piezo elements with the same electrode arrangement.

Both of these show greater displacements then conventional actuators.

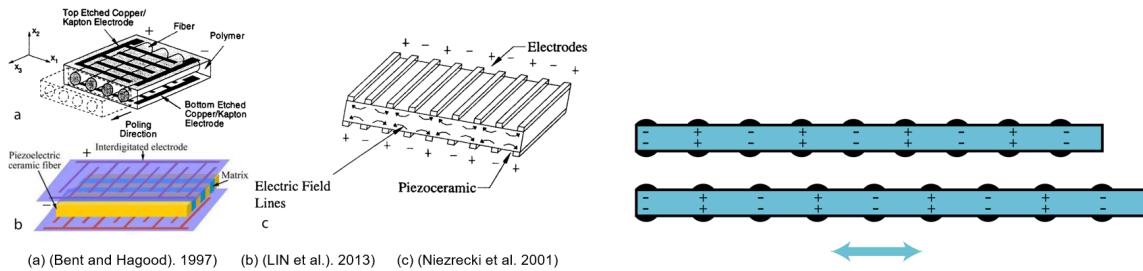


Figure 3.24: Left) a) Active Fiber Composite[27]. b) Macro Fiber Composite[28]. c) Interdigital Electrode Actuator[29]. Right) Shows the working principle behind this type of amplification

Torsional Piezo

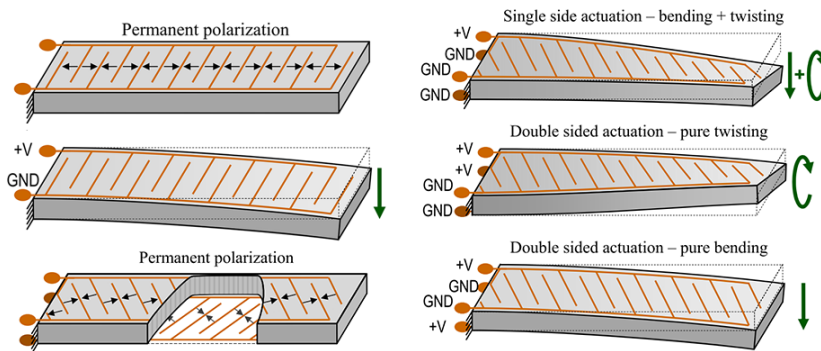


Figure 3.25: Compares the standard IDE (Top left and middle left) piezo, with the torsional piezo, this can be seen as an advanced variation of the inter digit electrode

The torsional piezo in Figure 3.25 angles the electrodes in such a way that the top and bottom layers expand at an angle causing the piezo to twist. However it can also be used in bend mode like normal IDE bending actuators.

Building Block Actuators

In this type of actuator a number of piezo actuation units are combined to produce larger displacements than they could alone.

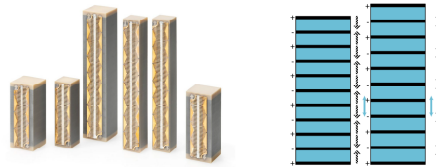
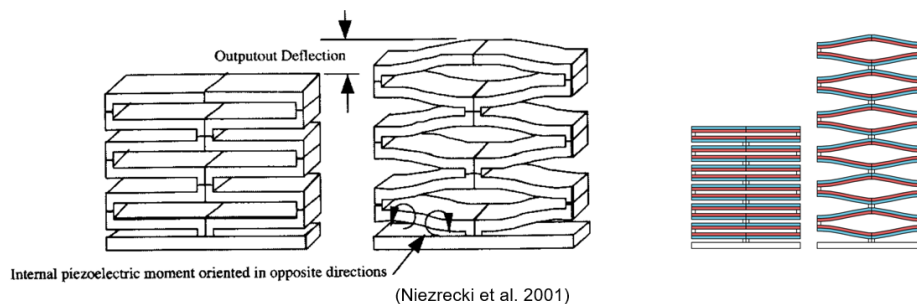


Figure 3.26: Left) Stack Actuator (piceramic). Right) Shows the working principle, Angled-dashed arrows represent polarization direction. Blue is expanding

The most simple and straight forward building block actuator is the stack actuator, as shown in Figure 3.26. This involves stacking actuators on top of each other. Each piece of the stack has a voltage difference applied to it. Two layers each with a voltage difference of 100V shows the same displacement as an imaginary monolithic piezo element of the same dimensions with a voltage difference of 200 V would have. All piezo's have a maximum voltage they can operate under though maximum voltage opposite to the direction of poling is about 10% of the max voltage in the direction of the polling. This is because a to high voltage in the opposite direction may cause depolling. And exceeding the max voltage may cause dielectric breakdown.



Internal piezoelectric moment oriented in opposite directions
(Niezrecki et al. 2001)

Figure 3.27: Left) Recuva type actuator[29]. Right) Working principle, blue is expanding and red is contracting.

Figure 3.27 shows the recuva actuator. Essentially the actuator is a clever way to use bimorph benders to create a straight movement. The individual beams making up the recuva actuator are fabricated so that one half of the beam bends in the opposite direction of the other. This produces a net displacement perpendicular to the main axis of the beams with no rotation of the endpoints of the beam.

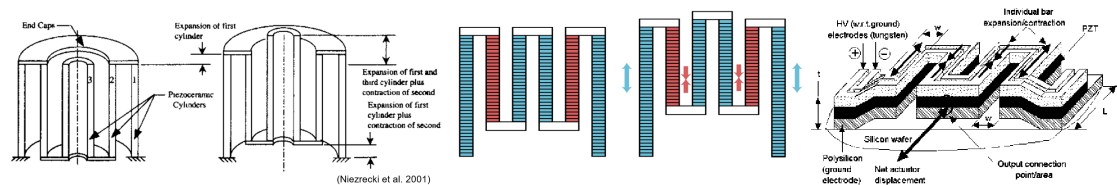


Figure 3.28: Left) Telescopic actuator[29]. Middle) The working principle. The blue ones are expanding, the red ones are contracting. Right) A planer version of the telescopic actuator called the meander line actuator.[30]

The actuator in Figure 3.28 is called a telescopic actuator. In this type of actuator neighbouring elements alternately expand and contract to produce a net motion in a single direction similar to how a handheld telescope unfolds A planer version of this type is called the meander-line actuator. The meander line actuator is used on millimeter or micrometer scales. The meander line actuator is shown on the right side of Figure 3.28

Spiral Actuators

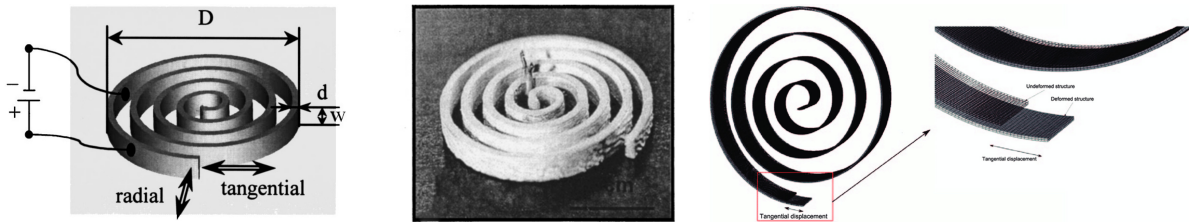


Figure 3.29: Spiral actuators [31][32][33].

Figure 3.29 shows examples of spiral actuators. Due to the spiral design the length of the piezo actuator is much longer for the same volume. Consequently the actuator produces much larger displacements in the tangential direction in comparison to it's volume compared to other piezo actuators. It also much more flexible then normal piezo actuators. It does produce much less force. And is less stiff, in the example from Figure 3.29 the eigenfrequency was 50 to 100 hz. Given the dimensions, and properties of PZT, the estimated stiffness of the spiral in the tangential direction is 111 N/m.

3.5.2. Externally leveraged Actuators

These actuators use external mechanism to amplify the stroke.

Lever Arm Actuators

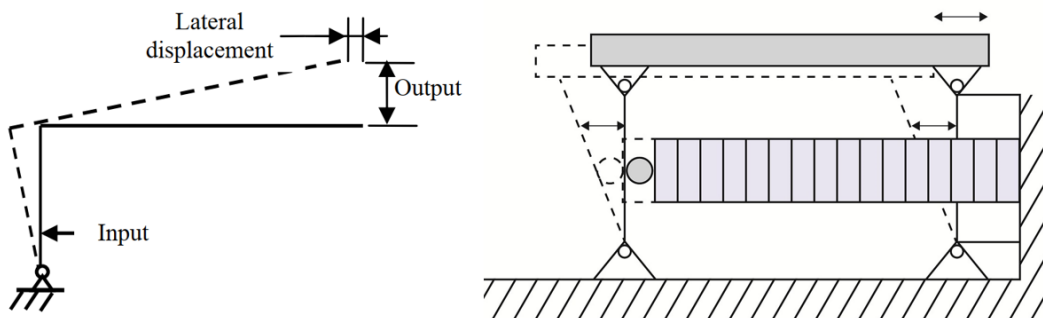


Figure 3.30: Lever type actuator[34].

Figure 3.30 shows the working mechanism of a lever type actuator. This involves a piezo stack pushing against a beam, at a spot much closer to the hinge, there by giving an initial amplification corresponding to the ratio of the total length divided by the distance the stack is pushing against. The beam is furthermore connected to a second which is longer, there by once again giving an amplification corresponding to the ratio of length of the longer beam divided by the shorter beam. The motion at the output is not one dimensional, as the output travels in a circular path

Flextensional, Flextensional + Lever, Flextensional + Bimorph

Flextensional actuators convert and amplify the stroke of piezo actuators in the transverse direction. All of them utilize some setup whereby a v-shaped mechanism is stretched or compressed to make the center tip move in a straight line.

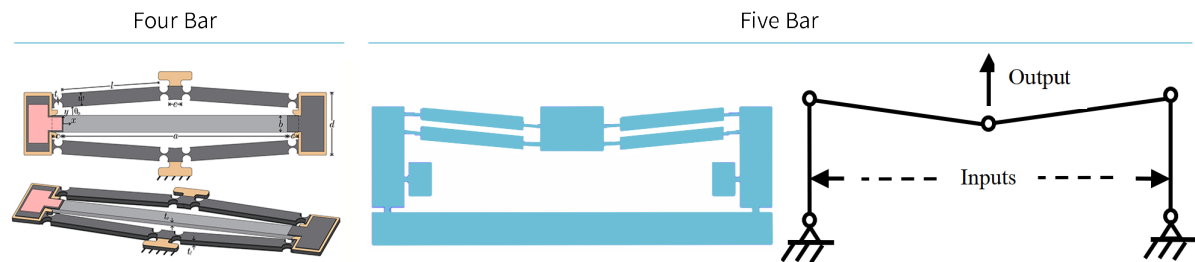


Figure 3.31: Left) The most common type of flextensional mechanism.[35]. Right) Shows the fivebar flextensional mechanism, which is a combination of flextensional and lever [36].

The left side of Figure 3.31 shows the most common flextensional actuator. The amplification is dependent on the angle of the v-shaped mechanism. The shallower the angle the bigger the amplification.

The middle and right side of Figure 3.31 shows a mechanism that combines lever type amplification with flextensional amplification. The mechanism is supposed to deliver increased amplification compared to most common flextensional designs of the same size.

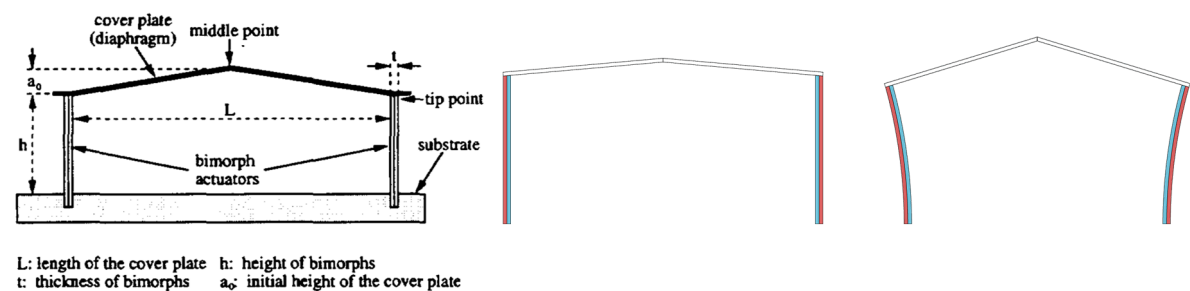


Figure 3.32: Left) Bimorph Double Amplifier[37]. Right) The working principle. Blue expands, red contracts

Figure 3.32 shows a mechanism that combines the flextensional mechanism with a bimorph actuator. The extension and compression is done by the bending action of bender actuators and not the extensions and compression of piezo stacks. Both the bending action as well as the flextensional deformation of the v shape give amplification.

3.5.3. Early concepts and ideas

Figure 3.33 shows some very early concepts just to test out some ideas and how they might be incorporated in to cells. A square shape was chosen for ease of use. a is just two four bar flextensional actuators. b and c use the lever arm concept, but the mechanism actually decreases the displacement of the piezo's, but amplifies the displacement of the cell. This could work in situation where the flexure flexes very little, but the piezo's need to deliver a lot of force. b uses a four-bar flextensional mechanism and c uses three bimorph patch actuators, the center one would be a sensor, the two outer would actuate. d is the most conventional and most practical design, it incorporates the actuators from c in a more conventional design. e is a bimorph patch, but just really inefficient. f uses double spiral actuators. g and h both use triangular arms so the arms themselves do not bend much, but transmit the force to the cell. And finally i is a 2D version of the telescopic amplification.

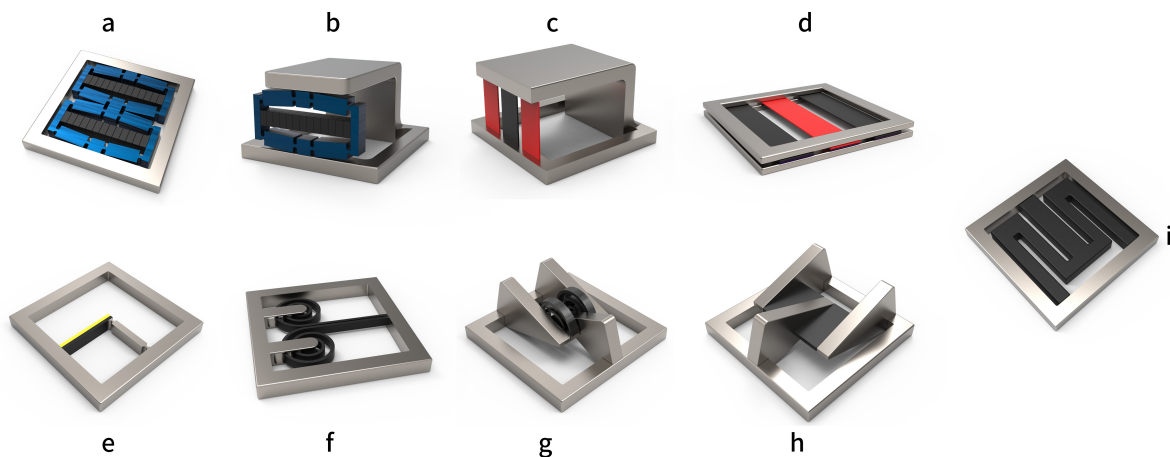


Figure 3.33: Some very early concepts just to visualize how these amplification methods might look in a cell. a) double fourbar flextensional. b) single fourbar flextensional. c) patch, center would be sensor d) patch center would be sensor. e) bimorph f) spiral g) spiral, h) torsional. i) telescopic

3.5.4. Suitability of the different amplification methods

At this stage of the work, most of the design and experimentation will have to be done with relatively few and big piezo elements, even if custom piezo elements are possible. If printing flexure with piezo elements becomes possible microscopic 3d structures could be created. But for now any amplification mechanism would have to be translated to a two dimensional variant. For example a two dimensional version of the telescopic amplification would have a contracting and expanding patches connected to each other instead of stacks. It would need to be applied to softer more flexible medium otherwise the actual expansion and contraction would be hampered.

A much more important problem is the decrease in stiffness, and the corresponding decrease in the first eigenfrequency. Currently smaller patch piezo actuators have eigenfrequencies in the hundreds herz. For example the T220-H4BR-1305XB shown in Figure 3.34, and used extensively in this projects, which is a bimorph bending piezo transducer with dimensions of 31.8 x 12.7 x 0.51 mm has an eigenfrequency of 350 hz. This is adequate, but even a reduction by two times to 175 hz would bring it dangerously close to the frequencies that need to be damped. Hence externally leveraged amplification is not very suitable yet unless the starting eigenfrequency is very high, as for example it is for stacks.

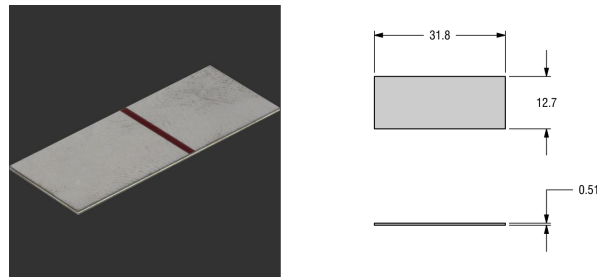


Figure 3.34: The T220-H4BR-1305XB Piezo electric Bimorph Bending Transducer with an eigenfrequency of 350hz [38]

Internally leveraged amplification is the most promising type of amplification. And bending actuators are widely available. Interdigital Electrode Actuators are more advanced version of the bender actuator which could achieve more displacement at no cost to the stiffness, and thus are even more desirable. And the torsional piezo is an more advanced version of the interdigital electrode. However the torsional piezo is not commercially available. Though one can immediately see the possibility of creating a fiber composite flexure with angled interdigital electrodes enabling the flexure itself to directly counter the first mode and the second torsional mode. This falls outside of the scope of this thesis. However smaller torsional patches inside cells could enable a cell to push and pull as well as twist, thus enabling more advanced damping.

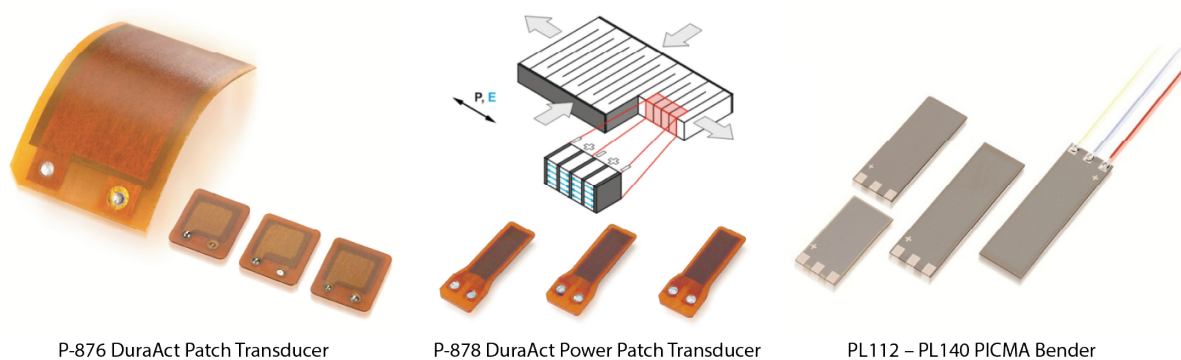
3.6. Commercially available piezo actuators

The simplest way to to make any mechanism would be to buy commercially available piezo actuators and integrate them in to a design. When looking for piezo actuators the most important criteria was the voltage they operate at, size and ratio of dimensions, and price. Most amplifiers can go in to the hundred of volts so piezo actuators operating on thousands of volts were not considered. As the flexure was to be kept as small and thin as possible, the piezo's themselves had to be as small as possible. At the core of all amplification mechanisms are either stack or patch actuators, patch actuator being just long and thin plates that in their most simple form make up extending or bending actuators.

Desirable characteristics of piezo patch actuators was how thin they were and the ratio of length to width. Thinner is better. The ratio of length to width is important as it determines directionality. A patch actuator that is square will extend/contract or bend the same in all directions. However if one dimension is longer then the actuating in that direction will larger. However if an actuator is much longer then wide it will just be strip that require a large hexagon cell but cannot deliver much force. Though this could be solved by having several next to one another. This does increase complexity of actuating and possible price.

The stack actuators had to be as small as possible, and ideally longer then they are wide and deep. In any flexure the stacks would have to be housed inside the flexure, their width and depth would determine the thickness of the flexure. If they had more length then width and depth they could deliver more displacement. Though again this could be solved by stacking, the stack actuators on top of each other.

Patch actuators



P-876 DuraAct Patch Transducer

P-878 DuraAct Power Patch Transducer

PL112 – PL140 PICMA Bender

Figure 3.35: Shows the three actuator from Pi Ceramic that were considered for buying

P-876 DuraAct Patch Transducer[39] As shown in the left image of Figure 3.35. This transducer has a laminated shell for protection, is flexible and with clear electrodes on a single side. The Full specification can be found in Figure A.9 in Appendix A.1. The laminated shell protects the piezo and could make it easier to remove glue or epoxy, but also adds unwanted thickness and diminishes the stiffness of the contact between the piezo and a flexure material. The coating also adds length and width to piezo which does not contribute to actuation. The electrodes on a single side would make connecting much easier, as all connection can be done on a single side.

The location of the connection is predetermined and reduces the options of any design. The biggest problems are the dimensions and voltage. The smallest transducer measures 16x13x0.5mm which makes it a bit too square and not directional enough, and it uses a voltage between -100V and 400V, which is a bit too much. The other transducers all have dimensions of 61x35x0.4 mm, which is too large. The price is 56,- for the 16x13x0.5 mm actuator

P-878 DuraAct Power Patch Transducer[40] As shown in the middle image of Figure 3.35. This transducer also has a laminated structure for protection. The coating also serves as a preload to make the actuator bendable. It has all the connections on one side, like the P-876. And like the P-876 the location of the connection is predetermined and reduces the options of any design. It requires a voltage between -20V and 120 V. This is an interdigital electrode type actuator. The full specifications can be found in Figure A.10 in Appendix A.1. The laminated coating has the same advantages and disadvantages as for the P-876. Though this coating is quite a bit larger proportionally. The transducer measures 27x9.4x0.6 mm, but the active area is only 15x5.4. Its main disadvantages are the thickness at 0.6 mm and the small active proportion of the whole package. The price is 98,- euro per actuator.

PL112 – PL140 PICMA Bender[41] As shown in the right image of Figure 3.35. This bender has no lamination. It is surrounded by ceramic insulation. It requires three connections. The connections are all located on one side at the bottom. The transducer comes in several sizes. The smallest ones are 18x9.6x0.67 mm, 25x9.6x0.67mm, and 31x9.6x0.67 mm. The displacement of the 18mm long actuator is $\pm 100 \mu$, for the 25 mm it is $\pm 310 \mu$, and for the 31 mm it is $\pm 450 \mu$. They operate at a voltage of ± 30 V. The resonant frequency for the 18 mm one is 1800 hz, 600 hz for the 25 mm one, and 420 hz for the 31mm actuator. The full specifications can be found in Figure A.11 in Appendix A.1.

The biggest disadvantage is their thickness at 0.67mm which would make them thicker than all of the piezo actuators discussed here. And the fact they require three connections per actuator. The location of the connections is on one side which is an advantage, but the location is also predetermined which gives less options when designing. Their price is 71,- euro for the 18x9.6x0.67mm actuator, 80,- euro for the 25x9.6x0.67 mm actuator and 83,- euro for the 31x9.6x0.67 mm

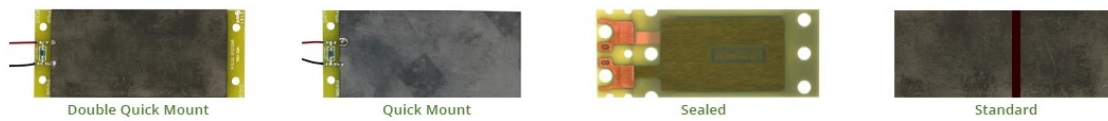


Figure 3.36: Shows the actuator versions of the T220-H4BR-1305XB and T220-H4BR-1305YE from piezo.com that were considered for buying.

T220-H4BR-1305XB Piezoelectric Bending Transducer and T220-H4BR-1305YE Piezoelectric Extending Transducer[38][42] As shown in Figure 3.36 These two transducer will be grouped together as their dimensions, construction and material use are identical. The only difference is the polling. The actuators come in several versions, standard with just a nickel coating, a sealed version, quick mount and double quick mount. The smallest dimensions are 31.8x12.7x0.51mm for the standard version, the sealed version is 53x20.8x.71mm although only 28x18 of that is active element, and it only comes with a single active layer, it is recommended for sensing and energy harvesting. The other types all come with two active piezo layers. The quick mound adds an element measuring 12.7x12.7x1.6mm for mounting and connections and the double quickmount adds two on both sides.

For the purposes of this project the standard is the best as it has the smallest dimensions. In fact it's thickness is the second smallest. It's whole surface can be used to attach connections. The bender has a displacement of $\pm .25$ mm, which is lower then the $\pm 310 \mu$ displacement of the PL122 with smaller length (25x9.6x0.67mm) but larger thickness. The benders operate at a voltage of ± 60 V and extenders at 120V. The resonant frequency is 350 hz for the bender, and 29500 hz for the extender. The price for the standard ones is 93,- euro's. The full specifications can be found in Figure A.12 in Appendix A.1.

T220-H4BR-1305XB Bender vs PL127 PICMA Bender Eventually it came down to these two benders. Their dimensions are similar 31.8x12.7x0.51 for the T220 and 21x9.6x0.67 mm for the PICMA. The PICMA has better performance, and more directionality as the ratio of length to width is better. But it comes at the cost of greater thickness and predetermined connection location. The greater resonant frequency of the PICMA of 420 hz vs 350 hz for the T220 is strictly better in terms of control, but it also means the actuator is stiffer and would require a thicker flexure. The PICMA als operates at a voltage of ± 30 V instead of ± 60 V. Both have very clean and rectangular shapes, that are easy to accommodate inside a design. It's a very difficult choice. But in the end the greater flexibility with regards to connections of the T220 and thinner size make it preferable to the PL127 PICMA.

Stack Actuators

This was terribly simple. As the SA Series 150V Piezo Stack Actuators[43] from piezodrive were available at the TU Delft. The size of the actuator chosen the SA030318 was 18x3x3 mm which is just small enough that it might work. The maximum displacement is 25μ , the eigenfrequency is 84 kHz. The price of these actuators is 46,- euros. Generally piezodrive is one of the cheapest if not the cheapest piezo vendor outside of Aliexpress resellers. These types of actuators are shown in Figure 3.37 the full specifications for these actuator can be found in Figure A.13 in Appendix A.1.



Figure 3.37: Shows the SA Series 150V Piezo Stack Actuators from piezo drive

3.7. Reflections

Laser sensor positioning. The initial Finite Element Analysis done in section 3.2 showed where the flexure would displace for several different modes and thus the sections a laser sensor should be pointed at.

Material All of the materials except for Aluminium are suited for a flexure. Aluminium was too stiff and it's first eigenmode at 142 Hz would be too high.

Hexagons The most important findings of this chapter deal with cell patterns. The conclusion is that Hexagonal cell patterns are the best suited for cellular flexures. Hexagons and triangles both have three useful rotational symmetries but the hexagon is easier to work with and can accommodate more mechanisms. A mechanism implemented in a hexagonal cell will always result in a smaller and more efficient cell than the same sized mechanism in a triangular cell.

Furthermore patterns where the hexagon corner points along the longest axes of a flexure (pointy pattern) are better than patterns where the hexagon flat edges point along the longest axis (flat pattern). This is because the pointy pattern can form straight lines of force to damp the bending modes. Whereas the flat pattern forms a zigzagging line.

The piezo inside a hexagon can be aligned with the flat edges or the corners. And a pointy pattern with piezos aligned with the corners is overall superior. The research also showed a lot of patterns which were bad.

More advanced hexagonal cells can be made by subdividing a hexagon into six smaller (piezo) cells. At their simplest these smaller elements have triangular or diamond shapes. The more complex hexagons with smaller inner hexagons have piezo elements which are rectangular or pentagonal. These can be driven in pairs, whereby opposite elements behave as one element or individually. Once again a hexagon in a pointy pattern with six diamond shaped inner elements is the best. Furthermore if these elements are separated by their adjacent neighbours with empty space, their force will only be directed from the center of the cell outwards. This will improve directionality, as normally piezo exert force all around them.

Amplifications The most useful amplifications researched were in the internally leveraged bimorph bending amplification family, more advanced versions of this include the interdigital electrode actuators and torsional inter digit electrodes which do not add extra amplification, but do allow for twisting in addition to bending. Another good amplification method is the flextensional amplification in conjunction with stack actuators.

T220-H4BR-1305XB Piezoelectric Bending Transducer This Piezo actuator is the most suited commercially available actuator for this project, but the PL127 PICMA Bender is a very close second, and could be reconsidered in the future.

4

Design and Finite Element Analysis

Design and Finite Element Analysis are intimately intertwined as any design is first put through Finite Element Analysis and the results of Finite Element Analysis inform future improvements in design.

Finite Element Analysis was done at all stages of the thesis. It was done to gain insight into the way flexures deform during their eigenmodes, this informed the research on basic cell shapes as was shown in the previous chapter.

Furthermore Finite Element Analysis was done to help integrate Piezo elements and PLA as both materials have different stiffnesses. Though other practical concerns like the total stiffness, debugging, manufacturing and practical integration concerns played an important role in the final design.

Finite Element Analysis was also used to test out some preliminary ideas and to compare designs. In total around 40 different cell and flexure designs were tested numerous times. Only the major designs and result will be discussed.

Finite Element Analysis was also used to test out some preliminary ideas and one big idea was even rejected based on the results, while this idea never made it into the final experimental flexure it will be discussed as it adds valuable knowledge. Some designs were tried but did not work out for various practical reasons these designs will also be discussed and the reason to abandon them. And some designs could not be made in a practical time frame but do seem to be promising ideas. These will be discussed along with their Finite Element Analysis results.

4.1. Flexensional Design and Finite Element Analysis

The initial assumption at the start of the thesis was that 3d printing and any kind of glue or epoxy would leave a flexure with too much inherent damping. This meant that ideally any design would require the laser cutting of a single sheet of metal and plastic. This makes piezo stacks inside a flexensional mechanism such as the one in Figure 3.31 more attractive due to the way the stacks are connected to a flexure, versus a piezo patch actuator. Figure 4.1 showcases this very well. The figure on the right side can be cut from a single plate. While the figure on the left requires the cutting and connecting of two plates. Beneath the 3d models are front-facing enlarged cutouts of the figure above showing how the flexure and piezo would fit together. The location of the cutouts is indicated by the red line in the 3d models.

At the time it was thought that a connection made out of glue or epoxy could act as a damping material. A single plate design would also have a more consistent thickness and stiffness over multiple models. Whereas with a multi-plate design the thickness and stiffness would vary due to varying thickness of the connecting layer.

As mentioned in the previous chapter, externally leveraged amplification methods reduce the stiffness and eigenfrequency but stacks have a very high eigenfrequency to begin with, in the kHz range. A particular range

of stack actuators was easily and cheaply available, had pretty small dimensions and a high eigenfrequency. The Stack Actuator in question is the SA030318 actuator from PiezoDrive [43], the actuator is 3 x 3 x 18 mm in dimensions. A thickness of 3mm is small enough to still be viable for a flexure, especially if the flexure is made out a skeletal structure as show in Figure 3.18. This would reduce the in plane stiffness of a 3mm thick flexure enough to make it flexible enough for practical use.

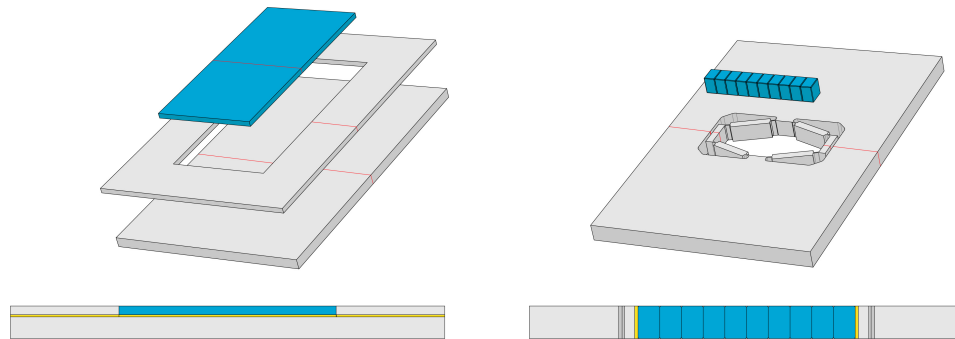


Figure 4.1: Top Left) design needed to fit a piezo patch inside the flexure Top Right) design needed to fit a stack. inside the flexure. Bottom Left) a front view of the design above housing the patch. Bottom Right) A front view of the design above with the stack. Grey is flexure material, blue is piezo and yellow is glue/epoxy.

Figure 4.2 showcases how a possible flexure might look. Though the render is just for showcase purposes, the piezo positions and directions are not optimized. There are three different cells. One containing two five bar mechanism, one containing a single four bar mechanism, and one with a patch actuator. One might envision a situation where the heavier double five bar piezo cells are positioned near the base where the most force and strain are required, the four bar a little higher and the patch actuators which are the lightest but provide the least force could be placed the highest.

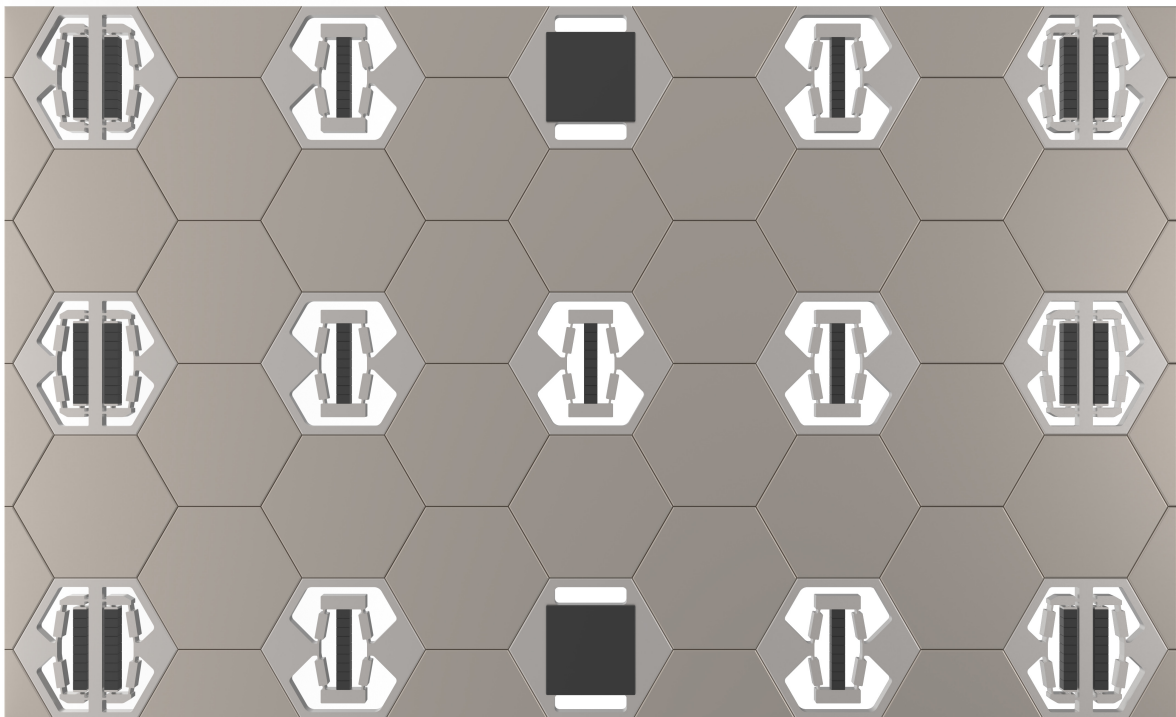


Figure 4.2: Example of how a flexure with flextensional mechanism might look. The purpose was to showcase different mechanisms, the cells are not positioned in an optimal way, as this is just to visualize the idea. The mechanism in this case are the four bar flextensional, five bar flex-tensional and simple patch..

4.1.1. Displacement and Force testing

The first priority was to test out if a flex-tensional mechanism could actually work inside a flexure. Meaning would it transmit the forces to the piezo during flexing and would the force the piezo creates be transmitted back to the flexure. If this was possible then the design would be adjusted for the needed stiffness if necessary and possible to achieve the desired first eigenfrequency.

Three designs were created for the Finite Element Analysis to find out how individual cells reacts to displacements at various points and directions. All the designs are based on the standard flex tensional amplification mechanism, and are shown in Figure 4.3. A square outer shape was used because it's computationally less intensive, and the square shape mimics the behaviour of a flexure better. Just as in a real flexure, forces from the outside will be spread along a horizontal edge on the top and bottom. The compliant joints are thicker than normally found on these types of mechanism because the flexure was expected to be made out of Polycarbonate or POM and not metal.

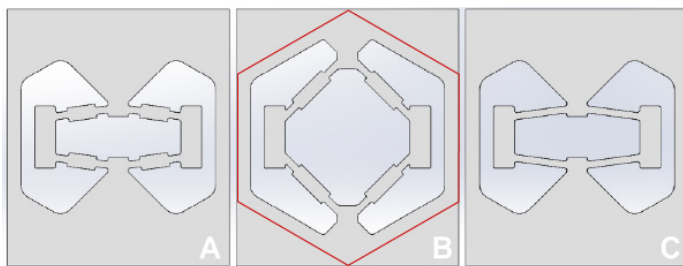


Figure 4.3: Three different cell variants to be tested in Comsol. A) standard. B) Arms at 45 degrees, to test the effect of arm angle. The red hexagon displays the physical limits the designs have to adhere to, to fit inside a hexagonal cell. C) No center stiffness elements, as the piezo would only extend the arms will only be in tensions, this could be more efficient.

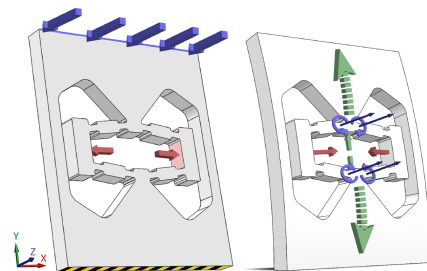


Figure 4.4: Left) showcases where all the places displacements were applied and/or calculated. The view is shifted up a bit to showcase certain surfaces. Right dashed arrows show the strain, normal arrows show the displacement or rotation.

- **Design A** resembles the standard design the most, where the arms have a low angle compared to the horizontal, this should maximize the amplification of the piezo stack. But will minimize the displacements transmitted to the piezo.
- **Design B** has the arms at 45 degree angles. In this case there is no amplification either way. This was done to test the effect of the angle of the arm. Cells with arm angles greater than 45 degrees were not tested as piezo displacements are tiny as is, and greater angles would not fit inside a hexagonal cell, 45 degrees is pushing it as is. The red hexagon around the middle cell showcases this.
- **Design C** has no central stiffening element. The piezo will be operating exclusively by extending, the arms will be constantly in tension, by removing the central elements the bending stiffness of the arms is reduced which result in less energy storage in the arms and more transmitted to the rest of the cell.

The analyses were performed by prescribing displacements at certain points of the cell and recording the resulting displacements at the other areas. The left image in Figure 4.4 shows where the displacements were applied and/or calculated, and defines the axes. The right image in Figure 4.4 shows the expected strain and displacement when a displacement is prescribed in the z-direction at the upper edge of the cell.

The bending of the flexure is approximated by applying a displacement in the z-direction at the upper edge of the cell, marked by the blue arrows and blue edge, while constraining the bottom of the cell marked with the black yellow stripes. The stretching will happen along the y axis in the frame of reference of the cell, shown by the green dashed lines. There will also be a movement in the y-direction shown by the solid green arrow. Due to the amplification mechanism, this stretching will be converted to a displacement in the x-direction as the arms rotate. The rotation is shown by the blue arrow in the right image in Figure 4.4, and the x-displacement of the areas marked with red is shown by the red arrows. The x displacement is taken from both sides and added together, as this is the maximal compression a piezo might experience. In reality the cell will not just stretch, the opposite half will compress. FEA can show whether one type of strain is dominant. If one type is not dominant then the system will not work.

Ideally one would like to see how displacement in the x -direction affects the z -direction, but when the cell is straight no displacement in the z -direction will take place.

4.2. Results

Table 4.1: Table shows the displacement in the x direction when a displacement is applied in the z direction. At the bottom of each column is the average attenuation. Meaning by how much less the the displacement in the x direction is compared to the z direction The displacement in the x -direction is calculated by adding the x displacement of both sides indicated by the red arrows and red colour in Figure 4.4 as this how much compression a piezo stack will experience maximally.

Cell A		Cell B		Cell C	
dz (mm)	dx(mm)	dz (mm)	dx(mm)	dz (mm)	dx(mm)
0.2	1.33E-05	0.2	3.74E-05	0.2	1.92E-05
0.4	5.83E-05	0.4	1.34E-04	0.4	7.55E-05
0.6	1.35E-04	0.6	2.90E-04	0.6	1.69E-04
0.8	2.43E-04	0.8	5.06E-04	0.8	3.00E-04
1.0	3.83E-04	1.0	7.80E-04	1.0	4.67E-04
1.2	5.54E-04	1.2	0.001113	1.2	6.72E-04
1.4	7.57E-04	1.4	0.001505	1.4	9.14E-04
1.6	9.91E-04	1.6	0.001956	1.6	0.001193
1.8	0.001257	1.8	0.002466	1.8	0.00151
2.0	0.001555	2.0	0.003031	2.0	0.001863
Average Attenuation		Average Attenuation		Average Attenuation	
2369		1173		1946	

The attenuation is in the thousands. Which is a lot. But the displacement in the z directions could be in millimetres, while the strain the piezo should receive and can produce is in the μm . The displacement of the piezo stack is $25 \mu m$, so ideally the attenuation should be in the hundreds. The normal mechanism in Cell a delivers the least amount of displacement in the x direction, which makes sense as it is intended to amplify the x displacement and thus reduce the displacement delivered in the x direction. Cell c has the same angle as Cell a and thus the same amplification but is less stiff and thus easier to deform. This design is superior if only pulling forces are applied in the arms. Cell B does not amplify, and as expected delivers the most displacement to a piezo stack.

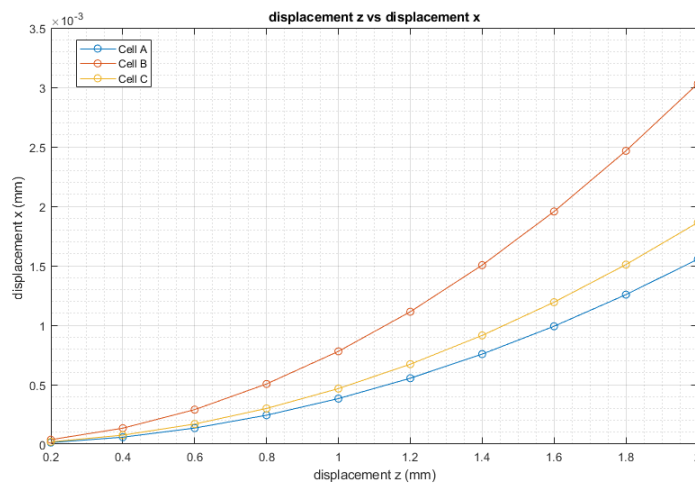


Figure 4.5: Graphs comparing the displacement in the x direction. due to the displacement in in the z direction at the upper edge of the cell.

4.3. Force testing

To test the validity of the concept even further forces were applied instead of displacements. The material specified was polycarbonate. Metals were ruled out due to being too stiff when 3mm thick. These Finite Element Analyses were done on a mesh resembling Cell C in Figure 4.3. As this cell performed reasonably close to the other two cells while having a much simpler mesh that is less computationally intensive. Two different approaches were taken.

In the first approach a force in the z direction was applied with a smoothed step function for 2 seconds. After those two seconds a smoothed force in the x-direction was applied simulating a piezo element extending. This approach failed miserably. The force in x direction had negligible effect. The force in x direction was more than 1000 times stronger yet had an effect of less than a percent.

A second approach was taken utilizing global equations where a z force was applied and the software was left to find the x force needed to reduce the displacement by some value. Most of these attempts did not return a solution. The ones that did were not encouraging. Prescribing a force in the z-direction of 0.2 N resulted in a z displacement of 0.074mm, to bring that down to 0.07 mm the force provided by the Piezo would have to be 1518 N.

If the results are correct then this approach will never work. Not only is it inefficient, it requires more force than a small stack can provide and the polycarbonate material would not be able to handle the stress these forces would create.

The displacement based FEA was done again on a simpler model to gain some insight into what could be wrong. The analysis was done with 4 different resolution meshes, all of the calculations agree with each other. The results of that analysis are shown in figure 4.6

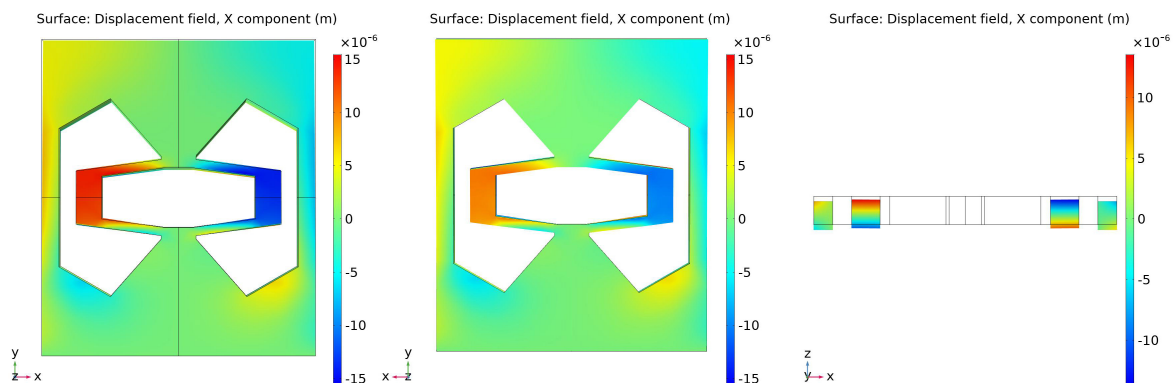


Figure 4.6: Three images showing the displacement in x-direction from three different perspectives. The rightmost image looks from the bottom, so the front of the cell is located on the top and the backside is at the bottom

The three images show the displacement of the model in the x-direction, the direction affecting the piezo. It can be seen that the back and front of the model, especially the parts where the piezo is supposed to be wedged, displace in opposite directions. But the net displacement as can be seen in the horizontal cut is towards the center, hence compressing the piezo. This once again confirms the notion that bending of the cell will compress the piezo. However since the surface touching the piezo is not evenly compressing it, and some surface areas are even extending it, the stack will experience torque, which is bad for the piezo. The displacement itself is small but it is in the micrometer range which is perfect for piezos. The average displacement of the surfaces the piezo stack is supposed to be attached to is 1.8 microns, as there are two of them, the total strain compressing the piezo would be 3.6 microns.

Another point of interest are the strain calculations shown in Figure 4.7.

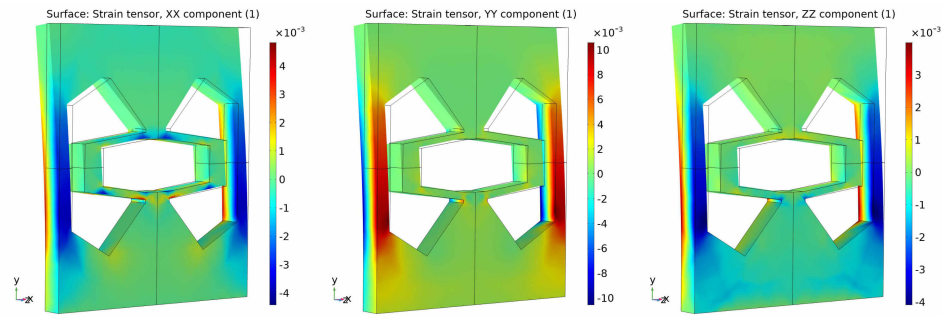


Figure 4.7: Three images showing the strain the x,y, and z-directions

These calculations seem to show that a piezo patch on the surface of the cell will experience much more strain than any equivalent piezo stack in the intended position. The initial idea behind the piezo stack with the amplification mechanism was that the mechanism would decrease the strains on the piezo to the order of microns, while increasing the the strain the piezo generates. The strain on the surface is in the order of magnitude of 10^{-3} , which would make the strains in the order of microns, as the dimensions of the cell are in the order of millimeters. The most relevant dimension for piezo patches is the Y direction where strains are between $5 \cdot 10^{-3}$ and 10^{-2} , as those parts are 20 mm long, this would make the patches stretch by 200 microns. This could be to much.

Piezo FEM

Finally the piezo module was used to analyse the current approach and it confirmed that this approach would not work. A piezo stack was put in and a force of 5 [N] was put in the z direction at the top of the cell. Without the piezo powered on the the displacement of the top of the cell was 1.2666 mm, with the piezo powered and extending $25 \mu m$ as per manufacturer specification the top of the cell moved 1.2597 mm, which is trivial. Figure 4.8 shows the model used for the FEM. The piezo stack is 18 mm long and has a surface $3 \times 3 \text{ mm}$, it extends $25 \mu m$

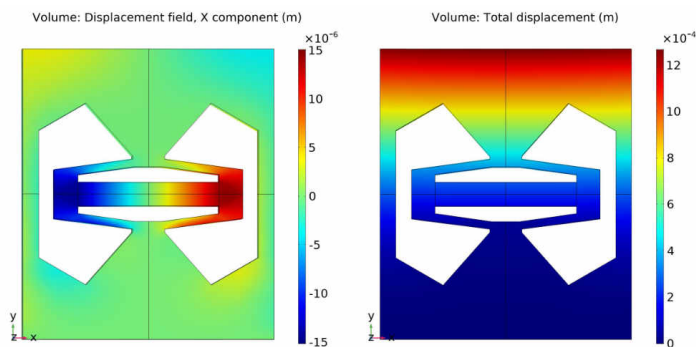


Figure 4.8: Left image shows the displacement in the x direction and the right the displacement in z direction

Since a piezo stack is so much more stiff than a polycarbonate flexure one possible problem envisioned early on would be the transmission of forces. The polycarbonate may not be able to compress the piezo stack, rather it's own body would deform and take up all the forces. Which is something that could still be a problem. However the analysis did not have the stack react against a compression, it worked by just applying a voltage to the piezo stack to have it elongate. Yet the design still did not work. Just to make sure it wasn't due to polycarbonate being much softer than the piezo material, the polycarbonate was replaced by aluminium. The results were pretty much the same. A force of 10 [N] was applied in the z direction at the top of the cell. Which lead to a Z-displacement of 0.26509 mm, when a voltage was applied to the stack it elongated by 17.861 microns, the z-displacement went from 0.26509 mm to 0.26436 mm.

The design itself absorbs too much of the strain applied to it by the piezo stack by deforming in ways not useful to damping the flexure.

The failure of these analysis prompted the research into the damping properties of a single 3d printed flexure as well as two printed pieces glued together using epoxy glue. The results for the single 3d printed flexure and flexure made out of two 3d printed elements glued together using epoxy were summarized in table 3.1 along with all the other materials.

4.4. Design and FEA for patch elements

With 3d printing being usable patch piezos could be integrated. Any initial design and experiment would use commercial patch actuators that can be bought. Two piezo actuators stood out, both having the same dimensions, but one being an extending type (T220-H4BR-1305YE) and the other a bending type (T220-H4BR-1305XB). The initial design and Finite Element Analysis focussed approximating the real world performance of these piezo patch transducer with FEA. Then the analysis proceeded by analysing the performance of the transducers inside a cell and a flexure. This included the amount of displacement they could induce at the end of a cell, the force they could exert and the stiffness they exhibited. Further testing was done by splitting the two layers of the transducers and positioning them on opposite sides of a cell, thereby mimicking two extending and contracting piezo patches of half thickness on both sides of a flexure. And finally a cell was designed with custom designed patch elements which could exert force in three different directions. Two version were made, one with central bender elements and one with split extender piezo patches.

4.4.1. T220-H4BR-1305XB vs Finite Element Analysis

First order of business was to find out how close the finite element analysis comes to performance of the T220-H4BR-1305XB bender actuator and what can be tweaked to make it better, after this the same was done for the T220-H4BR-1305YE extender transducer. The material properties were taken from the company website [44]. The bender actuator consist out of 5 layers. Two piezo layers each 0.19mm thick, one central brass layer 0.13 mm thick and 2 FR4 epoxy layers 0.02mm thick. The piezo and brass layers were modelled with their respective dimensions. The epoxy layers were replaced by a "Thin elastic layer" boundary condition. EPoxy properties were: Young modulus 5.54 GPa, Poisson Ratio 0.32, density 1.4. The exact type of epoxy used in these bender actuators is not know, so the epoxy values were taken from matweb [45]. The young modulus was approximated from the shear modulus 2.1 GPa by the following formula $E = 2G(1+\nu)$, wherein G is Shear Modulus, and ν is poisson ratio.

The specification for the T220-H4BR-1305XB Bender actuator are shown in Figure 4.9

General Specifications

Parameters	Specifications	Parameters	Specifications	Parameters	Specifications
Length (mm.)	31.8	Capacitance (nF)	24	Spring const (N/mm)	2.02
Width (mm.)	12.7	Rated Drive Voltage (+/-V) off of Resonance	60	Max Amplitude (mm)	0.647
Thickness (mm.)	0.51	Free Deflect (+/-mm)	0.25	Response Time (mSec)	0.63
Temperature Range	-60° C to 140° C	Blocked Force (N)	0.28	Resonant Freq (Hz)	350
Mass (grams)	1.6			Max Drive Volts @ Resonance (V)	20.6

Figure 4.9: The specifications for the T220-H4BR-1305XB Bender actuator [38]

Figure 4.10 shows the Finite Element Analysis of the T220-H4BR-1305X as well as where the boundary conditions were applied. As mentioned the bender in the Finite Element Analysis consist out of three layers, the

two piezo layers are coloured blue in the zoomed in section, the central brass layer is yellow. On the top a voltage of 60 V is applied and on the Bottom -60 V, this boundary condition is colored red. A "ground" boundary layer is applied on the interface between the piezo layers and the central brass layer, this is coloured purple. A fixed constraint is applied to one end of the piezo, this boundary condition is indicated by the green colour.

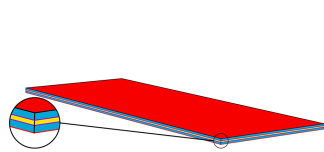


Figure 4.10: The FEA of the T220-H4BR-1305XB Bender actuator. The zoomed in section shows the layer makeup and boundary conditions. Blue is piezo layer, yellow is brass layer. Red top is +60 V boundary condition, red bottom is -60 V boundary condition. Purple is "ground boundary condition, and green is the "fixed constraint boundary condition".

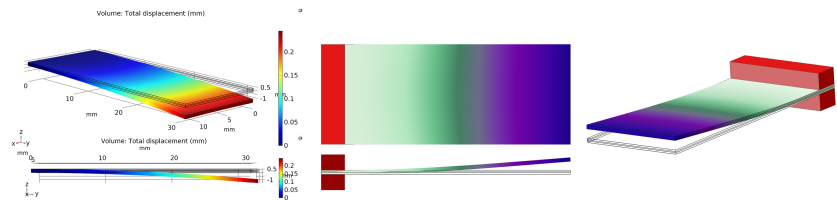


Figure 4.11: Two small blocks measuring 12.7x3x2 mm were added at one end of the piezo actuator. These blocks clamped the piezo actuator and increased the first eigenfrequency to 321 hz.

According to the specification shown in Figure 4.9 the piezo should have a maximum deflection of ± 0.25 mm, in the simulation the deflection is 0.238mm. A difference of 5%, pretty close. The eigenfrequency should be 350 hz, in the Finite Element Analysis this is 265 Hz, this is a difference of 25% which is pretty large. A possible explanation for this large discrepancy could be the boundary conditions. In the FEA the bender is constrained on just one edge at the outer end, it is likely that in real life the piezo was clamped down on one side, a clamp would increase the eigenfrequency. This idea was tested by creating a small clamp. The clamp consisted of two small steel pieces with the dimensions 12.7x3x2 mm clamping the piezo on both sides. The "fixed constraint" boundary condition was removed from the piezo and applied to these two small blocks. The eigenfrequency increased to 321hz. This is shown in Figure 4.11

Analysing the extender was fairly straightforward, as merely reversing the voltage on one of the sides would have the transducer extend instead of bend. Furthermore the voltage needed to be changed as the extender operates at ± 120 V, so not from 0 to 120, but ± 120 V. Doing that yielded an extension/contraction of 0.0035 mm which is 9% more then the official figure of 0.0032mm [42]. A figure of the specification will be omitted here as they are largely the same as for the bender shown in Figure 4.9, the citation should suffice.

4.4.2. Displacement

Cell Displacement

A displacement analysis was done to see how much displacement a piezo could induce inside a cell. The displacement analysis were done by placing the piezo transducers inside a hexagonal model as shown in Figure 4.12, applying voltage to the relevant surfaces, constraining one edge and calculating the average displacement of the opposite side in the z direction. Figure 4.12 also shows the surface in green used for the displacement calculation and the axis of the displacements given by the red arrows.

shown in Figure B.1 in Appendix B.1. The models measurements were derived from the length of the piezo transducer. The thickness of the outside walls and the height of the model were both 2 mm. Two mm was chosen as a 3 mm flexure was not needed any more and a thinner flexure was preferred as it could be driven easier by the piezos. However a flexure that is too thin could give issues when 3d printing. Figure 4.12 shows a cutout of these models look inside a cell.

Three different types of piezo transducers were tested, a bender, an extender, and a split design. All transducers are placed at the center of the cell, looking from the top as shown in Figure 4.12 and the top row of Figure 4.13. Looking from the side, as shown in Figure 4.12 and the middle row of Figure 4.13 the bender is placed at the center, the extender at the top, though it could be placed at the bottom. The split design simply takes the two piezo layers of a normal transducer and puts one at the top and one at the bottom. This design blurs the line between extender and bender, since a single patch can only extend or contract, but they would be driven in such a way so that when one is extending, the other is contracting, this way the flexure itself can be seen as

the substrate of a larger bender.

A voltage of 60 V was used for the bender and split piezo design and a voltage of 120 V was used for the extender design. The reason a voltage of 60 volts was used for the split design is because that is a lower voltage. The 120 V given for the extender design is suspect as the physical dimensions, materials used and construction are almost identical to the bender piezo.

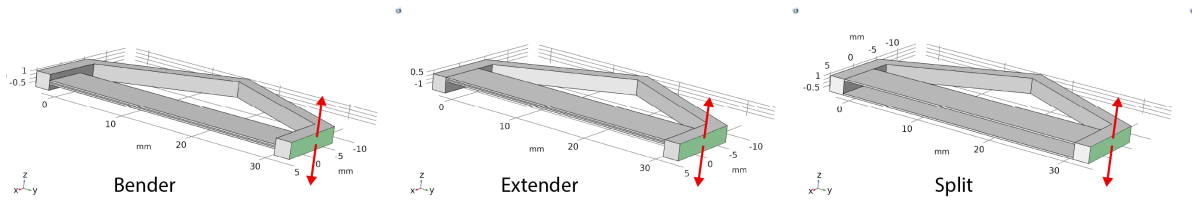


Figure 4.12: Left image shows the bender, middle the extender, right the split(extender/bender). Displacement was calculated for the green surface, the opposite surface was constrained. Red arrows give the axis of rotation.

Figure 4.13 showcases the results of the displacement analysis

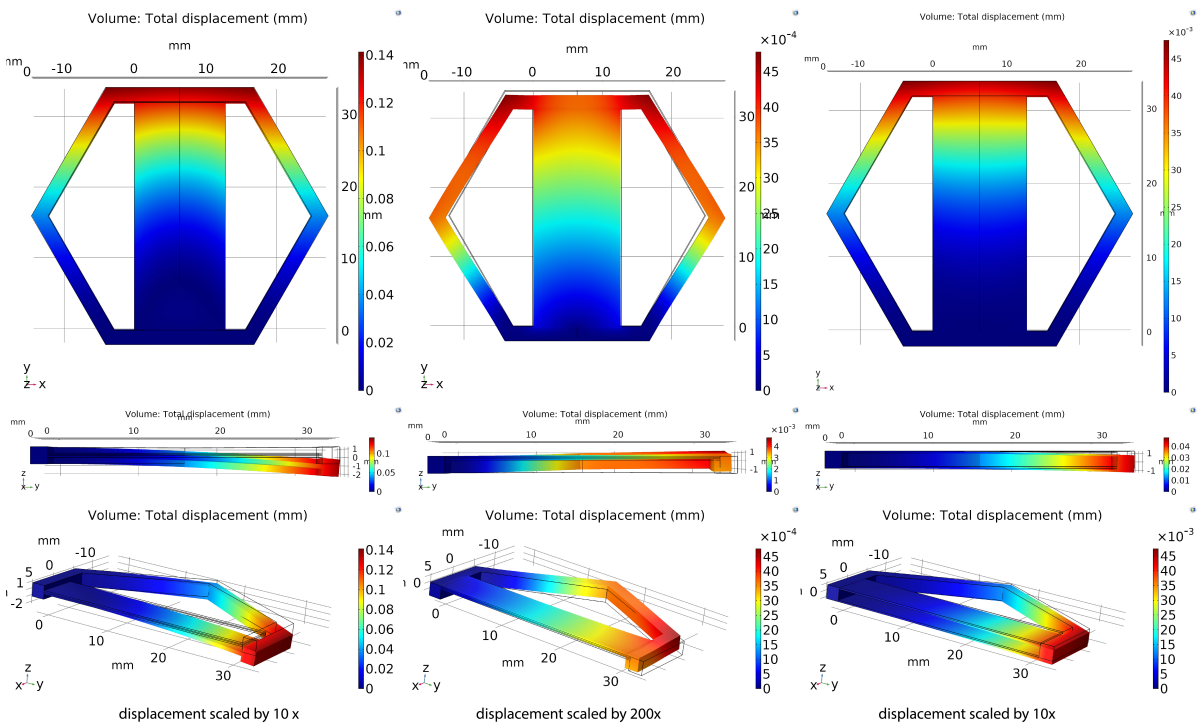


Figure 4.13: Fem Analysis of the models shown in Figure 4.12. Left image shows the bender, middle the extender, right the extender/bender split

As the displacement scaling in Figure 4.13 shows the extender design doesn't work, and it doesn't make sense given the way it is implemented. Later on the designs will be tested within the context of a full flexure where it will make much more sense. The analysis was included for completeness sake. Table 4.2 shows the results in mm. The bender design provides the most displacement, with the split design providing 3 times less displacement and the extender 66 times less displacement.

Table 4.2: Table shows the displacement in the z direction of the three different cell designs.

	Bender	Extender	Split
dz(mm)	0.1384	0.0020935	0.045924

4.4.3. Flexure displacement

Two separate flexure tests were done, one were the piezo without the hexagonal cell were placed in a flexure. And a second test where the piezos were kept inside the hexagonal cell and the cell was integrated in a flexure.

In the previous tests the bender actuator provided the most displacement, but given it's location at the center of the bending axis it should be able to exert the least amount of force. As a flexure is stiffer then a hollow hexagonal cell more force is needed to bend it. Therefore placing the piezos in a solid flexure might give the extender and split piezo design an advantage, as those design should be able to exercise more force. A longer flexure should also displace more at the outer end for the same bend angle, but at the same time it is stiffer, so harder to bend, and thus the piezo will induce a lower angle. It is interesting to see what the end result will be. The models, the placement of the piezo transducers and the results of the FEA are shown in Figure 4.14. The area the displacement was calculated for is coloured green, and the red arrows show the axis of displacement. The voltage used for the extender was 60 V for the sake of simplicity, and because the value of ± 120 is suspect, again that is ± 120 , not from 0 to 120 V as maybe expected. As mentioned before the construction, materials and dimensions are the same as for the bender.

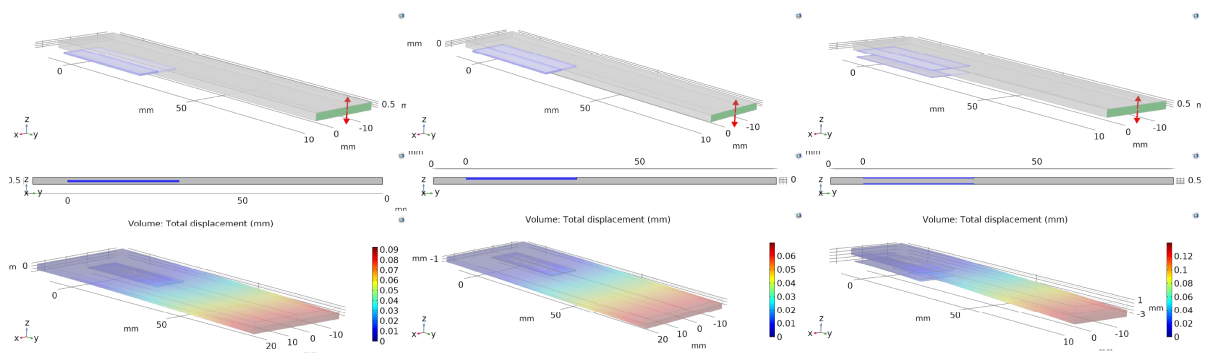


Figure 4.14: Left image shows the bender, middle the extender, right the extender/bender split

Table 4.3 shows the results in mm.

Table 4.3: Table shows the displacement in the z direction of the three different piezo transducer placements and designs

	Bender	Extender	Split
dz(mm)	0.092227	0.069522	0.13953

The results in Table 4.3 show that the displacement induced by the bender has decreased to 0.67 of what it was for the single cell, the displacement induced by extender has increased by 33 times, despite this the extender still produces .75 times the displacement of the bender. Though at 120 V the extender design would probably show greater displacement. The displacement of the split design has increased by 3 times, and now produces more displacement then the bender design, about 1.5 times as much. This means that the displacement that is produced by the piezo elements in a split design is more efficiently transferred to the flexure and it should be the best in damping in this context with this size flexure. This shows the importance of designing a cell within the context of a whole flexure.

A parametric sweep was done with the width and length independent of each other to research the effects of these dimensions on the behaviour of a flexure with a specific cell type. The expectation is that increasing the width will decrease the calculated displacements as it makes the flexure stiffer, while increasing the length will increase the calculated displacements as increasing the length does not make the flexure stiffer, but it does increase the distance the endpoint moves for the same bending. Figure 4.15 shows beginning and end states for both of the length sweeps as well as the width sweeps. The setup was otherwise identical to the previous analysis with the same surfaces being used to calculate the displacement. Figure 4.16 shows a graph of the results.

The overall behaviour falls within expectations. The simple displacement study showed the extender displacement improved by 33 times over its performance in a single hollow cell, the bender did worse than in a single cell, but still better in absolute terms, and the split design improved by over 3 times. The sweep shows how the differences developed over different dimensional scales.

The added stiffness of the piezo material did not offset the amplification advantage the bender has over the extender design, even when increasing the width and adding more stiffness. From the figures it is also clear that the split design displacement increases the fastest with the flexure length. This increase, or the slope of the line is essentially the angle of bending that the piezo induces, and length will amplify the difference caused by difference in angles.

The width has an inverse relationship with the displacement, the expectation was that the relationship would be linear, as the second moment of area increases linearly with the width. But the graphs show a non-linear relationship. The lines seem to be moving towards an asymptote, which is presumably zero. The Extender is decreasing the least amount. The lines may even cross each other for some higher width. But this sweep only went up to lengths and widths which a future flexure could reasonably have.

The conclusions from this is that the split design is the best, followed by the bender design.

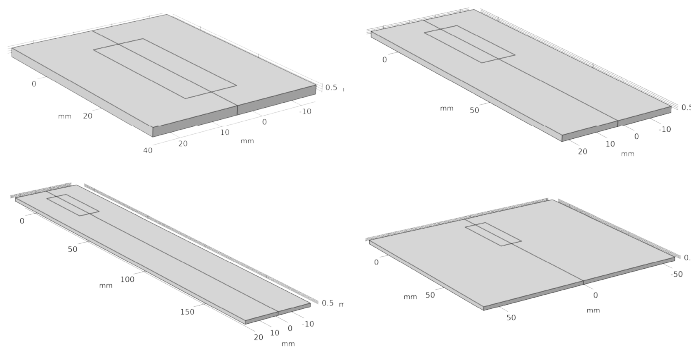


Figure 4.15: Left image shows the length sweep starting from a length of 50mm and going up to 200mm. Right shows the sweep for the width starting from 40 mm and going up to 115 mm.

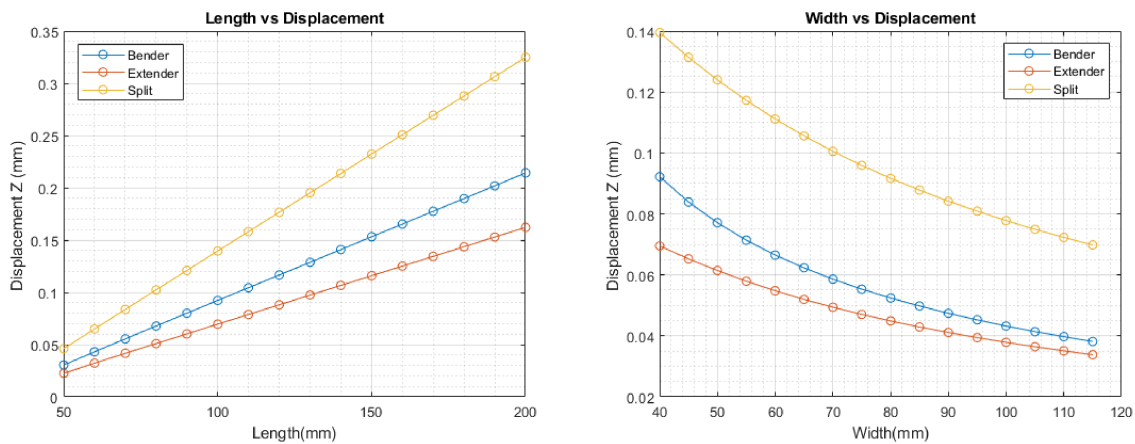


Figure 4.16: Left image shows the graph for the "Length vs Displacement", and the right shows the graph for the "Width vs Displacement" calculated by the sweep.

Table 4.4 shows the numeric results of the sweep in mm. This was data used to make the graphs of Figure 4.16.

Table 4.4: Table shows the numeric values used to make the graphs in Figure 4.16. Left shows the values for the "Length" sweep and the right shows the values for the "Width" sweep.

	Length(mm)	Bender	Extender	Split
Displacement Z-direction (mm)	50	0.030	0.022	0.046
	60	0.043	0.032	0.065
	70	0.055	0.042	0.084
	80	0.068	0.051	0.102
	90	0.080	0.060	0.121
	100	0.092	0.070	0.140
	110	0.104	0.079	0.158
	120	0.117	0.088	0.177
	130	0.129	0.097	0.195
	140	0.141	0.107	0.214
	150	0.153	0.116	0.232
	160	0.165	0.125	0.251
	170	0.178	0.134	0.269
180	0.190	0.144	0.288	
190	0.202	0.153	0.306	
200	0.214	0.162	0.325	

	Width(mm)	Bender	Extender	Split
Displacement Z-direction (mm)	40	0.092	0.070	0.140
	45	0.084	0.065	0.131
	50	0.077	0.061	0.124
	55	0.071	0.058	0.117
	60	0.067	0.055	0.111
	65	0.062	0.052	0.106
	70	0.059	0.049	0.101
	75	0.055	0.047	0.096
	80	0.052	0.045	0.092
	85	0.050	0.043	0.088
	90	0.047	0.041	0.084
	95	0.045	0.039	0.081
	100	0.043	0.038	0.078
	105	0.041	0.036	0.075
	110	0.040	0.035	0.072
115	0.038	0.034	0.070	

4.4.4. Second Flexure test

So now we do the same sweep test but with the piezo inside the cells. The expectation is that that the extender will do better here as well, it is now pulling on the top side of a flexure and has a longer arm them the bender, thus it can exert more force. But the longer arm, also means lower amplification of the bending. The sweep parameters are the same. Figure 4.17 shows the starting and ending sizes.

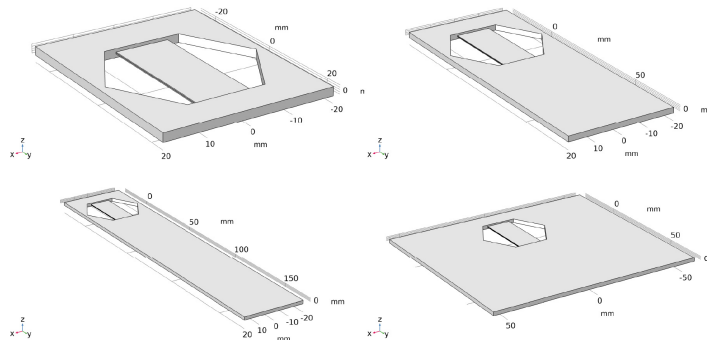


Figure 4.17: Left image shows the length sweep starting from a length of 50mm and going up to 200mm. Right shows the sweep for the width starting from 40 mm and going up to 115 mm.

Figure 4.18 shows the results, and Table 4.5 shows the numeric results of the sweep in mm used to make the Figure Figure 4.18.

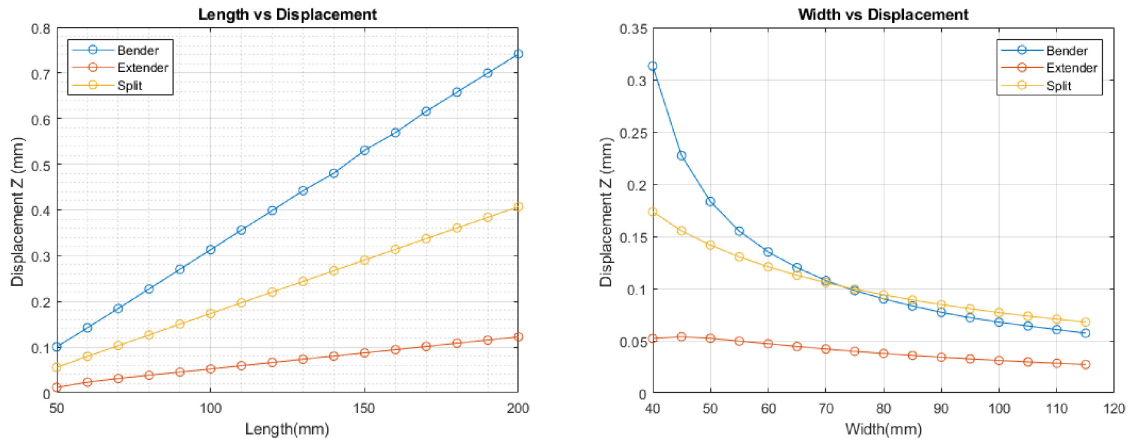


Figure 4.18: Left image shows the graph for the "Length vs Displacement", and the right shows the graph for the "Width vs Displacement" calculated by the sweep.

Using the cell design things have changed once again. When it comes to the length sweep the bender performs the best again, followed by the split design and then lastly extender. But the width sweep shows the bender initially starting strong but being overtaken by the split at a width of 75 mm. The extender design seems to produce better displacement at 45 mm than 40. This is probably a mistake in the FEA. But it also has the least steep curve. Meaning it is less affected by the width increasing. All the FEA were rerun several times to check if the results were correct.

Table 4.5: Table shows the numeric values used to make the graphs in Figure 4.16. Left shows the values for the "Length" sweep and the right shows the values for the "Width" sweep.

	Length(mm)	Bender	Extender	Split
Displacement Z-direction (mm)	50	0.100	0.012	0.056
	60	0.142	0.023	0.080
	70	0.185	0.031	0.103
	80	0.227	0.038	0.127
	90	0.270	0.045	0.150
	100	0.313	0.052	0.173
	110	0.356	0.059	0.197
	120	0.399	0.066	0.220
	130	0.442	0.073	0.244
	140	0.480	0.080	0.267
	150	0.531	0.087	0.290
	160	0.569	0.094	0.314
	170	0.616	0.101	0.337
	180	0.658	0.108	0.361
190	0.700	0.115	0.384	
200	0.741	0.122	0.407	

	Width(mm)	Bender	Extender	Split
Displacement Z-direction (mm)	40	0.313	0.052	0.173
	45	0.227	0.054	0.155
	50	0.183	0.052	0.142
	55	0.155	0.050	0.130
	60	0.135	0.047	0.121
	65	0.120	0.045	0.113
	70	0.108	0.042	0.106
	75	0.098	0.040	0.100
	80	0.090	0.038	0.094
	85	0.083	0.036	0.089
	90	0.077	0.034	0.085
	95	0.072	0.033	0.081
	100	0.068	0.031	0.077
	105	0.064	0.030	0.074
110	0.061	0.028	0.071	
115	0.057	0.027	0.068	

Table 4.6: Table shows the displacement in the z direction at the standard length of the flexures, which is 100x40mm

	Bender	Extender	Split
dz(mm)	0.31307	0.052185	0.17347

Looking at table 4.6 placing the the cells inside flexure did change stuff a bit, and in the way it was expected. The extender design displacement is now 6 times lower then the bender and the displacement for the split is 1.8 times lower. Though placing the piezos in solid flexure helped the extender and split design more. Still the extender performance improved by over 10 times. And the performance of the split design by 1.7 times.

4.4.5. Stiffness & Force

The next analysis involved testing the stiffness of each cell when no voltage is applied. Ideally the cell should not be stiffer than a solid hexagonal cell of the same dimensions made out of the same material as the flexure, PLA in this case. If the cell is less stiff than the solid PLA cell, the flexure as a whole could be made less thick or the cells not containing piezo actuators could have holes to reduce their stiffness.

Due to problems with the FEA, the discretization of the "Solid Mechanics" component had to be increased from quadratic serendipity to cubic serendipity in COMSOL. This means the interpolation of the finite elements is being approximated by a higher order. This makes the simulation more accurate and stable at the expense of increasing the computing time. And the designs had to be simplified. Instead of the bender and actuator piezo transducers being made out of 3 layers with a thin elastic layer in between, the models used for the stiffness testing were made out of 2 layers. Each layer was .51/2 mm (0.255mm) thick. The split design already used only two layers. However earlier those layers were 0.19 mm thick, as that was the thickness of the piezo layers in the bender and extender transducer. But for this test the layer thickness was increased to 0.255 mm to make the test more even. The stiffness test was done by putting a constraint on one side of the piezo and applying a force on an opposite edge. Then calculating the displacement of the surface opposite to the constrained surface. Everything was compared to a solid hexagonal cell of the same dimensions. Figure 4.19 shows this setup. The green surface is the surface that the displacement was calculated for. The blue arrow shows the direction of the force and the blue line on the bottom of the green surface is the line where the load was applied. Figure 4.19 also shows a red line. This was used for force testing and will be described just below.

As mentioned, force testing was done as well, namely the maximum force the piezo could exercise was tested. This was done by using FEA optimization. The standard voltage of 60 V was applied to the bender and split designs, and 60 as well as 120 volts to the extender design. A force was applied on the same edge as for the stiffness test, except the force was varied until the cell exhibited zero displacement. When there is zero displacement the force applied is equal to the force exercised by the piezo. The blue arrow shows the direction of the force, the red arrow shows the direction of the force exercised by the piezos.

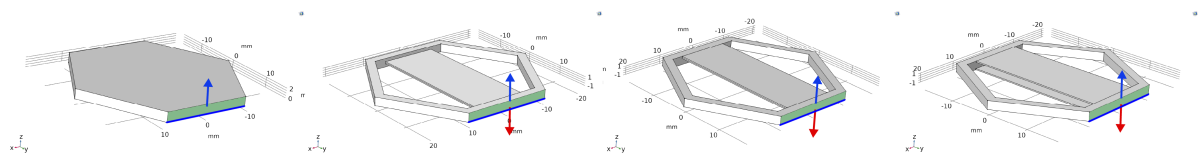


Figure 4.19: From left to right, solid cell, bender, extender, split. Force was applied on the blue line, blue arrows show the force direction. Red lines show the force direction of the piezos. The average displacement was calculated for the green area.

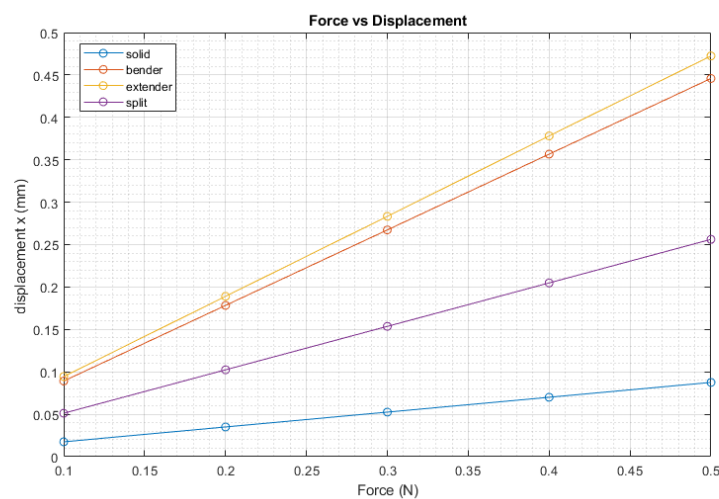


Figure 4.20: Image shows the displacement of the various cells for the force applied.

Table 4.7 shows the calculated stiffness for the different designs in Figure 4.19. It was calculated using the same data that was used for the graph in Figure 4.20

Table 4.7: Table shows the calculated stiffness for the different designs in Figure 4.19

	Solid	Bender	Extender	Split
K(N/m)	5.71E-03	1.12E-03	1.06E-03	1.95E-03

It is clear that all designs are less stiff than a solid 2 mm solid cell. The bender and extender are 5 times less stiff and the split design 2.5 times. The bender and extender should have the same stiffness as they are almost identical, except for the placement. The bender is in the central part of the cell, the extender near the top or bottom. However the FEA was done to confirm this.

Several solutions exist to make the cells equally stiff as the rest of the cells in a flexure. The thickness of the flexure could be reduced. Given that the bending stiffness is proportional to the cube, the flexure thickness could be reduced to roughly .5 its thickness, to make it about as stiff as the bender and extender, or 0.7 times as thick for the split design. Another solution might be to add flexure material to the cell alongside the piezos. In practice this solution will most likely be used as it offers a substrate for the piezos to be attached to. And yet another solution could be to make holes in the flexure. So instead of a solid design a skeletal design could be used resembling something from Figure 3.15. Of course all three solutions can be used to achieve an optimal design.

The result from the force testing are shown in Table 4.8

Table 4.8: Table shows the calculated force the different designs in Figure 4.19 can exert.

	Bender	Extender	Extender 120 V	Split
Force (N)	0.110	0.080	0.197	0.046

The expectation was that the stiffer something was the more force it could exert. As piezo actuators have the same dimensions, structural and material compositions the stiffness they add to a cell is derived from their positions. The same positions which give the cell more stiffness should also give the piezo a larger leverage arm to exert force. As the split design is farther away from the axes of bending it should be able to exert a greater momentum and thus the force it can generate at the measured surface should be higher. These assumptions hold true if we look at the result for the bender, extender and extender at 120 V. The extender is a bit less stiff than the bender and thus it can produce a bit less force, the extender at 120 V has twice the voltage so it should produce more force than the extender at 60 V, and it does by twice as much. But then we look at the result for the split design and see that it can produce a maximum force which is half that of the extender and bender design. This makes little sense as it has an inherent stiffness about 2.5 times that of the bender and extender design and the two piezos have a greater arm. It should take a greater force to displace the outer edge from the neutral position.

4.5. Advanced Cell designs

The following designs are based on the research done in Chapter 3. They are modified designs of the cells shown in Figures 3.10, 3.12, 3.13, 3.14. Figure 4.21 summarizes the research. These cell designs will be referred to as "Advanced Cells/Design" or "Flower Cells/Design", on account of the resemblance to flowers. The conclusion from those sections was that cells where the piezos are aligned with the corners (design b,c,d in Figure 4.21) are slightly better than the designs aligned with the edges (design a in Figure 4.21). This was based on comparing the patterns of force that the flexure in Figure 3.13 were capable of creating, with the strain the different modes produce as shown in Figure 3.9.

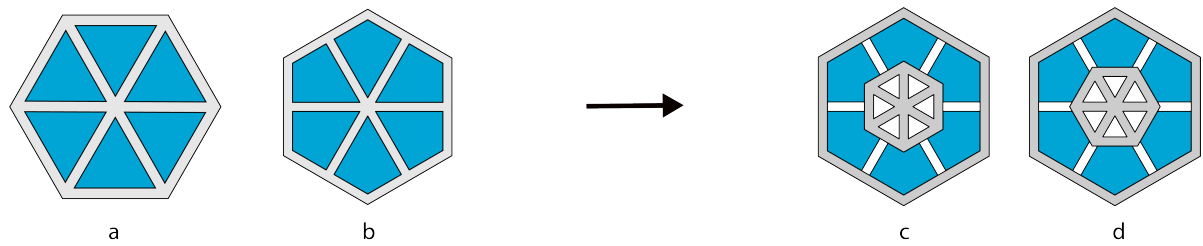


Figure 4.21: Left side shows two advanced designs taken from Figure 3.10, right side shows the better advanced design (b) being optimized further as shown in Figure 3.14

However as at this point the research is purely theoretical the design with the piezo aligned with the edges was chosen as that would allow a better comparison with the previous design based around commercial actuators. Seeing as the extender design is generally inferior, only the bender design and split design will be analysed. The outer dimensions of the cells were the exact same as before. The inner edges of the hexagon are 31.8 mm apart, exactly the same length as before, as that is the length of both the T220-H4BR-1305XB (bender) and T220-H4BR-1305YE (extender) actuators modelled before.

The advanced cells were subjected to the exact same analyses as the designs in the sections before. First a displacement study was done to see how much displacement the cells produced. Then a stiffness analysis was done with no voltage on the piezos, and finally a Force analysis. After the full cell analysis was done, a flexure displacement analysis was performed.

Figure 4.22 shows the setup and FEA results of the displacement study for the advanced cell designs. In Figure 4.22 the left images show the advanced bender, the right images show the split design. Blue line is the line the force was applied to. The blue arrow shows the direction of the applied force. The red arrow shows the force applied by the piezos. The light blue areas indicated which piezos were activated. Though only the top piezos are shown, coloured blue, the bottom piezo were also activated. They had to be to induce bending in the cells. The FEA images show the result of the displacement study where 60 V was applied to the piezo.

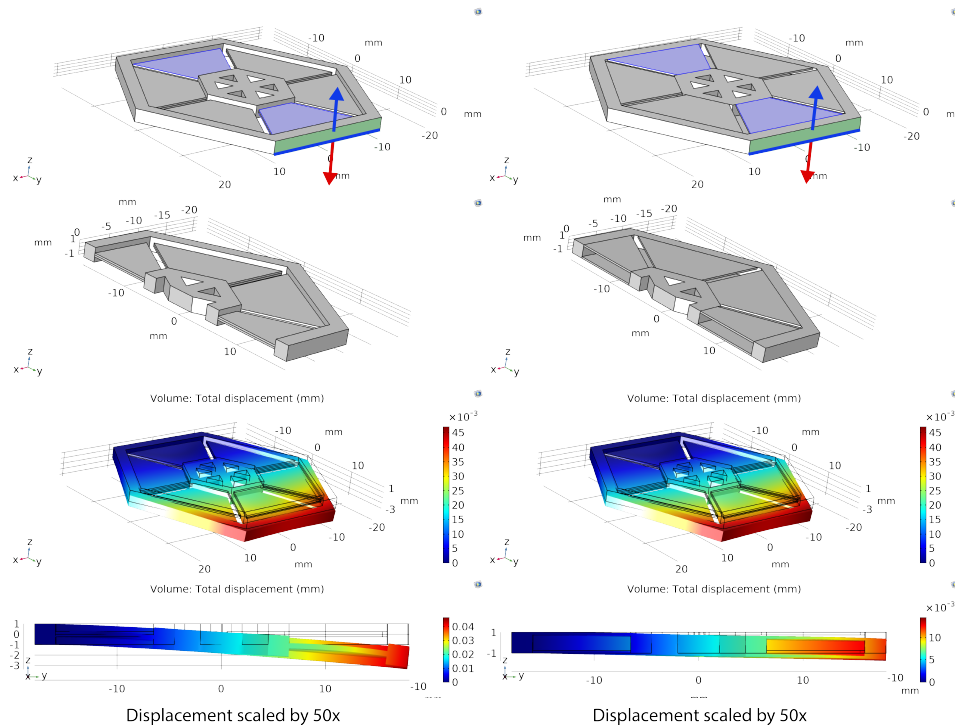


Figure 4.22: Left images show the advanced bender, the right images show the split design. Blue line is the line the force was applied to. The blue arrow shows the direction of the applied force. The red arrow shows the force applied by the piezos. The light blue areas indicated which piezos were activated. Though only the top piezo are shown coloured blue, the bottom piezo were also activated. The FEA images show the result of the displacement study where 60 V was applied to the piezo.

Figure 4.23 shows the results of the stiffness study, and same as before the solid cell is the stiffest as it shows the least amount of displacement when force is applied, followed by the split cell and finally the bender.

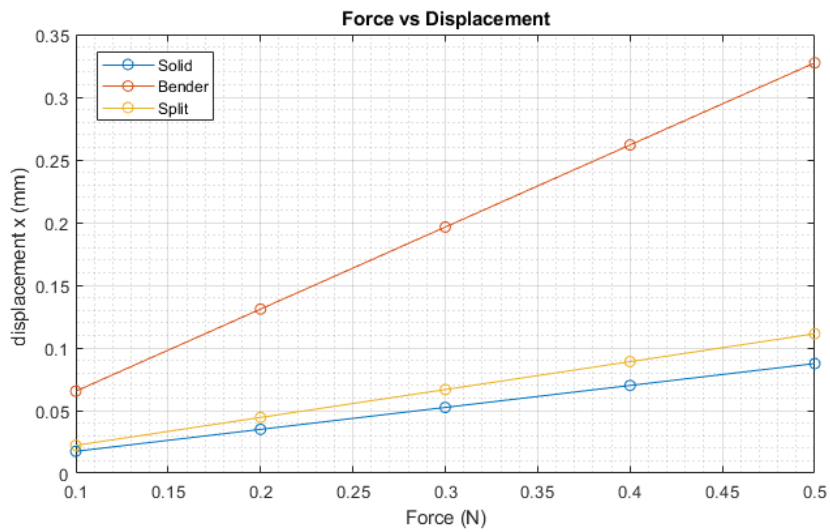


Figure 4.23: the figure shows the displacement of the green edge in Figure 4.22, as force is applied to the blue coloured edge in Figure 4.22.

The middle mini table in table 4.10 shows the numeric results of the analysis mentioned above and shown in Figure 4.23 and Figure 4.24. The displacement is the maximum displacement the cell and piezo combination can produce for 60V. The stiffness is the stiffness of the cell in combination with the piezo elements, but with no voltage on piezo. And the Force is the maximum force the piezos can provide with 60 V applied. The table shows furthermore the earlier results with the basic cells design in the left most mini table. The right most mini table shows the ratio between the results.

Table 4.9: Left table shows the results from the basic dedsigns. Middle table shows the results of the advanced design discussed just above. Right most table shows the ratio of the results.

	Basic Design		Advanced Design		Advanced Design/Basic Design	
	bender	Split	bender	Split	bender	Split
dz(mm)	0.1384	0.04592	0.04450	0.01338	0.32150	0.29142
K(N/m)	0.00112	0.00195	0.00153	0.00449	1.36174	2.30093
F(N)	0.11031	0.04563	0.06531	0.05366	0.59209	1.17615

The results shown in table 4.9 are in line with expectations. The advanced design has more piezos so it should be stiffer. The elements are shorter and less wide. So the piezo cell itself is stiffer and there is less piezo to bend it, so the displacements of the outer ends are smaller. The advanced designs having shorter and narrower piezos should also be able to exert less force. And this is true for the bender piezo, but not for the split design.

The designs were also tested in flexure. Figure 4.24 shows the flexure displacement test. The top row shows how the piezo were embedded in the flexure. The blue coloured piezo are used to induce bending.

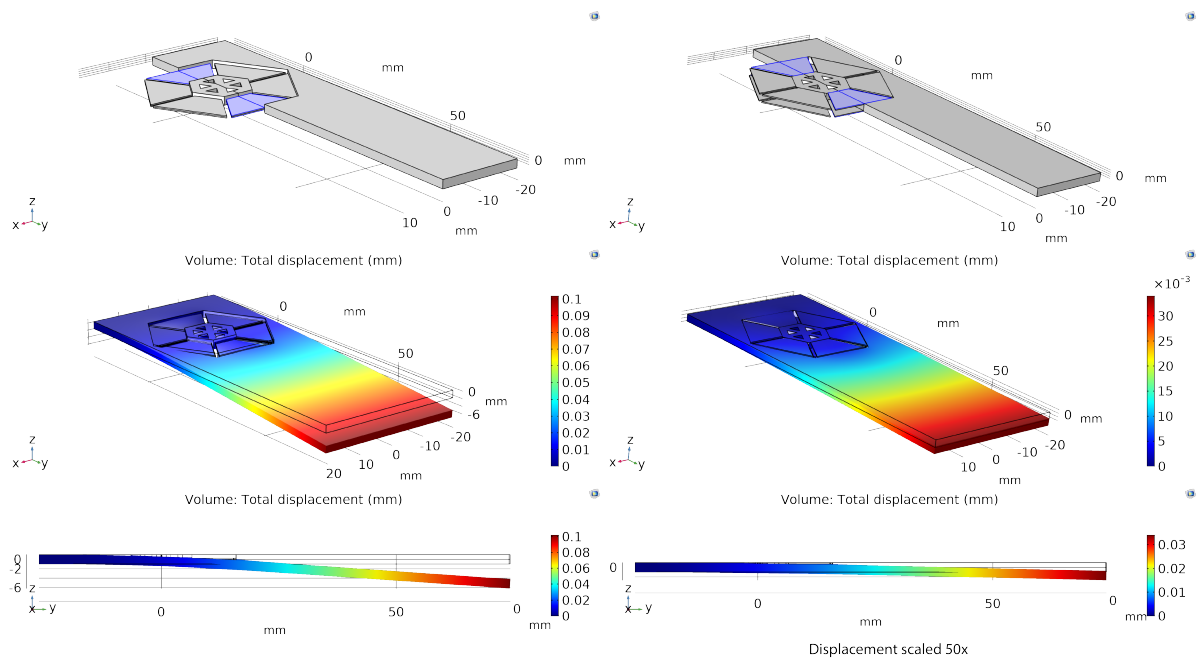


Figure 4.24: The top row shows how the piezo were embedded in the flexure. The blue colored piezos are used to induce bending, middle and bottom row show the results of the FEA.

Just like before, a sweep was performed to see the relationship between the length and width and the displacement. The expectations were to see roughly the same kind of relationship that was seen before between the bender and the split design. Figure 4.25 shows the starting and ending lengths and widths of the sweep.

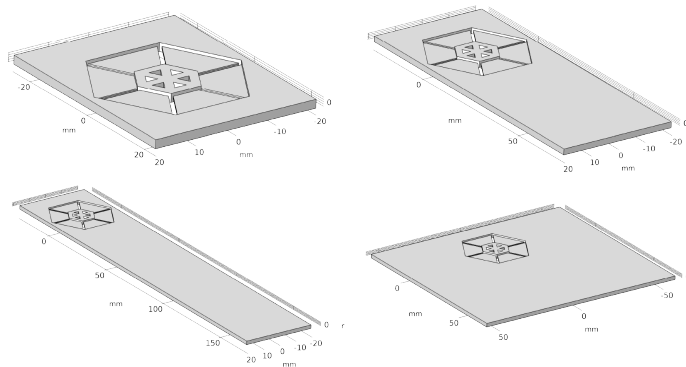


Figure 4.25: Left image shows the length sweep starting from a length of 50mm and going up to 200mm. Right shows the sweep for the width starting from 40 mm and going up to 115 mm.

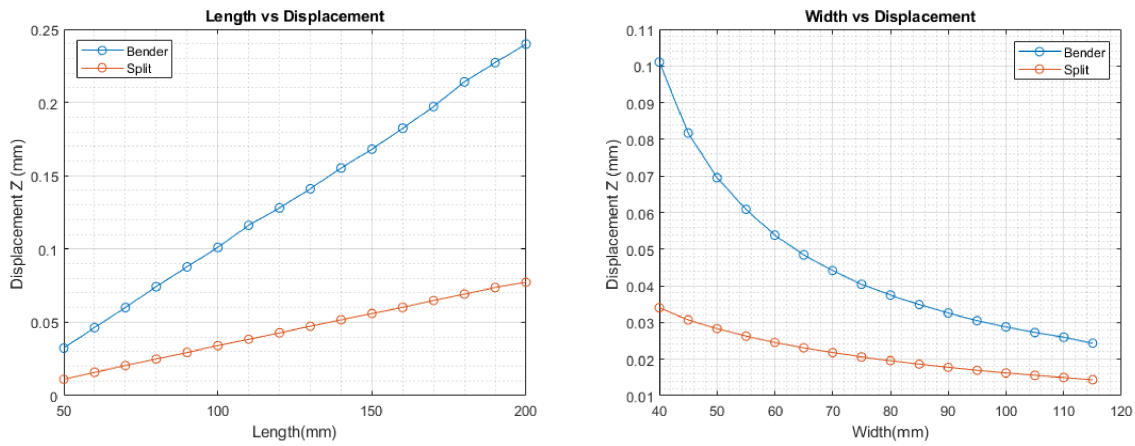


Figure 4.26: Left image shows the graph for the "Length vs Displacement", and the right shows the graph for the "Width vs Displacement" calculated by the sweep.

Table 4.4 shows the numeric results of the sweep in mm. This data was used to make the graphs of Figure 4.26.

Table 4.10: Table shows the numeric values used to make the graphs in Figure 4.16. Left shows the values for the "Length" sweep and the right shows the values for the "Width" sweep.

	Length(mm)	Bender	Split
Displacement Z-direction (mm)	50	0.032	0.011
	60	0.046	0.016
	70	0.060	0.020
	80	0.074	0.025
	90	0.088	0.029
	100	0.101	0.034
	110	0.116	0.038
	120	0.128	0.043
	130	0.141	0.047
	140	0.155	0.052
	150	0.168	0.056
	160	0.182	0.060
	170	0.197	0.065
	180	0.214	0.069
	190	0.227	0.074
	200	0.240	0.077

	Width(mm)	Bender	Split
Displacement Z-direction (mm)	40	0.101	0.034
	45	0.082	0.031
	50	0.070	0.028
	55	0.061	0.026
	60	0.054	0.025
	65	0.048	0.023
	70	0.044	0.022
	75	0.040	0.021
	80	0.037	0.020
	85	0.035	0.019
	90	0.033	0.018
	95	0.031	0.017
	100	0.029	0.016
	105	0.027	0.016
	110	0.026	0.015
	115	0.024	0.014

These results are in line with the sweep results from the basic cell design as shown in Figure 4.18. Both the sweeps with the basic designs and the sweeps for the advanced designs have been plotted in Figure 4.27. The advanced design does have much less displacement. This is expected as the advanced designs use smaller piezo to generate displacement. And the cells are stiffer due to the inactive piezo elements where as in the basic design the rest of the cell is empty. This would mean that the basic design is more suited for places on a flexure where force needs to be directed in only one direction. The results for the width sweep are the most important ones as there the stiffness changes.

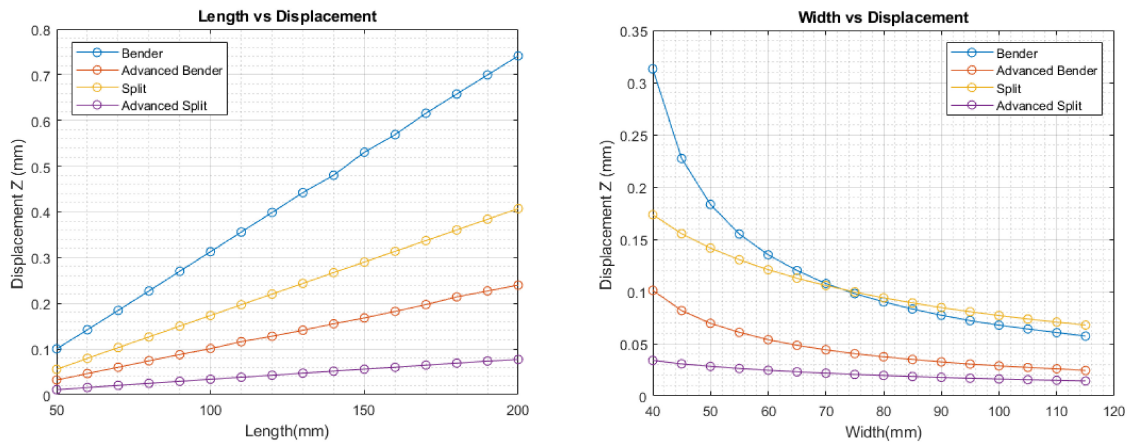


Figure 4.27: Left image shows the graph for the "Length vs Displacement", and the right shows the graph for the "Width vs Displacement" calculated by the sweep. Only this shows the results of both the sweep with the flexures containing normal piezo cells and advanced flower piezo.

4.6. Expectations check

4.6.1. Force at the outer end

One assumption made was that the split design would exert more force as its two piezo layers are farther apart from the bending axis. And that this could be tested by applying a force on the outer ends of a cell while activating the piezo and seeing how much force was needed to make sure the edge the force was applied to did not displace. This was then assumed to be the blocking force of the mechanism. However either the assumption is wrong or the test methodology is wrong. This was tested by using a model previously used to show that the bimorph bending mechanism amplifies less the farther the piezo are apart. The model and setup are shown in Chapter 3 in the section describing the amplification mechanism in Figure 3.23. The current setup and result are shown in Figure 4.28. The voltage and fixed constraint are the same, 60 V, and fixed constraints are applied to the green marked left edges of the model. The blue piezo is expanding and red piezo is contracting. But now a downward force was applied on the corners marked with the purple circles. For every distance between the piezos an optimization algorithm was run to see what the max blocking force was. The distance between the two piezo elements varied between 1 mm and 10 mm.

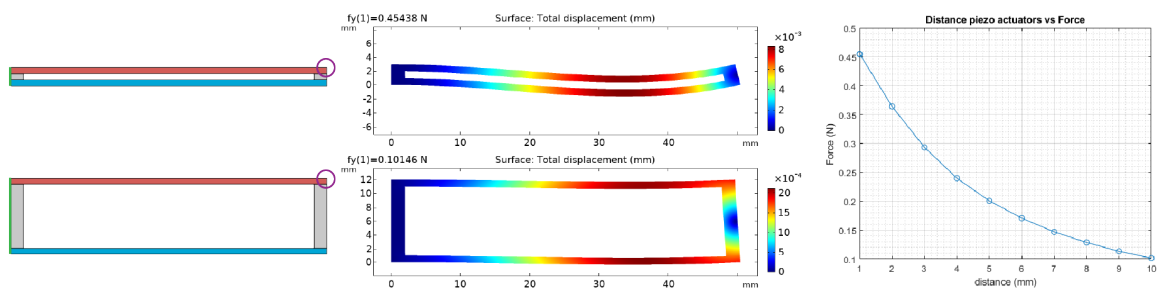


Figure 4.28: Left) Shows the setup and where the fixed constraints are applied. Middle image shows the outer extremes in distance. In the upper middle image the distance between the piezos is 1mm, in the lower middle the distance is 10 mm. A downward force was applied to the corner marked by the purple circle. Right) shows the relationship between the force a piezo can handle and the distance between the piezo actuators.

This Finite Element Analysis confirms what the earlier analysis showed. Namely that my assumptions were wrong. The position of the layers from the bending axis only gives it a bigger arm when exercising force along the axis. Not for a force which is applied perpendicular to the main flexure axis as was done in all the tests up until now.

Still the placement should matter. Consider a design with only a singular piezo element. If this element is placed in the center of a flexure, its extending and contracting will not bend the flexure, if it is placed off center it will start to bend the flexure. The more off center it is the more moment it can exercise on the flexure. As the Flexure bends due to the force along its length, it displaces in the direction perpendicular to its length and exerts force. But the farther away the piezo is from the bending axis, the less amplified the bending will be as was showed by the same model used above in chapter 4 Figure 4.28.

The middle images in Figure 4.28 also show that the distance is not the only thing that is important. While the ends of those models may be relatively close to their starting vertical position, they are also twisted. The thinner one is twisted more. If we imagine a flexure extending from the right edges of the models, the flexure would be pointing upwards.

4.6.2. Bender vs Split

Now we can test what matters more amplification or moment exerted on a flexure. To do this we can do another sweep. One with a bender, where material is added around piezo elements, so they stay close together. And another sweep were the material is added between the piezo elements and they move farther apart as the material is added. This decreases their amplification but increases the force they can exercise. Figure 4.29 shows the setup for the sweep. The top image shows a bender. This bender has 0.02 mm of PLA between the piezo elements. And 0.01 mm of PLA above and below those elements. As the sweep proceeds a total of 0.49 mm of PLA is added above and below. At the end there will be a total of 1 mm PLA added, two times 0.49 plus 0.02 mm that was between the two elements. The red piezo element is contracting and the blue expanding.

The lower image in Figure 4.29 show a split design. This starts with 0.04 mm of PLA between the two piezo elements and 0.96 mm is added to make it a total of 1 mm.

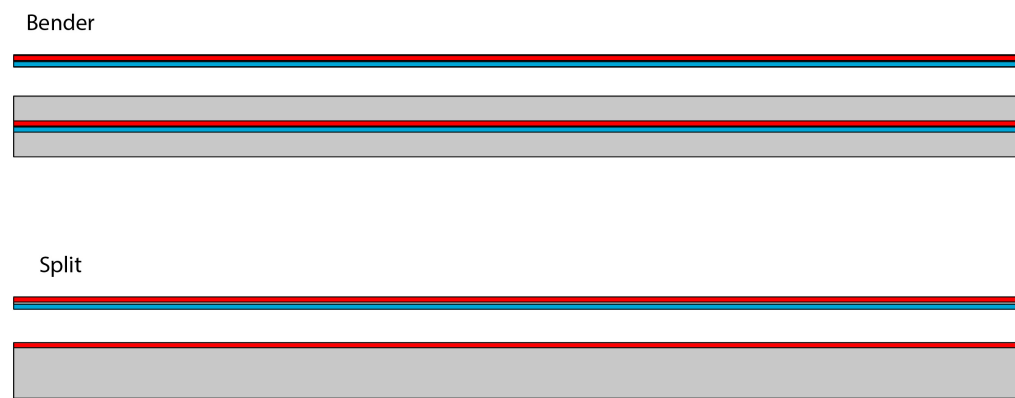


Figure 4.29: Shows the start and end conditions of the sweep. The top bender start with 0.02 mm pla between the layers and 0.01 mm layers above and below the piezo layers. At the end it has 0.49 mm above and below, add to that the 0.02mm layer in between and the piezo go's from 0.04 mm of PLA to a total of 1 mm of PLA. The bottom Split starts with 0.04 mm of PLA and that is increased to 1mm PLA in between.

Figure 4.30 shows the end results.

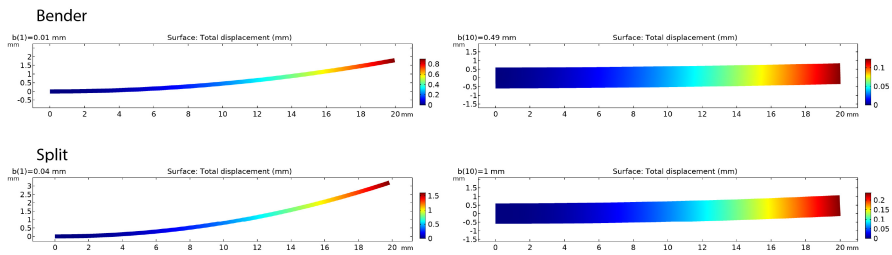


Figure 4.30: Shows the start and end Finite Element Results for the bender and split design of the sweep.

Figure 4.31 plots the results and Table 4.11 shows the numerical values used for the plot.

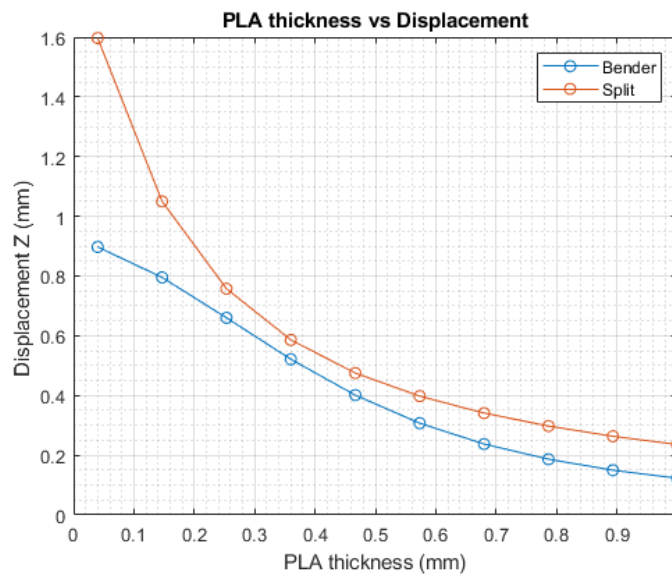


Figure 4.31: Shows The plots for the bender and split design.

Table 4.11: Table shows the numeric values used to make the graphs in Figure 4.31.

	Width(mm)	Bender	Split
Displacement Z-direction (mm)	0.040	0.897	1.597
	0.147	0.795	1.050
	0.253	0.660	0.758
	0.360	0.521	0.586
	0.467	0.401	0.475
	0.573	0.307	0.398
	0.680	0.237	0.341
	0.787	0.187	0.298
	0.893	0.150	0.263
	1.000	0.123	0.236

This result shows that the split design will always do better if it is totally incorporated in PLA material. The expectation was that the bender would be better initially but along the way the split design would generate more displacement. Off course this still maybe the case if we try a different less stiff plastic instead of PLA. But it is good to know that in any design where the piezos are surrounded in PLA, the Split design will always do better. Currently this is not the case, the cell designs have plenty of empty space. And in advanced designs there are inactive piezo elements contributing to the stiffness. So these results will not change the current design, but they should be kept in mind.

4.7. Advanced Real design

The previous advanced designs were made to be compared with the basic designs. The dimensions were dictated by the earlier basic designs. The current advanced design was conceived by considering how one can make the advanced design as easily and quickly as possible. Because the triangular piezo transducers do not need to be constructed from the basic materials. One can also buy a piezo transducer and cut it. The base for the current advanced design is the T220-H4BR-1305XB Bender as it is available and will be tested. Figure 4.32 shows the new designs. The zoomed in front sections show that the piezo construction uses three layers. Top piezo, middle brass, bottom piezo, and a thin elastic layer simulating the bonding material between the piezo and brass. This is the exact same thickness and composition as the real bender the piezo are based on. The zoomed in back sections shows cutout for at the backs where electric connections can be made with the piezos.

Figure 4.33 shows the T220-H4BR-1305XB Bender and the way three piezo triangular pieces can be cut-out from it. This design is fully focussed on actuating, the position for the sensor has not been thought about as at this point it is not known if laser sensors will be used or piezo sensors.

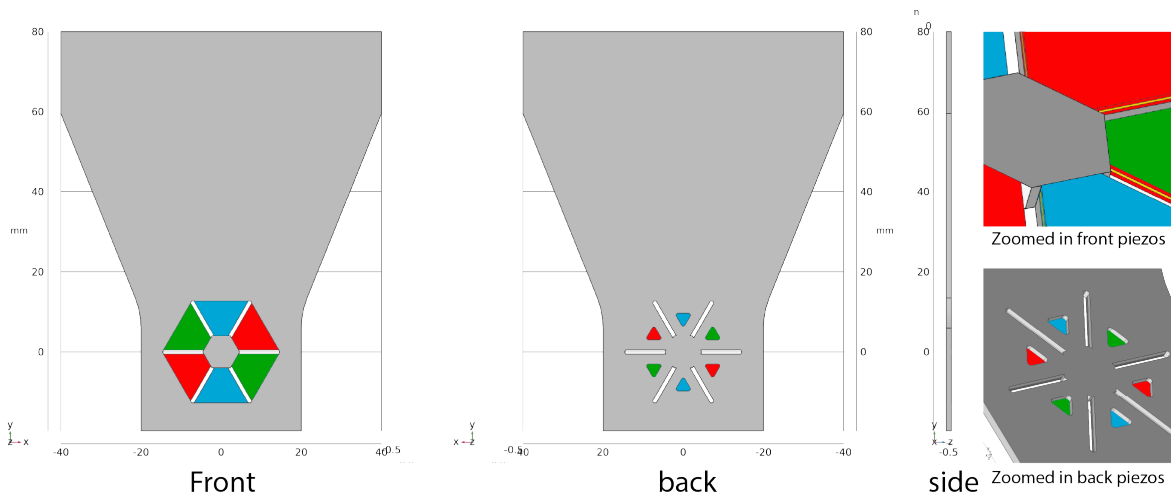


Figure 4.32: Showcases the new design. Blue, red and green are the piezos, grey is PLA. Note the yellow in the zoomed in front image, that is brass

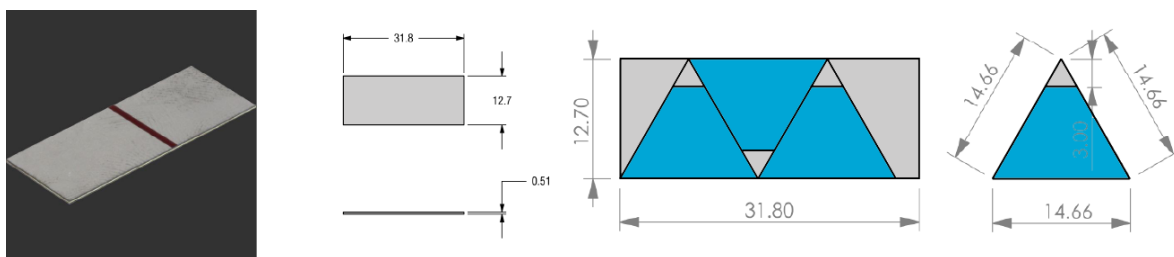


Figure 4.33: Left shows the real piezo bender (T220-H4BR-1305XB). Right shows how the triangular piezo pieces used in the model in Figure 4.32 can be cut. It shows all the relevant dimensions.

Figure 4.34 shows the modes that the piezo cell needs to damp. There are a total of 3 independent piezo pairs, represented by the blue, green and red colours. However the red and green piezo groups need to work together in a symmetrical fashion to damp the second torsional mode.

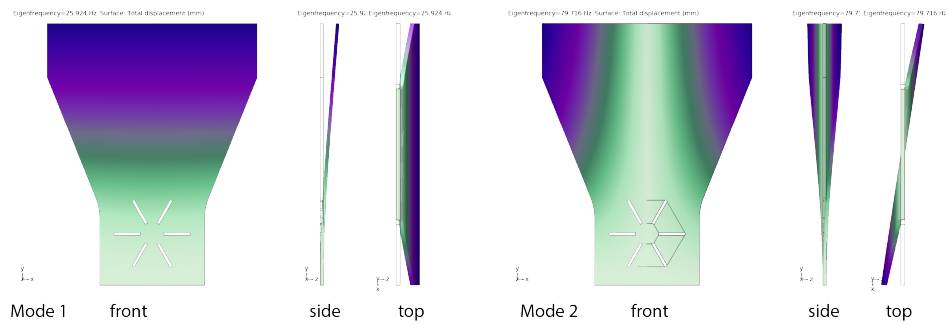


Figure 4.34: Shows the modes that need to be damped. Left shows mode 1, which is the bendy mode. This one can be damped by the vertical piezoss (blue). Right shows mode 2 which is the torsional mode. This mode can be damped by the rotated piezos(red and green).

Finite Element Analysis has been done on this model to see if activating different piezo produces different modes. Two displacement studies have been done. One with only the blue piezo activated, and one with the red and green piezo activated, but not the blue. Figure 4.35 shows the results of the analysis with only the blue piezo activated. It produces nice symmetrical one sided bending. Figure 4.36 shows the results of what happens when the green and red piezo are activated but not the blue. The red and green piezo were made to bend in opposite directions, the hope was to produce a reasonable torsional twisting in the piezo. However as can be seen this is not the case.

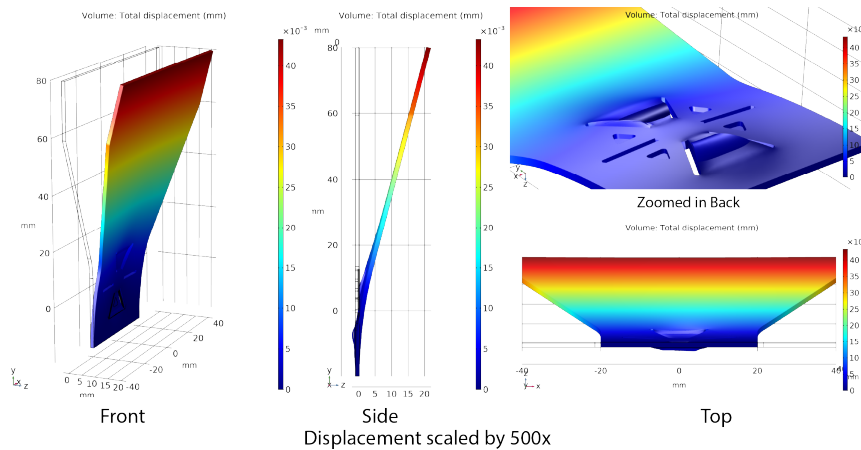


Figure 4.35: Shows the Finite Element Analysis when the blue actuators are activated. The produces symmetrical bending to one side.

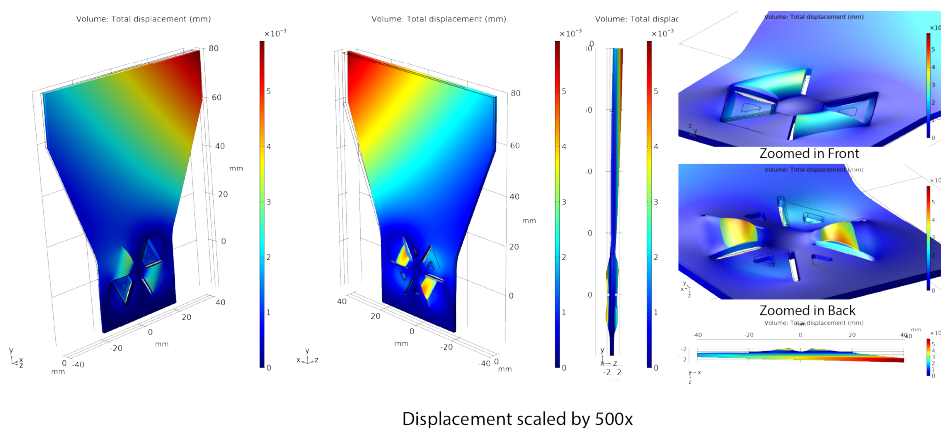


Figure 4.36: Shows the Finite Element Analysis when the red and green actuators are activated. The red and green actuators bend in opposite directions.

The most likely culprit is the asymmetry between the front and back of the flexure at the spot housing the piezos. The piezos are bonded to one half of the flexure by their backside, while their frontside is exposed, there is no flexure material to transfer forces to. The piezos should be connected to flexure material with their front and back in equal manner. This could be solved by having a symmetrical design where two halves of a flexure are printed. One half forming the front of the flexure and the other forming the back. These flexures could be bonded with the piezos sandwiched in between. This would make creating connections and bug fixing those connections harder. So a symmetrical version of was made, the overall thickness was kept the same and same torsional displacement study was done as the one in Figure 4.36. Figure 4.37 shows the new flexure. The flexure is front/back symmetrical and the piezos are sandwiched in between. Figure 4.38 shows the Finite Element Analysis done in this flexure. And this time the piezo create a nice symmetrical torsional flexing in the flexure.

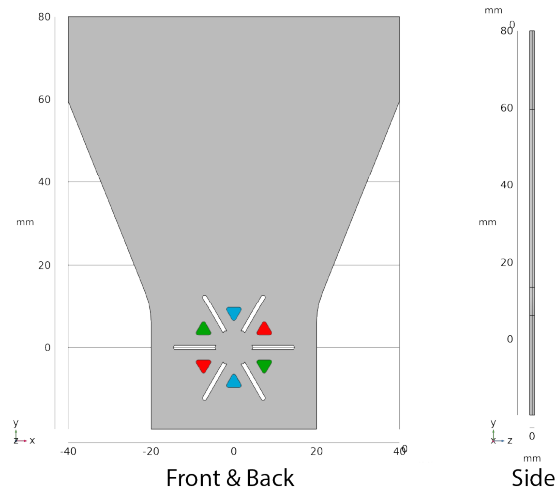


Figure 4.37: Shows The new front back symmetrical flexure. The piezos are sandwiched in between two front back halves. Colors indicated piezos.

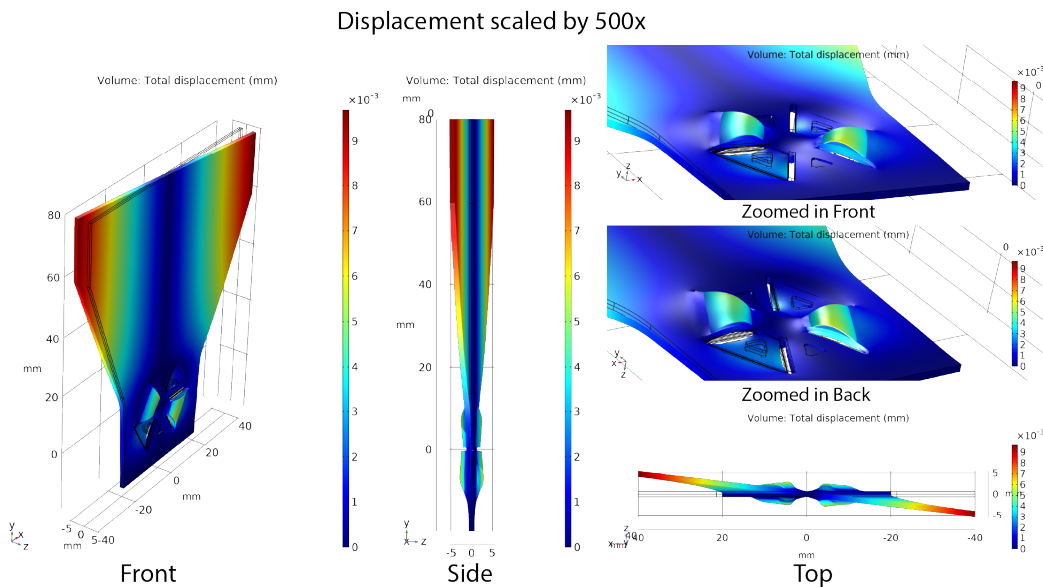


Figure 4.38: Shows the Finite Element Analysis when the red and green actuators are activated. The red and green actuators bend in opposite directions.

4.8. Reflections

Flex-tensional designs. The flex-tensional design was a long shot and proved to unworkable at the current time and at the current scales. Though one can imagine tiny stacks embedded in flex tensional mechanism off the bending axis. This could ensure either complete extensions or compressing. Being that these tiny stacks would have a higher eigenfrequency they could be used to damp higher modes. Also while there is a net compression of the stack in the tested model, it is not even compression across the surface that is being compressed, some parts touching the piezo are extending it, so the piezo will experience torque.

Length & width sweep For the basic design the width sweep showed that after a certain width increase the split design is better. The advanced designs results were similar to the basic design results but the split design never overtook the bender design as the best.

However all those cell designs have a hexagonal cell which is hollow and the piezos only make contact with their outer ends. The sweeps where the piezos were integrated in to flexures showed the split design as being the best. The same is true for the sweep in the expectations check. But these checks did not account for the empty spaces and inactive piezo elements as is the case in advanced designs.

In general extra flexure material adds stiffness and at some point the extra force the split design can exert exceeds the advantage in amplification the bender design has. In any real flexure the cells would have a flexure substrate to bind the piezos at the topside or bottom side and not just out ends. Depending on how much material is added the split or bender may be better.

Wrong expectations The Split design was expected to generate more force then the bender design, as the piezos of the split design are located farther from the axis of bending and the force they exert has a longer arm. But this proved to be wrong, and the extra FEA proved it.

Symmetrical flexures. The last Finite Element Analysis shows the importance of symmetrical flexures. However these kind of flexure enclosing the piezo need to be more precise, and are harder to make connection and bug fix the connections.

5

Practical Design and Experiments

Having done all of the analysis it is time to use that knowledge to design something that can be tested. Ideally both the bender and split design should be tested. But the split design requires custom cutting and assembly of a working piezo, while the bender design can be bought. So it was decided to go through with the bender design. And only test out the split design if an attempt is made to produce the advanced type of cells as those would need custom actuators anyway. Another advantage of the bender is that connections are easier. The last part of the previous chapter also showed the importance of a design that is symmetrical between the front and back when it comes to damping torsional modes. The piezos should ideally sit in the middle between the front and back of the flexure and their front and backsides should be connected to about the same flexure material. This calls for a closed off design where the piezos are housed inside a flexure. This also has the advantage of protecting the piezos from the environment which was already stated as being one of the advantages of producing flexures with integrated piezo elements. A closed off design might make debugging difficult especially when more complex flexures need to be designed.

5.1. Test Setup

For the sake of completeness and reproducibility all of the non obvious components used for testing will be listed below. Some are standard Thorlab components others are specifically designed and manufactured for this experiment and others are commercially available equipment.

- NI cRIO-9039 CompactRIO Controller[46]
- NI 9201 8 Channel $\pm 10V$ 12-Bit Analog Input [47]
- NI 9264 with DSUB 16 Channel $\pm 10V$ Analog output [48]
- OptoNCDT-1420 Laser Sensor measuring range 10 mm reproducibility of 0.5μ at 2 kHz [18]
- OptoNCDT-1750 Laser Sensor measuring range 2 mm reproducibility of 0.1μ at 2 kHz [49]
- Tektronix TDS 2014 digital oscilloscope[50]
- Custom 3d printed Laser Sensor Holder
- Custom Machined Aluminium Base to hold the flexures
- Delta elektronika ES150 SERIES Power Supply set to 24 V [51]
- Six BD300 Dual-Channel 300V (piezo) Amplifiers from piezo drive operating at 24 V [52]
- Two DT25/M - 25 mm Dovetail Translation Stages, M6 Taps [53]
- 25 mm Optical Construction Rail 300mm[54]
- Two Right-Angle Brackets for 25 mm Rails[55]
- Solid Aluminium Optical Isolation Breadboard [56]
- Lasercut plastic box to encase the test setup

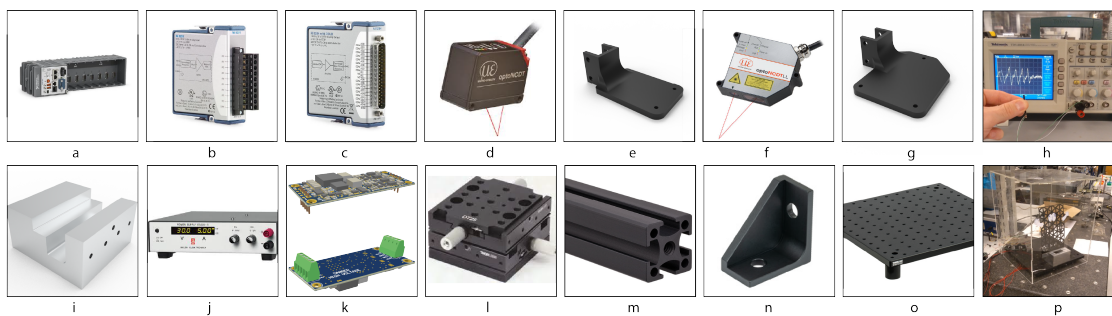


Figure 5.1: a) NI cRIO-9039, b) NI 9201, c) NI 9264, d) OptoNCDT-1420, e) Laser printed sensor holder for OptoNCDT-1420, f) OptoNCDT-1750, g) Laser printed sensor holder for OptoNCDT-1750, h) Tektronix TDS 2014 digital oscilloscope, i) Custom Machined Aluminium Base, j) Power Supply Unit, k) BD300 Dual-Channel 300V piezo Amplifier, l) DT25/M - 25 mm Dovetail Translation Stage, m) 25 mm Optical Construction Rail 300mm, n) Right-Angle Bracket for 25 mm Rails, o) Solid Aluminium Optical Isolation Breadboard, p) Lasercut plastic box to encase the test setup

5.2. BD300 Dual-Channel 300V encasing

The BD300 amplifier comes without an encasing, so a custom encasing was designed and 3d printed. The purpose of the encasing is to protect the amplifier but also people from the electric current generated by the amplifier. Furthermore the encasing needs venting so heat generated by the amplifier during operation can be dissipated. Figure 5.2 shows the amplifier with human fingers for scale. It also shows the design of the encasing. The encasing consists of a 3d printed bottom section that has four round pillars/cylinders. The amplifier has four holes at its edges. The amplifier sits in the bottom sections on top of the thicker pillars, the amplifier does not stick out above the walls of the bottom encasing. The 3d printed top part of the encasing has four holes, these are meant for the four smaller pillars of the bottom encasing. The top sits on the walls of the bottom casing. Some tape can be applied to the sides or some glue on the walls where the two parts meet to keep everything in place, otherwise the friction between the two parts does the job. It is all designed to be a tight fit. Figure C.5 in Appendix C.1 shows the part drawing with all the relevant dimensions.

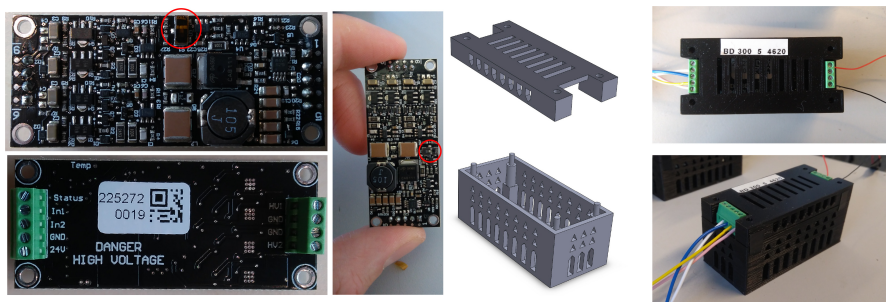


Figure 5.2: Shows the picture of the real life amplifier with fingers for scale. Middle are the top and bottom designs of the encasing. Right) Close up of the real life encasing

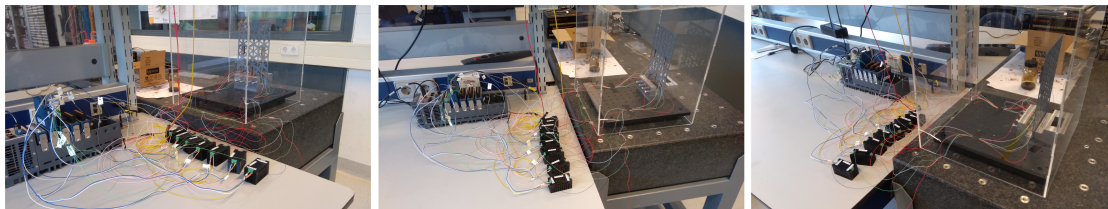


Figure 5.3: Shows how the amplifiers are setup in real life.

The piezo amplifier operated in two wire configuration. Meaning only Output 1 and Output 2 needed to be connected to a piezo. And Channel 2/ was configured to inverting mode by toggling a physical switch on the amplifier itself. This switch is marked by a red circle in Figure 5.3. A full description of using this mode with the piezo transducers used in this thesis is provided by piezodrive[57] and can be seen in Figure C.1 in Appendix C.1, In the same Appendix a closeup of the encasing and the switch that needs to be toggled is shown in Figure C.3.

5.3. Small flexure

In the early part of the testing phase only two bender piezo were available, this was done on purpose as piezo actuators are expensive, costing about 93,- euros per piece. A small flexure was build to test out the following things.

- Actuating
- Piezo recoverability/reusability
- Non adhesive piezo clamping
- Piezo Sensing
- Laser Sensing

The first three points **Actuating**, **Piezo recoverability/reusability**, and **Non adhesive piezo clamping** are interconnected and will be discussed together. Actuating and sensing are core features of damping. Normally piezos are connected through some adhesive to a surface, but that would make recovery much more difficult. The idea is to create a flexure that holds the piezos in place by clamping down on them and containing them in indentations, there would be no bonding material applied to the piezos. One way is to create two halves of a flexure with indentation in both sides to house the piezo and then bond the flexure together using epoxy, but not apply any of it on surfaces touching the piezos. As 3d printing is not that accurate and piezo have very small strains and displacements this could prove to be very inefficient and unworkable so it needed to be tested. By not having the piezo bonded recovery should be easier. But the piezo could still be damaged when opening up the flexure as the stresses applied to the flexure could be transmitted to the piezos.

Piezo sensing & Laser Sensing. For the sensing a few things are important. What modes can be observed. Is the sensor colocated. What is the resolution of the sensor. How fast can it acquire data (speed of acquisition). What are the limits. A mode needs to be observed to be able to damp that mode. Observability in turn is a function of the resolution, speed of acquisition, position and range limits of the sensor used. Piezo and laser sensors are fundamentally different. The Laser sensor measures distance, the piezo sensor measured velocity. Cost wise piezo are much cheaper than a laser sensor and can be colocated with the actuators.

Two piezo actuators Two piezos is the minimum needed to test out a multi piezo design. Having only two piezos makes it more simple to test out, do bug fixing, implement damping control, and with a smaller flexure it makes 3d printing faster. If the piezos cannot be recovered this would only affect two piezos. Having only two identical piezos and a laser sensor makes it so some modes like the torsional modes were not observable. Therefore a longer narrower flexure where the first two modes are bending modes was preferable at this point.

3d print dimensions test Piezos have very small displacements and 3d printed parts are never the exact dimensions specified due to errors and the shrinking of the model when cooling down. So first a couple of small models were printed to test out the dimensions that needed to be used. These were just rectangular 3d printed pieces with rectangular indentations of different dimensions where the piezo actuators could be fitted. Figure 5.4 shows some of these models and Figure C.4 in Appendix C.1 shows all of the models. Figure C.4 in Appendix C.1 will also show a row of models with identical indentations but more material on the sides this was done to test if more surrounding material influences the dimensions of the indentations. Eventually the third model from left with an indentation measuring 32x12.9 mm proved to be the best. So 0.1 mm needed to be added on each side of the piezo. Surrounding material did not make any difference.

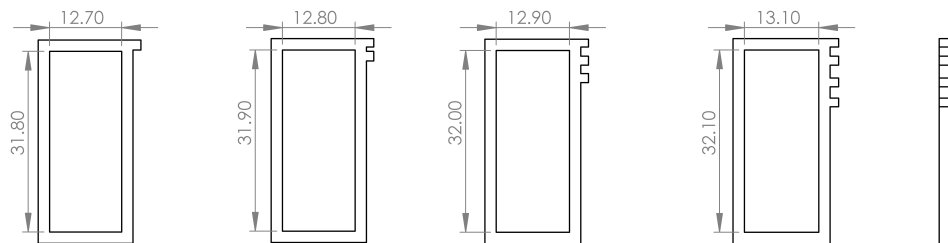


Figure 5.4: Shows the test models, each model has a different amount of "tooth" sticking out on the right upper side, to recognize which model it is. The third model with three teeth proved to be the best. The models on the lower row were used to test if more surrounding material influences the dimensions of the indentations.

Small Flexure The first flexure made that was tested is shown in Figure 5.5. The flexure is made out of two identical parts that are supposed to be clamped on top of another. The two parts are bonded using epoxy. The epoxy used is the UHU quickset[16]. The parts containing the piezos and wires have no epoxy. So the piezos are held in place by the contact of the flexures. This was done to make the recovering the piezo possible or at least easier. It was not known if glued/epoxied piezos could be successfully retrieved without breaking them. Or if any epoxy could be scrubbed off without also scrubbing the thin conducting layers of the actuators. The length of the free part of the flexure is 189 mm, the width is 40 mm and the thickness 2 mm (1 mm for each half). The indentations for the piezos are 32x12.9x.255 mm. The depth is 0.255 mm, no extra depth was designed to compensate for the shrinking of the flexure because there would be a layer of epoxy between the flexure to add to the thickness and it is desirable if the piezo is clamped with some pressure between the two flexure halves. The full dimensions and details of this flexure can be seen in Figure C.6 in Appendix C.1. The bottom of the flexure contains holes. Originally the bottom was meant to be clamped between metal plates held by screws that would go through the flexure. This was changed in the final setup, but the design was left unchanged by accident.

Picture e and f in Figure 5.5 shows the details of the flexure. The red square in "e" shows an indentation meant to accommodate a piece of tape, the green square shows an indentation to accommodate a piece of exposed wire with tape behind it. The blue circle shows a part where the extrusion for the wire gains more depth as the wire extrusion is 0.5 mm deep while the deepest part behind the piezo is 0.55 mm deep.

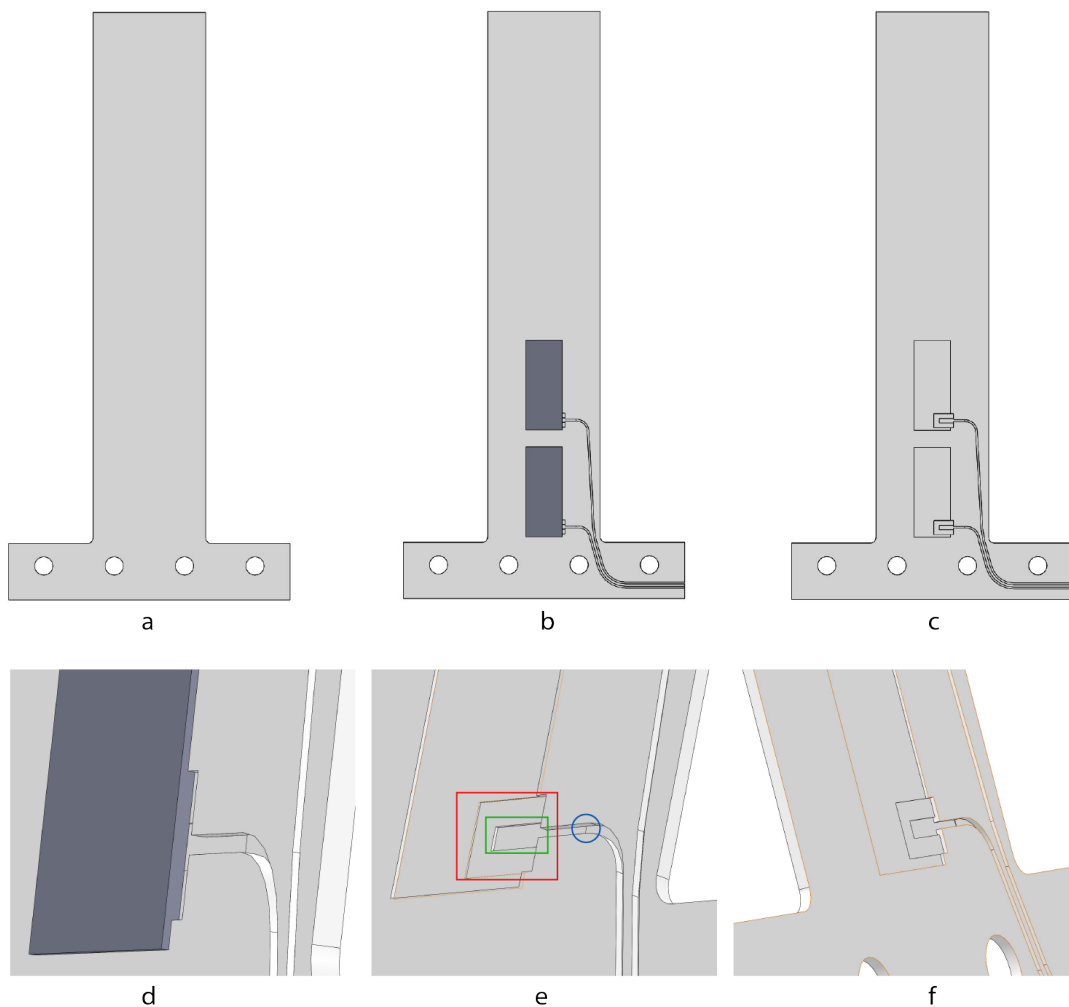


Figure 5.5: Shows the small flexure. a shows the flexure when it is complete and both halves are combined. b shows the one half of the flexure with the piezo inside. c shows one half without the piezo. d is a zoomed in version of b showing how the piezo fits and the small space behind it. e shows how the small space behind the piezo is constructed. f shows the same as e, but from another perspective

The procedure to construct the flexure is as follows. First one half is put on the table facing upwards, then the wires are put in the flexure, this is shown in Figure 5.6 "a" and "b", only in the real procedure the parts that connect to the piezo will have a piece of black tape behind them. Then the piezos are put inside. The piezos apply pressure on the wire and make contact with the tape behind. Some tape is used throughout to hold the wires in place, as can be seen in "c" and "d". The tape holding one of the piezos in place will be removed. The wires are put in the other flexure in the exact same way with the tape in the same positions serving the same purpose. Then epoxy is mixed and applied to all the parts of the flexure around the piezo, but not on the piezo self. The part not containing the piezos is held upside down over the flexure and brought down upon the flexure. A heavy object is placed on top of the two halves and the whole system is left to rest for a couple of hours.

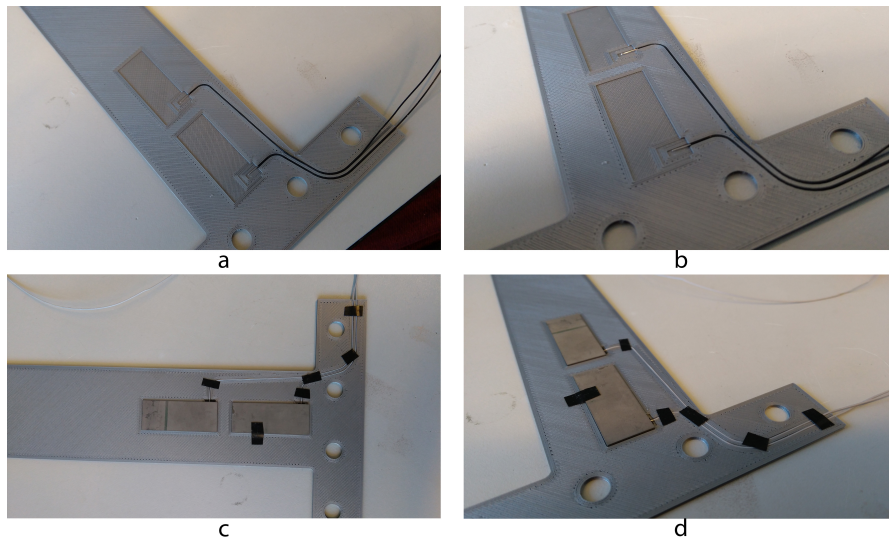


Figure 5.6: Shows the real life flexure and the way piezos and their wires are put inside. Tape is used to hold the wires in place. This is especially important for flexure half that is going to be inverted when it is placed on top of the half that is lying on the table with face up.

Figure 5.7 shows how to open up the flexure. This is done by taking a small blade to the outer end and wedging it in between the two halves, then carefully peeling the flexures apart and retrieving the piezos. This works very well, the piezo are undamaged and fairly clean. Only the glue from the tape has to be removed. The piezo are ready to be used again immediately.

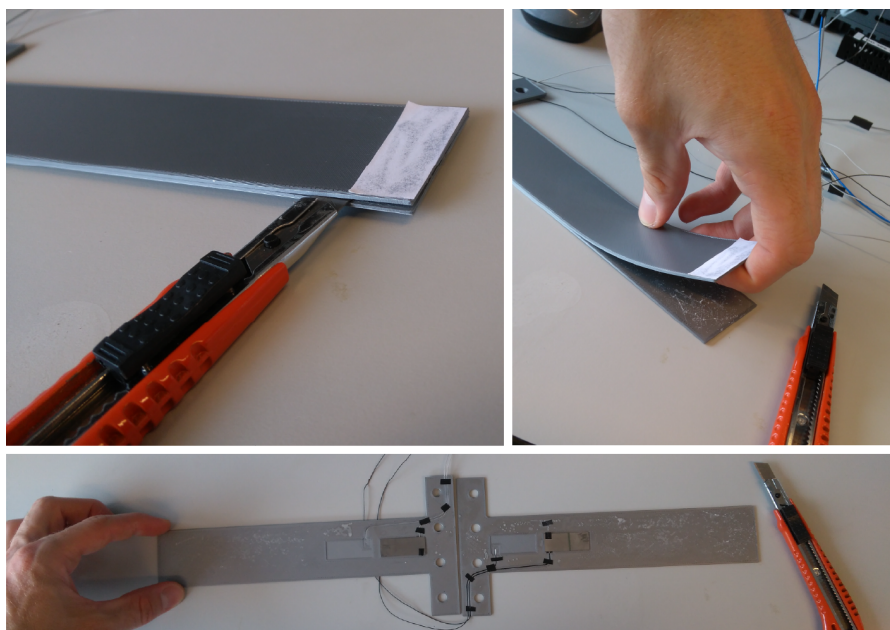


Figure 5.7: Opening up the small flexure and recovering the piezos.

Before opening up the flexure and taking everything apart the damping tests have to be performed. The setup can be seen in Figure 5.8. The flexure can be seen including the OptoNCDT 1750 laser distance sensor, and a small white paper on top of the flexure, this paper can also be seen in Figure 5.7. This paper is used to help the laser sensor. The paper forms a better surface to reflect the laser light. The laser sensor used for these experiments is a different from the one used during the damping tests. This laser distance sensor has a much shorter measuring range, 2mm instead of 10 mm, but better reproducibility at 0.1μ instead of 0.5μ . The laser sensor is connected to a 3d printed part, the dimensions of this part can be found in Figure A.2 in Appendix A.1.



Figure 5.8: Shows the flexure in the experimental setup. Do note the white paper on top of the flexure facing the laser distance sensor (OptoNCDT 1750), the paper is used to aid the laser sensor.

Comsol analysis was done beforehand on a simplified version of this flexure to confirm that the first two modes were bending modes and to see at which frequency they occurred. Figure 5.9 shows the comsol setup. The flexure material was PLA, the piezo material was PZT-5H, the flexure was constrained on the bottom. The first eigenfrequency occurs at 15.6 hz and second at 92.6 hz. This should be possible to observe and damp with the current setup.

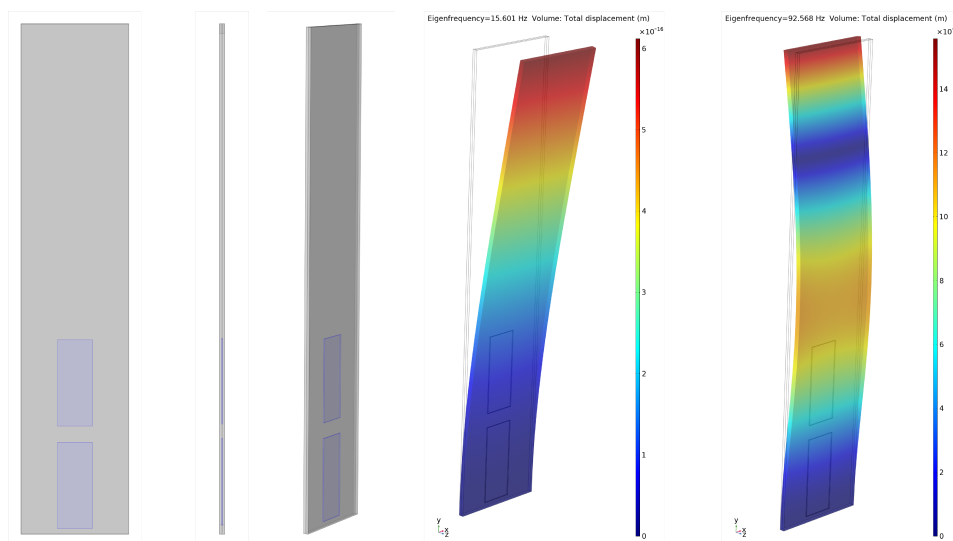


Figure 5.9: Shows the simplified flexure in comsol. and the results of the comsol analysis.

5.3.1. Small Flexure Experiments

Four different sensing experiments were done to test the sensing capabilities of the OptoNCDT 1750 laser distance sensor and the piezos themselves as sensing tools.

1. The flexure was actuated by the bottom piezo and the deflection was measured by the laser sensor.
2. The flexure was actuated by the bottom piezo and the deflection was measured by the top piezo.
3. The flexure was actuated by the top piezo and the deflection was measured by the laser sensor.
4. The flexure was actuated by the top piezo and the deflection was measured by the bottom piezo.

The following Figures show the results of these experiments. Figure 5.10 shows the result from the first experiment and Figure 5.11 from the second. It should be immediately clear that the piezo sensor is much better at sensing the modes in this flexure. One thing to be noted about these bode plots is the difference in axis limits, the bode for the laser sensor go up to 600 hz, the bodes where either of the two piezos was used as a sensor go up to 1100 hz.

The laser can sense the first mode at 15.3 hz, the second at 84.2 hz and the third at 125 hz. The piezo sensor can sense the modes up to 692 hz. Though it is noticeable less capable of sensing the third mode at 125 hz. The other thing to note in Figure 5.11 bode (top piezo is sensing) is the +1 slope at the beginning. This slope is due to the fact that piezos being capacitors act like high pass filters. The lower the capacitance of the piezo the higher the bandpass frequency. Meaning the lower the frequency you want to sense the more capacitance your piezo needs, which given the same material means a bigger sensor. A bigger sensor adds weight and stiffness. But the difference between the laser sensor and piezo sensor is so big that piezo sensors are clearly the way to go. It should also be noted that the FEA was accurate for the first mode, predicting 15.6 hz, but less so for the second mode, predicting 92.6 hz.

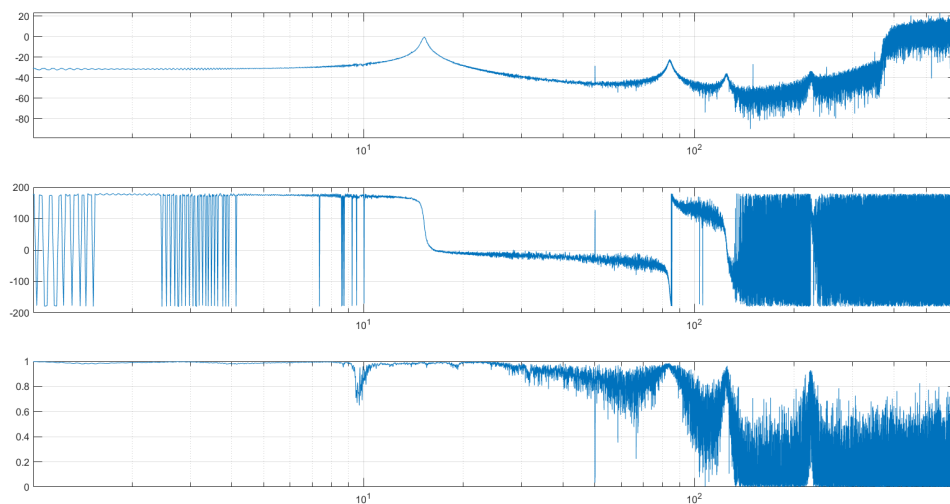


Figure 5.10: Shows the data when the flexure was actuated by the bottom piezo and the deflection was measured by the laser sensor.

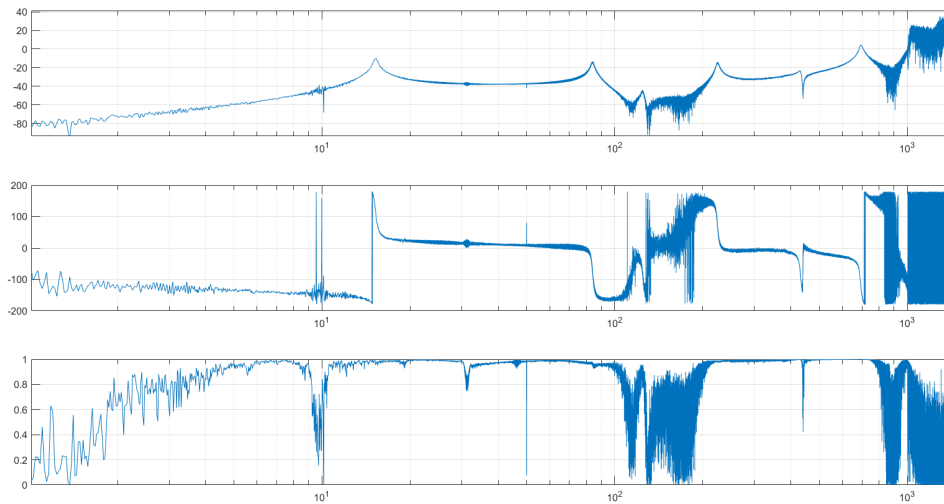


Figure 5.11: Shows the data when the flexure was actuated by the bottom piezo and the deflection was measured by the top piezo.

Figure 5.12 shows the result from the third experiment and Figure 5.13 from the fourth. The situation here is the same as before, the piezo is clearly the better sensor, apart from the +1 slope at the beginning.

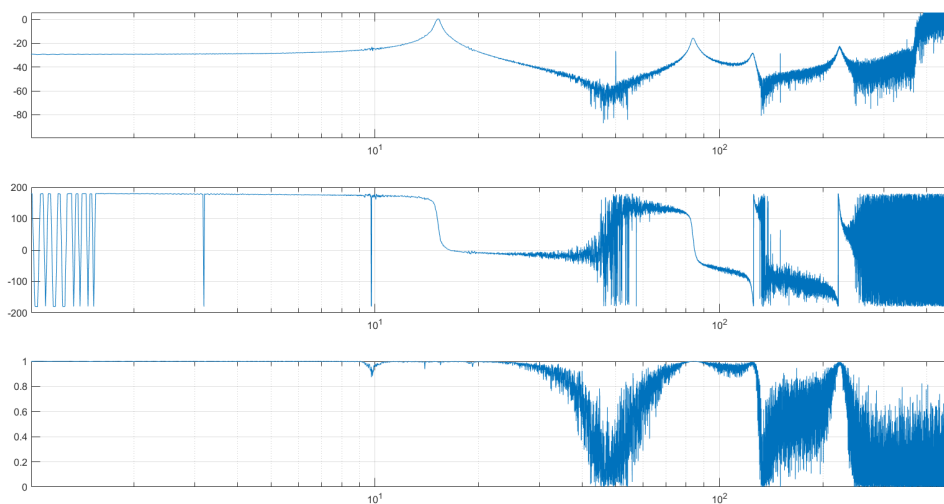


Figure 5.12: Shows the flexure was actuated by the top piezo and the deflection was measured by the laser sensor.

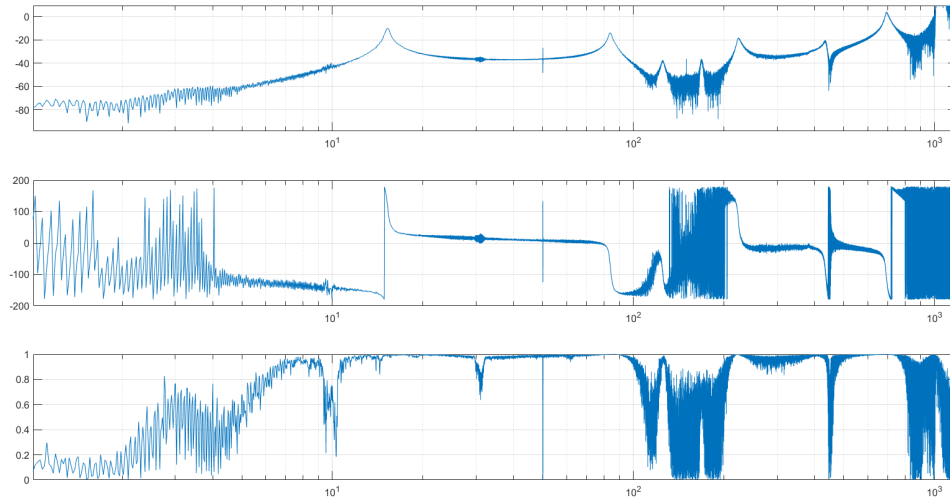


Figure 5.13: Shows the flexure was actuated by the top piezo and the deflection was measured by the bottom piezo.

Despite the shortcomings of the laser sensor it was decided to use the laser as the sensor during damping. As the laser sensor was adequate enough to observe the first two modes at 15.3 hz and 84.2 hz This way the top piezo could be used for damping the second mode. PPF was used to damp the modes. The Matlab file to make the PPF as well as the labview code was created by Niranjana Saikumar, the supervisor during this thesis. The design of the PPF filter was beyond the scope of this thesis. The damping filter just needed to be implemented. Two sets of three different sweeps were done to test the damping. One set had the bottom P1 actuator providing the disturbance and the second set had the top piezo P2 provide the disturbance.

Test 1

1. P1 was used to provide disturbance and P1 was also used to damp mode 1.
2. P1 was used to provide disturbance and P2 was used to damp mode 2.
3. P1 was used to provide disturbance and P1 was used to damp mode 1, while P2 was used to damp mode 2.

The results of these test are shown in Figure 5.14

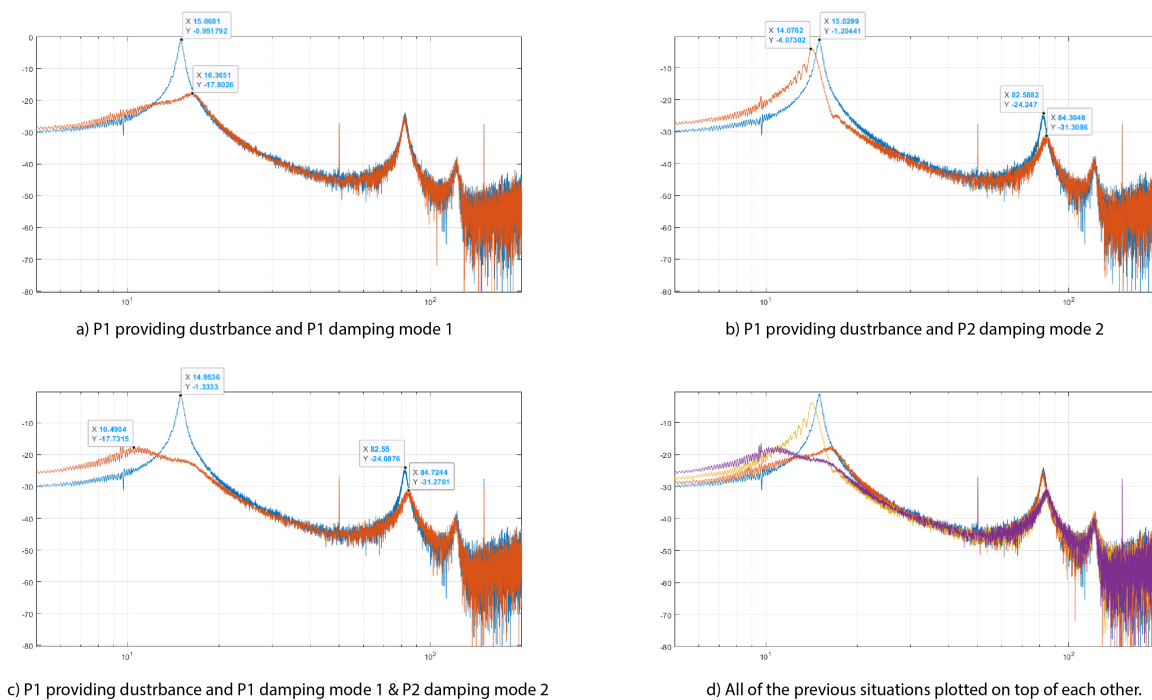


Figure 5.14: Shows the results of the damping. a) P1 provides disturbance and P1 damps mode 1. b) P1 provides disturbance and P2 damps mode 2. c) P1 provides disturbance and P1 damps mode 1 while P2 damps mode 2. d) Shows all of the previous plots together.

The full plots with the phase and coherence can be found in Figures C.7, C.8, C.9, C.10 in Appendix C.1.

The most important data is the one presented in Figure 5.14 c, as it shows the damping when all of piezos are working. The gain for the first mode goes from -1.33 dB to -17.7 dB, that means the first mode gets damped by 85%. The gain for the second mode goes from -24.09 dB to -31.27 dB, that means the second mode gets damped by 56%. Those are some very nice results.

Test 2

1. P2 was used to provide disturbance and P1 was also used to damp mode 1.
2. P2 was used to provide disturbance and P2 was also used to damp mode 2.
3. P2 was used to provide disturbance and P1 was used to damp mode 1, while P2 was used to damp mode 2.

The results of these test are shown in Figure 5.15

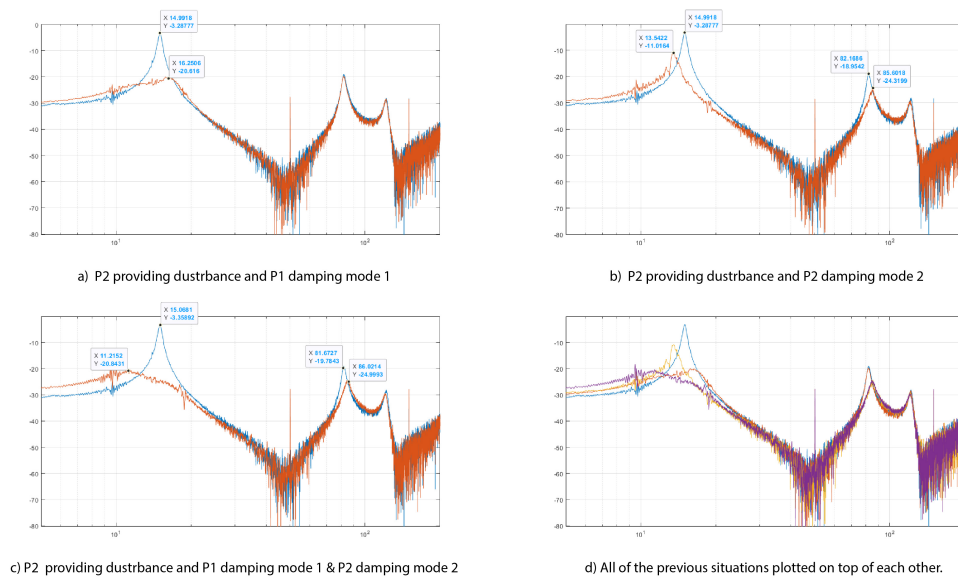


Figure 5.15: Shows the results of the damping. a) P2 provides disturbance and P1 damps mode 1. b) P2 provides disturbance and P2 damps mode 2. c) P2 provides disturbance and P1 damps mode 1 while P2 damps mode 2. d) Shows all of the previous plots together.

The full plots with the phase and coherence can be found in Figures C.11, C.12, C.13, C.14 in Appendix C.1.

The most important data is the one presented in Figure 5.15 c, as it shows the damping when all of piezos are working. The gain for the first mode goes from -3.36 dB to -20.84, that means the first mode gets damped by 87%. The gain for the second mode goes from -19.78 dB to -24.99 dB, that means the second mode gets damped by 45%. Those are some very nice results.

These results show that piezos can be integrated inside a flexure and used to actuate as well as to damp. By the very nature of being inside instead of on the outside some weight is reduced. Namely the weight that would have been taken up by the PLA material where the piezo sits now. The piezo also do not unbalance the flexure as they are located in the center. Due to limitations of 3d printing the stiffness could not be optimized. Ideally the areas above and below the piezo should have some material removed to equalize the stiffness with the rest of the flexure. However when printing such thin flexures at such precisions it is better to leave one side completely flat.

5.4. Octo Flexure

Having showed that piezos inside a flexure work it was time to attempt damping a full sized flexure. This flexure should make use of the hexagonal cellular structure previously researched and be able to damp torsional modes. Furthermore the test from the previous section showed that piezo could sense the vibrations of flexures much more accurately than laser sensors. Ideally a cell containing an actuator would also come with a piezo sensor. This prompted to search for piezo's that could be used as sensors. The main criteria was that the sensors were small and did not create much stiffness themselves and that they were cheap. The piezo actuators chosen for the task of sensing were the BA Series Insulated Piezoelectric Benders from piezodrive. Figure 5.16 shows such a transducer.



Figure 5.16: Shows a bender actuator from the BA Series Insulated Piezoelectric Benders from piezo drive.

The specific transducer chosen to be BA3502 used in this projects is the BA3502, it measures 35x2.5x0.7 mm. It is a very narrow actuator and fairly easy to incorporate in a hexagonal cell containing the T220 bender. It is however 4 mm longer and .2 mm thicker than the T220 actuator. Its main advantage is the price at 4.23 euro's per actuator. A trivial price compared to most other actuators. The biggest disadvantage are the connections. It comes with three connections. For use as a sensor only two are needed, the copper coating of one of the two piezo layers and the central copper layer. The connections are very small and at a predetermined location. The other parts are covered by insulating material. One can scrape this layer off, if one is very careful. However it is very easy to scrape the copper layer underneath. This was found out during testing unfortunately.

The new flexure would be based on the same principles as the small flexure. It would feature two halves that would be bonded together with epoxy without any of the epoxy touching the piezo actuators and sensors. The actuators and sensors would be clamped down and held in place by the side walls and pressure of the two halves squeezing them on each side. This was not a problem with the large actuator that has a large surface area where a wire can be connected. But it would be more tricky with the sensors.

Knowing the dimensions of the two actuators to be used, the T220-H4BR-1305XB as actuator and BA3502 as sensor hexagonal cells were designed and incorporated inside a flexure. Figure 5.17 shows the cells designed and Figure 5.18 shows how these cells are incorporated in a flexure. Looking at Figure 5.18 and Figure 5.17 the names of the cells in Figure 5.17 can be explained. The cell named "Mirror" is located in the left side of flexure half A, while the cell called "Main" is located on the right side. The cell named "Mirror Opposite" is located on the left side of Flexure B and the cell named "Main Opposite" is located on the right side of Flexure A. The full dimensions of the cells can be found in Figure C.18 in Appendix C.1. The part drawings of the cells in the Appendix C.1 will reveal that the indentations for the piezo actuator are not 32x12.9x0.255 mm but 32.10x13.10x0.255 mm. This change was needed as otherwise the piezo would not fit. The fit was especially a problem for the piezos that were placed at an angle. This difference in size between the vertical facing indents and angled indents is most likely due to the way the 3d printer lays down the layers.

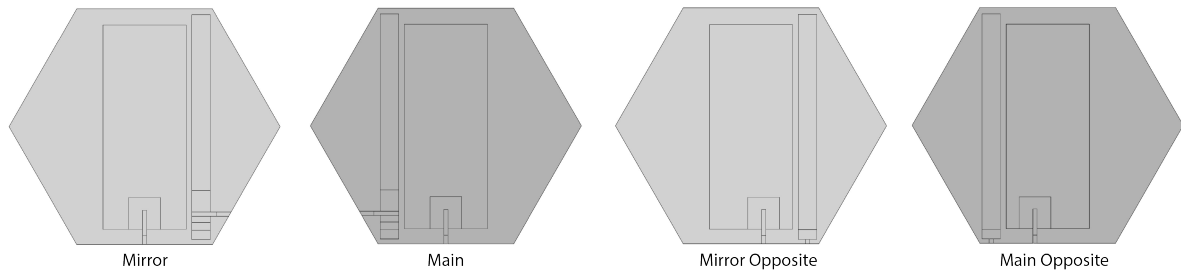


Figure 5.17: Shows the four types of hexagonal cells containing a piezo actuator sensor pair. Figure 5.18 shows how these cells are incorporated in a flexure.

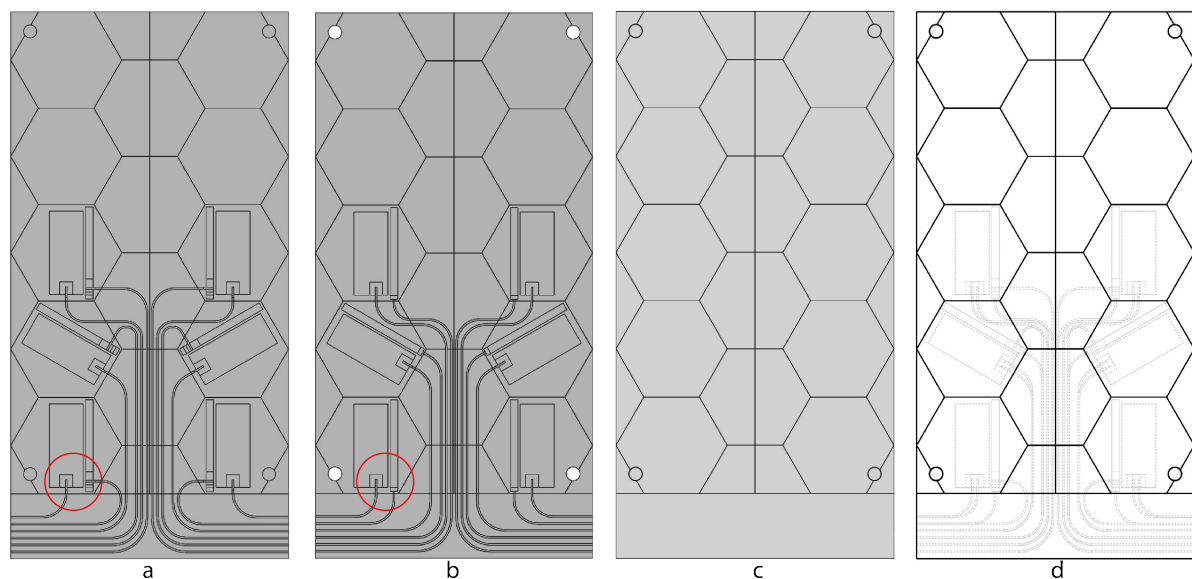


Figure 5.18: a) shows Flexure Half A, b) shows flexure half B, c) shows the two flexure when combined, d) shows the flexure combined but in see through mode. The red circle indicate the important difference between the cells in A and cells in B. The wire holes coming out of cells in A and B are offset from the center in the opposite directions for the actuators. And perpendicular to the sensor.

The cells are designed in such a way that the actuator is positioned in the center. Being hexagonal they can turn 60 degrees. The wiring of the sensors was by far the hardest part to do. As the connections for the different layers were very small and very close. The sensor cells that have wire indents going straight down are meant for the wire connecting to the central copper plate of the sensors. The indents going sideways out of the sensor are meant for wires connecting to the copper coating of one of the piezo layers. The indents for the wiring out of the actuators are just offset from one another so there is no chance that the two opposite wires will connect.

In terms of design and placement of the cells. The bottom row of cells will be used to damp the first mode. The middle angled cells will be used to damp the second torsional mode, and the top row of vertically aligned cells will be used to damp the third mode. Given the complexity of the flexure no comsol simulations were done on these models, just a plain PLA flexure of the same size was used as an approximation. Figure C.19 in AppendixC.1 shows the Finite Element Analysis and the expected eigenfrequencies for this flexure. The first bendy mode is expected at 16 hz, the second torsional mode at 60 hz, and the third bendy mode at 100 hz. Figure 5.19 shows the assembly of the real flexure. Notice the colour coding of the wires. Red goes from output 1 of the amplifier to one side of the piezo actuator, black goes from output 2 to the other side of the piezo actuator. White goes from one of the piezo layers of the sensors to an analog input, and green goes from the central copper plate of the sensor to a grounded input. The assembly proceeds in the exact same way as for the small flexure.

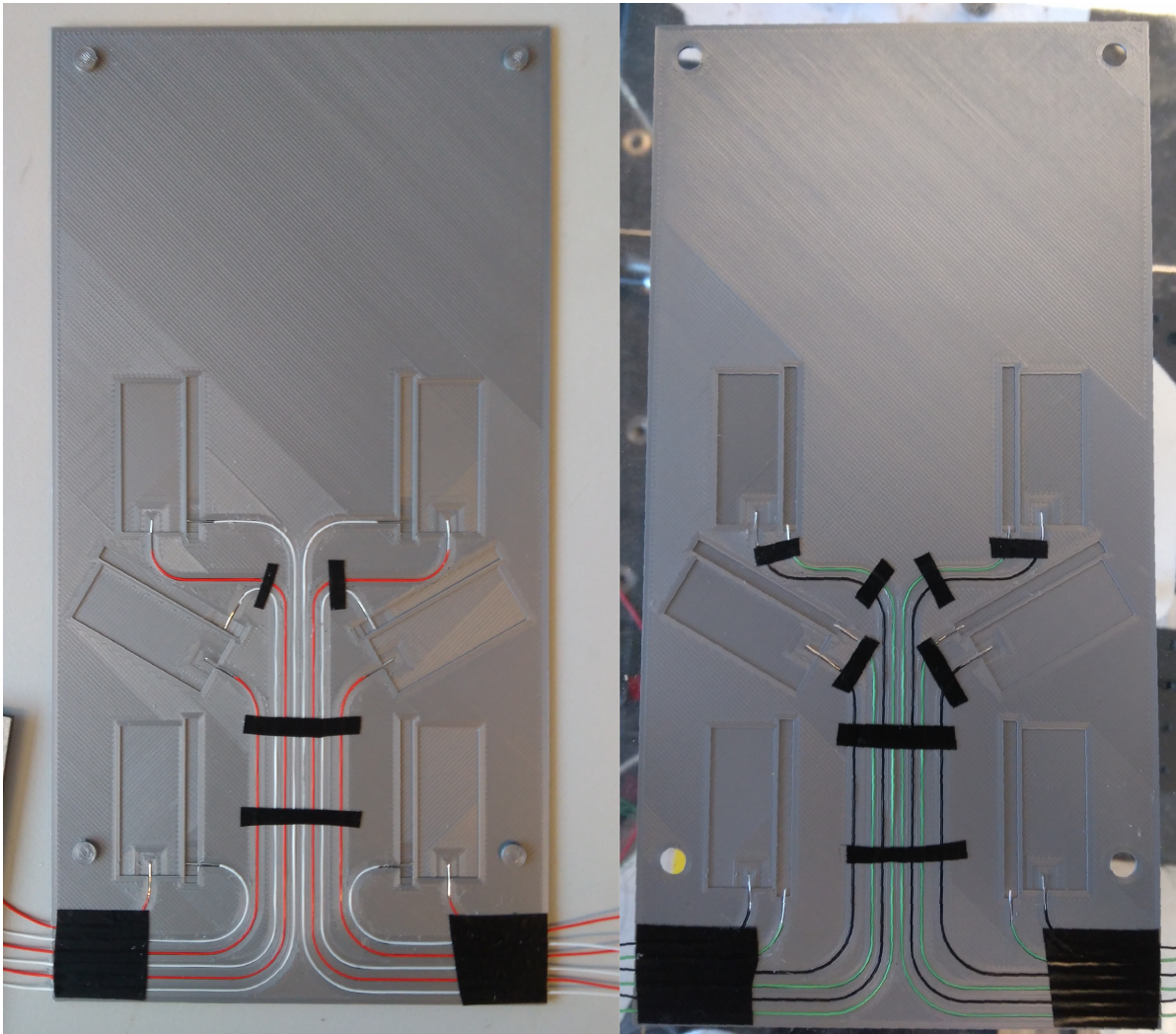


Figure 5.19: Shows the real life flexure with the wires put inside. The colour coding is as follows. Red goes from output 1 of the amplifier to one side of the piezo actuator, black goes from output 2 to the other side of the piezo actuator. White goes from one of the piezo layers of a sensor to an analog input, and green goes from the central copper plate of the sensor to a grounded input.

The procedure for putting in the wires and piezo is the same as for the small flexure. The flexure in a test setup can be seen in Figure 5.20. This figure should also explain the name. Those multiple coloured wires sticking out of the bottom are reminiscent of an octopus, hence the name Octo Flexure. Looking at the flexure one doesn't quit know if the flexure will damp modes or jump at them and try to eat their face.

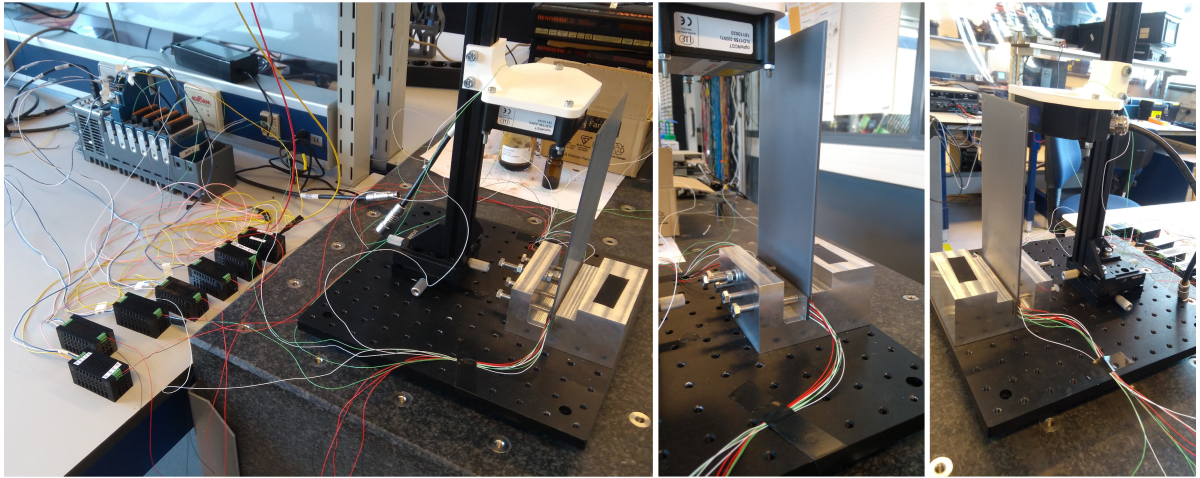


Figure 5.20: Shows the real life flexure in the test setup. Note that the laser sensor is not being used.

While the flexure looks cool, it doesn't work. Most of the sensors did not give any signal, and 2 of the 6 actuator piezos did not work. Those that do work do not produce any noticeable vibration in the flexure. They do produce noise, so they are connected. Though some times they lose connection temporary.

The flexure was disassembled in the same way as the small flexure before it and another attempt was made with this flexure, only this time conductive epoxy was applied to all of the surfaces where wires were supposed to connect. Unfortunately there was no improvement.

5.5. Open Flexure

The previous result showed how difficult it was to get the connections correct in a completely enclosed flexure. One solution might have been to not print out two halves of equal thickness but with one thicker side where all the piezos are put in together with their connections. And all the wires are routed through this thicker piece. Then once the piezos are put in, they are checked, and then the other side is bonded to the thicker half with epoxy in a similar way as the previous flexures. But this would still leave no way to fix the connections if something went wrong during testing. At the same time it wasn't clear if the piezo actuators could transfer their force efficiently enough to vibrate a much wider, heavier and stiffer flexure in the current setup. Especially as the tolerances had to be increased. With an increased cavity to move around in the piezo displacement wasn't being effectively transferred to the flexure.

The new flexure would have some key differences with the old ones. Those are

- Open design
- Epoxy bonded piezo
- Reduced stiffness through holes
- Better topological placement of the piezo sensors and actuators

Figure 5.21 shows the three main flexures produced. Left is the oldest and right is the newest. Their names refer to the Epoxy that was used to bind piezos to the flexure. But there are more differences between them.

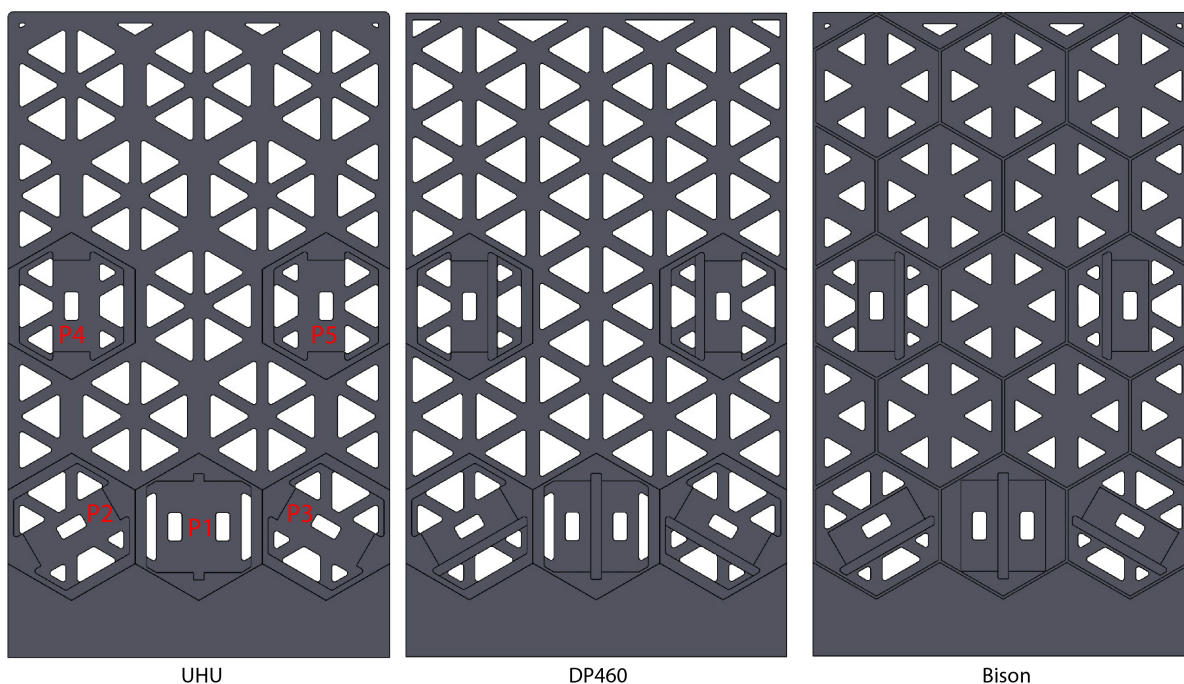


Figure 5.21: Shows the three main open flexures produced. The names indicate the epoxy that was used to bind the piezo actuators and sensors to the flexure. P1 to P5 designate the actuator sensor pair cells that will be referred to later on.

The open design is there to aid with the electric connections and in bugfixing. The piezos are bonded using epoxy to increase the efficiency of transfer of displacement. And the stiffness of the whole flexure is reduced by making holes. But the holes had a hexagonal pattern to maintain the cellular structure. At the same time the holes made sure the rest of the flexure had about the same stiffness as the cells containing the piezos, as the cells containing the piezos had large indents with reduced thickness to hold the piezo actuators and sensors. Another significant change is the Hexagonal pattern. These patterns have been extensively written about in Chapter 3, the previous pattern resembled flexure b1 in Figure 3.11 while the current pattern resembled flexure c1. Figure 5.22 shows these two flexures once again for convenience sake.

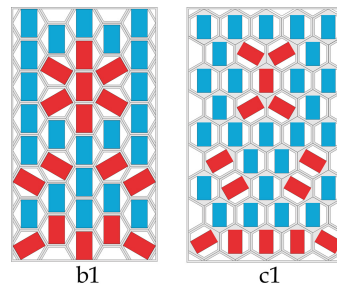


Figure 5.22: Shows the two different patterns that can be used with a hexagon. Previously the pattern on the left was used, the new open flexures use the pattern on the right.

Being that the flexure is open on one side with indentations it is not symmetrical between the front and back. This will hamper the damping of torsional modes as was shown in section 4.7 Advanced real design.

The last significant difference is the placement of the sensor actuator pairs. Now there are only two rows. And one cells contains two actuators paired with one sensor. The double actuator cell is used to damp the first bendy mode, the two angled cell on either side are to damp the second torsional mode and the upper two cells with vertical alignment are to damp the third bendy mode. All of the cells with actuators in them have a hole, the hole is for connections to the backside of the actuator. All of the connections for the sensor are on the front. P1 to P5 in Figure 5.21 designate the actuator sensor pair cells that will be referred to later on.

In total three main flexures were produced, and one small test flexure. The small test flexure was just used to test the cell design and if the actuators could produce vibration which the sensor next to them could detect. And it was used to test if and how the piezo actuators and sensors could be recovered after the bonding process. Figure C.20 shows the dimensions of the small flexure. Figure C.21 shows the 3d model. And figure C.22 shows the real life open flexure. All can be found in Appendix C.1

The construction procedure is as follows. First epoxy is placed on the relevant surfaces then the piezo sensor and actuator are placed, a weight is put on them, which sits there for a while. The sensor and actuator are bonded at the same time as they stay very close together and any epoxy will spill over between the surfaces they sit on. The same procedure is repeated for all the cells. The connections to the sensors are soldered on. The connections to the actuators are a bit more complicated as the nickel layer of the actuator piezo are very difficult to solder. The wires are soldered to a copper tape with conductive adhesive, this tape is then put on the front and back of the actuators. The procedure for each flexure was a little different as lessons from the previous flexures are applied. The differences will be discussed later on.

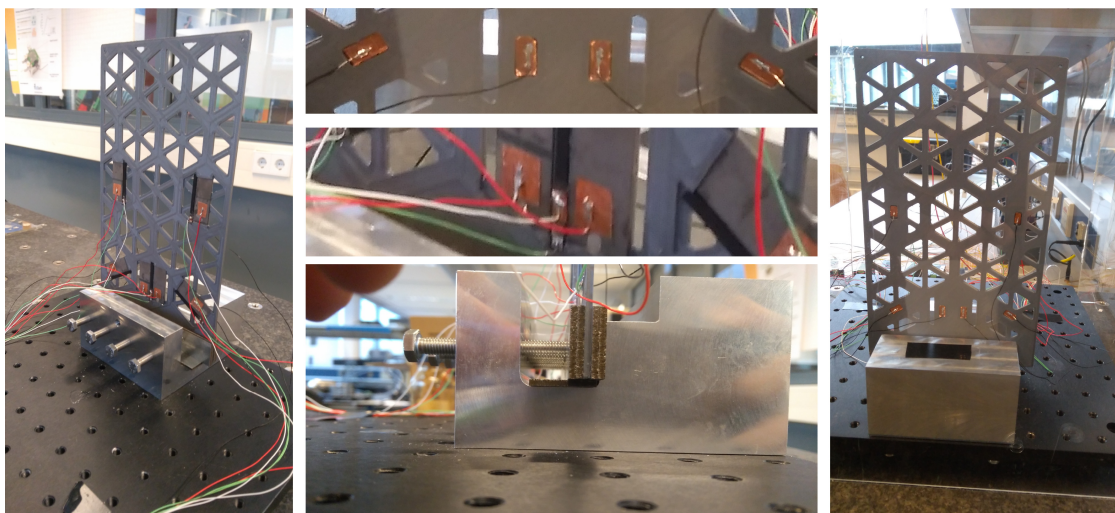


Figure 5.23: Shows the UHU flexure from the front, back and side. Notice how metal plates are used to offset the flexure from the floor and backside because the fillet would interfere with it's placement.

5.5.1. Finite Element Analysis

A flexure is designed around the cells containing one piezo actuator and one sensor. First the cell is designed with a goal in mind. Then that cell is put through FEM. Where its stiffness is calculated, then based on that stiffness the rest of the cells are designed. The PLA only cells are made out of struts forming triangles. The width of these struts is varied to achieve the desired stiffness. The procedure will be described in more detail just below. The design of the double actuator cell is dominated by the need to fit in two piezo actuator and a sensor, it is not designed with compatible stiffness in mind.

The Finite Element procedure is shown in Figure 5.24 and Figure 5.25. A load is applied to one end of a hexagonal cell containing a piezo sensor and actuator. The displacement in the z direction is calculated for the surface where the load is applied. Then a cell made out of PLA material is placed with similar constraints and load. But now there is a live link connection between COMSOL and Solid works and an optimization algorithm (Nelder-Mead) is used to change the width of the struts/arms that make up the solid hexagon. The closest match is selected and displayed.

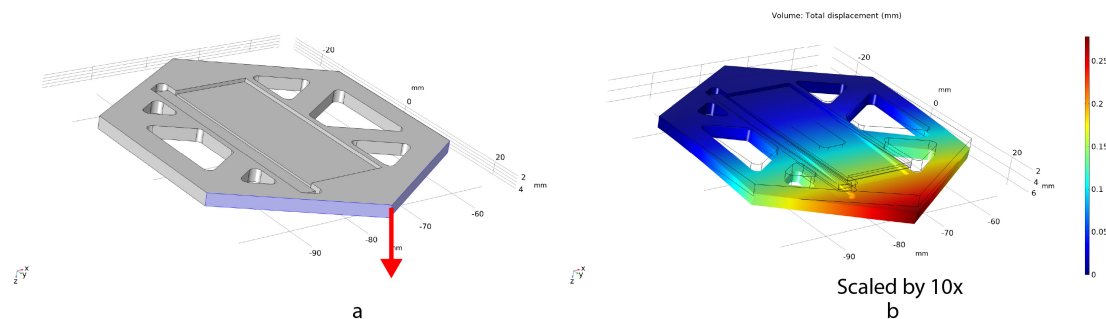


Figure 5.24: a) blue area shows where the force is applied, and red arrow shows the direction. b) Shows the result.

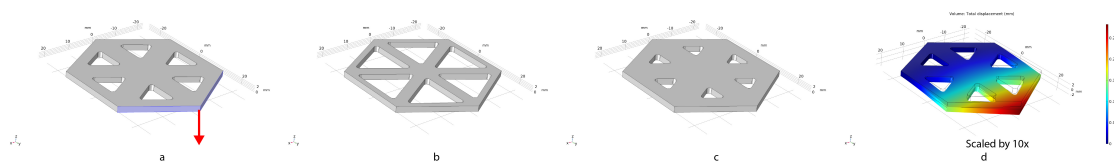


Figure 5.25: a) blue area shows where the load is applied, red arrow the direction. b) shows the lower limit of strut thickness. c) shows the upper limit of arm thickness. d) shows the end result.

This kind of stiffness matching is not perfect. It is very much dependent on the boundary conditions. The results will differ a bit, depending if the load is applied to an edge, point, or surface. It will also change if the displacement is calculated at a point, edge or surface. And it only tests for one direction, whereas forces in a flexure are transmitted in all directions. With significant diagonal forces during torsional modes. However going beyond this would be too complex.

5.5.2. UHU Flexure

The different flexures were not made out to test different designs out. Each flexure was designed based on the lessons learned from the previous flexures. The flexures will be discussed in the order of their making. The damping results will be discussed in the end, though the main results and lesson learned from a flexure will be discussed in each section dedicated to that flexure.

The first flexure was designed with the lessons from the Octo flexure and the small open flexure. The small open flexure showed that the UHU quickset epoxy[16] could be carefully scraped off with a blade and the small rests could be cleaned by scrubbing with isopropyl alcohol, this is shown in Figure C.23 in AppendixC.1. It was not known how the UHU epoxy would behave in the flexure, the most important factor was the fact it could be removed. So if something went wrong another epoxy could be used.

Figure 5.26 shows the cells of the UHU flexure. The full dimensions of the flexure and its cell can be seen in Figure C.24 in Appendix C.1. The thickness of the flexure is 2 mm, the thickness of the indentations for the piezos are 1 mm thick. The indentations are flat. This was done to give the piezos a large area to sit in, so any 3d print errors would not ruin the experience. This flexure took 22 hours to print. So redoing the print would take up a lot of time. The most crucial dimension is the length from top to bottom of the indentations. The top and bottom of a piezo actuator should be connected with the top and bottom walls of the indented area. These areas are marked by red rectangles in Figure 5.26. These areas maybe small but a lot of force can be transmitted through them and by connecting them the piezo actuator forms a kind of continuous surface with the top and bottom the cell, which serves well in transmitting forces.

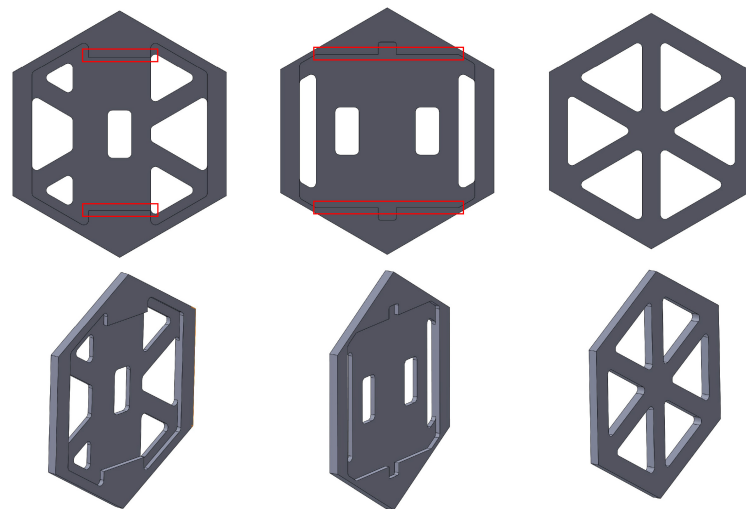


Figure 5.26: Left) single actuator sensor pair cell. Middle) double actuator single sensor cell. Right) PLA only cell. Red rectangles mark areas where the connection between piezo and flexure is crucial.

One big problem with this flexure was immediately apparent when the first identification runs were done. Namely that the second torsional mode was barely detected. At first this was puzzling. But no eigenfrequency analysis was run on the model as it was too complex and it would take a long time. It was assumed that the flexure would behave like a normal flexure. And generally it does. But given the test result, a Finite Element Analysis was run and it showed the problem. Figure 5.27 shows the stress during the different modes. The first mode generates the most stress in the sensor piezo located inside the central double flexure. The second mode however does not generate the most stress in the angled piezo beside the central double actuator, it generates more stress in the upper row of piezos. The third mode does generate the most stress in the upper row of piezos meant to damp that.

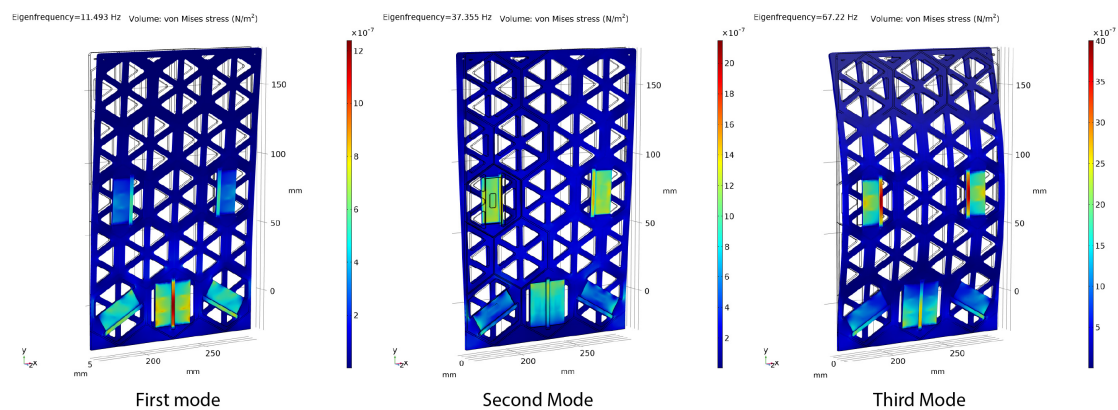


Figure 5.27: Left) Shows the first bendy mode. Middle) Shows the second torsional mode. Right) Shows the third bendy mode.

The biggest issue however is that the gain plotted in the bode plots was steadily decreasing. This was most likely do the epoxy steadily coming looser as the piezo vibrated. This meant the system was consistently changing. And a damping filter designed for data taken on one day would not be as valid the next day during implementation.

Further issues were with the electric connections and National Instruments equipment. The copper tape with conducting adhesive proved to be very unreliable, but the nickel layer made soldering more unreliable. The connections on the sensors very also very weak. Not due to soldering but because they copper layers they were soldered to were very thin. One wrong move and the connection would be torn off and could not be re soldered as the copper would come lose with the solder. Despite this, the most successful damping attempts were made with this flexure and will be discussed later on.

5.5.3. DP460

The second flexure attempted to solve the problem with the epoxy. Quick research was done to find an epoxy which could handle vibrations better. An epoxy that was recommended by high tech industry contacts for these applications is the 3M Scotch-Weld Epoxy Adhesive DP460 [58]. The manufacturer described it with the following important points.

- 60 minute work life with handling strength in four hours allows sufficient time for re-positioning
- Toughened for impact resistance and high fatigue resistance to withstand demanding conditions
- Outstanding environmental performance
- High peel and shear strength for strong bonds in critical applications

"Whether you are joining, adhering, attaching, repairing, potting, panel or structural bonding, our epoxy resin provides the highest shear, peel, impact, **vibration** and fatigue resistance in our Scotch-Weld™ Epoxy Adhesive family."

Apart from the change in epoxy, the procedure to construct the flexure was changed which was allowed by the fact that DP460 has a working life of 60 minutes. But that will be explained later on. First the focus will be on two changes made to the design of the cells. Figure 5.28 shows the new cell design. The full dimensions of the flexure and it's cell can be seen in FigureC.25 in AppendixC.1

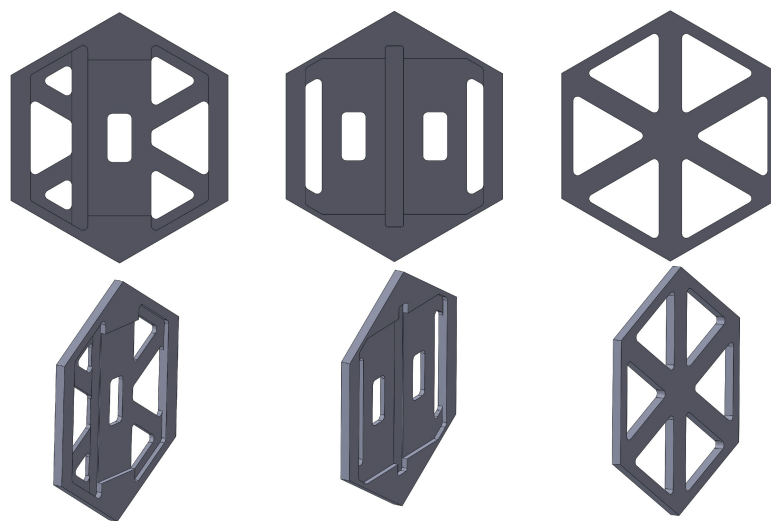


Figure 5.28: Left) single actuator sensor pair cell. Middle) double actuator single sensor cell. Right) PLA only cell.

The first change is an extra indentation of 0.2mm for the sensor. This makes the sensor and actuator surfaces the same height, which helps during the construction. After the piezos are put in to the cells a single flat weight can sit on their surfaces and distribute its weight among them. When the two surfaces are uneven the weight placed on top will sit askew. The second change is to the width of the arms of the PLA only cell. The outer edges are narrower than the six central arms. They are in fact half the width. However when the cells are arranged in a hexagonal pattern the outer walls will combine with their neighbours to form struts of equal thickness to the inner arms. So when the cells are arranged in a hexagonal pattern all struts/arms have the same thickness. This way a single cell stiffness analysis approximates the behaviour of a full flexure much better. In the UHU flexure you would have hexagons with walls that had twice the width as the inner arms. Now every strut/arm is equal. This should help the dynamics. The flexure as a whole is a bit less stiff but also weighs less. So the eigemodes should not shift, but the flexure should be easier to drive.

Construction A new procedure was made for construction. Figure 5.29 will serve as a reference in this section. First epoxy was applied to all the relevant areas, then the sensors and actuator piezos were put in their respective place. Then specially 3d printed pieces were put on top of them. And on top of that some heavy equipment was placed. In this case a scale or heater. The flexure was left in this condition for 24+ hours. Later it was discovered that neither the bottom or top of the equipment used as a weight was flat, so pressure was not evenly applied to all the piezos. This could be fixed by placing something flat on top of the 3d printed pieces and then something heavy on top. After the 24+ hours period, the weight was removed and the relevant soldering connections were made. A new type of copper with adhesive was used, this one had tin on the outside which made soldering the wires to the copper tape easier. Figure 5.30 shows the DP460 flexure from different perspectives.

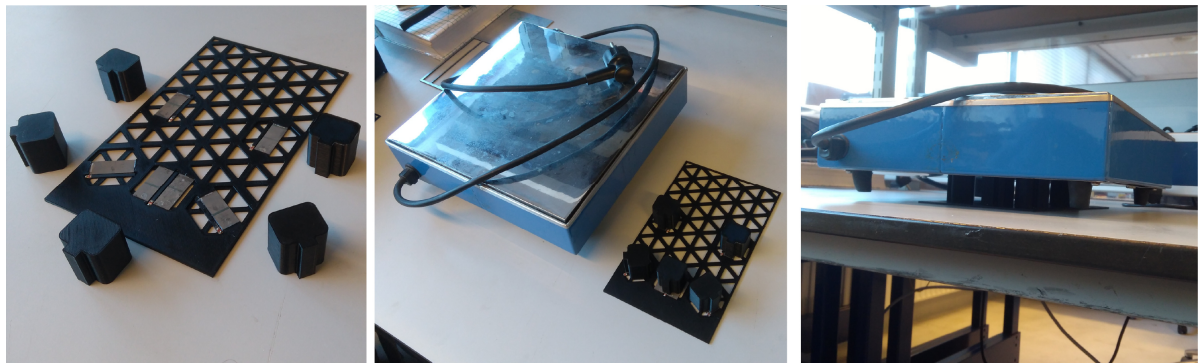


Figure 5.29: Left) The actuators and sensors in their respective places Middle) The 3d printed pieces on top of the piezos Right) A heavy piece of equipment is put on the 3d printed pieces.

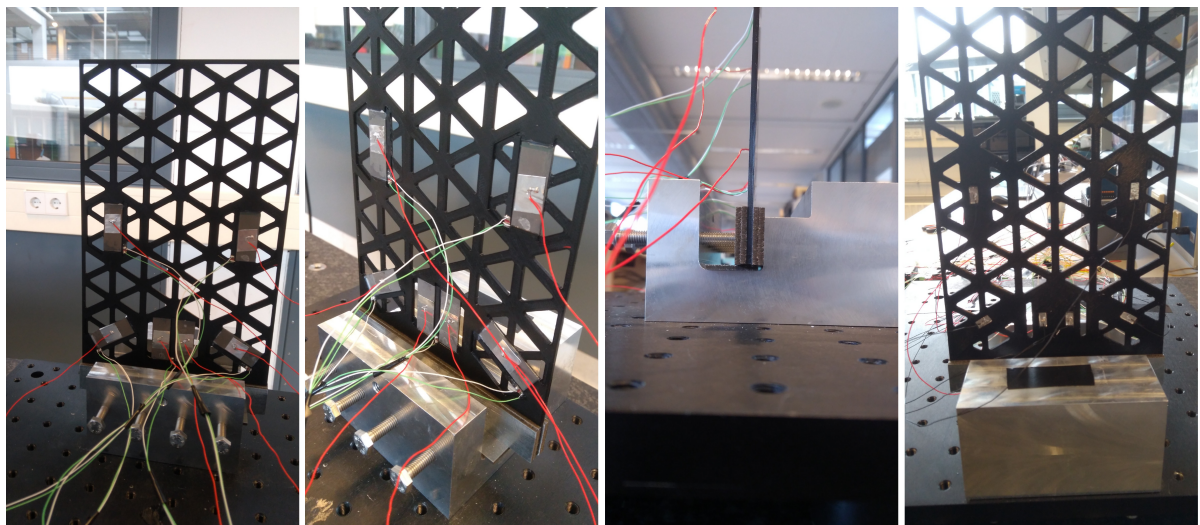


Figure 5.30: Shows the DP460 flexure from different perspectives

Testing System identification showed that this new flexure had lower gains than the previous one. This was unexpected as the new epoxy and procedure should have created a stiffer connection between the piezo actuators and the flexure, and also between the flexure and the sensors. So not only should the vibrations have been transmitted better from the actuators to the flexure, the vibrations should have been transmitted better to the sensors from the flexure.

All of the sensors were checked manually using an oscilloscope before being put in to the new flexure. The actuators could not be checked, they were just visually inspected for damage and a resistance meter was used to check the conductivity of the surface. So that is most likely not the case.

Furthermore the system identification test showed the same loss of gain as before.. The biggest problem however was with the control system. Before doing a full sweep every mode and piezo would be checked individually. First by running the disturbance at the specific frequency the piezo was meant to damp and turning on the damping and seeing what happened. Second by running a sweep using only one piezo and checking if it could damp the frequency it had to damp. P4 and P5, those are the piezos in the upper row meant for mode 3 could damp the system in the first instance. Namely when the flexure was run at the frequency they had to damp and then the damping was turned on. But when a sweep was done the damping would actually increase the peak. Numerous adjustments were made to the gain, even a negative gain was tried out. But during a sweep the system could not be damped. Given the limited time available, further damping attempts were abandoned, as the flexure would never damp better than the UHU flexure. Figures C.26, C.27, C.28, C.29, C.30 in Appendix C.1 show the undamped system identification plots.

5.5.4. Bison

A simple test was performed to check the strength of the bonding of the DP460 epoxy compared to the old UHU quickset and an epoxy bought at a local store the "Bison Combi Plastic" [59] acrylic epoxy.

The test was not very rigorous, however the differences were so large that it did not have to be. First a chunk of epoxy was left to dry on a PLA layer, then the next day a knife was used to try to scrape it off. The UHU and DP460 would come off quickly and easily. The blade would get between the epoxy and PLA and the chunk would fall off. The Bison could not be scraped off at all.

The second test was performed by bonding a piece of left over PLA material to an old PLA flexure with each epoxy, then leaving a small weight on top of all three test pieces for a day. The next day an attempt was made to peel the piece off. The pieces bonded by the UHU and DP460 came off easily, the piece bonded by the Bison was almost destroyed during the de-peeling process. So the Bison forms the strongest connection, which should help with the gain, but will make removing the piezos impossible.

If more time was available then the most straightforward avenue of research would be to find out what epoxies are used to bind the layers of piezo actuators. These kinds of epoxy should be the best suited to bind the piezo actuator to a flexure. Assuming the epoxy binds to flexure material.

These tests do not tell us anything about the ability of the epoxies to withstand vibrations. But at this point there was no point in not trying a flexure with the strongest epoxy. As there would be no need to retrieve the piezos any more. So we go to the third flexure, the Bison Flexure. The full dimensions of this flexure can be seen in Figure C.31 in Appendix C.1.

This flexure also has two big changes. This time an attempt was made to increase the observability of the second torsional mode to cells P2 and P3. Those are the two angled cells in the bottom corners. Figure 5.31 shows the new cells. The indentations were made much smaller, essentially we have gone back to the earlier design of holes for the piezos to be put inside. The idea behind this is that the piezos now also make contact with the flexure with their sides. And because the inner parts of a cell surrounding the piezos are thicker now they transmit more of the forces. In the previous cells the thick outer walls would bear most of the burden and the stress, now the stresses should be transmitted better to the piezo sensors, and the piezo actuator should be transmitting its displacement a bit better. Because the stiffness has been increased in the piezo cells, the stiffness had to be increased for the rest of the cells. And the PLA only cells now have much wider struts/arms. This increased stiffness will

mean lower gain. But hopefully that will be made up by a better connection and better observable second torsional mode.

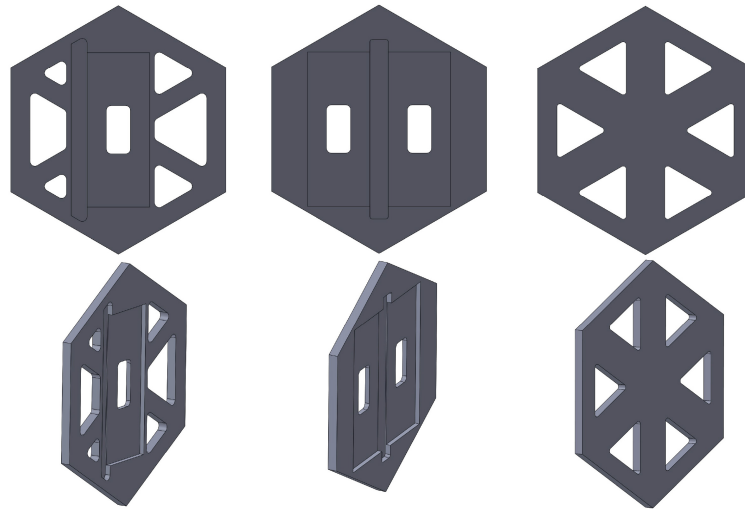


Figure 5.31: Left) single actuator sensor pair cell. Middle) double actuator single sensor cell. Right) PLA only cell.

Finite Element Analysis was run on the flexure with and without piezos inside to see the patterns of stress.

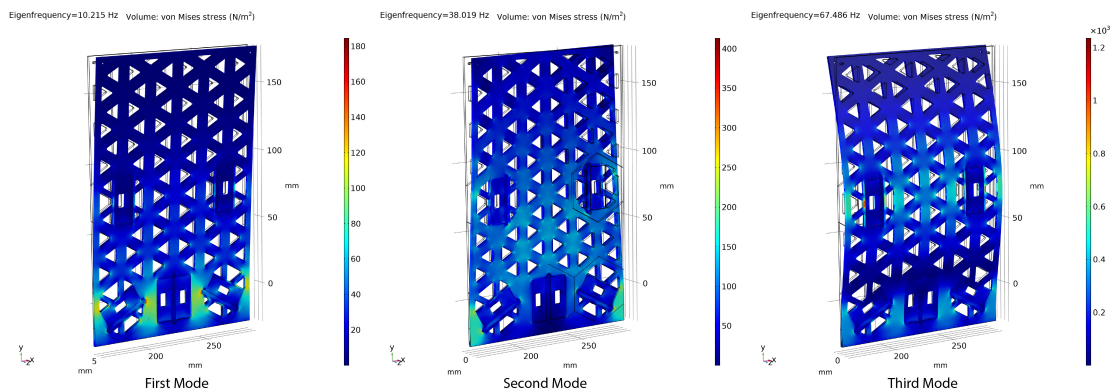


Figure 5.32: Shows the first three eigenmodes without any piezos in the cell. Left) Shows the first bendy mode. Middle) Shows the second torsional mode. Right) Shows the third bendy mode.

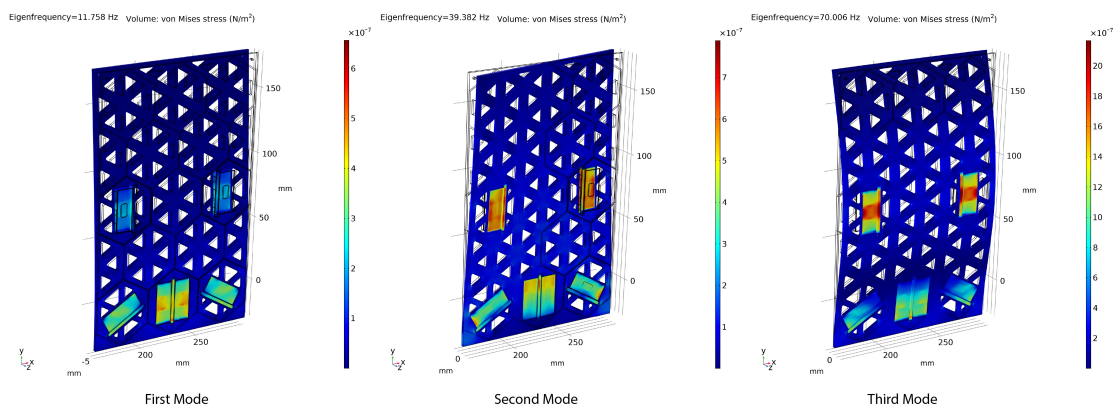


Figure 5.33: Shows the first three eigenmodes with the piezos in the cell. Left) Shows the first bendy mode. Middle) Shows the second torsional mode. Right) Shows the third bendy mode.

The stresses in Figure 5.32 look promising. Yes the first mode shows the highest stresses at the corners of cell P2 and P3, but that is because of the corners. The middle piezo should be strained adequately. But the best picture is the middle one showing the stresses caused by the second torsional mode exactly where we want them. The most right picture shows that the upper row of piezo cells will receive the most stress from the third mode, which is exactly as it should be.

But then we take a look at Figure 5.33 and things don't look that good any more. The first mode stresses the central piezo the most as it should. the third mode stresses the upper row of piezos the most as it should. But the second torsional mode again stresses the upper row the most. And stresses the central piezo more then the the two angled ones in the corner meant to damp the second mode. However the results are still better then for the first flexure. where the corners piezos barely showed any stress. Now at least they do seem to be stressed and thus strained.

The procedure for this flexure was once again different then for the previous one as this epoxy only has 3 minutes of working time. So each individual cell was done separately. The printed pieces were still used, it is just that a smaller weight was placed on top of them and left there for 30 minutes. And before the weight the piece was pressed down hard.

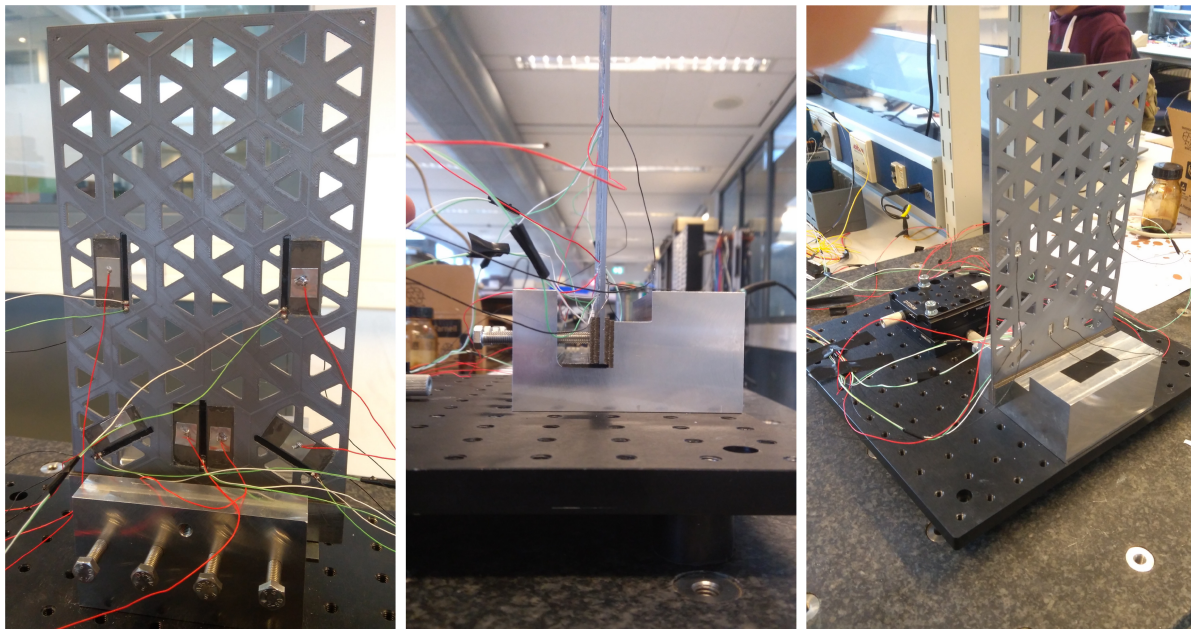


Figure 5.34: Shows the Bison Flexure in real life.

The system identification showed this flexure to be the worst of the lot. The data for P2 and P3 is so bad that the sensors and analog inputs were rechecked. The wires from P2 and P3 were put in to the ports of P4 and P5 and vice versa. But the data stayed bad. So it is not the input ports of the NI-9002 module. This is something that needs to be checked as one input, port 0 already stopped working. But in this case the input ports are not the problem. It could be three things, the flexure, the way the sensors are attached or the sensors themselves. It is highly unlikely that two mirror opposite sensors just failed at the same time and in the same way. So it is the flexure itself or the the connection. The plots of the system identification are shown in Figures C.32, C.33, C.34, C.35, C.36 of Appendix C.1.

The identification data is so bad that it's pointless to try to damp the flexure, with much worse observability damping the modes will be harder then with the previous flexures.

5.6. Damping results UHU Flexure

The damping experiments were divided in 5 sets/runs, and each set/run consisted of 3 tests/sweeps. There was one set/run per piezo cell. In each set one of the piezo cells would be used to provide the disturbance. First an undamped run would be done. Immediately followed by a run where only the piezo providing disturbance is damping, and then that would be followed immediately by a run where the same piezo is still providing disturbance but all of the piezos are trying to damp their respective modes. The piezo cells were designated P1 to P5, this was indicated in Figure 5.21. P1 is the middle double actuator cell, this one is meant to damp the first mode. Which is a bending mode. The two angled cells in both of the corners are P2 and P3 and they were supposed to damp the second mode. But during system identification that mode had very poor observability so it was decided to damp the seventh mode located at 256 hz. This mode is shown in Figure 5.35, this mode is all kinds of crazy. P4 and P4 are the two cells in the upper row. These cells have to damp the third mode, which is a bending mode.

The data is going to be presented per piezo cell run. Each run will have four figures. The first figure will show the Gain,Phase and Coherence of all three tests gathered from the sensor of that cell. The other figures will show the Gains for all the sensors. They will show the gains for the single damped test, and then the all damped test, and once again the all damped tests, but now some plots will be zoomed in at the respective frequency the piezo were supposed to damp. The all damped plots are repeated twice to show the overall influence of all the damping turned on, as well as how well damped each of the individual modes the piezos were supposed to damp were. And finally the data will be summarized and a short analysis given.

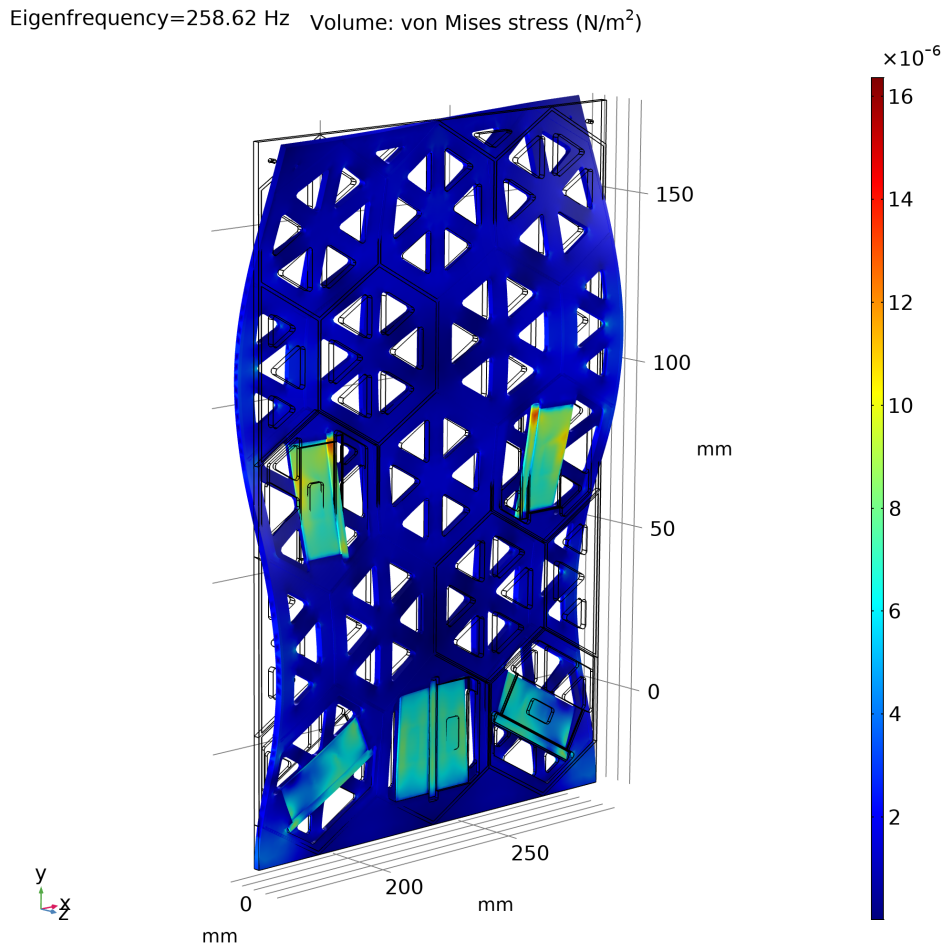


Figure 5.35: Shows the seventh mode of the UHU flexure

5.6.1. P1 Cell

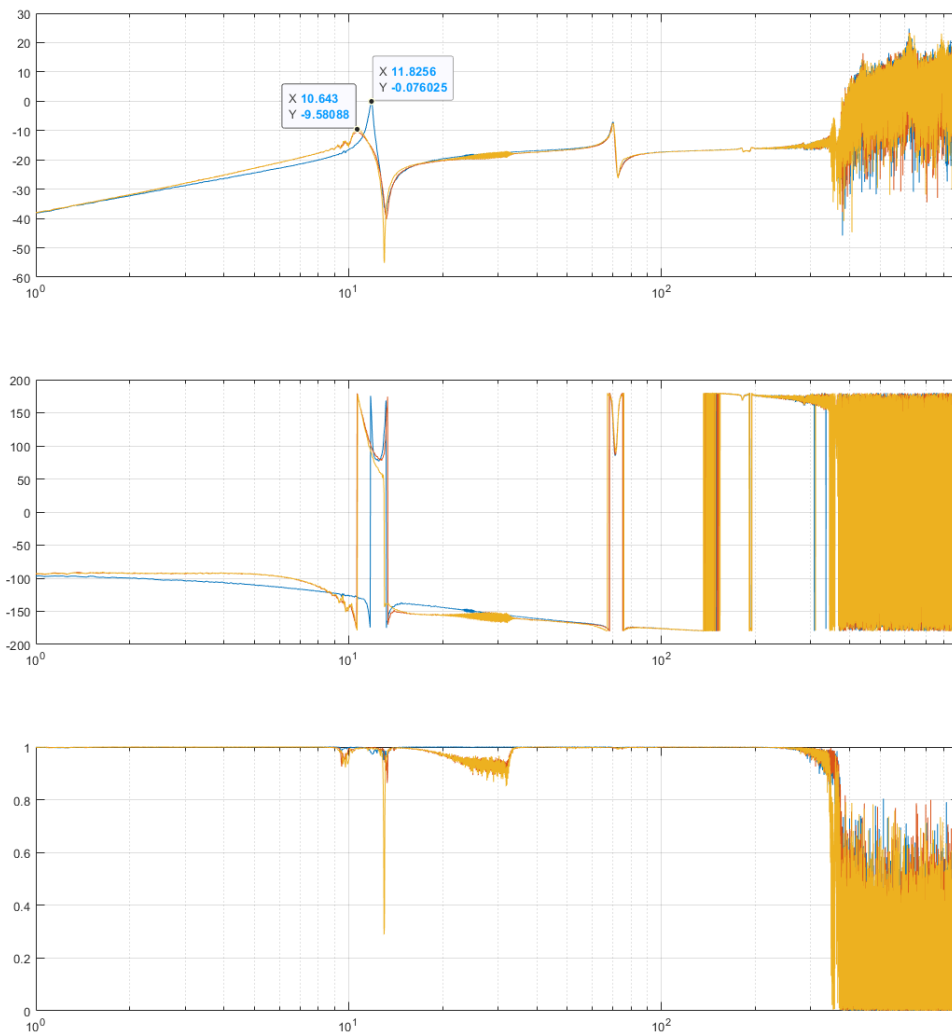


Figure 5.36: Shows the Gain, phase and coherence of all three sweeps when P1 provided the disturbance

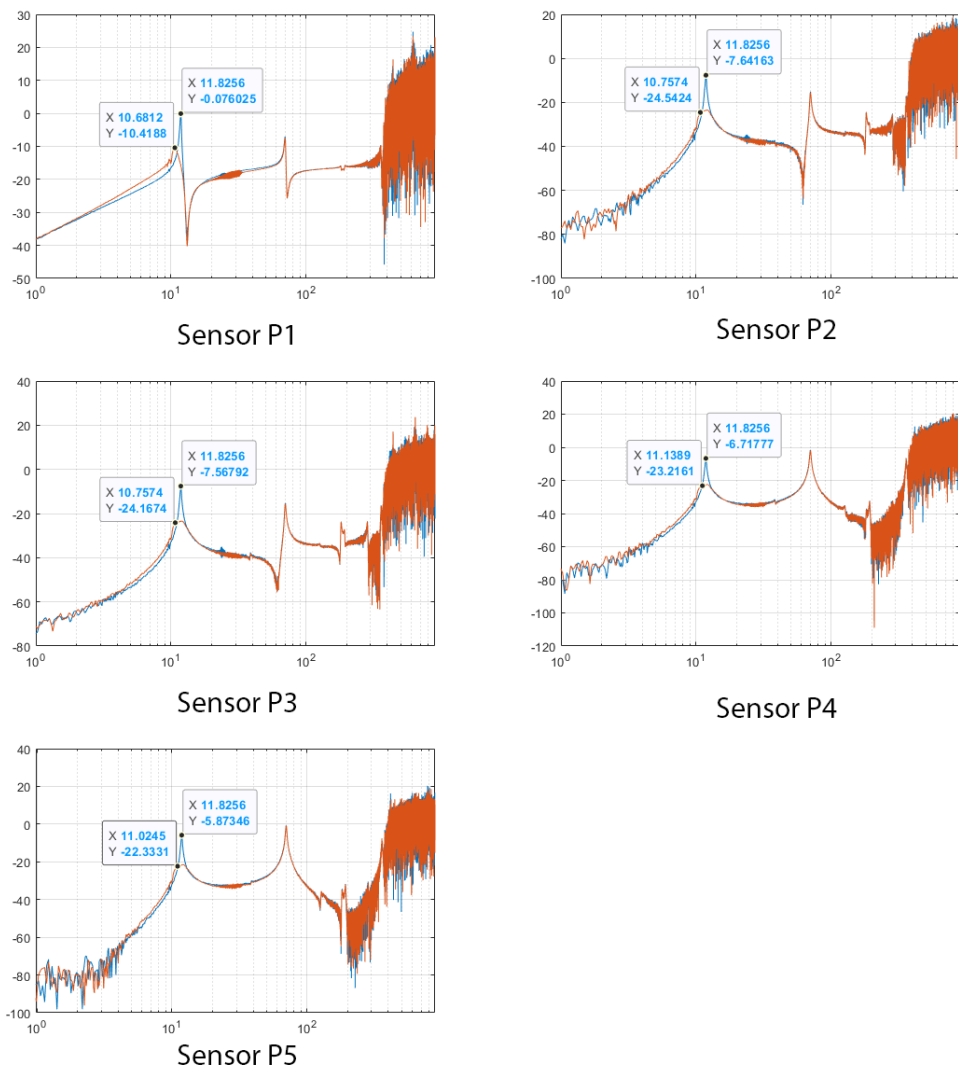


Figure 5.37: Shows the damped Gain from the perspective of all of the piezos when P1 provided the disturbance , and was the only one to damp

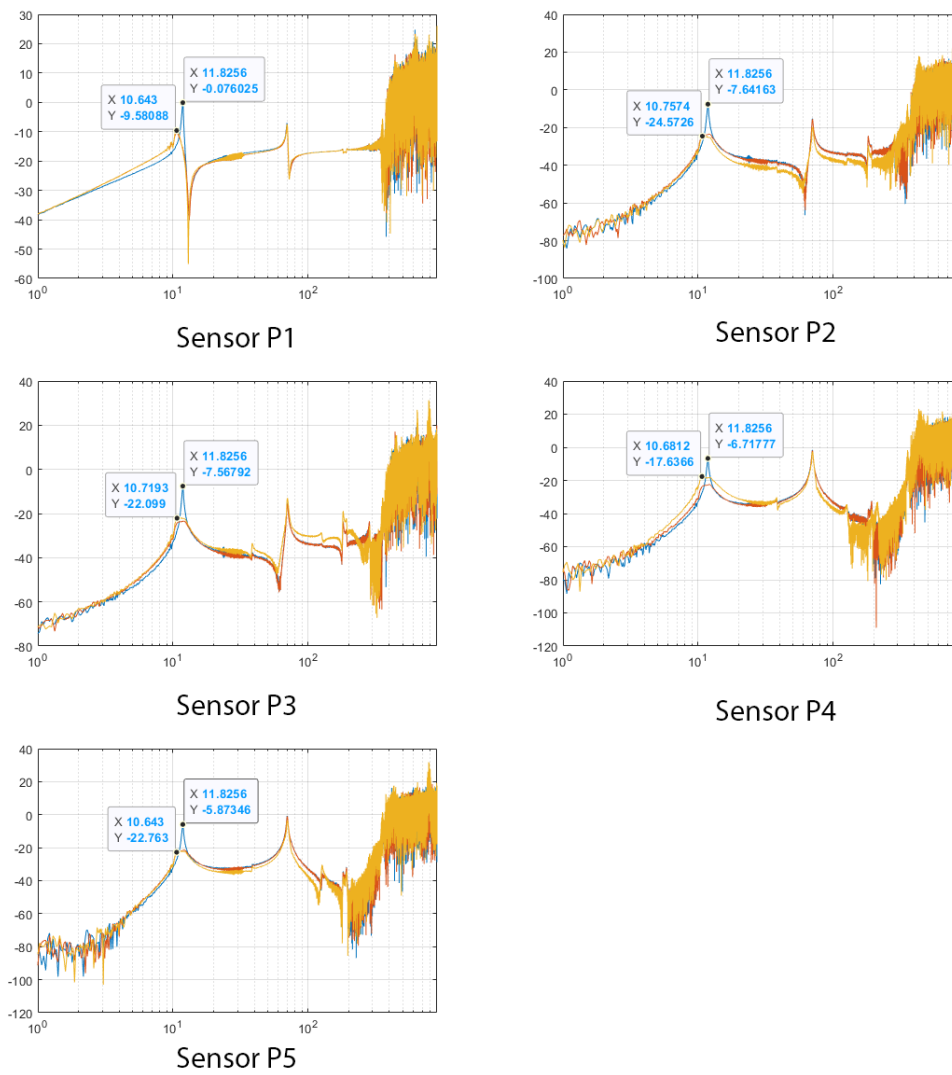


Figure 5.38: Shows the damped Gain from the perspective of all of the piezos when P1 provided the disturbance , and all of the piezos were used to damp

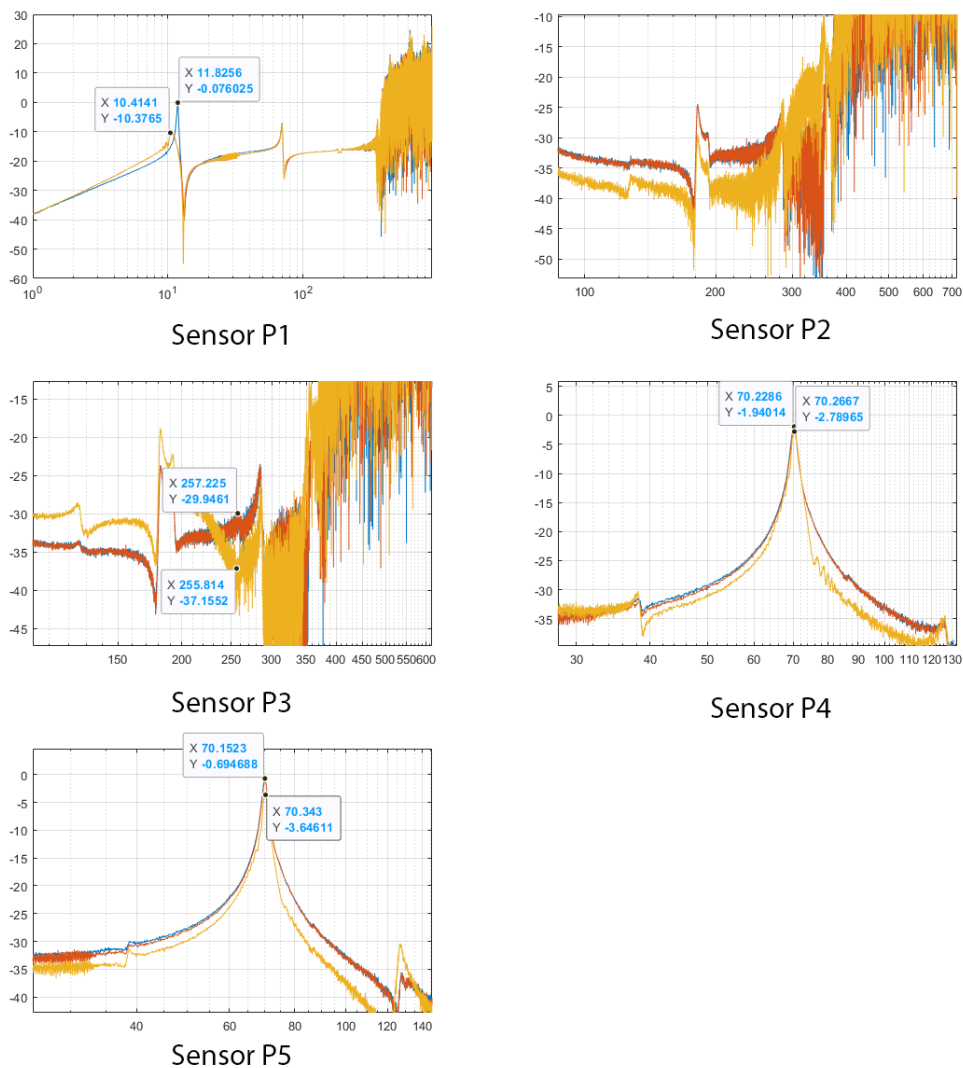


Figure 5.39: Shows the damped Gain from the perspective of all of the piezos when P1 provided the disturbance, and all of the piezos were used to damp, only now some plots are zoomed in at the respective frequency the piezo is supposed to damp.

The gain of the first mode goes down from -0.076 dB to -9.58 dB, which means it decreases by 67% from the perspective of P1. P2 data is just a mess unfortunately there are no peaks visible though the overall gain around 257 is lower with all damping turned on then without. P3 shows a slight peak, though the data is pretty bad. But if we take it as face value the 7th mode is damped by P2 and P3 from the perspective of the sensor of P3 by 56%. The damping of the third mode by P4 and P5 from the perspective of P4 is tiny, about 9%. Damping by P4 and P5 from the perspective of P5 is respectable at 34%. Overall not bad.

5.6.2. P2 Cell

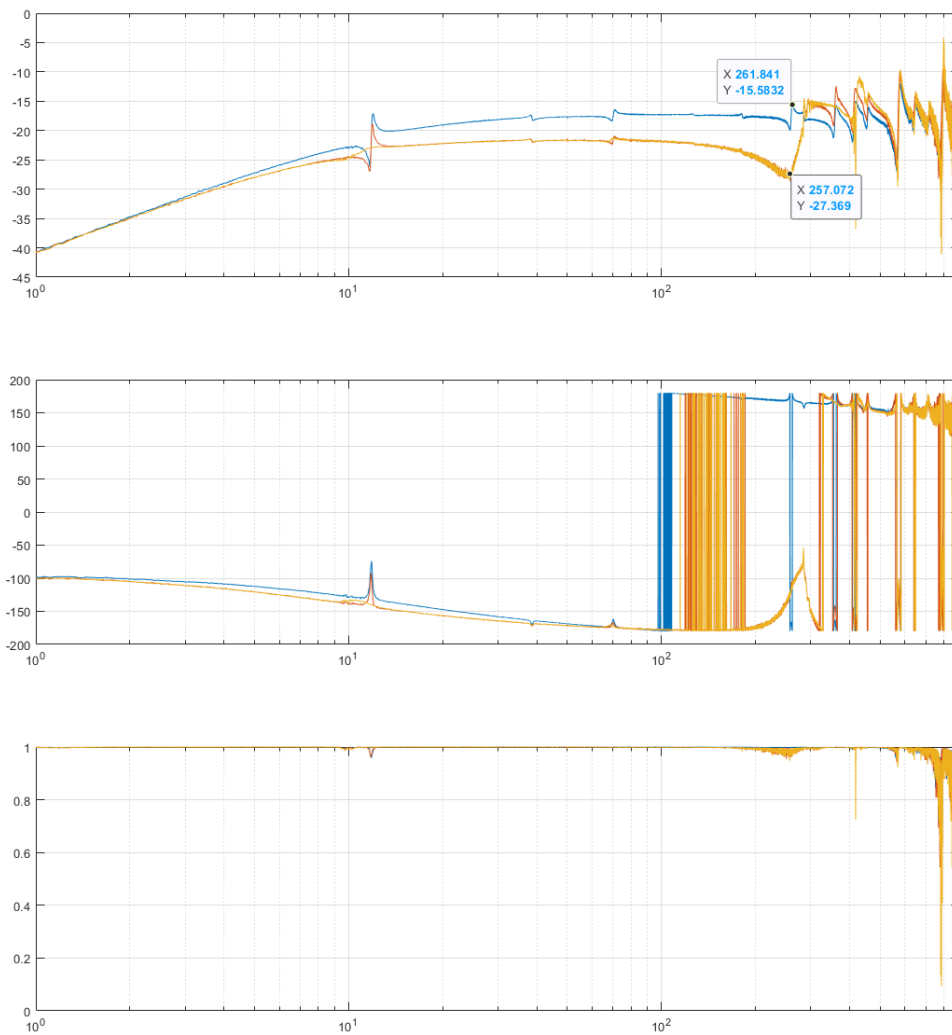


Figure 5.40: Shows the Gain, phase and coherence of all three sweeps when P2 provided the disturbance

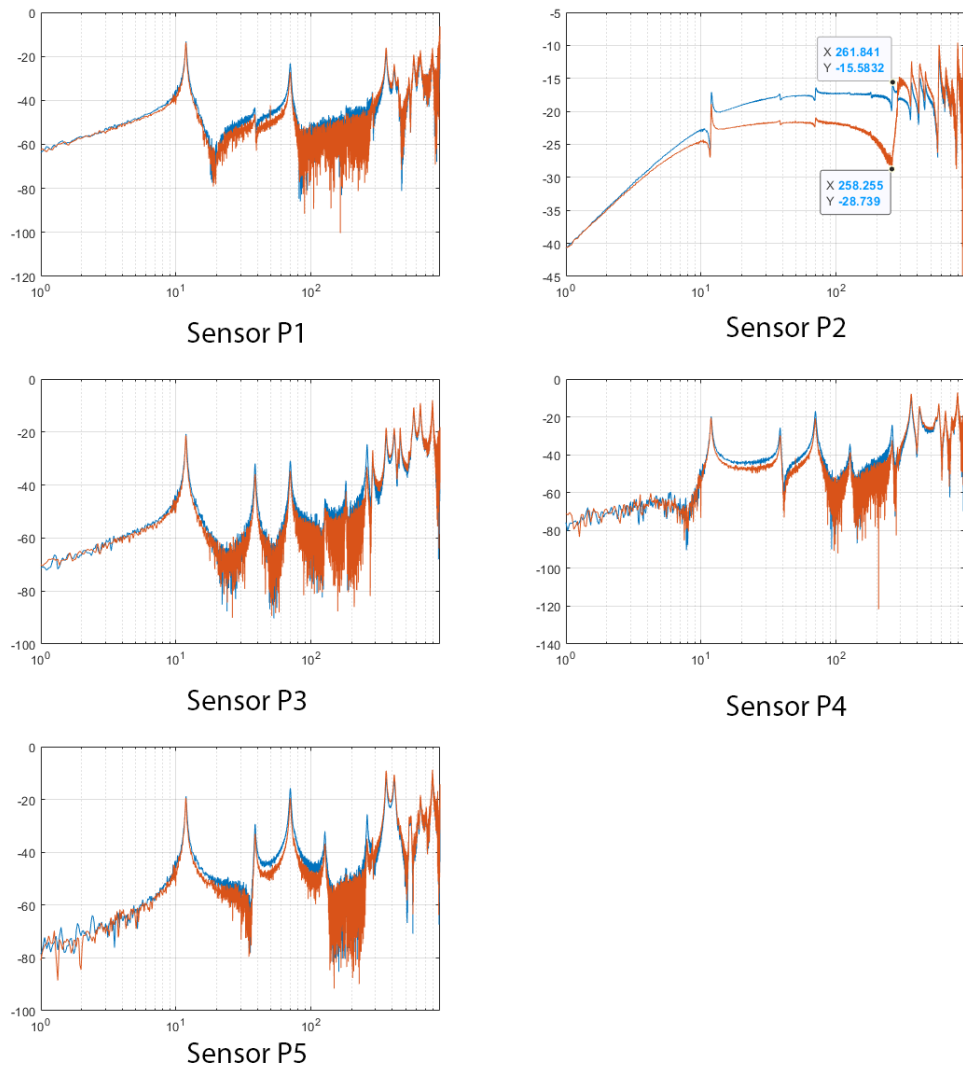


Figure 5.41: Shows the damped Gain from the perspective of all of the piezos when P2 provided the disturbance, and was the only one to damp

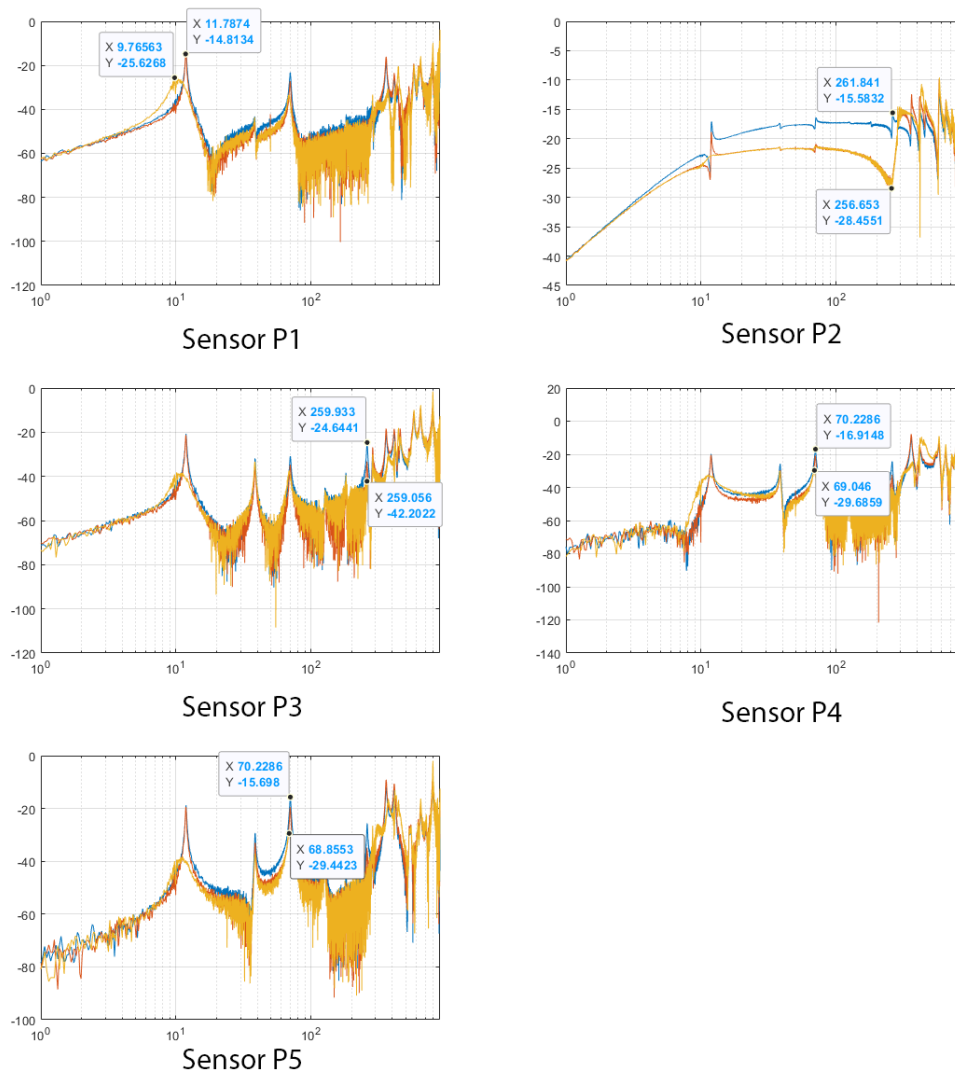


Figure 5.42: Shows the damped Gain from the perspective of all of the piezos when P2 provided the disturbance , and all of the piezos were used to damp

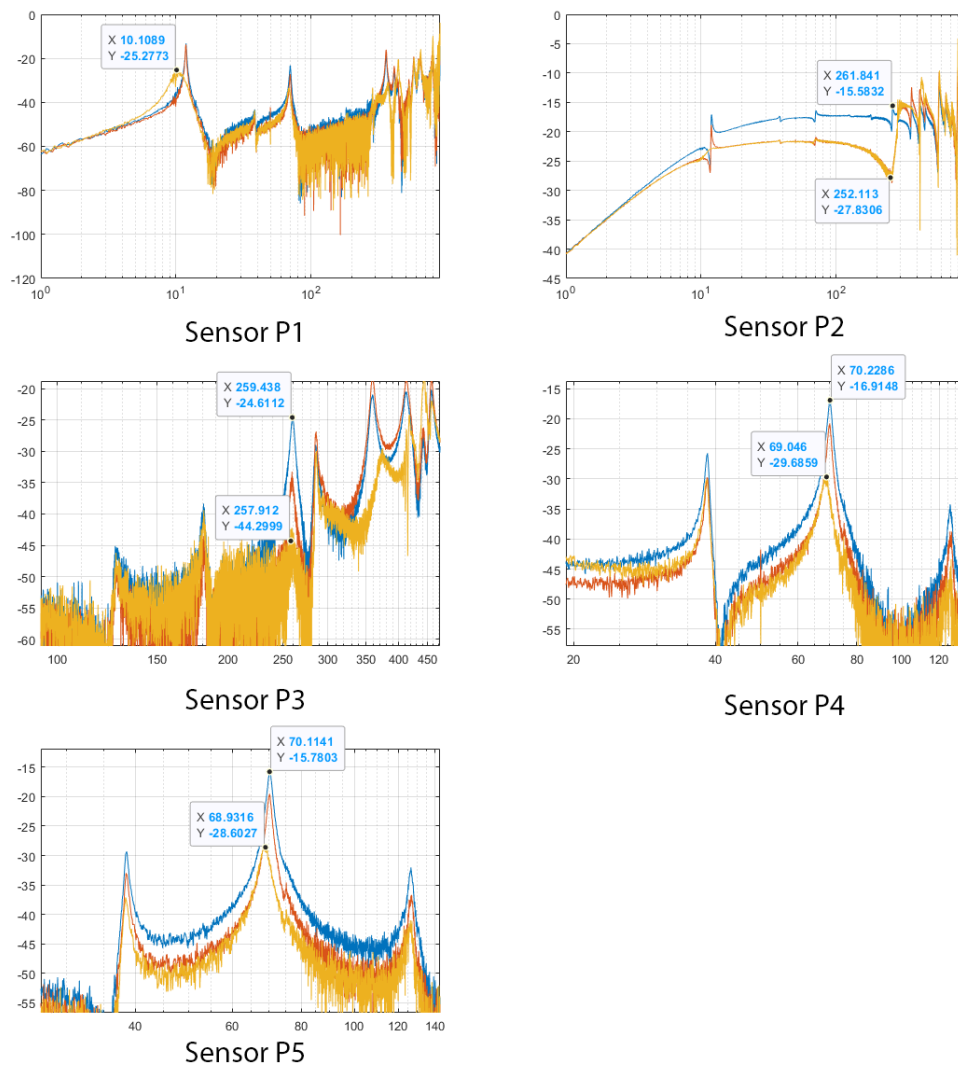


Figure 5.43: Shows the damped Gain from the perspective of all of the piezos when P2 provided the disturbance, and all of the piezos were used to damp, only now some plots are zoomed in at the respective frequency the piezo is supposed to damp.

The damping for the first mode is 71% from the perspective of P1. This was calculated based on data from Figure 5.42, as the data tip is not visible in Figure 5.43. P2 is not damping it is just increasing stiffness and lowering the gain. The gain is about 76% lower at the 7th mode from the perspective of its own sensor, though this is also partly due to the damping from P3. P3 seems to be damping the seventh mode by a whopping 90% from the perspective of its sensor, but off course a large part of that is due to P2 lowering the gain. P4 and P5 are damping the third mode from the perspective of P4 by 77%. And P4 and P5 are damping the same mode by 77% from the perspective of P5, so the P4 and P5 data matches up nicely. Again, the overall results are positive.

5.6.3. P3 Cell

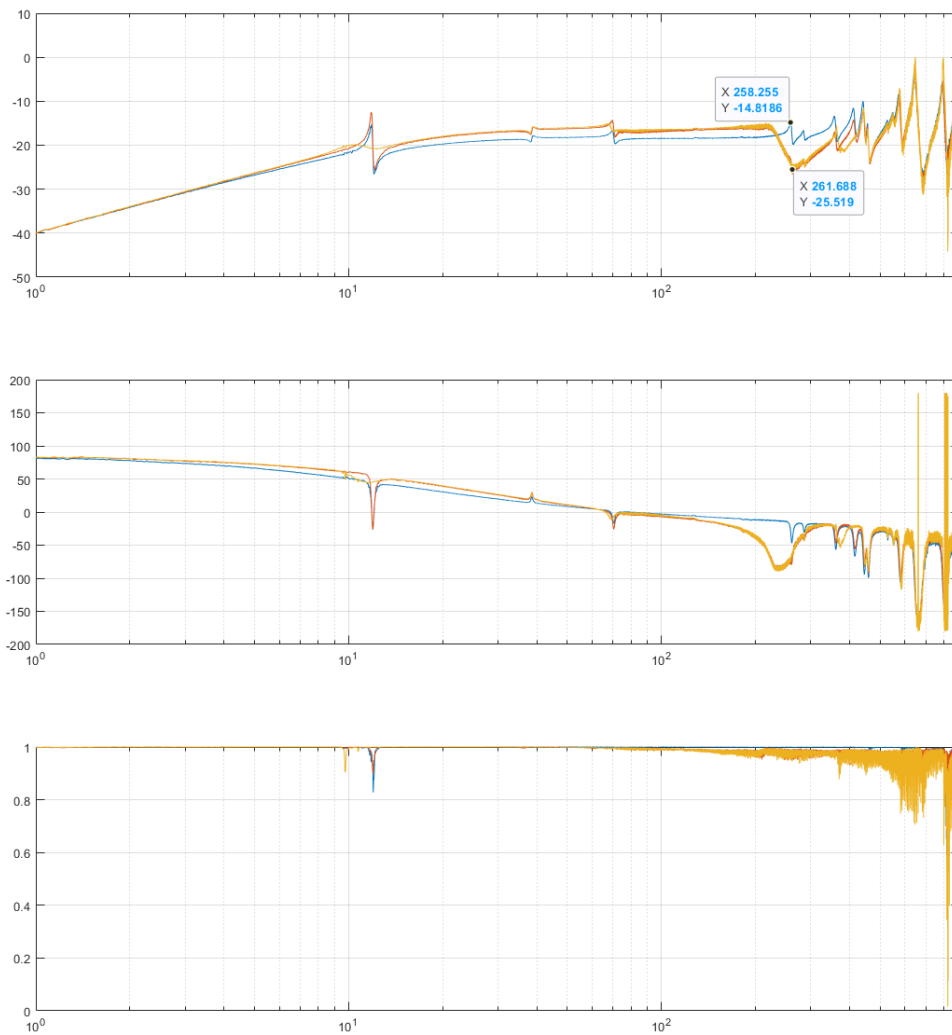


Figure 5.44: Shows the Gain, phase and coherence of all three sweeps when P3 provided the disturbance

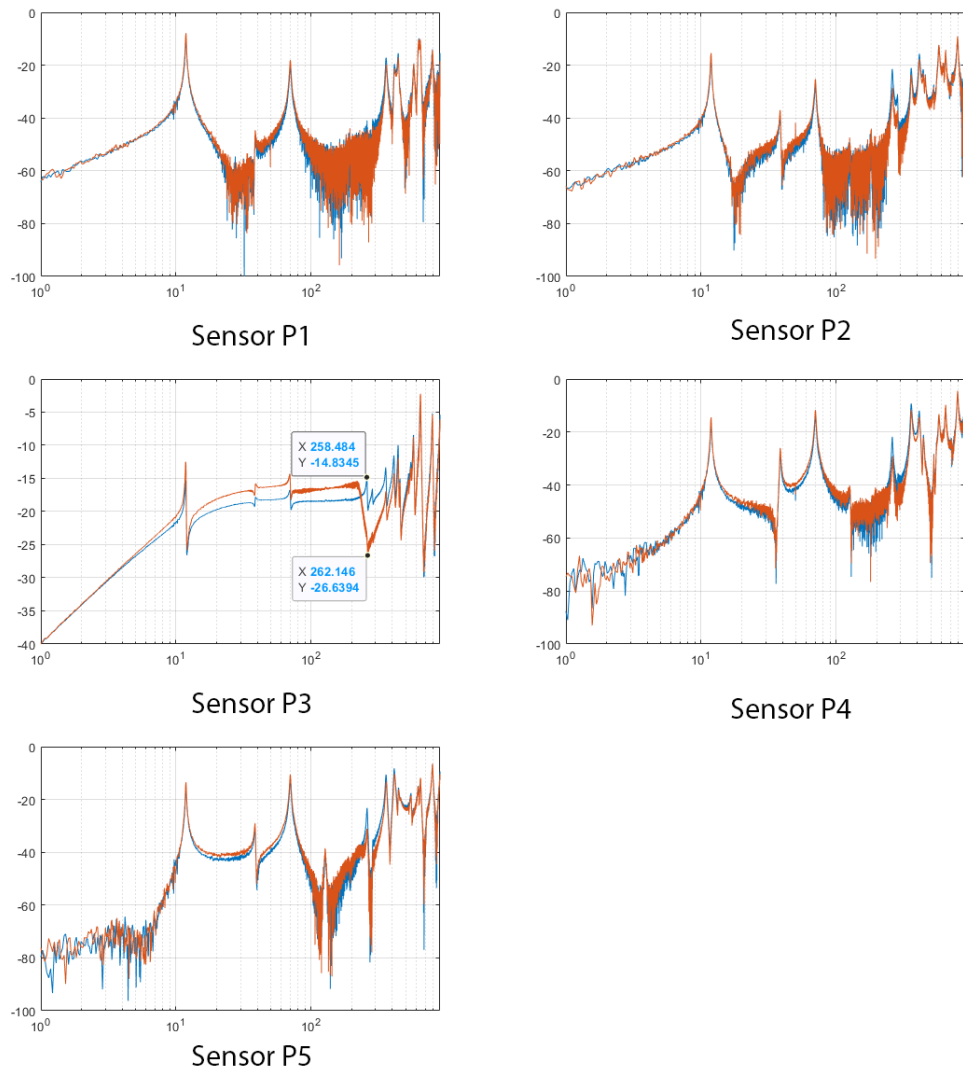


Figure 5.45: Shows the damped Gain from the perspective of all of the piezos when P3 provided the disturbance, and was the only one to damp

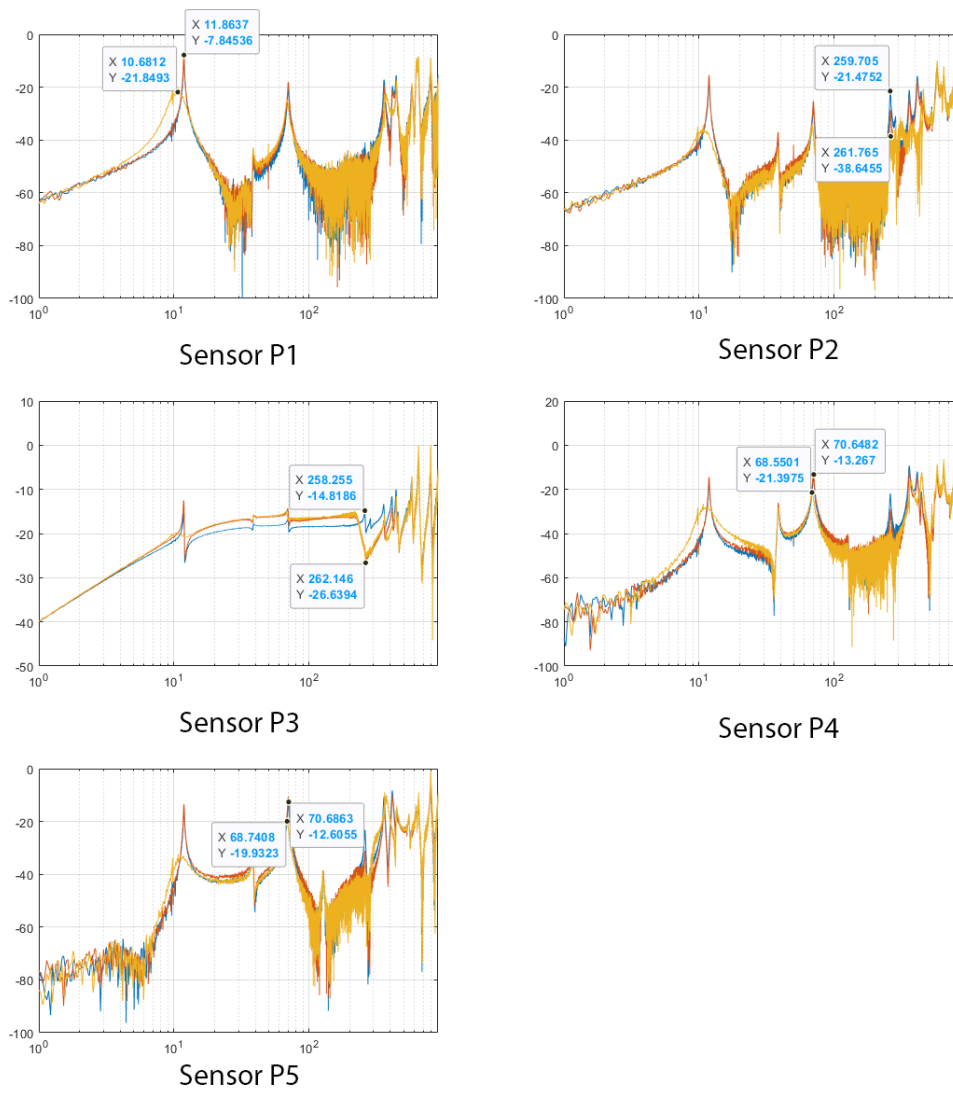


Figure 5.46: Shows the damped Gain from the perspective of all of the piezos when P3 provided the disturbance , and all of the piezos were used to damp

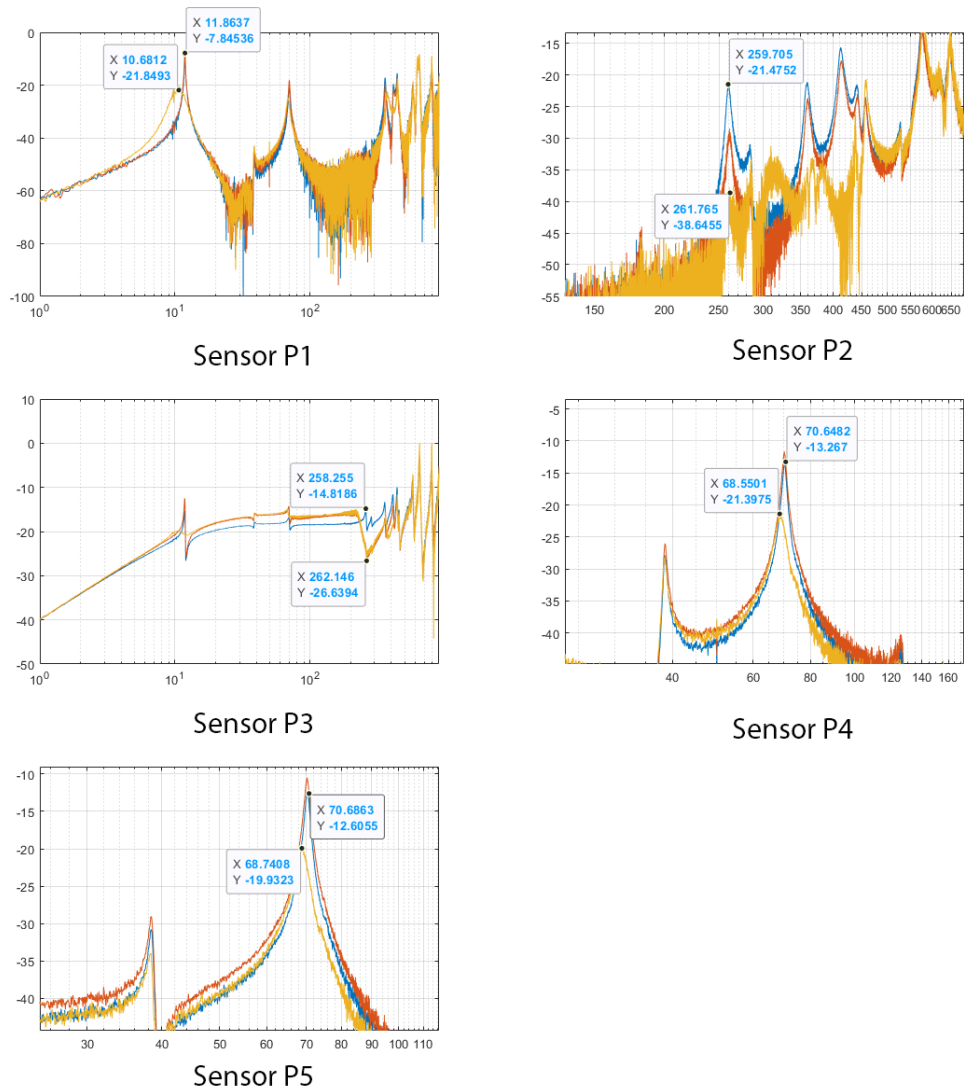


Figure 5.47: Shows the damped Gain from the perspective of all of the piezos when P3 provided the disturbance, and all of the piezos were used to damp, only now some plots are zoomed in at the respective frequency the piezo is supposed to damp.

The first mode is damped by 80% from the perspective of P1. P2 is once gain not damping, it is adding stiffness. Due to this the gain is about 86% less at the seventh mode from the perspective of its own sensor, though the damping from P3 contributes to this. The seventh mode is damped by 74% from the perspective of P3, but once again this is partly due the lowering of the gain by P2. The third mode is being damped by 61% by P4 and P5 from the perspective of P4, and 57% from the perspective of P5. Once again, good results overall.

5.6.4. P4 Cell

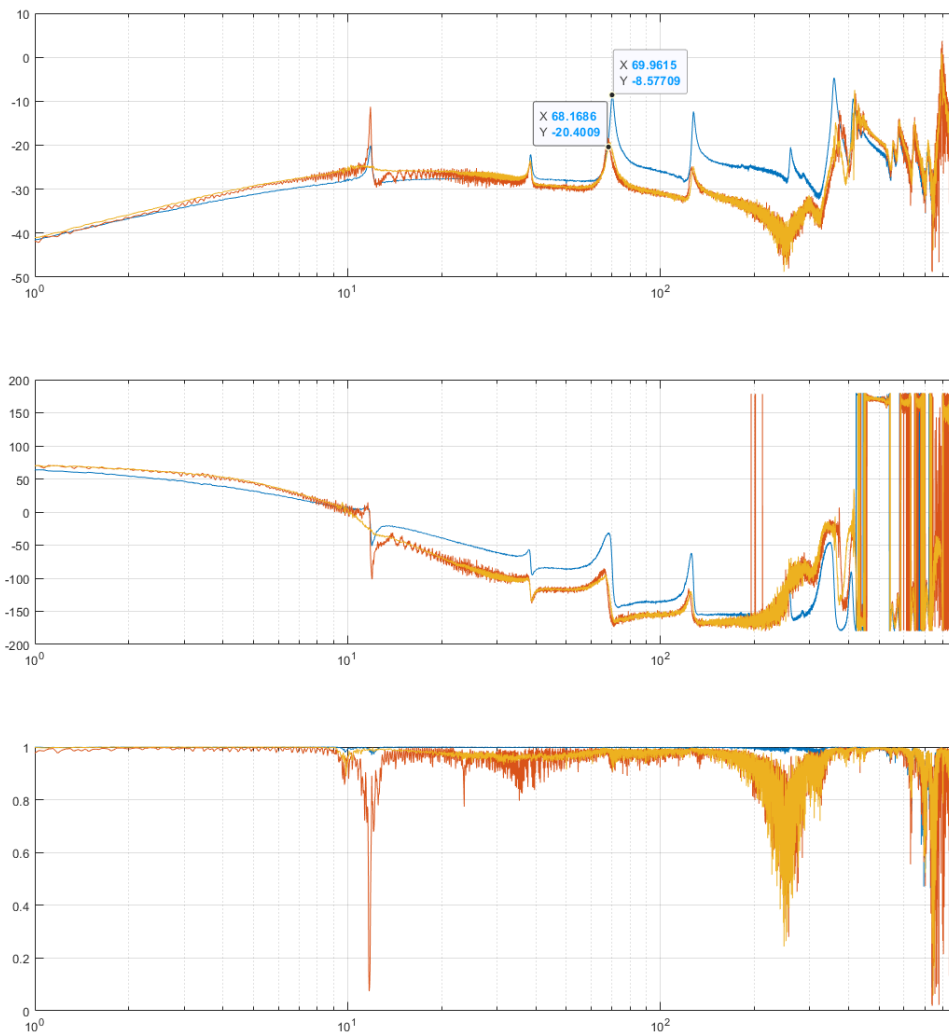


Figure 5.48: Shows the Gain, phase and coherence of all three sweeps when P4 provided the disturbance

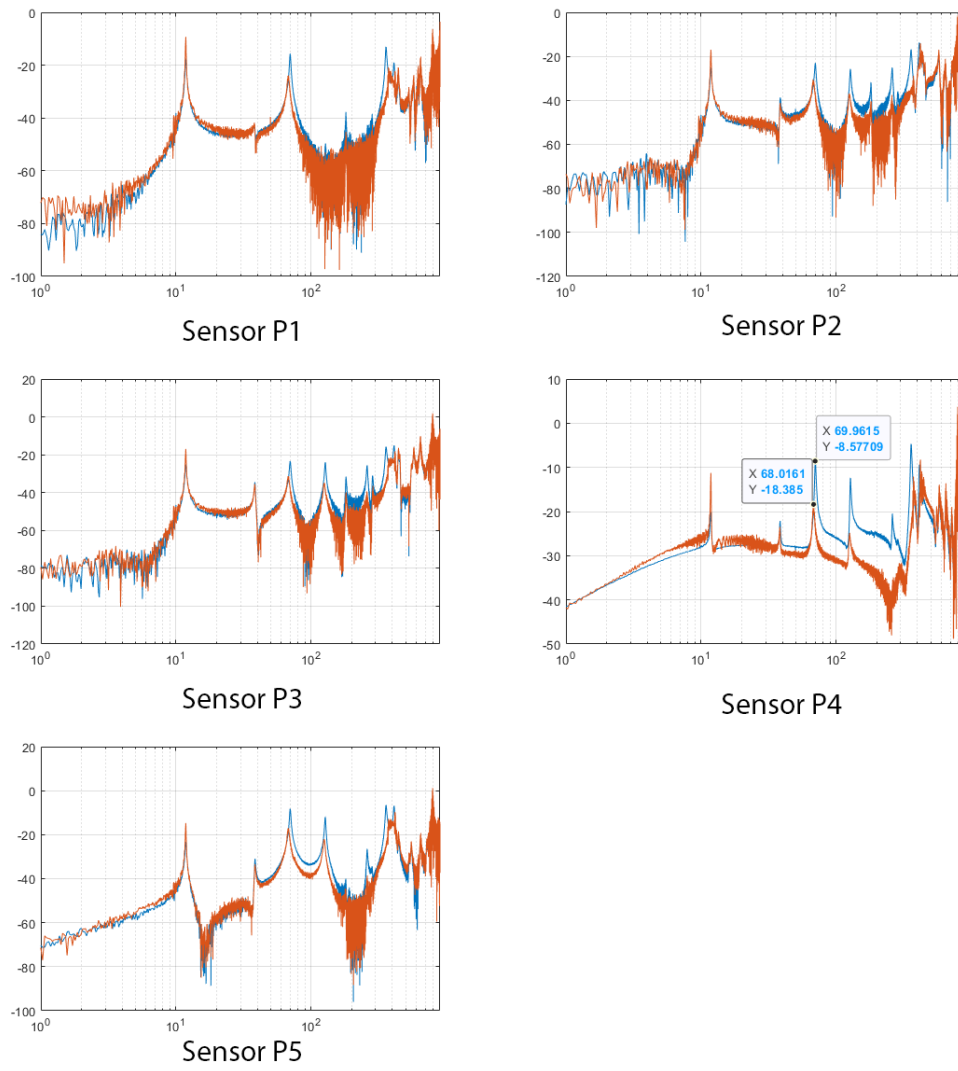


Figure 5.49: Shows the damped Gain from the perspective of all of the piezos when P4 provided the disturbance, and was the only one to damp

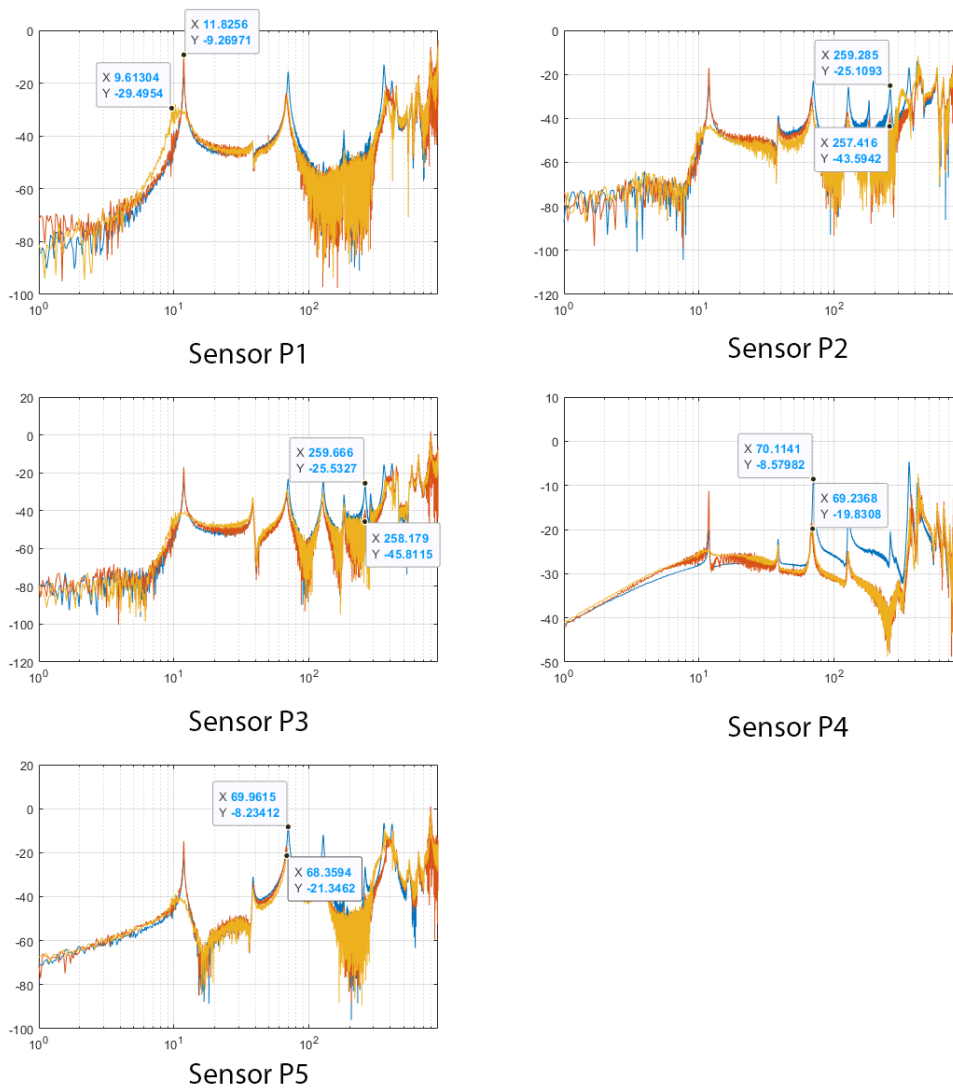


Figure 5.50: Shows the damped Gain from the perspective of all of the piezos when P4 provided the disturbance , and all of the piezos were used to damp

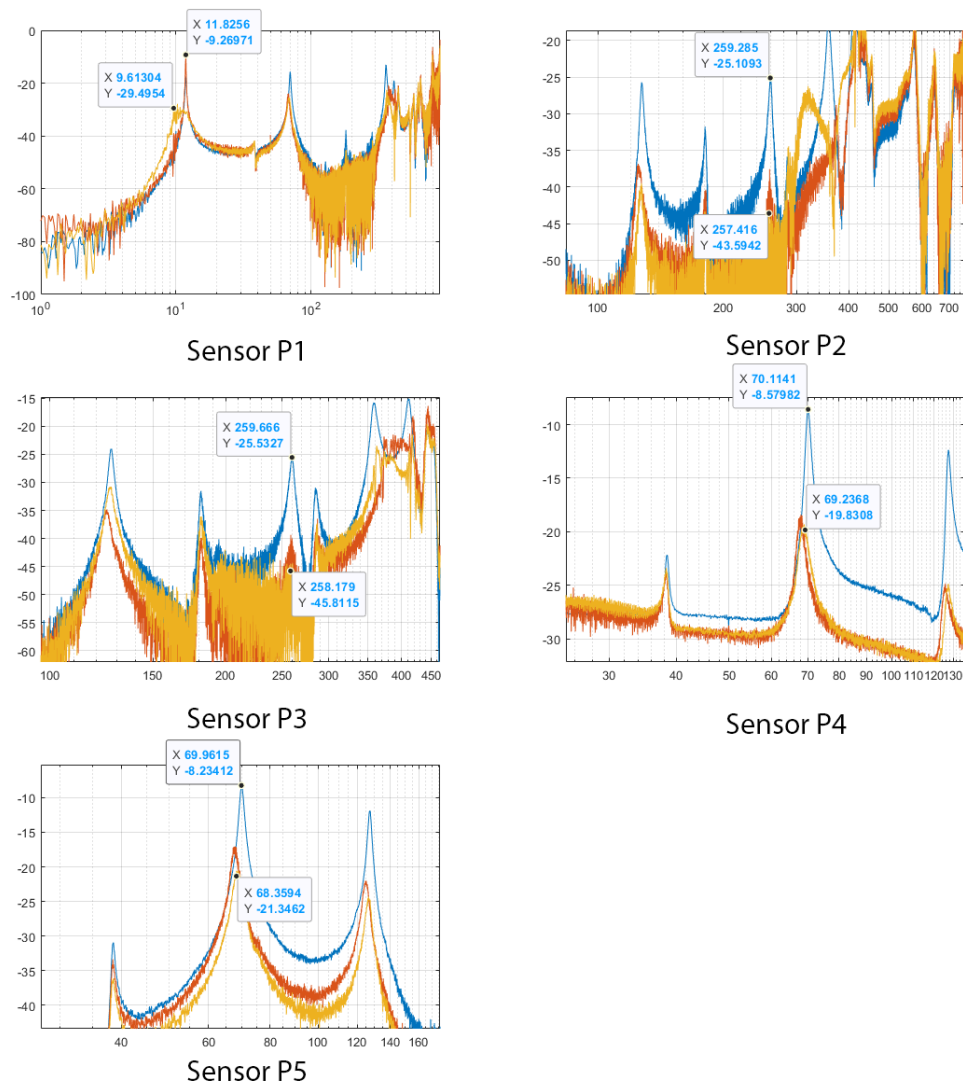


Figure 5.51: Shows the damped Gain from the perspective of all of the piezos when P4 provided the disturbance, and all of the piezos were used to damp, only now some plots are zoomed in at the respective frequency the piezo is supposed to damp.

The first mode is being damped by 87% from the perspective of P1. The data for P2 and P3 is really bad when any damping is turned on. Still they show lower gain at the 7th mode. Having said that, the gain at the 7th mode is 88% lower from the perspective of P2, due to damping from P3 and adding of stiffness by P2. The gain at the 7th mode is 90% lower from the perspective of P3. The gain at the third mode is 73% lower from the perspective of P4, due to the damping of P4 and P5. And the gain is 78% lower at the same mode from the perspective of P5, due to the damping of P4 and P5.

5.6.5. P5 Cell

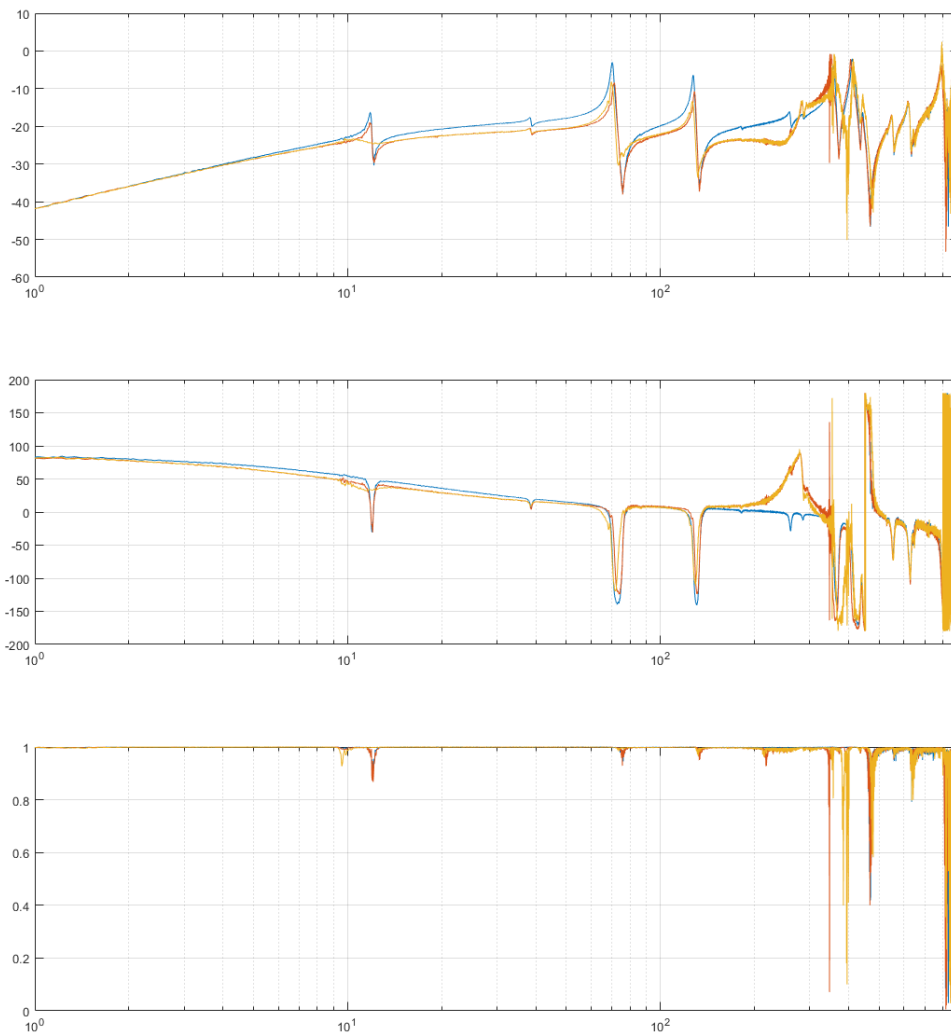


Figure 5.52: Shows the Gain, phase and coherence of all three sweeps when P5 provided the disturbance

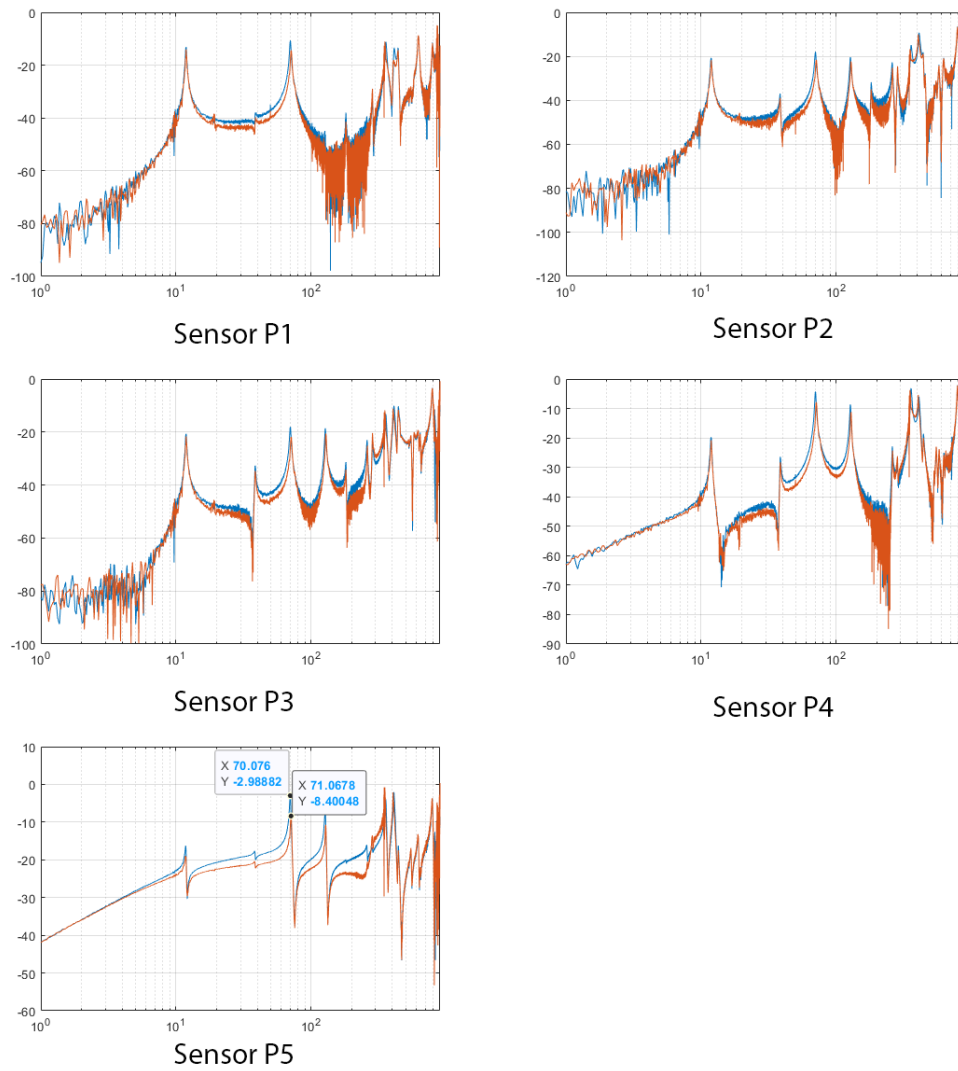


Figure 5.53: Shows the damped Gain from the perspective of all of the piezos when P5 provided the disturbance , and was the only one to damp

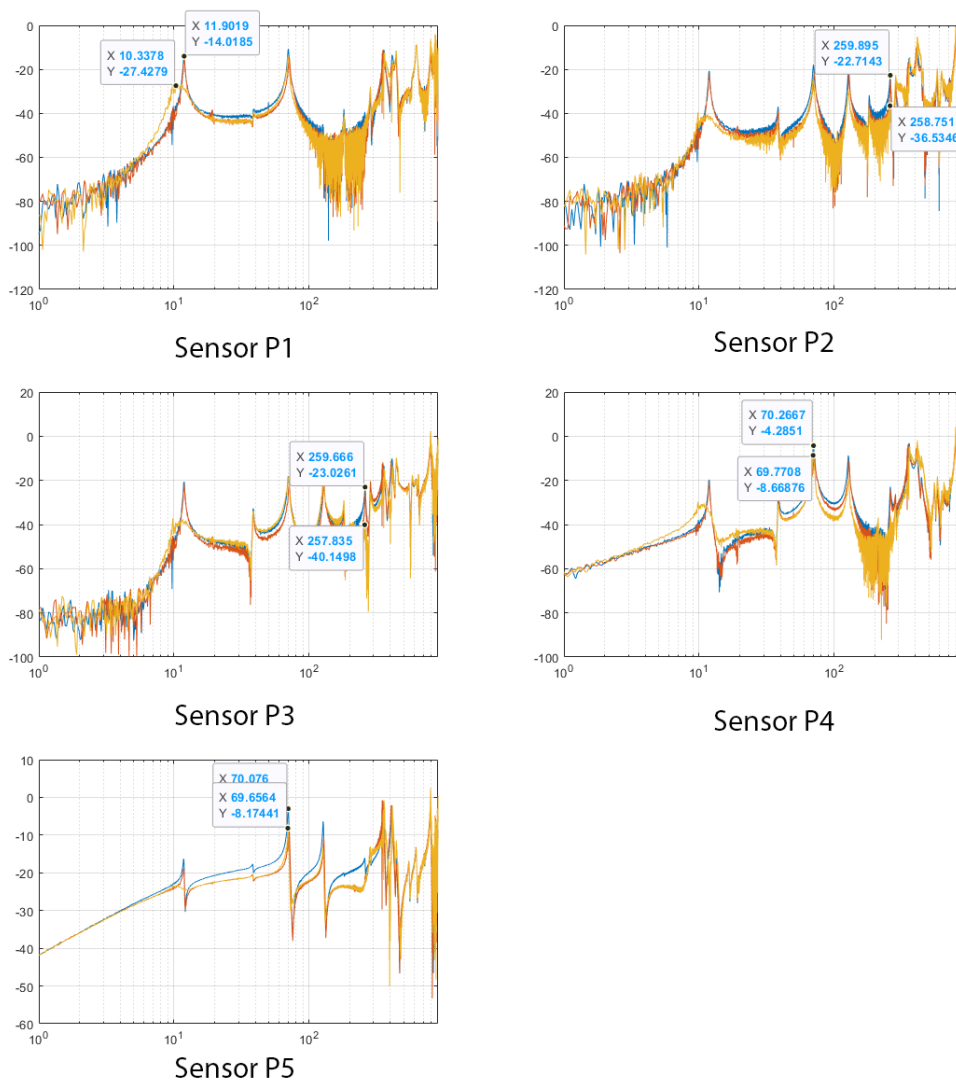


Figure 5.54: Shows the damped Gain from the perspective of all of the piezos when P5 provided the disturbance , and all of the piezos were used to damp

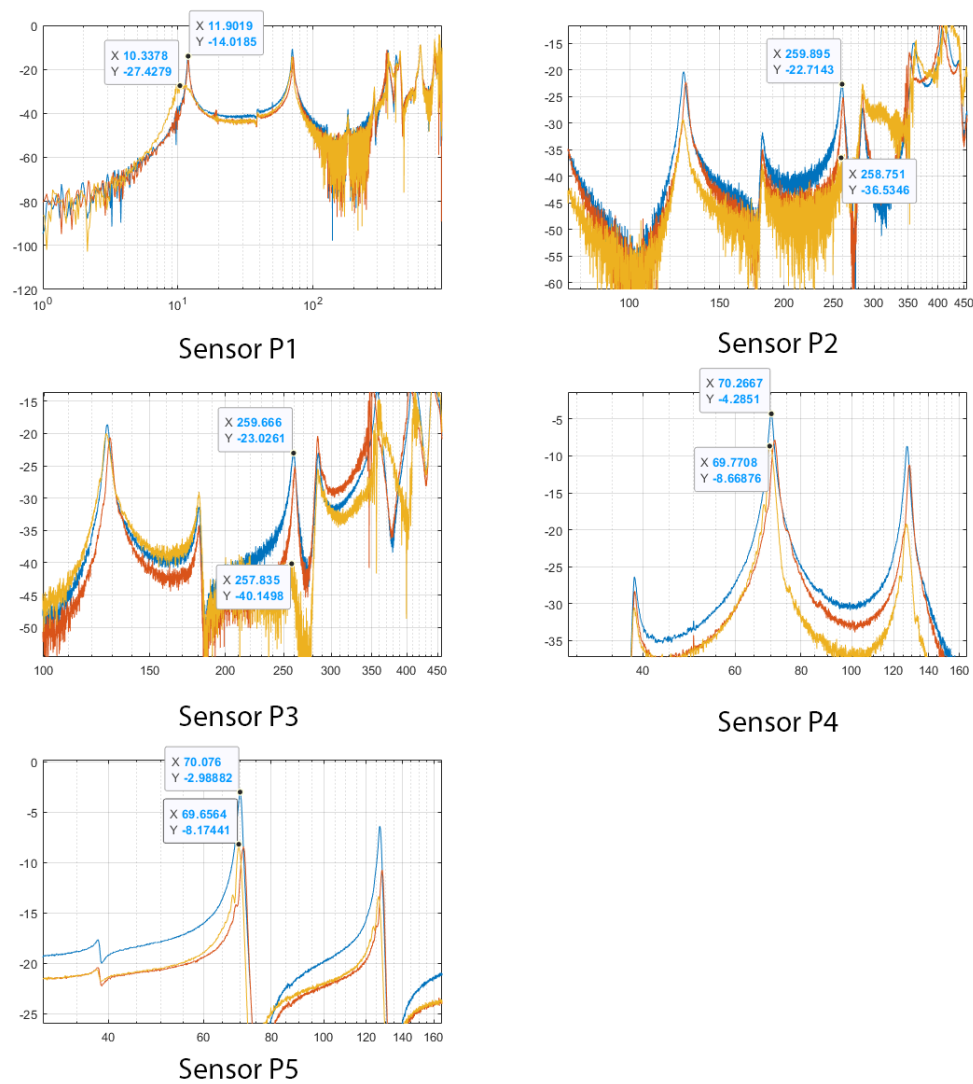


Figure 5.55: Shows the damped Gain from the perspective of all of the piezos when P5 provided the disturbance, and all of the piezos were used to damp, only now some plots are zoomed in at the respective frequency the piezo is supposed to damp.

The first mode is damped by 79% from the perspective of P1. The gain at the 7th mode is 80% lower from the perspective of P2, due to the influence of P2 and P3. The gain at the same mode is 86% lower from the perspective of P3, due to the influence of P2 and P3. The gain of the third mode is 40% lower from the perspective of P4 due to the influence of P4 and P5. And the gain at the same mode is 45% less due to the influence of P4 and P5 from the perspective of P5.

However looking at the plot of sensor 5, the mode is not being damped. But stiffness is being added. This is even more clear in the zoomed out bode plots. So P5 is not damping. It is doing the same thing that P2 is doing. Which is adding stiffness. These results are not consistent with what we saw previously. The third mode was always being damped from the perspective of P5. One possible explanation is that the damping of P4 was more powerful than the effect from P5. But why is that not the case now when all of damping is turned on?

5.6.6. Damping Result summarization

P1 The first mode is nicely damped by P1. And turning on all the piezo does not destabilize or increase the peak of the first mode. Every sensor in the flexure observes the first mode being damped. Only P4 sees a higher peak for the first mode when all of the dampers are turned on. The average damping of the first mode was 76.8%

P2 It does not look like damping. It looks like P2 is increasing the stiffness and thus reducing the overall gain. The good news is there were no problems when all of the piezos were damping. The average gain decrease of the seventh mode with the data from P2 and P3 combined is 80.7%, though this should be taken with a grain of salt, as this is also due to the stiffness adding effect of P2 and not just damping.

P3 The seventh mode is being damped but at the expense of increasing the gain in the lower frequencies. However looking at the other sensor this increase is not much due to the overall low gain of P3. So even though the sensor data from P3 makes it look like the gain is increasing a lot in the lower frequencies it is not. The P2 sensor seems to have picked up the damping of the seventh mode as well. The average gain decrease of the seventh mode with the data from P2 and P3 combined is 80.7%, though this should be taken with a grain of salt. As this is also due to the stiffness adding effect of P2 and not just damping.

P4 The third mode is being damped well by P4. And when all of the piezos are turned on everything works fine. There is a bit of increase in the gain of the lower frequencies due to spillover as is the case for P3, but it is minor. The average gain decrease at the third mode with the data from P4 and P5 combined is 55.1%. Though P5 seems to be adding stiffness and not damping, so the gain decrease can only partially be attributed to damping.

P5 This once again seems to be a case of not damping, but adding stiffness to the system. It lowers the gain but it is not damping. Though most of the time, the third mode is getting damped due the influence of P4. Only when the disturbance was provided by P5 did the damping of P4 not dominate the effects of P5. The average gain decrease at the third mode with the data from P4 and P5 combined is 55.1%. Though P5 as discussed here seems to be adding stiffness and not actually damping, so the gain decrease can only partially be attributed to damping.

Overall this can be considered a reasonable success. Given the FEA from chapter 4 it was known that damping torsional modes was always going to be difficult with front back asymmetric flexures. But the most important point is that all of the modes were damped by at least one of the pairs assigned to damp them. The first mode is the most important mode to damp as it produces the highest displacements and stresses, and it is being damped by at least 67%. The results are not as good as for the small flexure where the first mode was damped by 87%, but that flexure was smaller, lighter and narrower. And thus much easier to damp by the piezos than the bigger Open Flexures. Also that flexure was symmetrical from the front and back. Though in that flexure the piezos were not bonded and were free to move by a tiny bit due to the imperfect 3d printed cavities being slightly to big.

5.7. Reflections

Closed Flexures vs Open Flexures, Going in to the experiments the Finite Element Analysis favoured front back symmetrical flexures, where the piezos are in the center between the front and back, and their fronts and backs are connected to an equal amount of flexure material. But this type of design proved to be difficult to work with when it comes to connections and bugfixing. When those issues are sorted this type flexure should be explored once again. In fact now that adhesives are used this type of flexure may have other advantages. If a piezo is bonded on only one side, then every time the piezo bends away from that side, the piezo is peeling itself of the flexure. However when a piezo is bonded on both sides and clamped in between two halves of a flexure, pressure is applied on both sides, and the peeling is countered by the other side pressing the piezo back.

In the future a good option might be buying the PL112 – PL140 PICMA Bender actuators, putting them inside one half of a flexure and bonding them with adhesives, solder all the connections, test the flexure out as if it were an open flexure. If everything is fine, place the other half of the flexure with epoxy on it on top of the half containing the piezos, adhesive should be used on the parts containing the piezos. Given that adhesives are used one can make the cavities for the solder points and wires a bit larger. One big problem with the previous closed designs was the fact that the wires were tightly integrated in to the flexure halves, so the connections could not be made before hand. Of course another way to do this would be to leave holes where the connections are supposed to come, soldering does not need much space, so small holes can be made. Currently copper tape with conductive adhesive is used, and that requires a large surface area to be reliable.

Connections, this was a big problem to say the least. The notion of connections was given thought but only in the sense that the position of the connections should not be predefined so piezo actuators like the T220-H4BR-1305XB were preferred as it was thought that a connection could be applied anywhere. This is still a desirable characteristic. However the problem was with making the actual connections. In the case of the T220 actuator the nickel layer made it very difficult and unreliable to solder, while conductive adhesive and conductive epoxy proved to be unreliable as well. Plus it requires backside connections where as the competitors that have predetermined connecting points usually have them on all sides, and they are designed for soldering.

The soldering itself on predefined points works fine, but the point should not be vulnerable as it was with the BA series Bender actuators used as sensors. The soldering points have a very thin layer of copper on top of plastic, this layer can easily disconnect and since that spot is the only place the piezo can make a connection the piezo cannot be used any more This is doubly problematic if the piezo is already bonded to a flexure.

In conclusion making connections should have been researched more. But given the current experiences, piezo actuators like the PL112 – PL140 PICMA Bender series with predefined soldering points are more desirable. These Actuators were discussed at the end of Chapter 3 in section 3.6. Though these specific piezo actuators need 3 connections per piezo to make them work, which is not a desirable characteristic, as it makes it more complex and the amplifiers have to be used in a different mode which would mean the working of the amplifiers would have to be researched once again, they would have to be characterised again and the software partially rewritten.

Adhesives, initially the design was trying to avoid applying adhesives directly to the piezo. But that has shown to be too unreliable. Maybe in the future when 3d printing technology improves it can be attempted again. But at this point adhesives have to be used. And more research needs to be done to see which adhesives are the best suited for use with epoxy. As mentioned in 5.5.4 the Bison section, research should be done on which epoxies are used in the construction of piezo benders as these seem to be suited to the task. desirable characteristics of adhesives for a project like this are:

- Working time between 30 and 60 minutes
- Stiff but tough
- Resistance to impact and vibrations
- Dissolvable with specific non common and non hazardous agents

A longer working time is desirable as it gives more time to mix and spread the epoxy. To position the piezos and apply proper pressure. Obviously the stiffer it is the better the adhesive will transmit the displacement of the piezos, but it needs to be able to flex when strained by the piezos and not deform plastically or crack. It should be able to handle impacts and vibrations so the connections do not deteriorate too fast when the piezos vibrate. Ideally there should be some non hazardous agent to dissolve epoxy so the piezos can be easily and safely removed. Then there are some obvious required characteristics like compatibility with plastics, ceramics and metals, and being non poisonous.

Gain loss, the gain loss noticed during testing can be due to a few factors. Below is a list of the possible reasons.

- Adhesive deterioration
- PLA flexure deterioration
- Unreliable and/or deteriorating connections
- setup loosening
- Piezo actuators deterioration

It was assumed that the gain loss was mainly due to adhesives deteriorating. And given that this loss was not noticed in the smaller flexures where the piezos were not bonded, this is the most likely culprit. But at the same time, there is not much repeated data left from the small flexures and attention was not specifically paid to gain loss. So this might have just been missed. Also the smaller flexures were bonded by epoxy to one another. But this connections was over a larger surface, a surface that received less stress. And the connections between PLA and PLA maybe better then between Piezo and PLA.

However other reasons for gain loss might be the deterioration of the PLA flexure itself. The flexure may produce micro cracks. 3d printing lays down layers, these might be slowly coming loose due to vibrations. Another reason might be deteriorating connections. Connections that are not soldered are unreliable and could deteriorate.

The flexure was held by pressure coming from four screws, these could have been loosening during the experimentations. They were checked and seem to be holding, but it was not possible to check how much force they were applying to the flexure to clamp it down.

And the final reason for the gain loss might be piezos themselves, this seems unlikely as piezo should be good for many cycles. But they could be exposed to too much heat or voltage by accident during operation which could shorten their lifespan.

Flexure Material, PLA was chosen as it showed low inherent damping, it is cheap, available and works with the 3d Printers available. However there might be other materials more suited for this task. Materials which can be 3d printed with more accuracy, have lower inherent damping, or can handle vibrations better.

Amplifier phase lag, this wasn't tested in this project unfortunately but the amplifiers themselves most likely have phaselag which will influence the ability to damp higher modes.

5.8. Recommended future designs

Given what is know now, what would the recommendations be for a future design.

5.8.1. PICMA PL Symmetrical Flexure

Given the trouble with connections, the first thing I would do is use different actuators. In this case one from the PICMA PL series, these are shown in Figure 5.56. They were discussed in Chapter 3, section 3.6. They have three soldering points on a single side to make the connections. The points themselves look to be structurally strong. This would allow for reliable connections. This type of actuator is a bit thicker, but it can provide almost twice as much displacement and has a higher eigenfrequency. The biggest drawback is the need for three connections to drive the actuator instead of two.

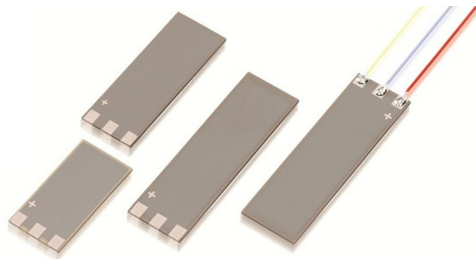


Figure 5.56: Shows the PICMA PL series actuator from Pi Ceramic. Note the three soldering points on one side.

I would recommend creating a symmetrical flexure made out of two halves, with the piezos in the center and everything bonded with epoxy including the piezos. So the piezos would be bonded on both the flexure halves. For sensing the same piezos should be used as were used in this thesis. They have structurally weak soldering points, but they are narrow and do not add to much stiffness to the structure. Figure 5.57 shows the design of this new flexure. It is called the PICMA flexure. And Figure 5.58 shows a couple of nice renders of this flexure. As the flexure is just an idea, none of the dimensions are final, it is just a mock-up, so not part drawing will be provided.

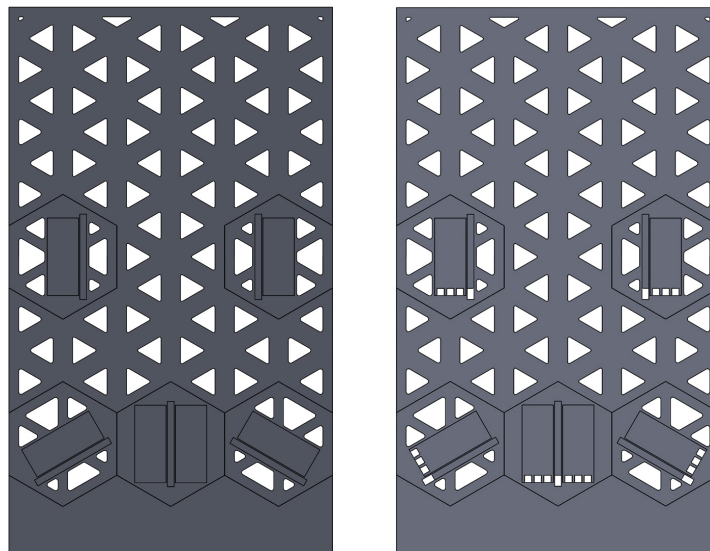


Figure 5.57: Left shows one flexure half, and right the opposite flexure half. Note the opposite flexure half has holes for connections to the sensors and actuators.

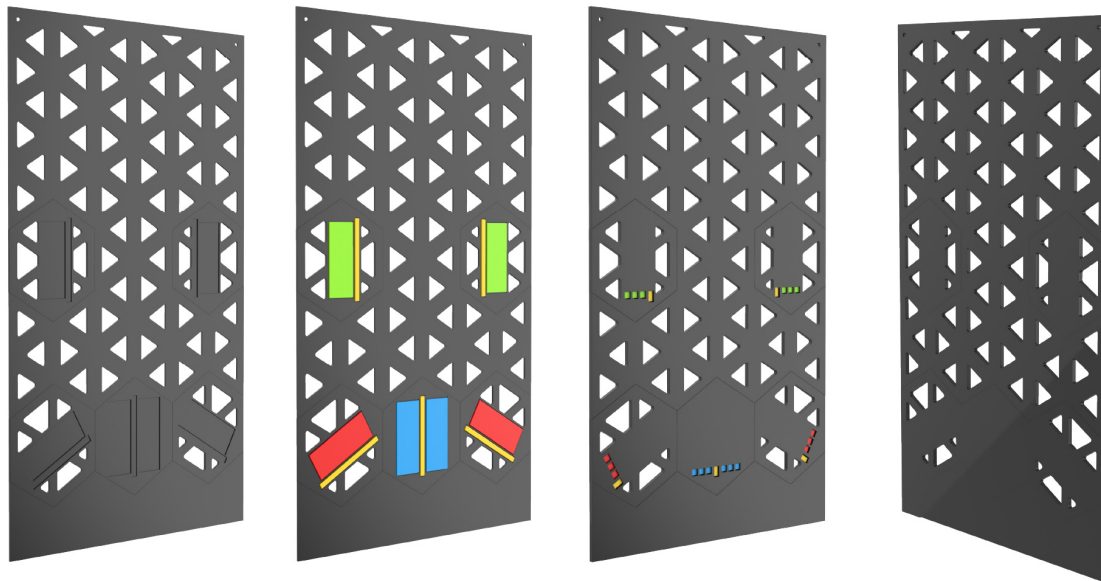


Figure 5.58: Shows the PICMA Flexure. From left to right we have a naked flexure half, same half with piezos, with the other half bonded, and finally the backside.

5.8.2. Advanced Real Flexure

If the above PICMA flexure works out, then work should be put towards a flexure with more advanced cells. The best we can do with current technology are hexagonal cells with six individual elements. The design of these cells has been extensively discussed in Chapter 3, section 3.3.

At the end of Chapter 4, in 4.7 two more realistic designs were analysed using Finite Element Analysis. I recommend one of these, namely the Advanced Real Symmetric Flexure. It is shown in Figure 5.59 and Figure 5.60. It uses a single hexagonal cell filled with six piezo elements made by cutting two commercially available bending actuators as shown in Figure 5.61. The piezos should be run in pairs, as marked by their colours. It does need some way to integrate sensors or it could use a laser sensor. A laser sensor could be aimed at the upper right or left corner to detect the first mode, which is a bending mode, and the second mode which is a torsional mode. The flexure is designed to flair out so the second mode is the torsional mode.

A more advanced version could use split piezos located in either flexure half and in between then sensing piezos.

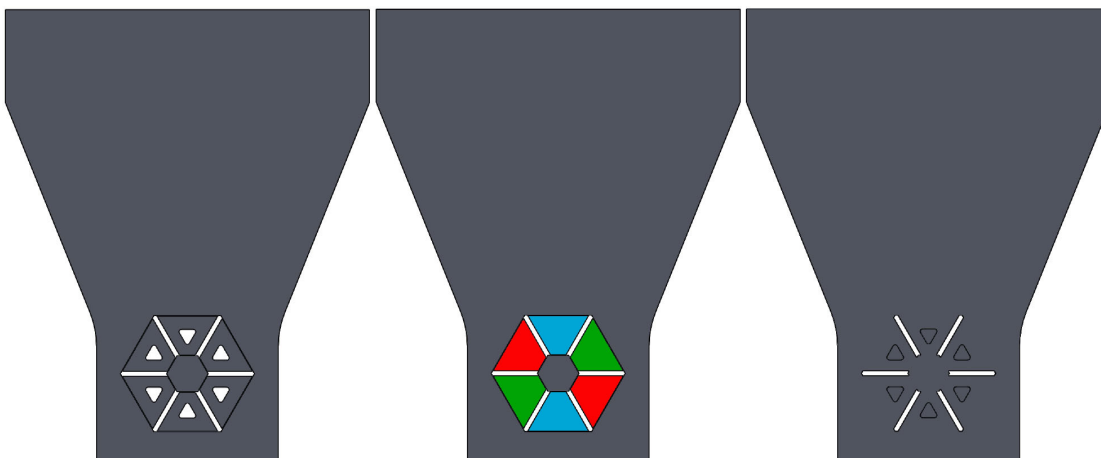


Figure 5.59: Shows the advanced real flexure. Left with no piezos, middle with six bending actuators (pairs are marked by colour), and right with the other half on top

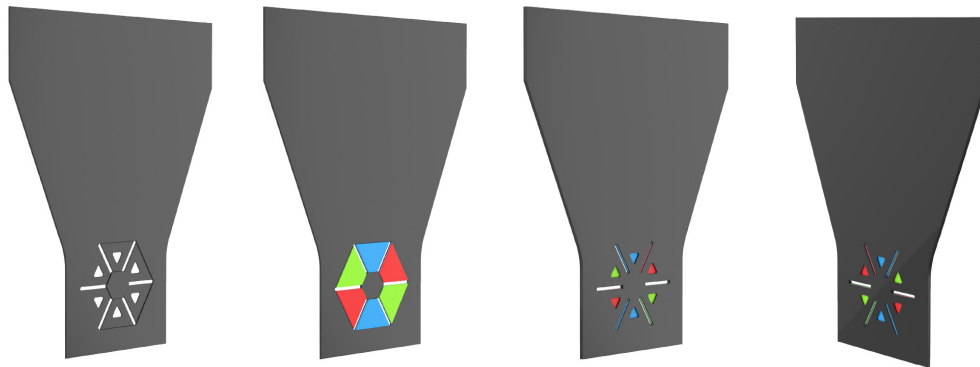


Figure 5.60: Shows the advanced real flexure. From left to right, shows a naked flexure half, same half with piezos, with the other half bonded, and finally a backshot.

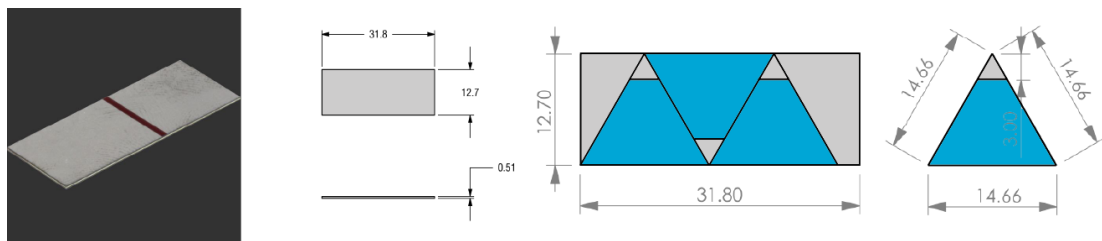


Figure 5.61: Left shows the real piezo bender (T220-H4BR-1305XB). Right shows how the triangular piezo pieces used in the model in Figure 5.59 and 5.60 can be cut. It shows all the relevant dimensions.

If a full flexure is ever made I recommend using a different type of advanced cell and pattern than the one used in the advanced design above. I recommend using the cell shown in Figure 5.62, and in the same cell pattern as the PICMA flexure. The advantages of this cell design are discussed in Chapter 3, section 3.3. But to cut a long story short, this type of cell and pattern can create better lines of force to damp the various modes. The reason for using the other type of cell in the flexure above is because that type of shape can be more efficiently cut out of a rectangular bender. It should be noted that bigger benders can be bought, for example a bender of the same type as the bender in Figure 5.61 but measuring 63.5x31.8x.51 can be bought for 1.5 times the price, though it is five times the size. It is called the T220-H4BR-2513XB Piezoelectric Bending Transducer[60], it's from the same company. The biggest problem with these piezos is that their coating makes soldering unreliable, hence the PICMA actuators in the PICMA Flexure. So maybe conductive epoxy could be tried to make the connections, though that is not as reliable as soldering.

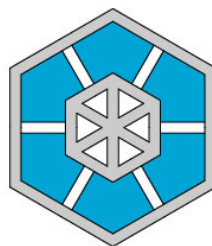


Figure 5.62: Shows a better type of advanced cell.

6

Conclusions & Recommendations

This thesis set out with the goal to develop the first prototype demonstrator of a metamech flexure with integrated piezo elements. Research revealed the potential to create flexures with advanced cells capable of exerting force in multiple directions. The initial end goal was to create a flexure housing such advanced cells. However this turned out to be too ambitious. Two working flexures were created, one relatively simple. But both demonstrated that the concept of integrating active damping elements worked well. However much of the useful knowledge generated during this thesis came from the initial research and Finite Element Analysis. Overall the project succeeded in showing the potential of metamech flexure, but did not achieve the more advanced goals nor do a comparison between metamech active damping and traditional ways to do active damping.

6.1. The Research

Materials

The initial research on the inherent damping of several materials showed those materials had very low damping ratios and thus could be used for damping tests. Those materials are Aluminium (Alu), Polycarbonate (PC), Polyoxymethylene (POM), 3d printed Polylactic acid (PLA), and PLA in combination with an Epoxy, the epoxy was the UHU quickset.

Cell Patterns

A more important conclusion was that Hexagonal cell patterns were the best suited for cellular flexures. Hexagons and triangles both have three useful rotational symmetries but the hexagon is easier to work with and can accommodate more mechanisms. A mechanism implemented in a hexagonal cell will always result in a smaller and more efficient cell than the same sized mechanism in a triangular cell.

But not all hexagon patterns are equal, research showed that patterns where the hexagon corner points along the longest axes of a flexure (pointy pattern) are better than patterns where the hexagon flat edges point along the longest axis (flat pattern). This is because the pointy pattern can form straight lines of force to damp the bending modes. Whereas the flat pattern forms zigzagging lines.

But it doesn't end there, piezos inside a hexagon can be aligned with the flat edges or the corners. And a pointy pattern with piezos aligned with the corners is overall superior. The research also showed a lot of patterns which were bad.

The research also focused on more advanced hexagonal cells that were subdivided into six smaller (piezo) cells. Which at their simplest had triangular or diamond shapes. These could be driven in pairs, whereby opposite elements behaved as one element or individually. Research showed that a hexagon in a pointy pattern with six diamond shaped inner elements was the best.

Further research showed that if those elements were separated by their adjacent neighbours with empty space, their force would only be directed from the center of the cell outwards. This would improve directionality, as normally piezos exert force all around them. But to do this the cell would need an inner smaller hexagon, and the diamond shapes would have to be turned in to pentagonal shapes, or six sides shapes, these are shown in Figure 3.14. Figures an text explaining this properly can be found in Chapter 3 section 3.3

6.2. Finite Element Analysis

Symmetrical Flexures

The most useful conclusions from the Finite Element Analysis comes from the last section. It is the fact that front and back symmetrical flexures where piezos sit in the center and have equal contact with their front as well as their backside with the flexure are better for damping torsional modes. For bending modes it does not matter much.

Flextensional mechanisms

Another conclusion was that flextensional mechanism with stack actuators do not work. At least not in the configuration they were tested in. Which is with one stack in the center of the bending plane of the flexure. Maybe some more advanced designs with smaller stacks inside flextensional mechanisms located in front of, and behind the flexing plane could work as in those positions the flextensional mechanism would more clearly be stretching or compressing the stack. Though the Finite Element Analysis showed the problem to be with the force transfer from the stack to the flexure, so even this suggested solution might not work.

Bender vs Split

A bender design is one where two piezo layers are close together and placed along the bending plane of the flexure. A split design is where the two layers are taken apart and put near the front and back surface. Several analysis were done on cells containing these designs, and also where these designs were integrated in to flexures. Furthermore there were basic designs, consisting out of piezo elements that can be bought and advanced design like those talked in the section above, with cells containing six different piezo elements.

Several sweep studies were done with the models integrated in to flexures, where the width and length was changed. These showed the bender as the best overall design. The basic split design was better in certain situations where the width of a flexure exceeded 75 mm. But the difference after those 75 mm were exceeded was not that big. While the bender design showed much better displacement in narrower flexures. In the advanced design the same pattern was observed, but the split design never exceeded the performance of the bender design.

However all of the cells were hollow hexagons, when flexure material is added as it most likely would be in any real design the split design can work better as shown in the flexure sweeps where the piezos were incorporated inside a flexure without the hexagonal cell. In a real design the piezo elements would most likely be bonded by their back and/or front surfaces instead of just the top and bottom like in the FEA. And this is where the split design shines, although it matters how much flexure material is added. At some point, the extra force the split design can exert exceeds the amplification advantage the bender has.

6.3. Practical design & Experiments

Small Flexure

This was the first attempt. It was a narrow long flexure with two piezos inside, one near the bottom (designated P1) end and one closer to the center (designated P2) when looking from above at the flexure. The piezo were clamped in between two flexure halves which were bonded by epoxy, though no epoxy was used on the

piezo actuators themselves. All wires were contained inside the flexure and led out through the bottom. This flexure worked very well. Two important test runs were done. One where P1 provided the disturbance and both piezos damped, and one where P2 provided the disturbance and both piezos damped. In the first run, with P1 providing the disturbance the first mode was damped by 85% and the second by 56%. In the second run, where P2 provided the disturbance, the first mode was damped by 87% and the second by 45%. This was a great success and showed the potential of meta mech flexures.

Big Closed Flexure

This was a bigger version of the smaller flexure with six piezo actuators and six sensors. Clamped in the same fashion as the small flexure, with all the wires routed through the flexure. This turned out to not work as getting the connections right failed in the two attempts at this flexure. Plus routing all the cables through the flexure made it way too complex. At the same time, the cavities/indentations housing the piezos had to be made larger as angled cavities turned out to be too small. But this made the other ones too big, so piezos had too much space to move freely around and thus could not efficiently transfer forces to the rest of the flexure. Being bigger the flexure was also stiffer.

Open Flexure

This can be seen as the grand final flexure of this experiment. This is an open flexure with skeletal hexagonal design. It has the piezos positioned in more optimal spots than the big closed flexure. And uses the pointy pattern, with piezos facing a corner. Being open the connections can be fixed. The flexures were intended to damp the first three modes. The first is a bendy mode, the second is a torsional mode, and the third is also a bendy mode.

Three were produced. The first one yielded the best results. The second and third were attempts at improvement. But yielded worse results. The second flexure optimized the stiffness a bit, improved the positioning of the sensor piezos and used a different epoxy. It produced good data during the identification process but in practice the third mode could not be damped. No matter what was tried the damping would always produce a higher gain peak than without damping. Due to time constraints this flexure was dismantled and a third was produced.

The third flexure changed the cell design containing the piezos, it made them stiffer and thicker, it also used a different epoxy. Unfortunately the system identification for this flexure was so bad that no damping attempts were made.

As mentioned the first flexure yielded the best results. Three modes were damped with this flexure. The first, the third and the seventh. Originally the second mode, a torsional mode was to be damped, but the piezo cells assigned to it could not observe it properly, so a higher mode, the seventh was chosen. One cell with double actuators was assigned to damp the first mode, two cells with a single actuator were assigned to damp the third mode and two cells with a single actuator were assigned to damp the seventh mode. The average gain decrease at the first mode was 76.8%, the average gain decrease at the third mode was 55.1% and the average gain decrease at the seventh mode was 80.7%. Though two cells were later found not to be damping but just adding stiffness and decreased the gain that way. One of the cells was assigned to damp the seventh mode and the other was assigned to damp the third mode. Luckily their counter pair did actually damp. The overall the damping was good, and remained good when all of the cells were damping at the same time.

Connections

Getting the connections right was very difficult. The actuators had a large area where connections could be made but the nickel coating made soldering difficult and conducting adhesive proved to be unreliable. The sensor piezos had really small spots where connections could be soldered. But these spots were structurally weak and could easily be pulled free leaving no spot to make connections. Talking about connections seems like it has no place in a conclusion to a thesis. But this proved to be so influential in the design of flexures that it has to be mentioned. The conclusions are, go for soldering and go for a piezo actuator with structurally sound soldering points. This will give more freedom in designing a flexure to house the actuator.

Gain loss

One thing noticed during experimentation was that flexure would steadily loose gain. There are several mechanism that could be responsible.

- Adhesive deterioration
- PLA flexure deterioration
- Unreliable and/or deteriorating connections
- Setup loosening
- Piezo actuators deterioration

These are talked about in more detail in Chapter 5, but adhesive deterioration is the most likely culprit. The problem is that in an open flexure the piezos are peeling themselves off every time they bend away from the flexure. This means that the system changes as more experiments are done. So a filter designed for a system today may not function as well tomorrow. This is an important point that needs to be addressed in future research.

6.4. Recommendations

Symmetrical Closed Flexure (PICMA Flexure)

This flexure is discussed at the end of chapter 5 in section 5.8, and the design is shown in Figure 5.57 and Figure 5.58. The finite Element Analysis showed a closed symmetrical flexure to be superior when it comes to damping torsional modes. These were the modes that none of the flexures in this thesis were able to damp. My proposition would be to go back to the two halves design only now with different actuators and using epoxy on the actuators themselves. Also this closed design should use the hexagonal pattern and piezo direction of the open Flexures.

What I propose is to use the PL112 – PL140 PICMA Bender actuators from piezo ceramic. These are actuators with a simple rectangular shape with what seems structurally sound soldering points at one end, all facing the same directions. Make two halves with square indents, put epoxy on the whole surface and in the indents. Put the piezo actuators inside. Do the same for the other half and put it on top. The design should have one rectangular hole or three smaller square or round holes where the soldering points are. Once the flexure epoxy has dried simply solder the connections to the piezo trough the holes. Now you have a closed of flexure with piezo elements in the center. The front and back of these piezo benders will have roughly the same surface to grip. These particular actuators are also a bit thicker and can exert more force then the T220-H4BR-1305XB Bender, so they should be able to deflect a stiffer flexure more easily. Put the sensors next to them and leave holes to solder the sensors. The only weak point of this flexure would be the sensors, as their connections are structurally weak. Also the PL PICMA series is more complex to drive as it needs three connections per actuator instead of two.

Piezo 3d printing

3d printing helped enormously in this project. And being able to print the piezo elements along with the flexure would be revolutionary. Research is being done in to this as part of the metamech project and we are a long way off. But I would like to reiterate the need for this. It would enable much more advanced designs.

Advanced designs

If the above mentioned "Symmetrical Closed Flexure (PICMA Flexure)" is a success then a working version of the symmetrical real advanced flexure shown at the end of Chapter 4 in Figure 4.37 could be attempted. This is also discussed at the end of Chapter 5 in section 5.8. And Figure 5.59 and Figure 5.60 show the design.

The design is fairly complete except a way to integrate sensors in to that flexure needs to be found. But the multi direction hexagonal cell is the goal to work towards with today's technology. Since that cell makes use of cut pieces of the T220-H4BR-1305XB Bender, which cannot be soldered reliably, one could put conductive epoxy inside the holes and put wires in those to connect the wires with the piezo surface. Though conductive epoxy was found to be not all that reliable.

The biggest problem with this design is that it does not account for any sensors. A split design could have the sensors in the center bending plane of the flexure and the actuators in front of and behind that plane. This would however be much more difficult when it comes to connections and it would require the cutting of extender piezo actuators instead of bending piezo actuators.

Routing and connections

Signal and power routing become a problem with more advanced designs. Even the single hexagonal advanced bender design proposed just above would have 12 connections without any sensors. A flexure with five of those cells instead of the more basic ones used in this thesis would have 60 connections, where as the most complex flexure used in this thesis had 22 with 10 of those being for sensors. Given that LED panels have millions of tiny independent connections in a flat panel, research should be done how to use that with these flexures.

Integrated electronics & amplifiers

This is an idea for a bit farther in to the future, but while integrating sensors and actuators in flexure, one should also consider integrating cells with microprocessors and piezo amplifiers. Or integrating the amplifiers inside the cell containing the piezos. This would drastically reduce the lag and enable to cells to damp much higher modes.

Bibliography

- [1] N. Lobontiu, *Compliant mechanisms: design of flexure hinges*. CRC Press, 2003.
- [2] "About compliant mechanisms." [Online]. Available: <https://www.compliantmechanisms.byu.edu/about-compliant-mechanisms>
- [3] D. S. C. W., *Vibration damping, control, and design*. Taylor and Francis, 2007.
- [4] S. O. R. Moheimani and A. J. Fleming, *Piezoelectric Transducers for Vibration Control and Damping*. Springer-Verlag London Limited, 2006.
- [5] P. Aumjaud, C. Smith, and K. Evans, "A novel viscoelastic damping treatment for honeycomb sandwich structures," *Composite Structures*, vol. 119, no. 119, p. 322–332, Jan 2015.
- [6] P. Aumjaud, J. Fieldsend, M.-A. Boucher, K. Evans, and C. Smith, "Multi-objective optimisation of viscoelastic damping inserts in honeycomb sandwich structures," *Composite Structures*, vol. 132, no. 132, p. 451–463, Nov 2015.
- [7] B. Yan, K. Wang, Z. Hu, C. Wu, and X. Zhang, "Shunt damping vibration control technology: A review," *Applied Sciences*, vol. 7, no. 5, p. 494, 2017.
- [8] F. dell'isola, C. Maurini, and M. Porfiri, "Passive damping of beam vibrations through distributed electric networks and piezoelectric transducers: Prototype design and experimental validation," *Smart Materials and Structures*, vol. 13, 02 2004.
- [9] F. Tateo, B. Beck, M. Collet, M. Ouisse, K. Cunefare, and M. Ichchou, "Vibration control of plates through a periodic array of shunted piezoelectric patches with negative capacitance circuits," vol. 9057, 04 2014, p. 90572E.
- [10] M. Tawfik, "Vibration control of plates using periodically distributed shunted piezoelectric patches /," Ph.D. dissertation, 05 2003.
- [11] M. Tsai and K. Wang, "On the structural damping characteristics of active piezoelectric actuators with passive shunt," *Journal of Sound and Vibration*, vol. 221, no. 1, p. 1–22, Mar 1999.
- [12] S. S. Aphale, A. Fleming, and R. Moheimani, "Integral resonant control of collocated smart structures," *Smart Mater. Struct.*, vol. 16, pp. 439–446, 04 2007.
- [13] L. Marinangeli, F. Alijani, and S. H. HosseinNia, "Fractional-order positive position feedback compensator for active vibration control of a smart composite plate," *Journal of Sound and Vibration*, vol. 412, pp. 1 – 16, 2018. [Online]. Available: <http://www.sciencedirect.com/science/article/pii/S0022460X17306727>
- [14] A. denHamer, G. Angelis, and N. Roozen, "Broad-band active vibration suppression using ppf focused on industrial application," *IEEE/ASME Transactions on Mechatronics*, vol. 10, no. 2, p. 146–153, Apr 2005.
- [15] M. Thomas, "Flexures," 2019. [Online]. Available: <http://web.mit.edu/mact/www/Blog/Flexures/FlexureIndex.html>
- [16] [Online]. Available: <https://www.uhu.com/en/product-page/plus-schnellfest/5485>
- [17] [Online]. Available: <https://www.ni.com/nl-nl/support/model.usb-6002.html>
- [18] [Online]. Available: <https://www.micro-epsilon.com/download/manuals/man--optoNCDT-1420--en.pdf>
- [19] G. Bautista, "Tessellation: The mathematics of tiling," 2014.

- [20] —, “Regular tessellations: Why only three of them?” May 2016. [Online]. Available: <http://mathandmultimedia.com/2011/06/04/regular-tessellations/>
- [21] “What is a tessellation? definition, examples and types of tessellations. funmaths.com,” 2018.
- [22] Q. Zhang, X. Yang, P. Li, G. Huang, S. Feng, C. Shen, B. Han, X. Zhang, F. Jin, F. Xu, and T. J. Lu, “Bioinspired engineering of honeycomb structure – using nature to inspire human innovation,” *Progress in Materials Science*, vol. 74, pp. 332 – 400, 2015. [Online]. Available: <http://www.sciencedirect.com/science/article/pii/S0079642515000377>
- [23] Z. Wang, Y. Zhang, and L. Jiefu, “Comparison between five typical reinforced honeycomb structures,” 01 2015.
- [24] S. J. Rupitsch, *Piezoelectric Sensors and Actuators: Fundamentals and Applications*. Springer, 2019.
- [25] J. Sirohi and I. Chopra, “Fundamental understanding of piezoelectric strain sensors,” *Smart Structures and Materials 1999: Smart Structures and Integrated Systems*, 1999. [Online]. Available: <http://www2.pitt.edu/~qiw4/Academic/ME2082/references/FundamentalPiezo1.pdf>
- [26] D. Haller, A. Paetzold, N. Losse, S. Neiss, I. Peltzer, W. Nitsche, R. King, and P. Woias, “Piezo-polymer-composite unimorph actuators for active cancellation of flow instabilities across airfoils,” *Journal of Intelligent Material Systems and Structures*, vol. 22, no. 5, p. 461–474, 2011.
- [27] A. A. Bent and N. W. Hagood, “Piezoelectric fiber composites with interdigitated electrodes,” *Journal of Intelligent Material Systems and Structures*, vol. 8, no. 11, p. 903–919, 1997.
- [28] Xiu-Juan, K.-C. Zhou, X.-Y. Zhang, and D. Zhang, “Development, modeling and application of piezoelectric fiber composites,” *Transactions of Nonferrous Metals Society of China*, vol. 23, no. 1, p. 98–107, 2013.
- [29] C. Niezrecki, D. Brei, S. Balakrishnan, and A. Moskalik, “Piezoelectric actuation: State of the art,” *The Shock and Vibration Digest*, vol. 33, no. 4, p. 269–280, 2001.
- [30] K. Denishev and V. Tabakov, “Meander-line piezoelectric actuator,” 11 2020.
- [31] F. Mohammadi, A. L. Kholkin, B. Jadidian, and A. Safari, “High-displacement spiral piezoelectric actuators,” *Applied Physics Letters*, vol. 75, no. 16, p. 2488–2490, 1999.
- [32] M. Allahverdi, A. Hall, R. Brennan, M. Ebrahimi, N. Hagh, and A. Safari, “An overview of rapidly prototyped piezoelectric actuators and grain-oriented ceramics,” *Journal of Electroceramics*, vol. 8, pp. 129–137, 08 2002.
- [33] W. Zouari, T. Ben Zineb, and A. Benjeddou, “A fsdt-mitc piezoelectric shell finite element with ferroelectric non-linearity,” *JOURNAL OF INTELLIGENT MATERIAL SYSTEMS AND STRUCTURES*, vol. 20, pp. 2055–2075, 11 2009.
- [34] I. (PI), “Pi (physik instrumente) l.p.” 2019. [Online]. Available: <https://www.pi-usa.us/en/apps-tech/technology/piezoelectric-drives/piezo-actuators/>
- [35] P. A. York, N. T. Jafferis, and R. J. Wood, “Meso scale flextensional piezoelectric actuators,” *Smart Materials and Structures*, vol. 27, no. 1, p. 015008, 2017.
- [36] P. R. Ouyang, W. J. Zhang, and M. M. Gupta, “Design of a new compliant mechanical amplifier,” *Volume 7: 29th Mechanisms and Robotics Conference, Parts A and B*, 2005.
- [37] B. Xu, Q. Zhang, V. Kugel, Q. Wang, and L. Cross, “Optimization of bimorph based double amplifier actuator under quasistatic situation,” *ISAF 96. Proceedings of the Tenth IEEE International Symposium on Applications of Ferroelectrics*, 2001.
- [38] [Online]. Available: <https://piezo.com/collections/piezoelectric-actuators-motors/products/piezoelectric-bending-transducer-t220-h4br-1305xb>

- [39] P. C. GmbH, “P-876 duraact patch transducer.” [Online]. Available: <https://www.piceramic.com/en/products/piezoceramic-actuators/patch-transducers/p-876-duraact-patch-transducer-101790/#description>
- [40] —, “P-878 duraact power patch transducer.” [Online]. Available: <https://www.piceramic.com/en/products/piezoceramic-actuators/patch-transducers/p-878-duraact-power-patch-transducer-101795/#description>
- [41] —, “Pl112 – pl140 picma® bender.” [Online]. Available: <https://www.piceramic.com/en/products/piezoceramic-actuators/bender-actuators/pl112-pl140-picma-bender-103000/>
- [42] [Online]. Available: <https://piezo.com/collections/piezoelectric-actuators-motors/products/piezoelectric-extending-transducer-t220-h4br-1305ye>
- [43] [Online]. Available: <https://www.piezodrive.com/actuators/150v-piezo-stack-actuators-2/>
- [44] “Material properties.” [Online]. Available: <https://support.piezo.com/article/62-material-properties>
- [45] “Overview of materials for epoxy adhesive.” [Online]. Available: <http://www.matweb.com/search/datasheettext.aspx?matguid=c1ec1ad603c74f628578663aaf44f261>
- [46] [Online]. Available: <https://www.ni.com/nl-nl/support/model.crio-9039.html>
- [47] [Online]. Available: <https://www.ni.com/nl-nl/support/model.ni-9201.html>
- [48] [Online]. Available: <https://www.ni.com/nl-nl/support/model.ni-9264.html>
- [49] [Online]. Available: https://www.micro-epsilon.com/displacement-position-sensors/laser-sensor/optoNCDT_1750/?sLang=en
- [50] [Online]. Available: <https://www.tek.com/datasheet/digital-storage-oscilloscopes-0>
- [51] [Online]. Available: <https://www.delta-elektronika.nl/en/products/dc-power-supplies-150w-es150-series.html>
- [52] “Bd300 dual-channel 300v amplifier.” [Online]. Available: <https://www.piezodrive.com/product/bd300-300v-dual-channel-amplifier/>
- [53] [Online]. Available: <https://www.thorlabs.com/thorproduct.cfm?partnumber=DT25/M>
- [54] [Online]. Available: https://www.thorlabs.com/newgrouppage9.cfm?objectgroup_id=194
- [55] [Online]. Available: <https://www.thorlabs.com/thorproduct.cfm?partnumber=XE25A90#ad-image-0>
- [56] [Online]. Available: https://www.thorlabs.com/newgrouppage9.cfm?objectgroup_id=159
- [57] [Online]. Available: <https://www.piezodrive.com/modules/bd300-dual-channel-drivers/>
- [58] Dec 2019. [Online]. Available: https://www.3m.com/3M/en_US/company-us/all-3m-products/~-/3M-Scotch-Weld-Epoxy-Adhesive-DP460/?N=5002385+3293241275&rt=rud
- [59] [Online]. Available: <https://www.bison.nl/nl/product.2288>
- [60] [Online]. Available: <https://piezo.com/collections/piezoelectric-actuators-motors/products/piezoelectric-bending-transducer-t220-h4br-2513xb>

Appendices

A

A.1. Appendix A (H3 Research)



Figure A.1: UHU Quickset Epoxy. This is the epoxy used to bond tow halves of a 3d printed flexure and test out the damping

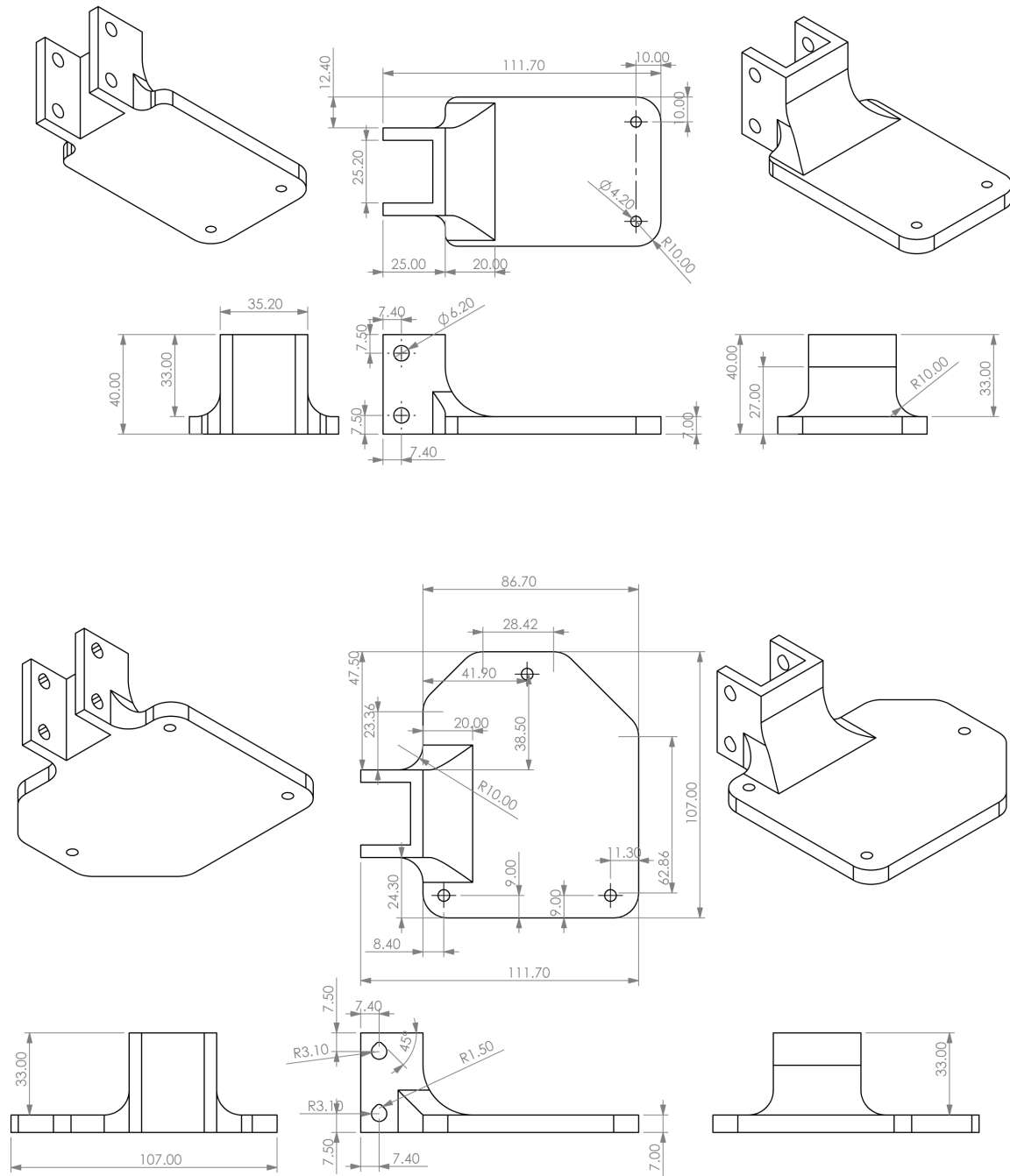


Figure A.2: Upper drawing) Laser Holder for the OptoNCDT 1420. Lower drawing) Laser Holder for the OptoNCDT 1750. Both are custom designed and 3d Printed.

Matlab Code used to find the eigenfrequencies and damping ratio in 3.2

```

1 clear all ,
2 close all ,
3 format compact ,
4 clc ,
5
6 % Sampling frequency in Hz

```



```

7     Fs     = 2e3                                     ;
8
9     % Retrieve all the files in a directory
10    %names = dir('D:\Google Drive\Thesis\Testing\06 Damping Test\013 01-11-2020 PLA\*.
        txt ');
11    names = dir('E:\Google Drive\Thesis\Testing\06 Damping Test\013 01-11-2020 PLA\*.txt
        ');
12
13    % the .\ indicates the home directory, so I can easily run this
14    % script between different PC's.
15    % names = dir('.\Damping Test\010 17-02-2020 PLA 3D 3mm\*.txt ')          ;
16    names = {names.name}                                     ;
17
18    % function to calculate the number of subfigs, downloaded from
19    % mathworks.
20    p = numSubplots(size(names,2))                               ;
21
22    for i = 1:size(names,2)
23        import = readmatrix(string(names(i)))                   ;
24        PC(1:length(import),i) = import(:,2)                   ;
25    end
26
27
28    for i = 1:size(PC,2)
29
30        % Need to calculate the mean so I will only use the values near
31        % the end after 3000, when the oscillation has been stabilized.
32        PC2 = PC(1000:end,i)                                     ;
33
34        % At the end there are values that dip really low, clearly error
35        % values. I want to remove them so I only use the values above 2.
36        k = find(PC2>2)                                         ;
37        PC3 = PC2(k)                                           ;
38        % subtract the mean so the oscillation oscillate around the zero
39        PC4(1:length(PC(:,i)),i) = PC(:,i) - mean(PC3)        ;
40
41        % Two plots to see if the above worked, figure 1 is the raw data
42        % from PC and figure 2 is the mean adjusted data from PC4
43        figure(1)
44        subplot(p(1),p(2),i)                                     ;
45        plot(PC(:,i))                                           ;
46        grid on                                               ;
47        grid minor                                             ;
48        axis tight                                             ;
49        xlabel('time in 1/2000 second')                         ;
50
51        figure(2)
52        subplot(p(1),p(2),i)                                     ;
53        plot(PC4(:,i))                                          ;
54        grid on                                               ;
55        grid minor                                             ;
56        axis tight                                             ;
57        xlabel('time in 1/2000 second')                         ;
58
59    end
60

```

```

61 % Preallocate the memory for the eigfreqs vector, not needed but
62 % a bit faster
63     eigfreqs    = zeros(1, size(PC4,2))           ;
64
65 for i = 1:size(PC4,2)
66
67 % I want to analyse the data but I do not want the bad data at
68 % the beginning or the end, and I want to calculate the damping
69 % ratio, so I first find the peaks
70     [pks, locs] = findpeaks(PC4(:, i))           ;
71
72 % Findpeaks produces negative values, which just don't
73 % make sense or fit so these three lines below remove those.
74     false      = find(pks<0)                     ;
75     pks(false) = []                               ;
76     locs(false) = []                             ;
77
78 % Weirdly some of the data has peaks of increasing amplitude at
79 % the beginning, so I want the my data to start after those
80 % shenanigans. Therefore I search for the max value and start
81 % the data from there.
82     maxpks     = find(pks == max(pks))           ;
83     pks        = pks(maxpks:end,1)               ;
84     locs       = locs(maxpks:end,1)              ;
85
86 % The above removed most of the problems, but not all, so now I
87 % want to directly remove all the peaks that are rising.
88 % I first find them by the for & if loop below and give them
89 % the value -20 so they can be easily identified.
90
91     for n = 1:length(pks)-1
92         if (pks(n+1)-pks(n)> 0.1) && (pks(n) > 0.2)
93             pks(n) = 20                           ;
94         end
95     end
96
97     for n = 1:length(pks)-1
98         if pks(n)< 0.005
99             pks(n) = -50                           ;
100
101         end
102     end
103
104 % Now I find the locations with the -20, and use the last
105 % location that has -20+1 as the starting point. This should
106 % just give me peaks which are descending. However not all of
107 % the data contains those bad behaving peaks so I use an if
108 % loop to identify those that need to be fixed.
109
110     pkstart = find(pks == 20)                     ;
111     if length(pkstart)> 0
112         pks  = pks(pkstart(end) + 1:end)         ;
113         locs = locs(pkstart(end) + 1:end)         ;
114     end
115
116     pkstart = find(pks == -50)                     ;

```

```

116     if length(pkstart)> 0
117         pks(pkstart(1):end) = [];
118         locs(pkstart(1):end) = [];
119     end
120
121 % I do not want the bad data at the end, so I just use the data
122 % that exists between the first and last peak.
123     ante = find(pks>1);
124     pks(ante) = [];
125     locs(ante) = [];
126
127     %{
128     post = find(pks<-1);
129     pks(post) = [];
130     locs(post) = [];
131
132     ante = find(PC4(:,i)>1);
133     PC4(ante) = [];
134     PC4(ante) = [];
135
136     post = find(PC4(:,i)<-1);
137     PC4(post) = [];
138     PC4(post) = [];
139     %}
140
141     false = find(pks<0);
142     pks(false) = [];
143     locs(false) = [];
144
145     PC5 = PC4(locs(1):locs(end),i);
146     PC6(1:length(PC5),i) = PC5;
147
148
149
150
151     data = PC5;
152
153 % Findin the peaks once again, just to make a nice plot on top
154 % of the oscillating data in figure 3.
155
156
157
158
159     figure(3);
160     subplot(p(1),p(2),i);
161     plot(locs(1):locs(end),data);
162     grid on;
163     grid minor;
164     axis tight;
165     xlabel('time in 1/2000 second');
166     hold on;
167     plot(locs,pks);
168     hold off;
169
170     figure(4);
171     subplot(p(1),p(2),i);

```

```

172     plot(locs , pks) ;
173     grid on ;
174     grid minor ;
175     axis tight ;
176     xlabel('time in 1/2000 second') ;
177
178     n = length(pks)-1 ;
179     d = (1/n)*log(pks(1)/pks(length(pks))) ;
180     z(i) = 1/sqrt(1+((2*pi)/d)^2) ;
181
182     yft = fft(data) ;
183     % I took the floor in both the yft2 and DF because matlab
184     % was giving warnings, however ceil and round produce errors
185     % as the vector are not equal
186     yft2 = yft(1:floor(size(data,1)/2+1)) ;
187     % frequency increment
188     DF = Fs/floor(size(data,1)) ;
189     freqvec = 0:DF:Fs/2 ;
190
191     figure(5) ;
192     subplot(p(1),p(2),i) ;
193     semilogx(freqvec,abs(yft2)) ;
194     %semilogx(2*pi*freqvec,abs(yft2)) ;
195     title('Frequency domain plot') ;
196     xlabel('Frequency in herz') ;
197     grid on ;
198     grid minor ;
199
200     % Find the eigenfrequency
201     [M,I] = max(yft2) ;
202     eigfreqs(i) = freqvec(I) ;
203
204     end
205
206     % The eigenfrequencies the means and standard deviation
207     eigfreqs
208     mean_eigfreq = mean(eigfreqs)
209     standard_deviation = std(eigfreqs)
210
211     % damping ratio using the first method
212     zmean = mean(z)
213     zstd = std(z)
214
215     % return formatting to default state
216     format loose

```

A.2. Damping Figures PLA

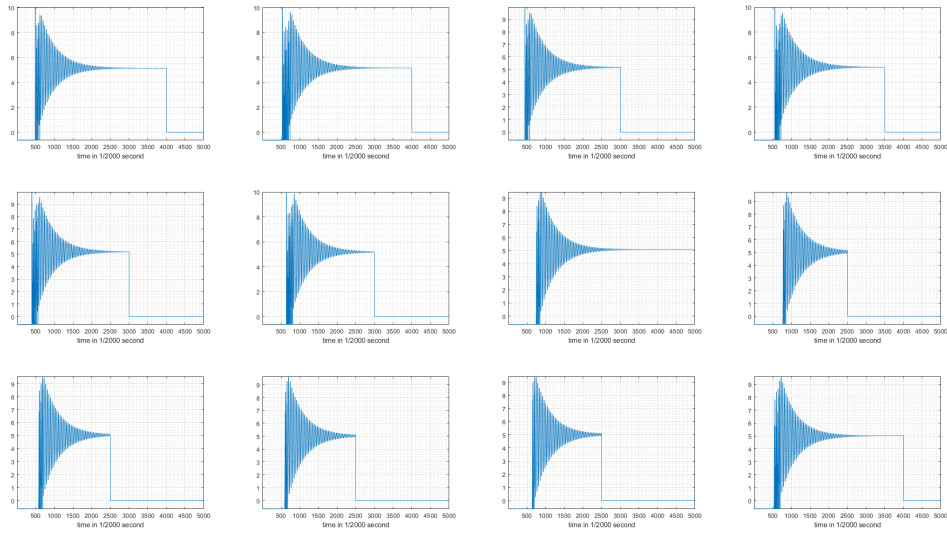


Figure A.3: The raw data for the PLA flexure, corresponding to image a in Figure 3.3

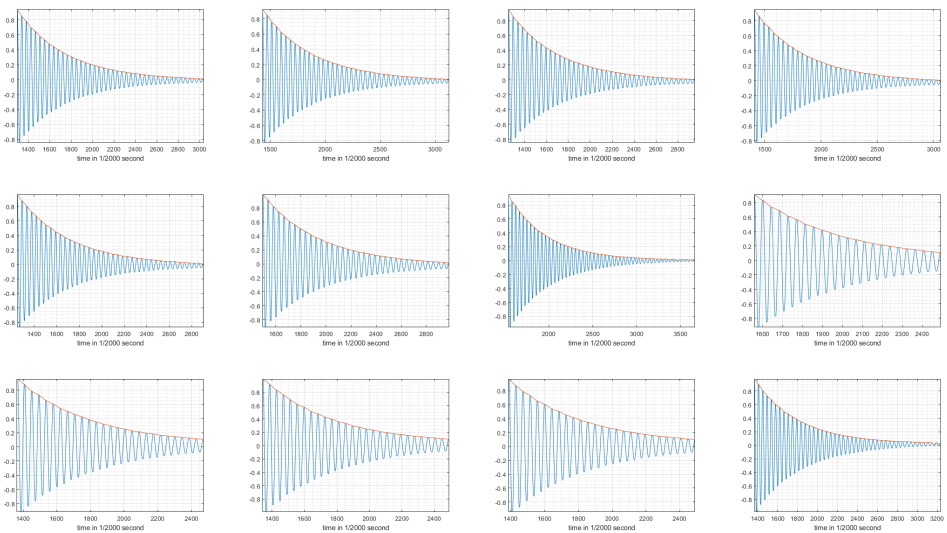


Figure A.4: The data for PLA after the mean adjustment and cutting of bad part. The red line plots the relevant peaks used to calculate the damping ratio. These plots corresponds to image c in Figure 3.3

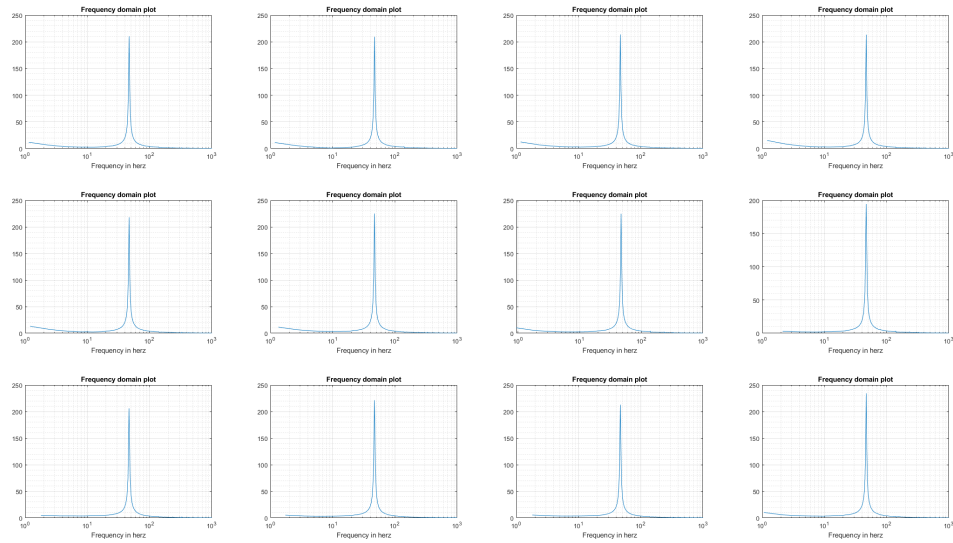


Figure A.5: The frequency domain plot for PLA based on the data from the previous Figure, FigureA.4. These plots corresponds to image e in Figure 3.3

A.3. Damping Figures Aluminium

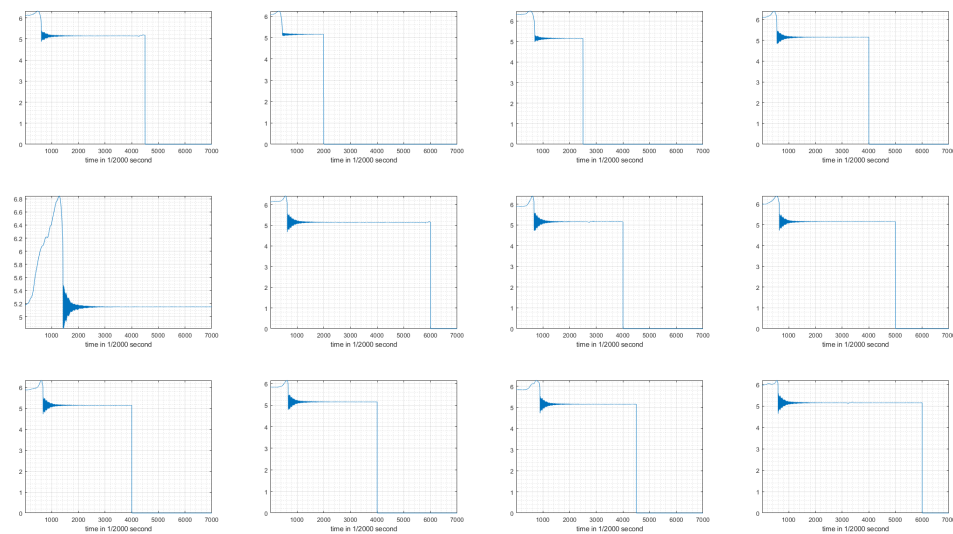


Figure A.6: The raw data for the Alu flexure, corresponding to image a in Figure 3.3, only now for Alu instead of PLA

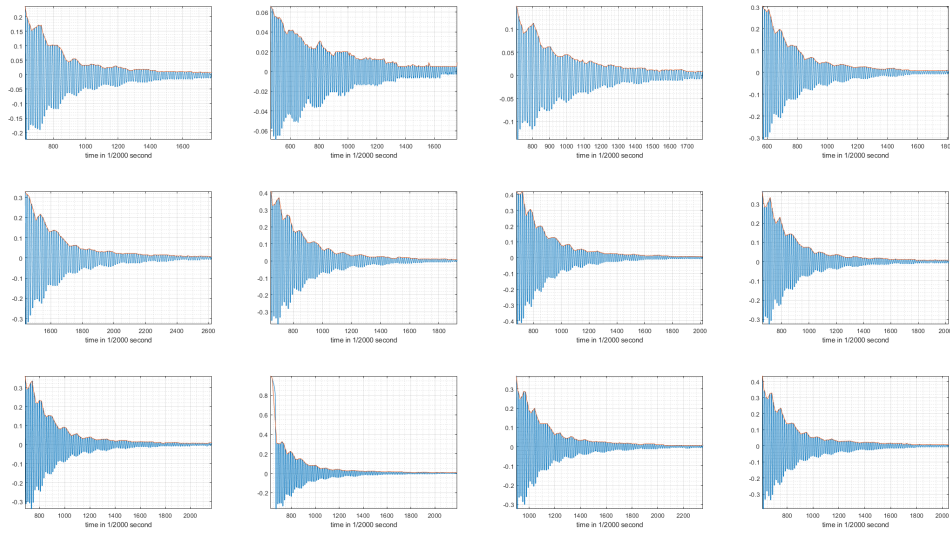


Figure A.7: The data for Alu after the mean adjustment and cutting of bad part. The red line plots the relevant peaks used to calculate the damping ratio. These plots corresponds to image c in Figure 3.3, only for Alu

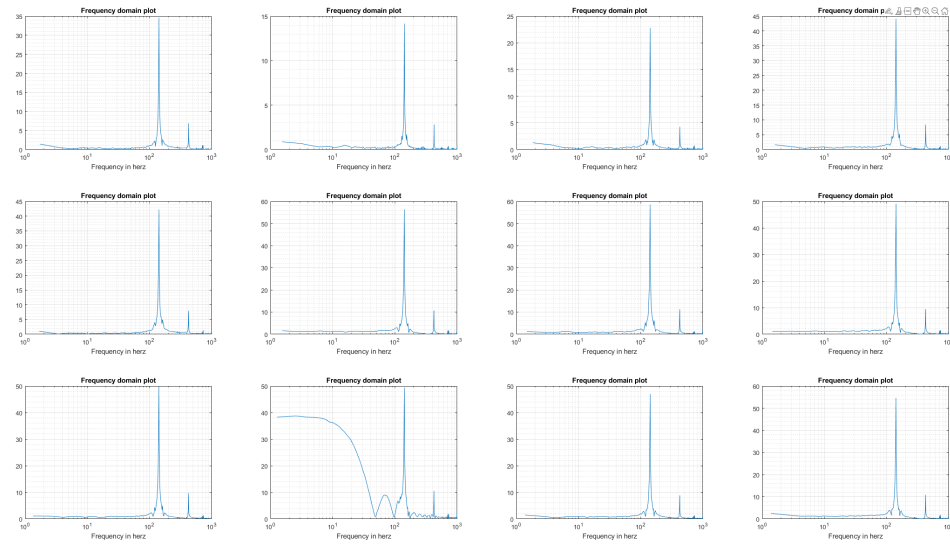


Figure A.8: The frequency domain plot for Alu based on the data from the previous Figure, FigureA.7. These plots corresponds to image e in Figure 3.3, except for Alu now.

A.4. Commercial Actuators Appendix

Specifications

	P-876.A11	P-876.A12	P-876.A15	P-876.SP1	Unit	Tolerance
Operating voltage range	-50 to 200	-100 to 400	-250 to 1000	-100 to 400	V	
Motion and positioning						
Min. lateral contraction	400	650	800	650	μm/m	
Rel. lateral contraction	1.6	1.3	0.64	1.3	μm/m/V	
Mechanical properties						
Blocking force	90	265	775	280	N	
Min. bending radius	12	20	70	–	mm	
Drive properties						
Electrical capacitance	150	90	45	8	nF	±20 %
Piezo ceramic	PIC255	PIC255	PIC255	PIC255		
Piezoceramic height	100	200	500	200	μm	
Miscellaneous						
Voltage connector	Soldering points	Soldering points	Soldering points	Soldering points		
Dimensions	61 mm × 35 mm × 0.4 mm	61 mm × 35 mm × 0.5 mm	61 mm × 35 mm × 0.8 mm	16 mm × 13 mm × 0.5 mm		
Recommended electronics	E-413, E-821, E-835	E-413, E-821, E-835	E-413, E-821, E-835	E-413, E-821, E-835		

Operating temperature range: -20 to 150 °C.

Custom designs or different specifications on request.

Figure A.9: The specification for the P-876 DuraAct Patch Transducer

Specifications

	P-878.A1	Unit
Operating voltage range	-20 to 120 V	
Motion and positioning		
Min. axial strain	1200	µm/m
Rel. axial strain	10	µm/m/V
Min. lateral contraction	250	µm/m
Rel. lateral contraction	1.2	µm/m/V
Mechanical properties		
Blocking force	44	N
Min. bending radius	24	mm
Drive properties		
Electrical capacitance	100	nF
Piezo ceramic	PIC252	
Active element	15 mm × 5.4 mm	
Miscellaneous		
Voltage connector	Soldering points	
Dimensions	27 mm × 9.4 mm × 0.6 mm	
Recommended electronics	E-503, E-504, E-505, E-506, E-610, E-617, E-618, E-663, E-821, E-831, E-836	

Electrical capacitance: Measured at 1 V_{pp}, 1 kHz, RT, tolerance ±20 %.

Operating temperature range: -20 to 150 °C.

Custom designs or different specifications on request.

Figure A.10: The specification for the P-878 DuraAct Power Patch Transducer

Specifications

	PL112.10	PL122.10	PL127.10	PL128.10	PL140.10	Unit	Tolerance
Operating voltage range	0 to 60 (± 30)	0 to 60 (± 30)	0 to 60 (± 30)	0 to 60 (± 30)	0 to 60 (± 30)	V	
Displacement	± 100	± 310	± 450	± 450	± 1000	μm	$\pm 20\%$
Remaining length L_F	12	22	27	28	40	mm	
Length L	18	25	31	36	45	mm	$\pm 0.5\text{ mm}$
Width W	9.60 ± 0.2	9.60 ± 0.2	9.60 ± 0.2	6.15 ± 0.1	11.00 ± 0.2	mm	
Height TH	0.67	0.67	0.67	0.67	0.55	mm	$\pm 0.1\text{ mm}$
Blocking force	± 2.1	± 1.25	± 1.1	± 0.55	± 0.5	N	$\pm 20\%$
Electrical capacitance	2×1.1	2×2.5	2×3.4	2×1.2	2×4.1	μF	$\pm 20\%$
Resonant frequency	1800	600	420	360	160	Hz	$\pm 20\%$
Operating temperature range	-20 to 150	-20 to 85	-20 to 85	-20 to 150	-20 to 85	$^{\circ}\text{C}$	
Piezo ceramic	PIC252	PIC251	PIC251	PIC252	PIC251		
Recommended electronics	E-650, E-651 • E-614	E-650, E-651 • E-614	E-650, E-651 • E-614	E-650, E-651 • E-614	E-650, E-651 • E-614		

Electrical capacitance: Measured at $1 V_{pp}$, 1 kHz, RT, clamped on one side with remaining length L_F , no load.

Resonant frequency: Measured at $1 V_{pp}$, clamped on one side with remaining length L_F , no load.

Standard connections: Solderable contacts (PL1xx.10) or PTFE-insulated stranded wires, UHV compatible, 100 mm, AWG 32, \varnothing 0.49 mm (PL1xx.11).

Recommended mounting: Epoxy resin adhesive.

All specifications depend on actual clamping conditions and mechanical load applied.

Custom designs or different specifications on request.

Figure A.11: The specification for the PL112 – PL140 PICMA Bender

General Specifications

Parameters	Specifications
Length (mm.)	31.8
Width (mm.)	12.7
Thickness (mm.)	0.51
Temperature Range	-60° C to 140° C
Mass (grams)	1.6
Capacitance (nF)	24
Rated Drive Voltage (+/-V) off of Resonance	60
Free Deflect (+/-mm)	0.25
Blocked Force (N)	0.28
Spring const (N/mm)	2.02
Max Amplitude (mm)	0.647
Response Time (mSec)	0.63
Resonant Freq (Hz)	350
Max Drive Volts @ Resonance (V)	20.6

T220-H4BR-1305XB Bending Transducer

General Specifications

Parameters	Specifications
Length (mm.)	31.8
Width (mm.)	12.7
Thickness (mm.)	0.51
Temperature Range	-60° C to 140° C
Mass (grams)	1.6
Capacitance (nF)	24
Rated Drive Voltage (+/-V) off of Resonance	120
Free Deflect (+/-mm)	0.0032
Blocked Force (N)	29.00
Spring const (N/mm)	2.02
Max Amplitude (mm)	0.647
Response Time (mSec)	0.63
Resonant Freq (Hz)	29500
Max Drive Volts @ Resonance (V)	20.6

T220-H4BR-1305YE Extending Transducer

Figure A.12: Left image shows the specs for the T220-H4BR-1305XB Piezoelectric Bending Transducer and right image shows the specs for the T220-H4BR-1305YE Piezoelectric Extending Transducer

Specifications

Order Code	Range +/-10%	Length	Cross Section	Cap. +/-20%	Mass	Blocking Force	Stiffness	Res. Freq.	\$USD	Buy Now
SA030305	5.6um	5mm	3x3mm	140nF	0.53g	330N	80N/um	300kHz	\$26	Buy Now
SA030310	14um	10mm	3x3mm	300nF	1.1g	330N	33N/um	150kHz	\$45	Buy Now
SA030318	25um	18mm	3x3mm	500nF	2.0g	330N	18N/um	83kHz	\$54	Buy Now
SA050510	14um	10mm	5x5mm	630nF	2.0g	900N	108N/um	150kHz	\$40	Buy Now
SA050520	31um	20mm	5x5mm	1.8uF	4.0g	900N	41N/m	74kHz	\$64	Buy Now
SA050536	56um	36mm	5x5mm	4.3uF	7.1g	900N	28N/um	42kHz	\$112	Buy Now
SA070718	28um	18mm	7x7mm	4.1uF	7.0g	1800N	120N/um	83kHz	\$73	Buy Now
SA070742	70um	42mm	7x7mm	10uF	15g	1800N	51N/um	36kHz	\$200	Buy Now

Figure A.13: The specifications for the SA Series 150V Piezo Stack Actuators

B

B.1. Appendix B (H4 Designs & Finite Element Analysis)

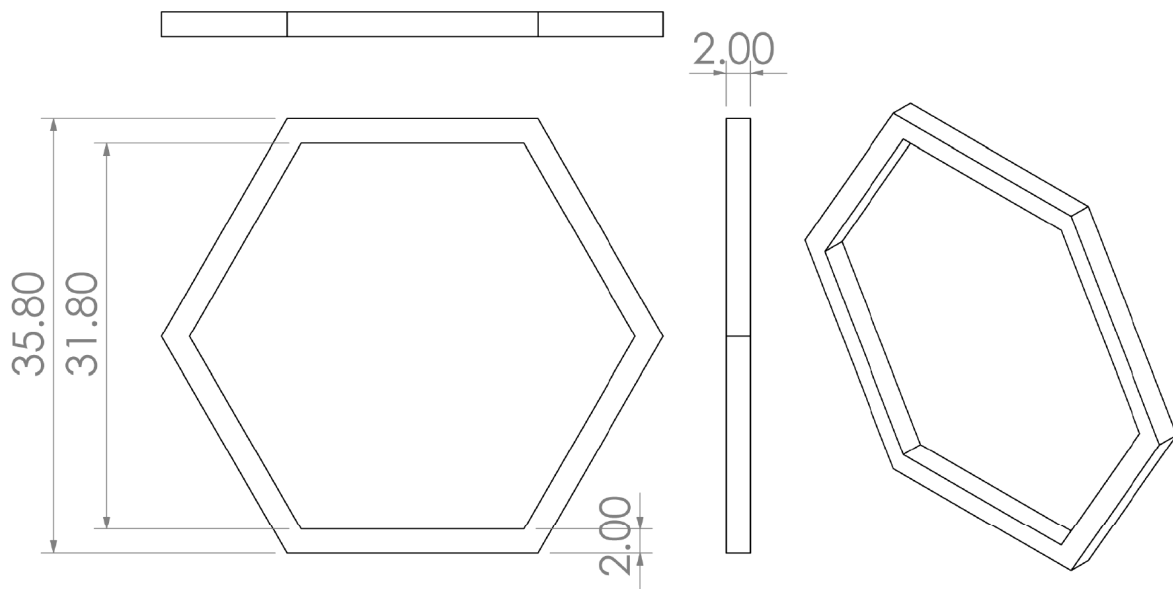
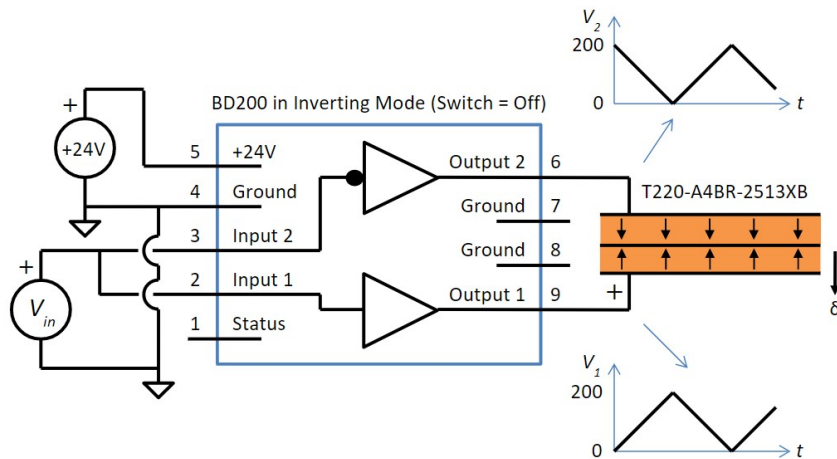


Figure B.1: Shows the model inside which different piezo transducers were placed.

C

C.1. Appendix C (H5 Practical Design and Experiments)

Application Example: +/-200V Piezo Driver



This example shows a series poled bender driven in the “two-wire” configuration [1]. A 0V to 3V input signal produces +/-200V output. Note that the load is driven differentially and cannot be connected to ground. Channel 2 is configured in the inverting mode by setting the switch to “off”. The voltage at output 1 is $V_1 = KV_{in}$, and the voltage at output 2 is $V_2 = K(3 - V_{in})$, where $K = 67.7$ for the BD200. Therefore, the voltage across the load is

$$V_{Load} = V_1 - V_2 = 2K(V_{in} - 1.5)$$

Therefore, a 0V input produces -200V across the load, 1.5V input produces 0V across the load, and 3V produces +200V across the load.

When the output voltage is positive, the actuator bends downward. The deflection δ is

$$\delta = 2K(V_{in} - 1.5) \frac{\delta_{pp}}{V_{pp}}$$

where δ_{pp} is the peak-to-peak displacement of the bender, and V_{pp} is the maximum peak-to-peak voltage. For example, $\delta_{pp} = 1.048$ mm, and $V_{pp} = 360$ for the T220-A4BR-2513XB actuator www.piezo.com.

Figure C.1: Shows how the two wire operation mode works on the BD300 Dual-Channel 300V (piezo) Amplifier

The description for the in Figure C.1 is for a BD200 Amplifier that go's up to 200 V. The BD300 can go up to 300 V and has a higher Gain (K) namely K is 100 The National Instruments equipment needs to output a voltage between 0 and 3 volts. Around 1.5 volts the piezos would see zero volts. At 1.8 volts they would see +60 V and at 1.2 they would see -60. In practice there were slight differences between the piezo amplifiers,

and they had to be calibrated. Each Amplifier in the setup is marked by a strip showing the Model name "BD300", the number of the amplifier, meaning which piezo it corresponds to, this goes from 1 to 6, and a number designating the labview value that needs to be entered in the code used to have the Amplifier output 0 V, an example is "4615". Generally these numbers corresponds to an output out of the Nation instruments equipment of 1.47V. In practice The amplifier outputs zero volts when it sees this voltage at it's input. Figure C.2 shows a screenshot of the program used to damp these flexures. Red circle marks this offset value for amplifier 1. There are either differences between the amplifiers or between the output ports of the NI-9264 which cause differences. In this setup the amplifiers are marked and not the output ports. Though the output ports seem to be the main culprit. if these amplifiers are ever connected to different output ports or different modules the software should be calibrated again.

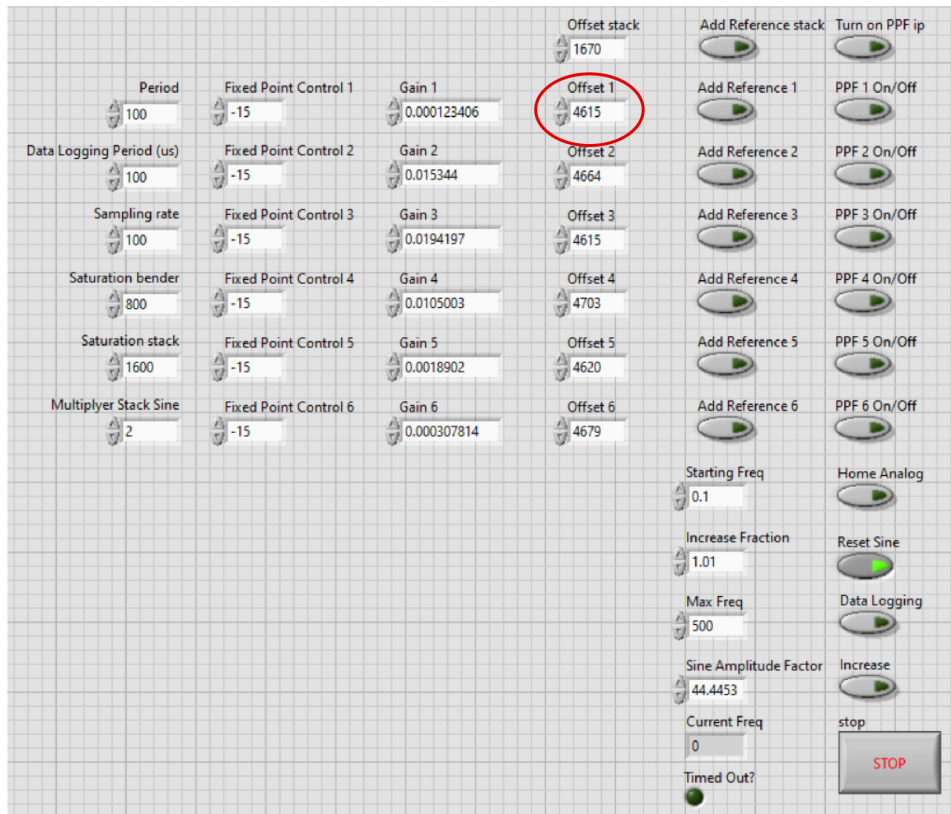


Figure C.2: A screenshot of the labview program used to damp the flexures. Red circle marks the offset value where the amplifier will output around zero volts.

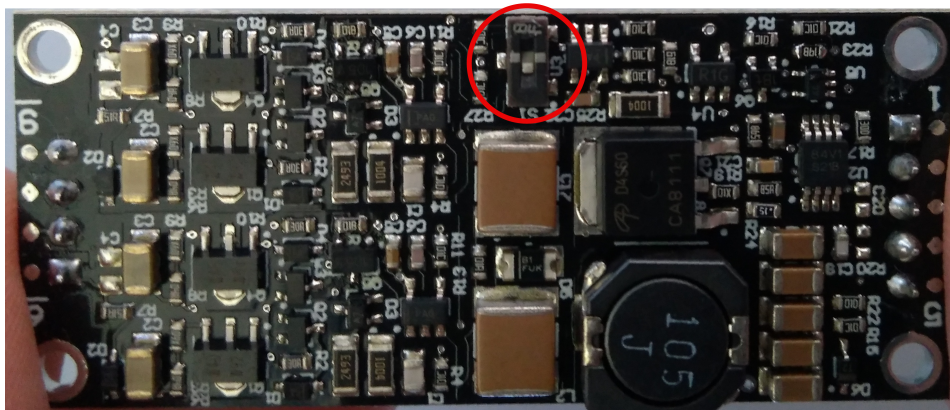


Figure C.3: A close up of the BD300 Dual-Channel 300V (piezo) Amplifier showing the switch that toggles inverting mode on and off.

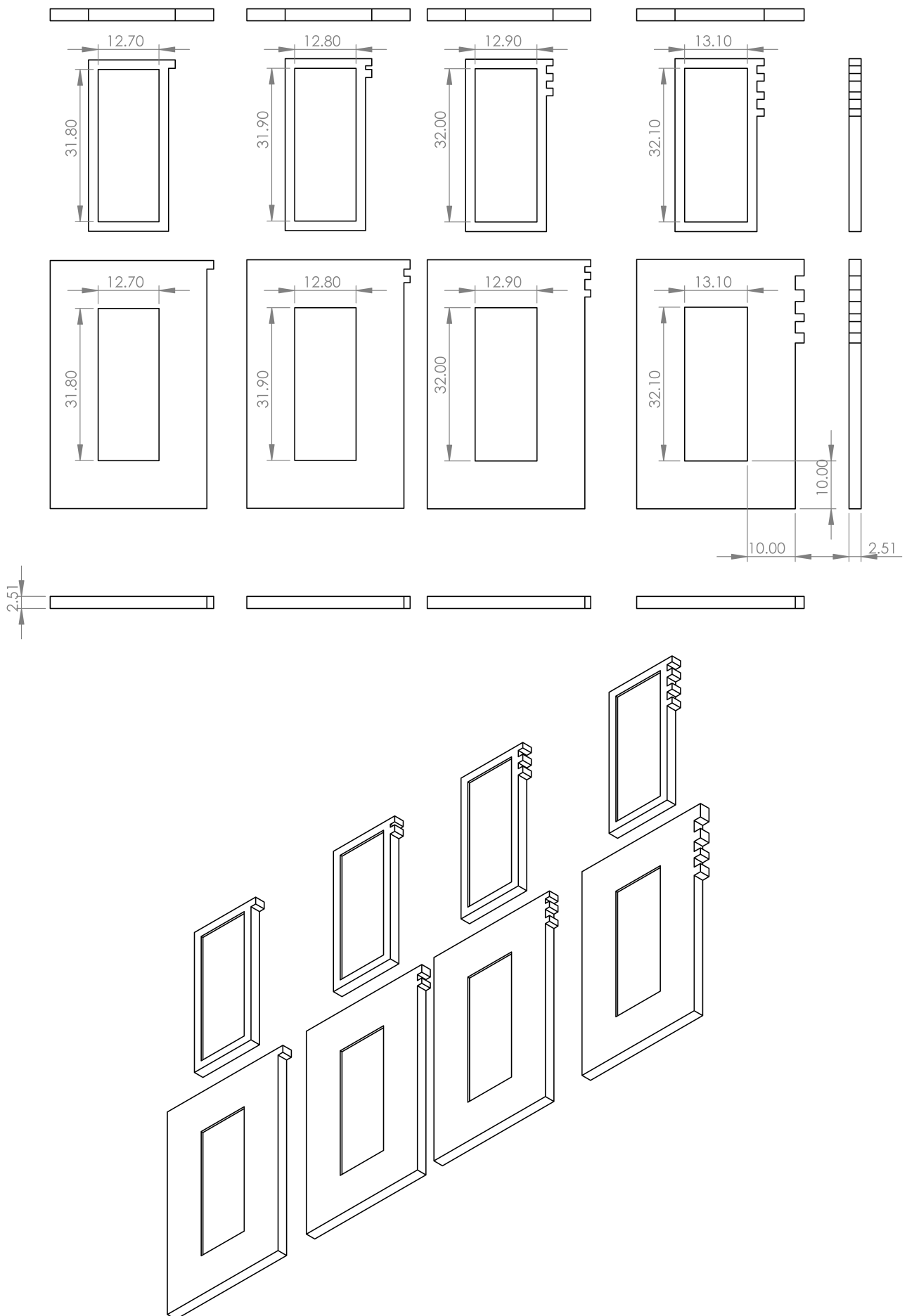


Figure C.4: Part drawing for one half the small flexure showing all the important dimensions. Two identical half's are meant to be glued together.

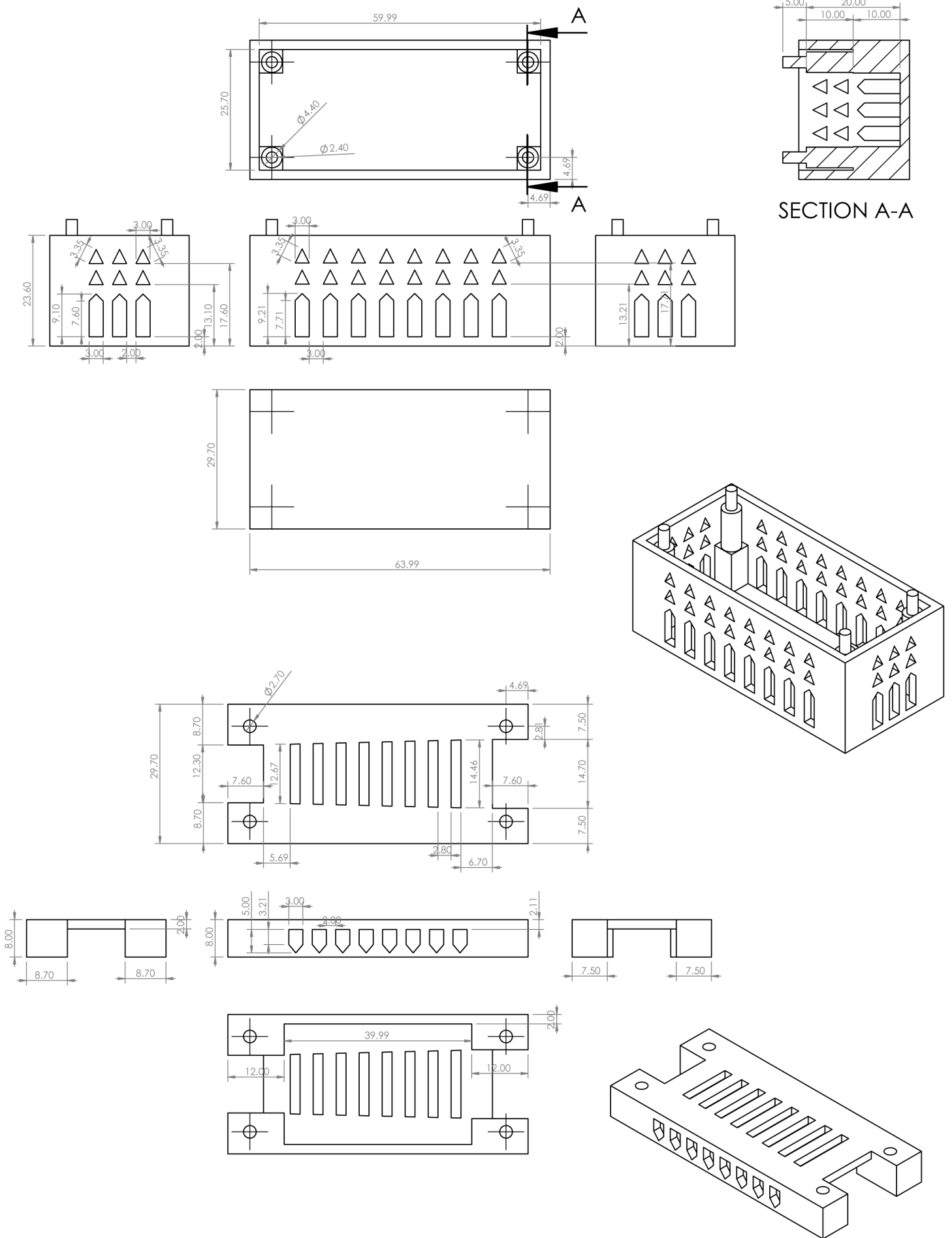


Figure C.5: Part drawing for both parts that make up the amplifier encasing

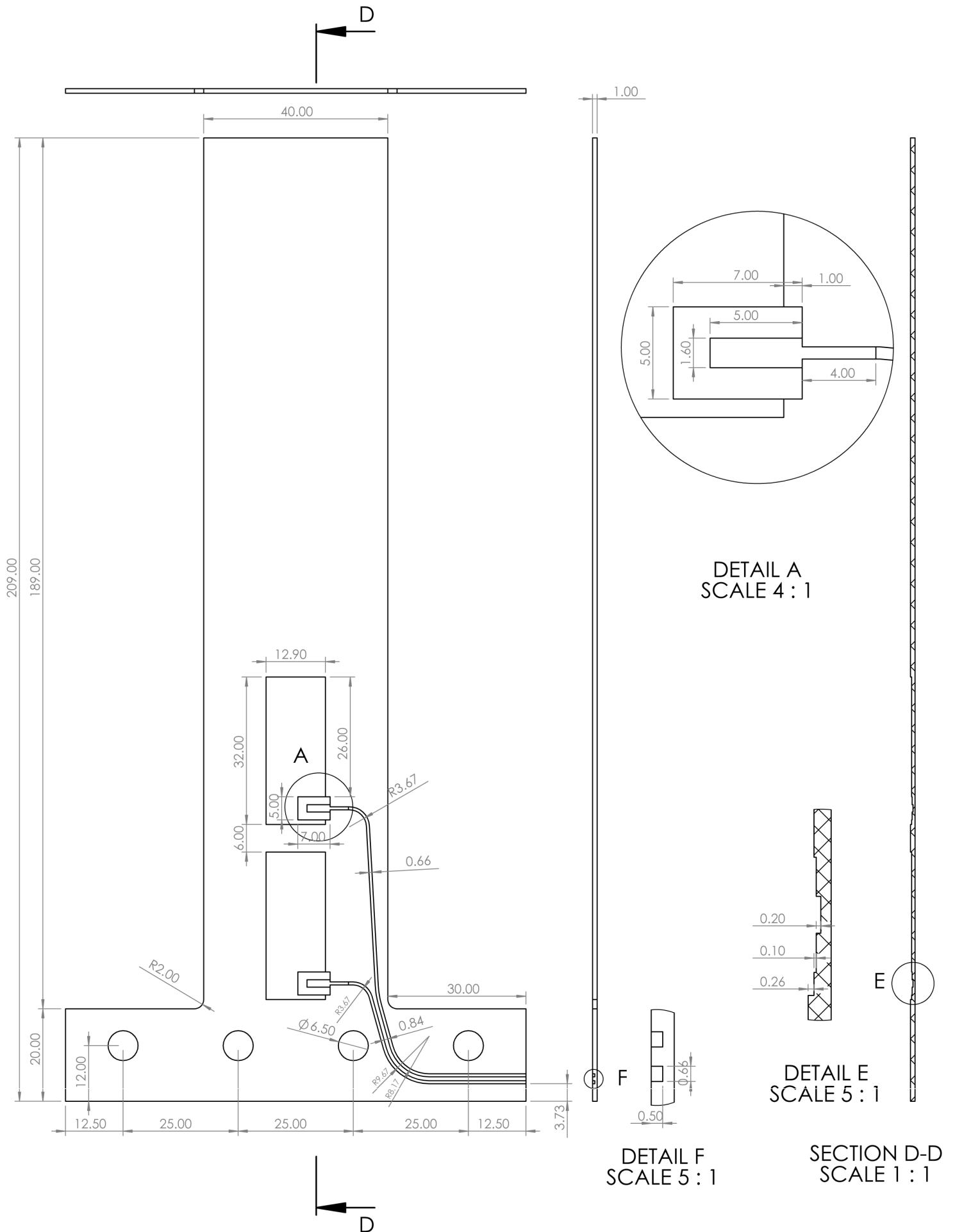


Figure C.6: Part drawing for one half the small flexure showing all the important dimensions. Two identical half's are meant to be glued together.

C.2. Small Flexure Appendix

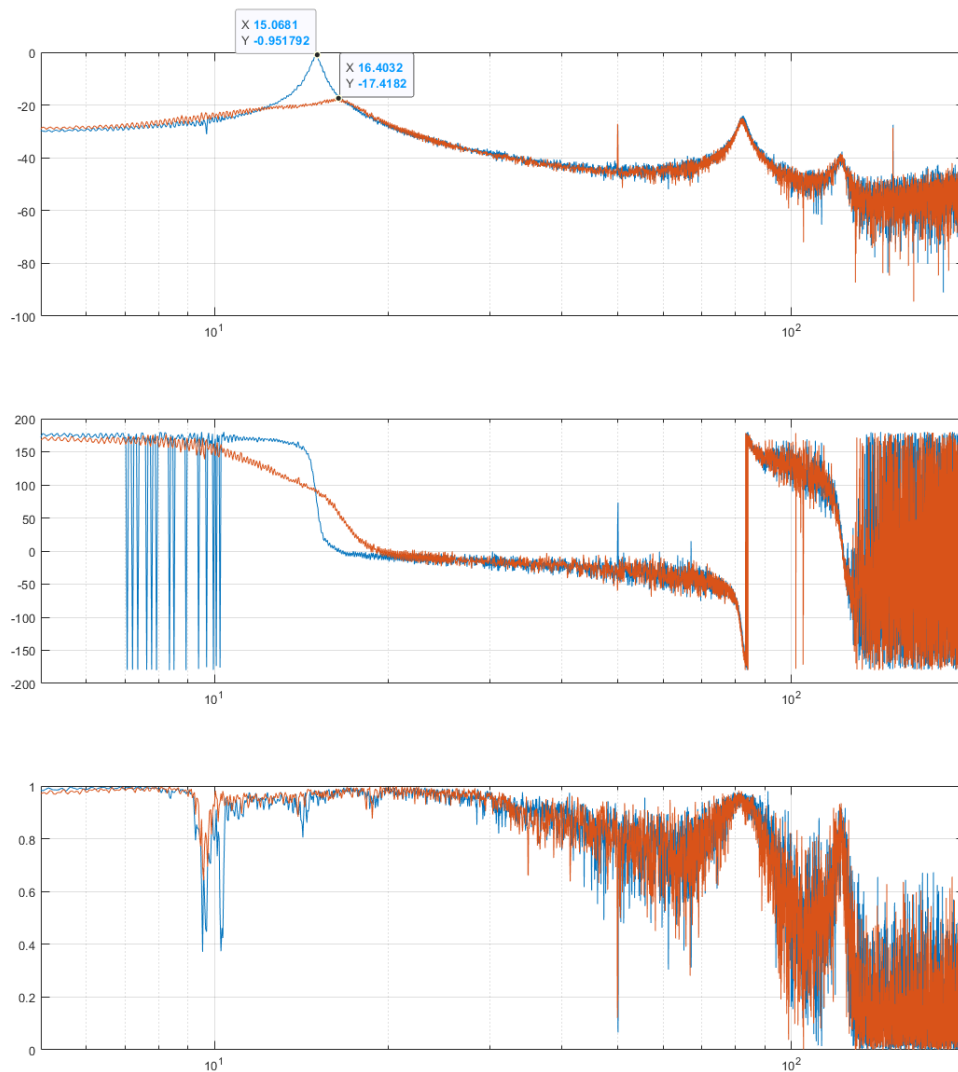


Figure C.7: Shows bode, phase and coherence plot when P1 was used for disturbance and P1 was also used to damp Mode 1

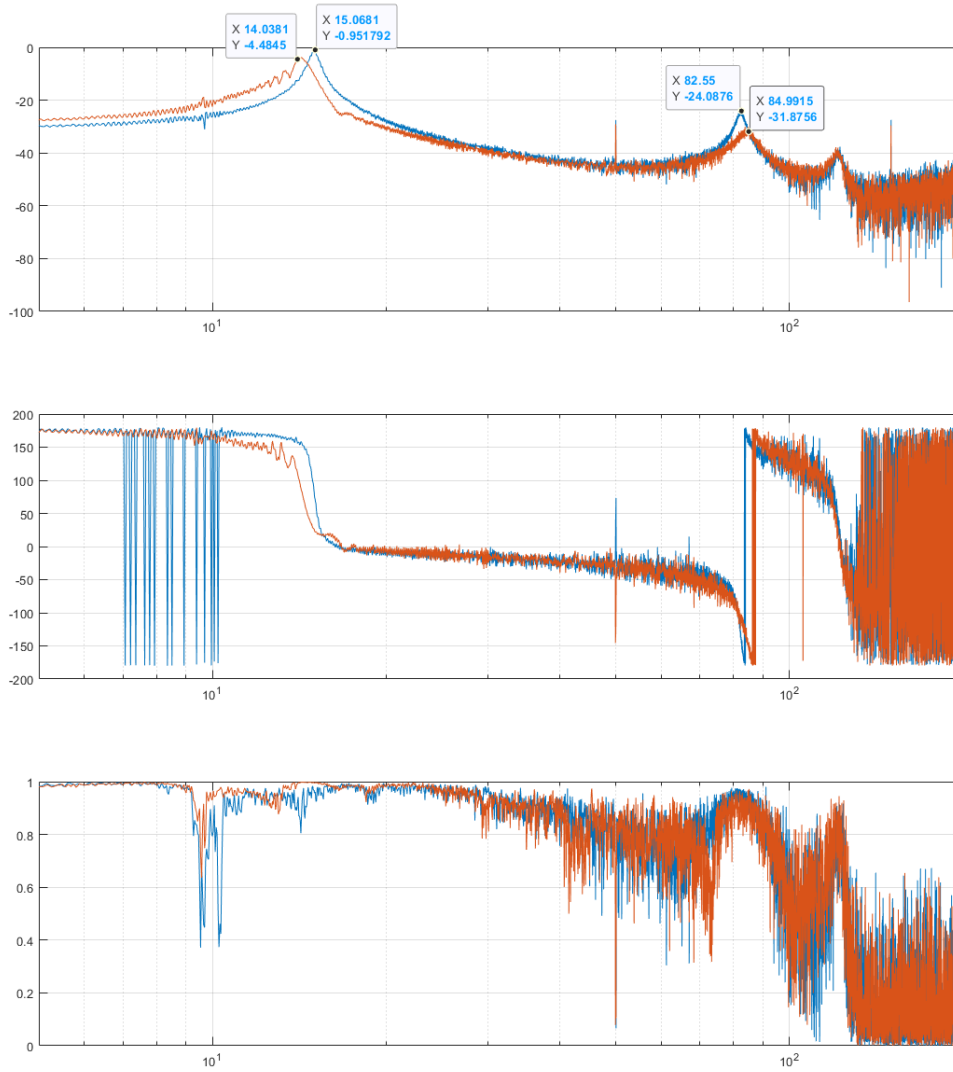


Figure C.8: Shows bode, phase and coherence plot when P1 was used for disturbance and P2 was used to damp Mode 2

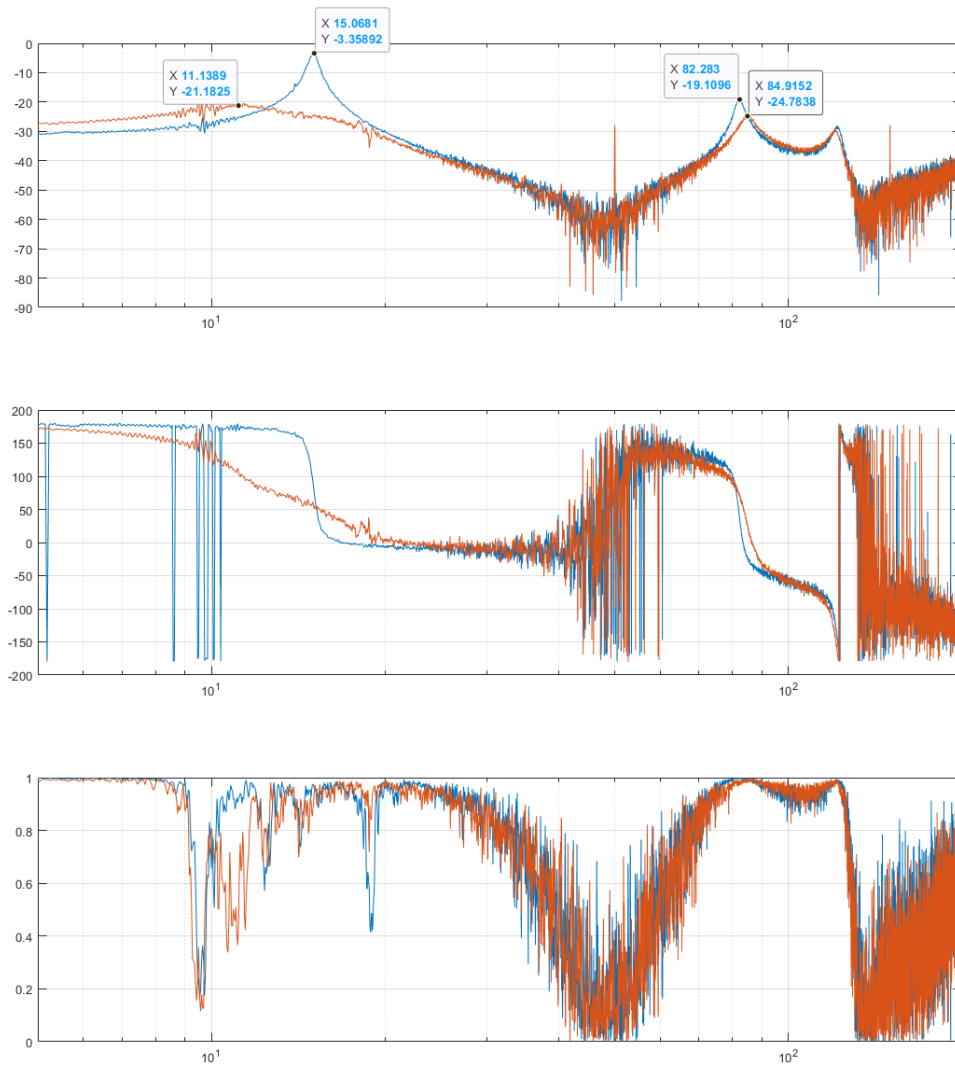


Figure C.9: Shows bode, phase and coherence plot when P1 was used for disturbance and P1 was also used to damp mode 1, at the same time P2 was used to damp Mode 2

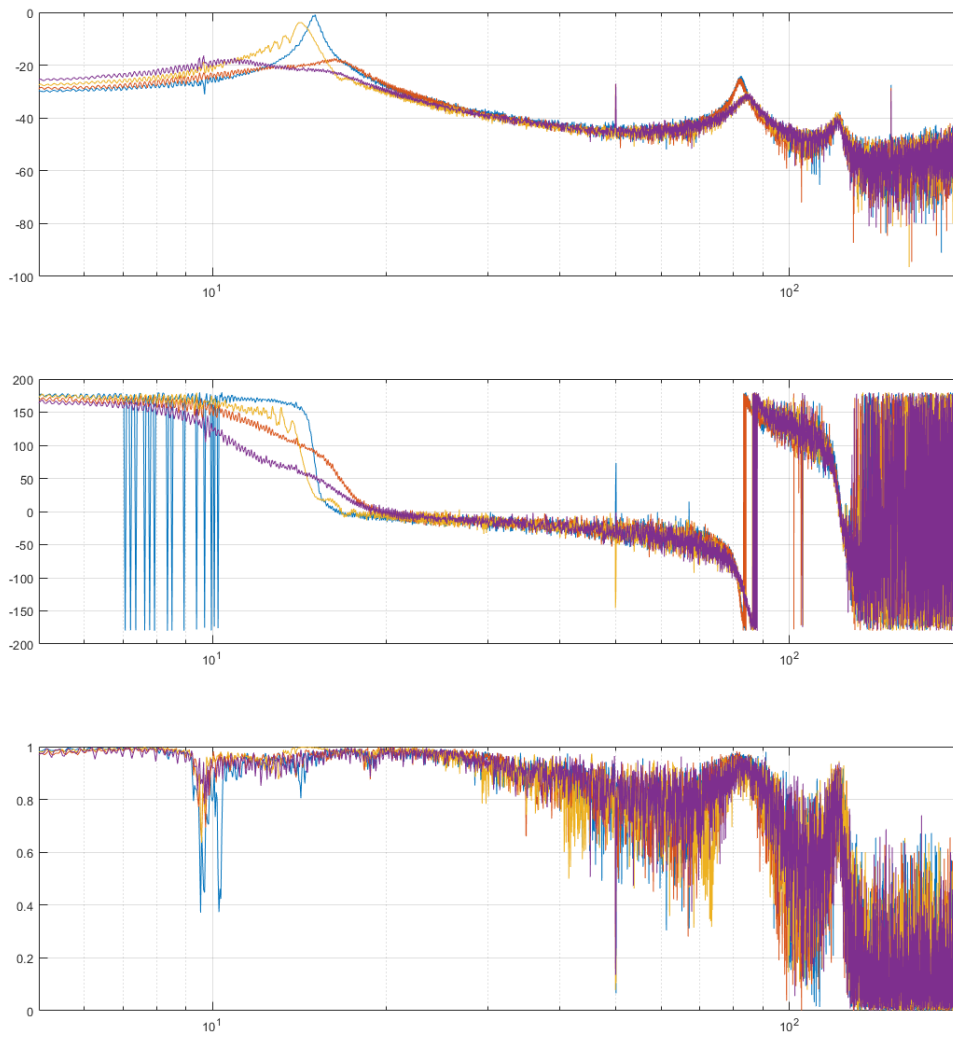


Figure C.10: The three plots from Figure C.7, Figure C.8, Figure C.9 in a single plot

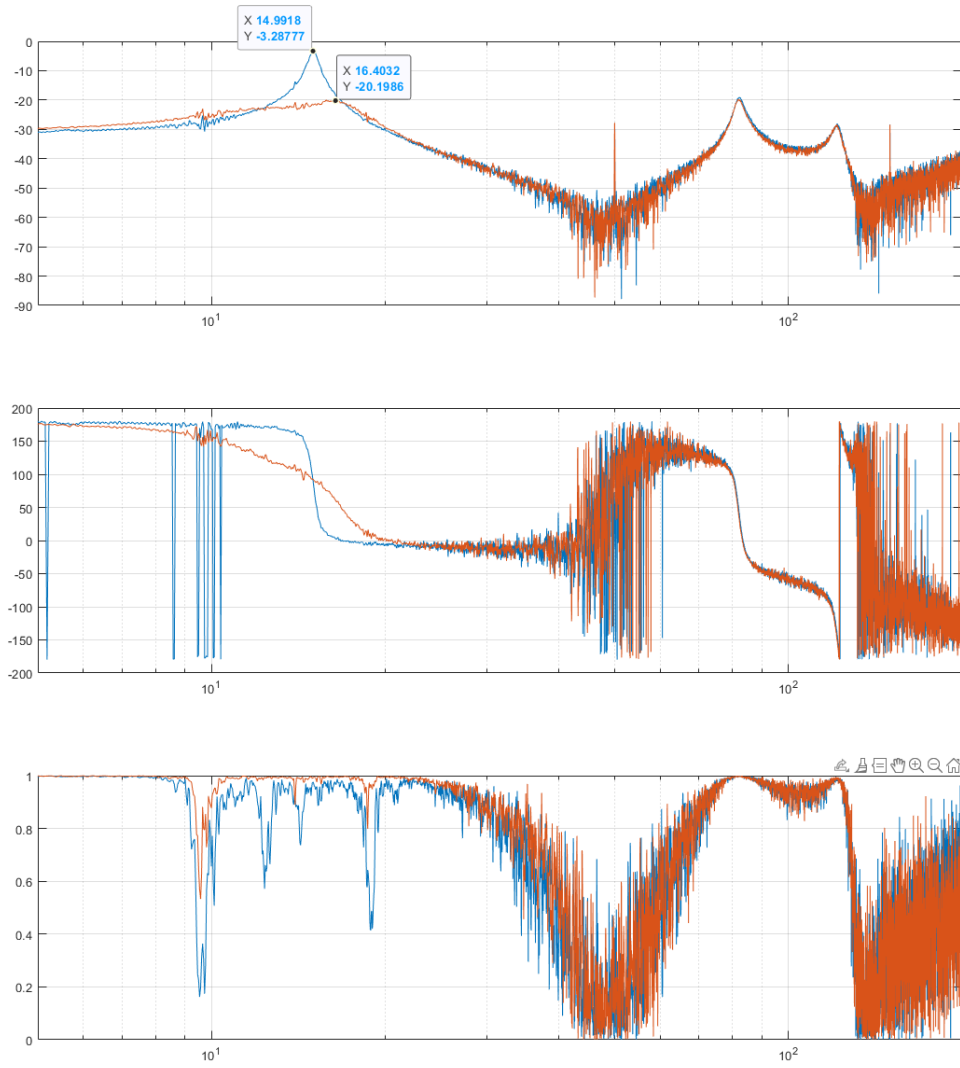


Figure C.11: Shows bode, phase and coherence plot when P2 was used for disturbance and P1 was used to damp Mode 1

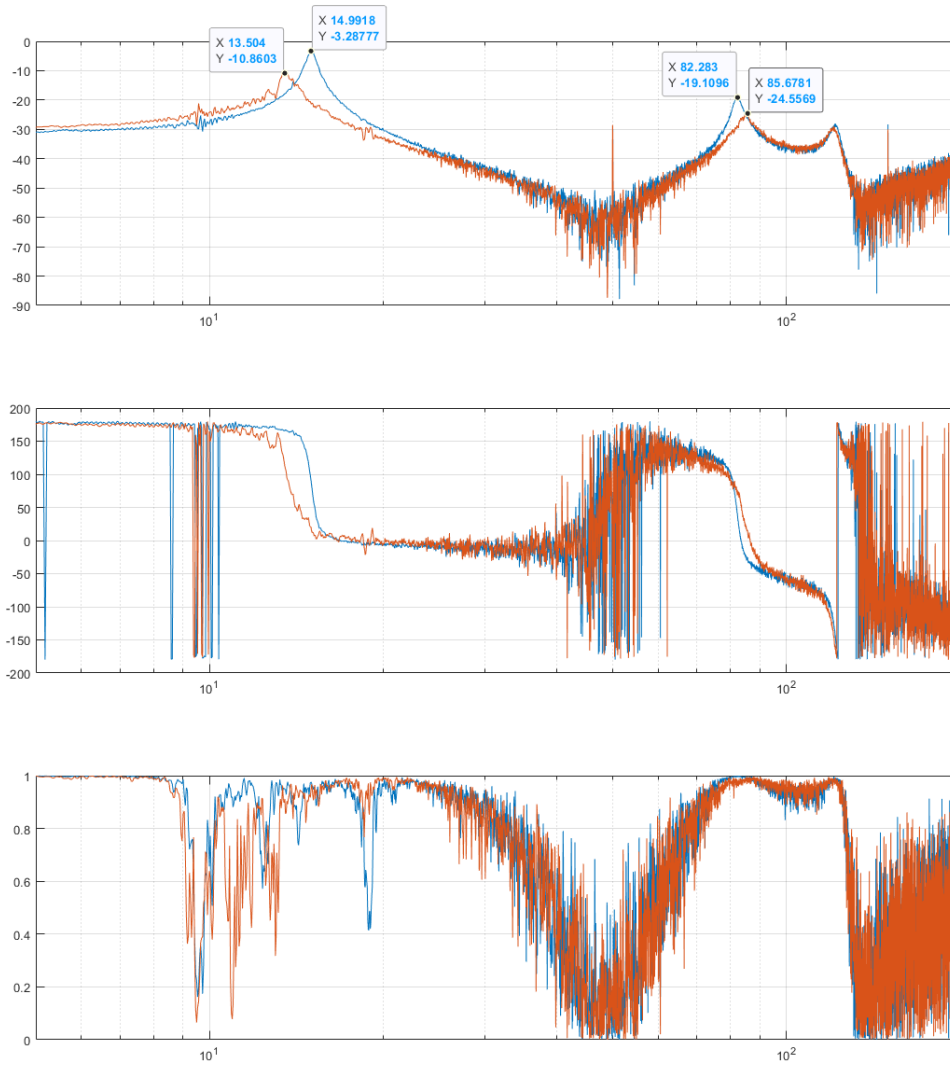


Figure C.12: Shows bode, phase and coherence plot when P2 was used for disturbance and P2 was also used to damp Mode 2

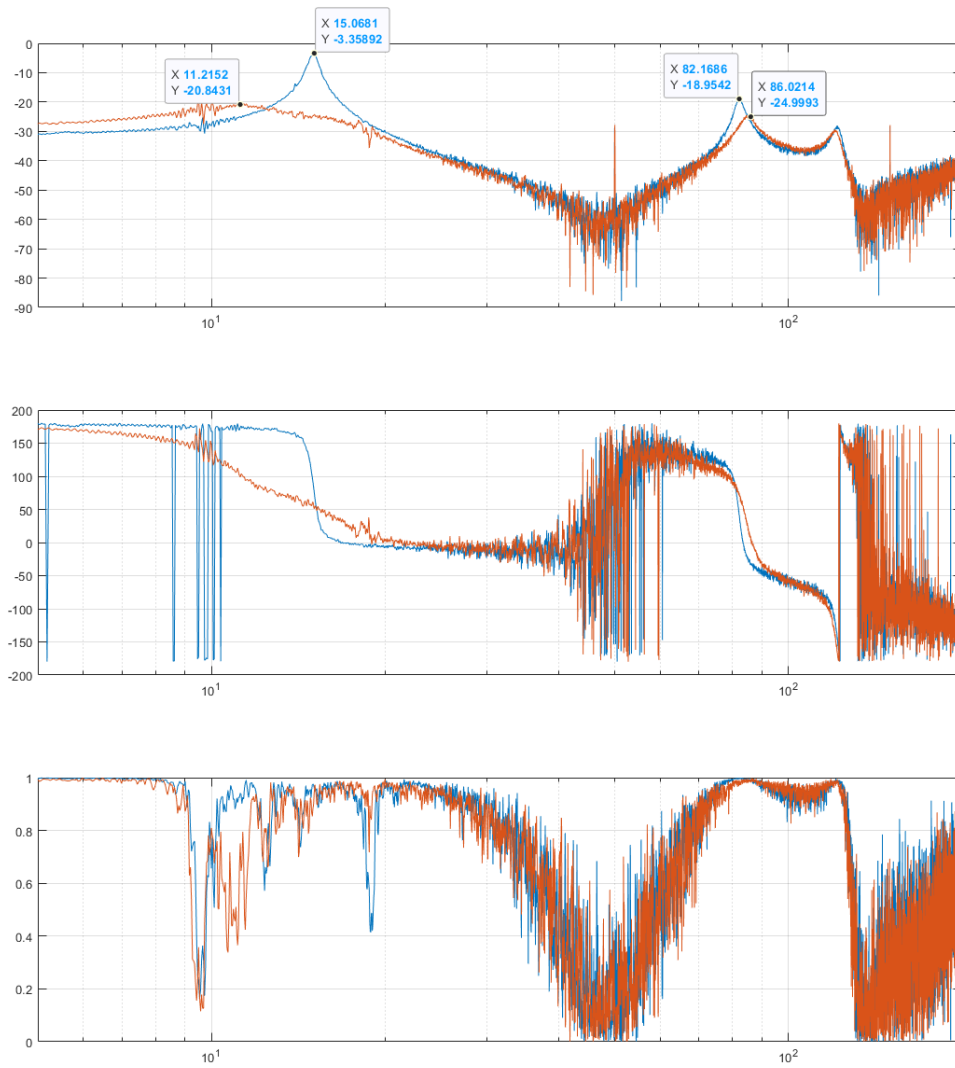


Figure C.13: Shows bode, phase and coherence plot when P2 was used for disturbance and P1 was used to damp mode 1, an besides providing disturbance P2 was also used to damp Mode 2

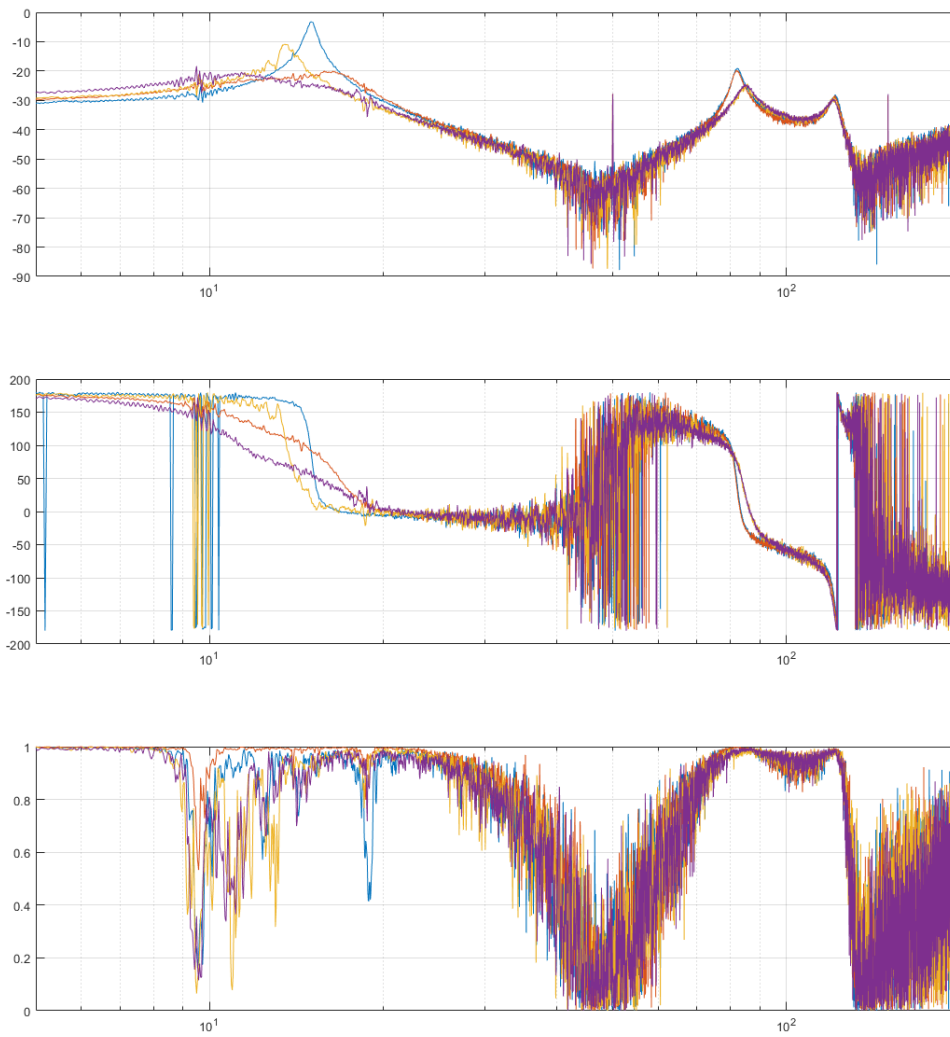


Figure C.14: The three plots from Figure C.11, Figure C.12, Figure C.13 in a single plot

C.3. BA Sensor Specs

Specifications

Order Code	Deflection	Force	Dimensions	Thickness	Free Length	Voltage	AC Voltage	Cap. [1]	Stiffness	Res. Freq.	Mass	\$USD	Buy Now
BA3502	0.7 mm	0.08 N	35 x 2.5 mm	0.8 mm	28 mm	+150 V	+/-90 V	20nF	220 N/m	230Hz	0.3 g	\$5	Buy Now
BA4902	1.3 mm	0.07 N	49 x 2.1 mm	0.8 mm	42 mm	+150 V	+/-90 V	28nF	100 N/m	140Hz	0.4 g	\$6	Buy Now
BA4010	1.1 mm	0.18 N	40 x 10 mm	0.8 mm	33 mm	+150 V	+/-90 V	100nF	327 N/m	250Hz	1.7 g	\$14	Buy Now
BA5010	1.5 mm	0.3 N	50 x 10 mm	0.8 mm	43 mm	+150 V	+/-90 V	125nF	400 N/m	200Hz	2.1 g	\$18	Buy Now
BA6020	2.6 mm	0.3 N	60 x 20 mm	0.8 mm	53 mm	+150 V	+/-90 V	300nF	230 N/m	60Hz	5 g	\$30	Buy Now

Notes:

1. Capacitance of both sides in parallel. This value should be used for calculating the required current in the three-wire or parallel configuration. Tolerance is +/-30%

Figure C.15: The specifications for the BA Series Insulated Piezoelectric Benders from piezodrive

C.4. Octo Flexure Appendix

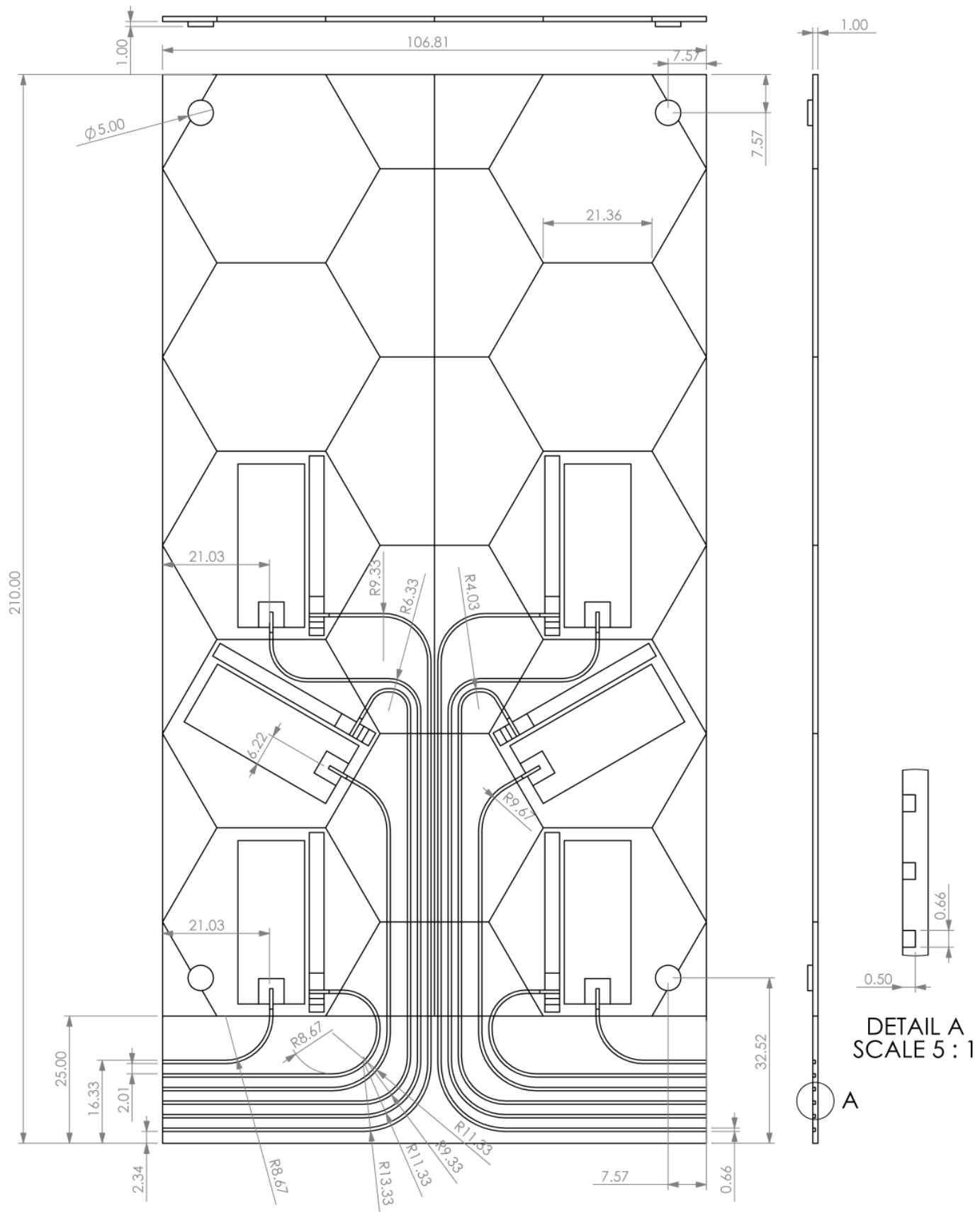


Figure C.16: Part drawing for one half the Octo Flexure. This is part A, the part with four round cylinders near its corners which fit in to the round holes of Part B, and where the sensing piezo have the wire coming straight down out of the piezo.

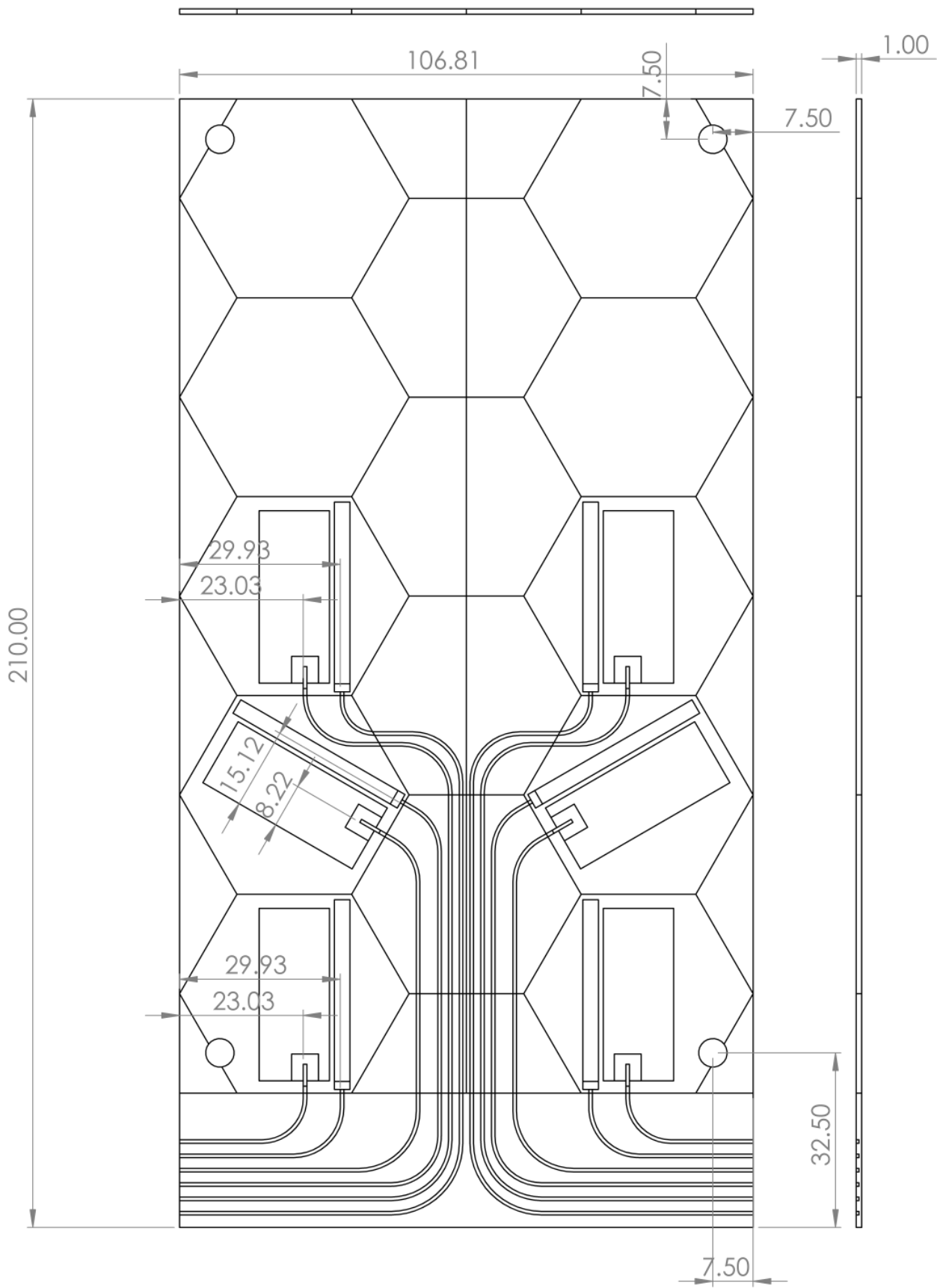


Figure C.17: Part drawing for one half the Octo Flexure. This is part B, the part with four round holes near its corners where the round cylinders of Part B fit into, and where the sensing piezo have the wire coming from the sides out of the piezo.

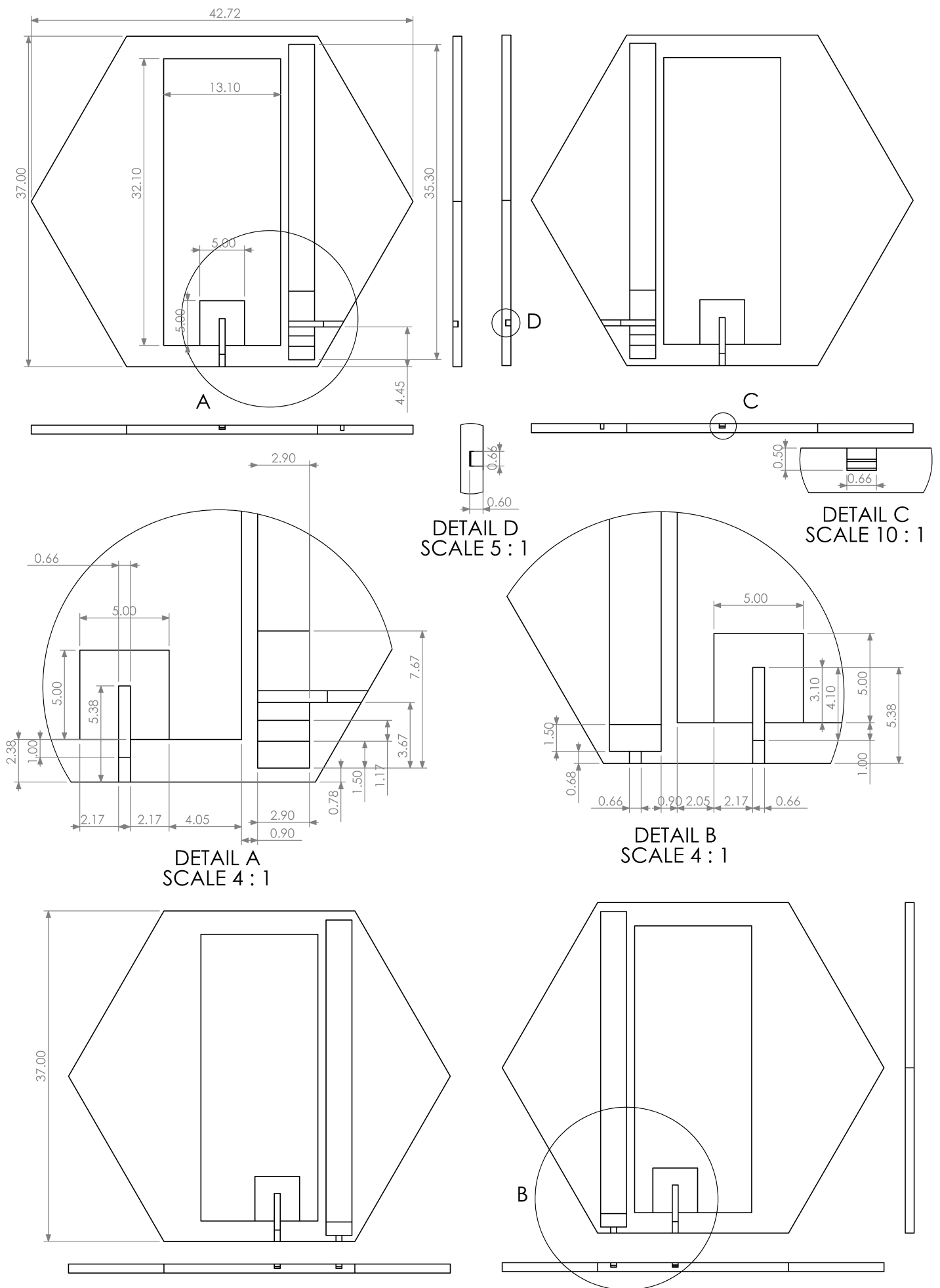


Figure C.18: Part drawing for the four types of cells that house piezo actuator sensor pairs in the Octo Flexure shown in Figure 5.18

Eigenfrequency=16.117 Hz Surface: Total displacement (mm) Eigenfrequency=59.662 Hz Surface: Total displacement (mm) Eigenfrequency=100.01 Hz Surface: Total displacement (mm)

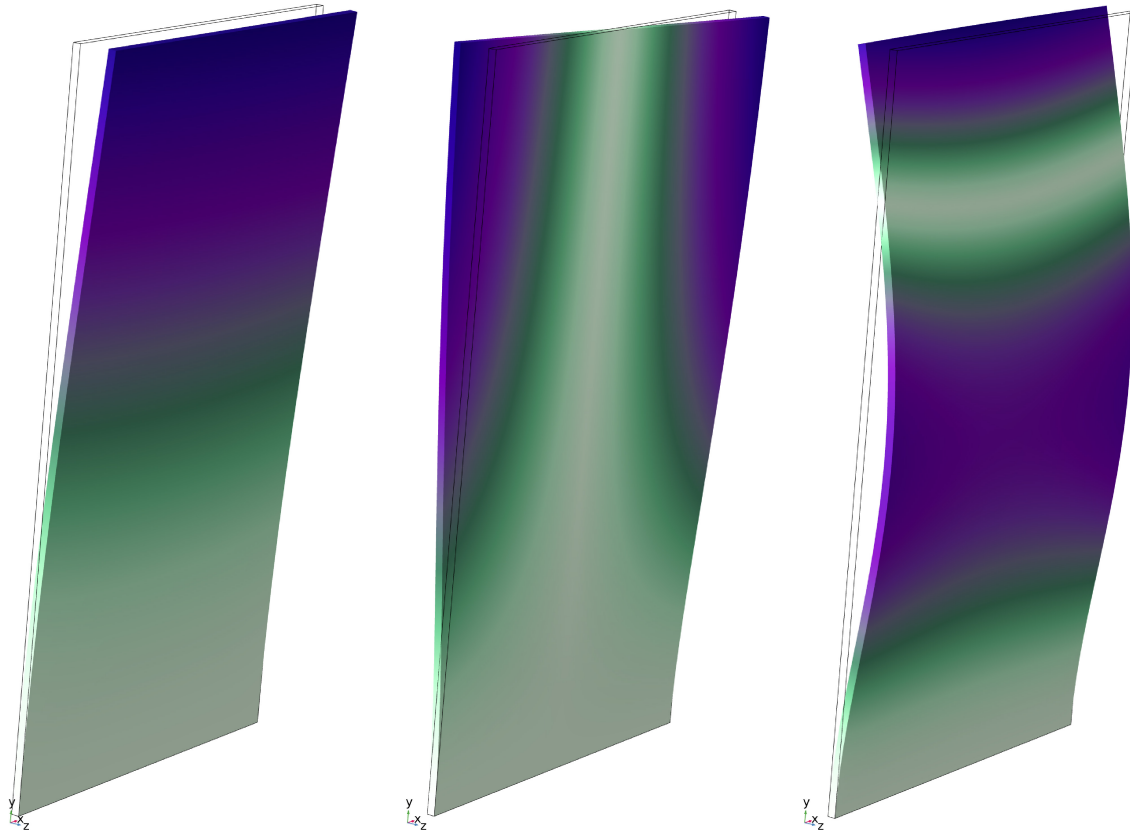
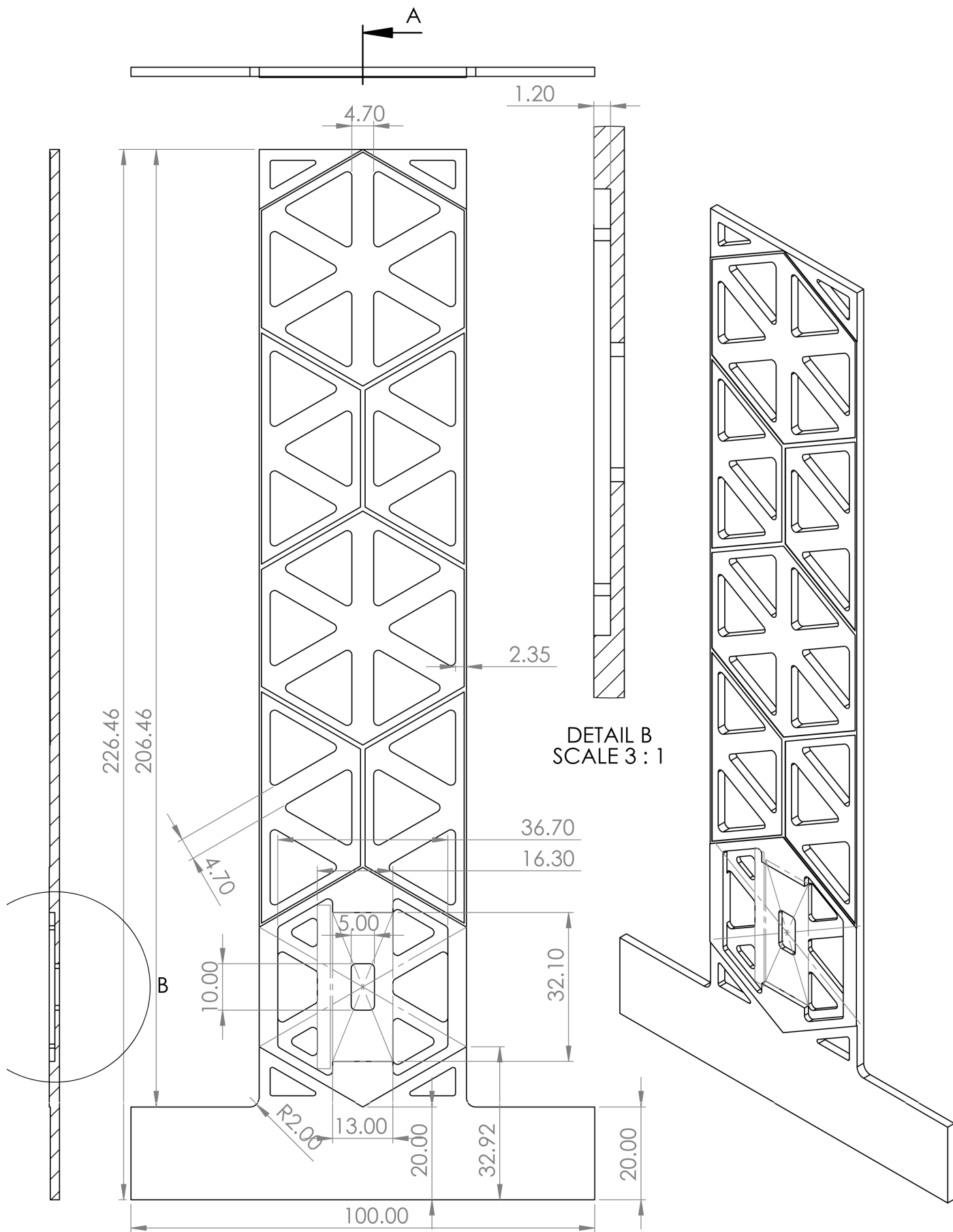


Figure C.19: Shows the three expected eigenmodes of the Octo flexure that the piezos need to damp.

C.5. Open Small Flexure



SECTION A-A
SCALE 1 : 1



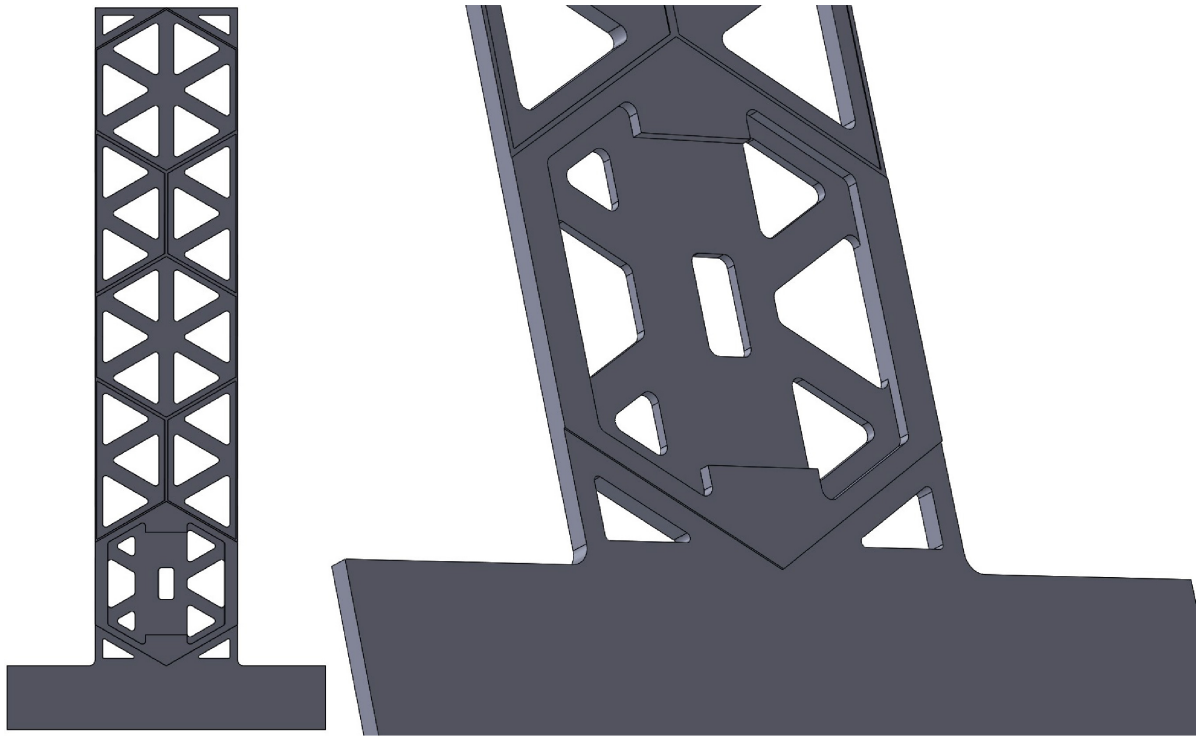


Figure C.21: Shows a model of the small open flexure that was used to test out the new sensor actuator arrangement and whether piezo could be successful removed after bonding with epoxy

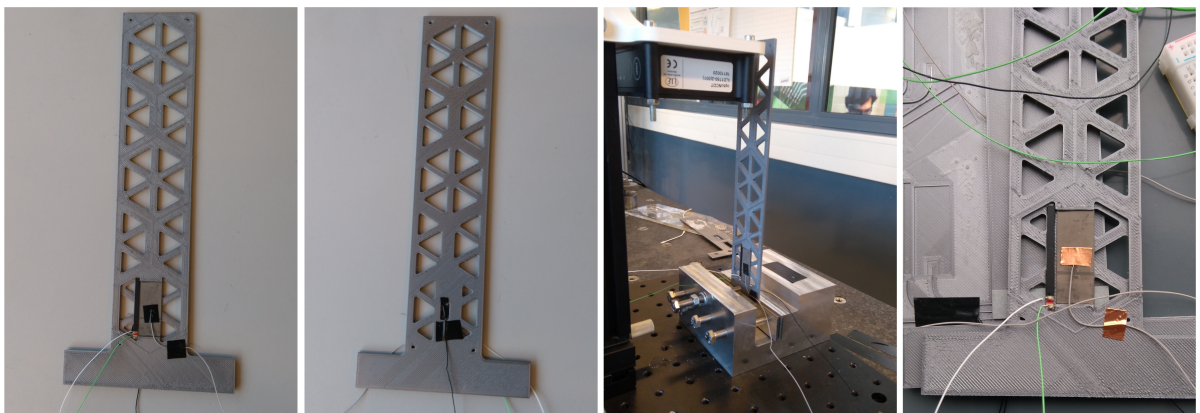


Figure C.22: The real version of the small open flexure. Note in the rightmost image the conductive copper tape connections. These would play a big role in the main flexures.

C.6. UHU Appendix



Figure C.23: Shows how the epoxy is scraped off a piezo actuator. In the end the actuator is cleaned and scrubbed with isopropanol.

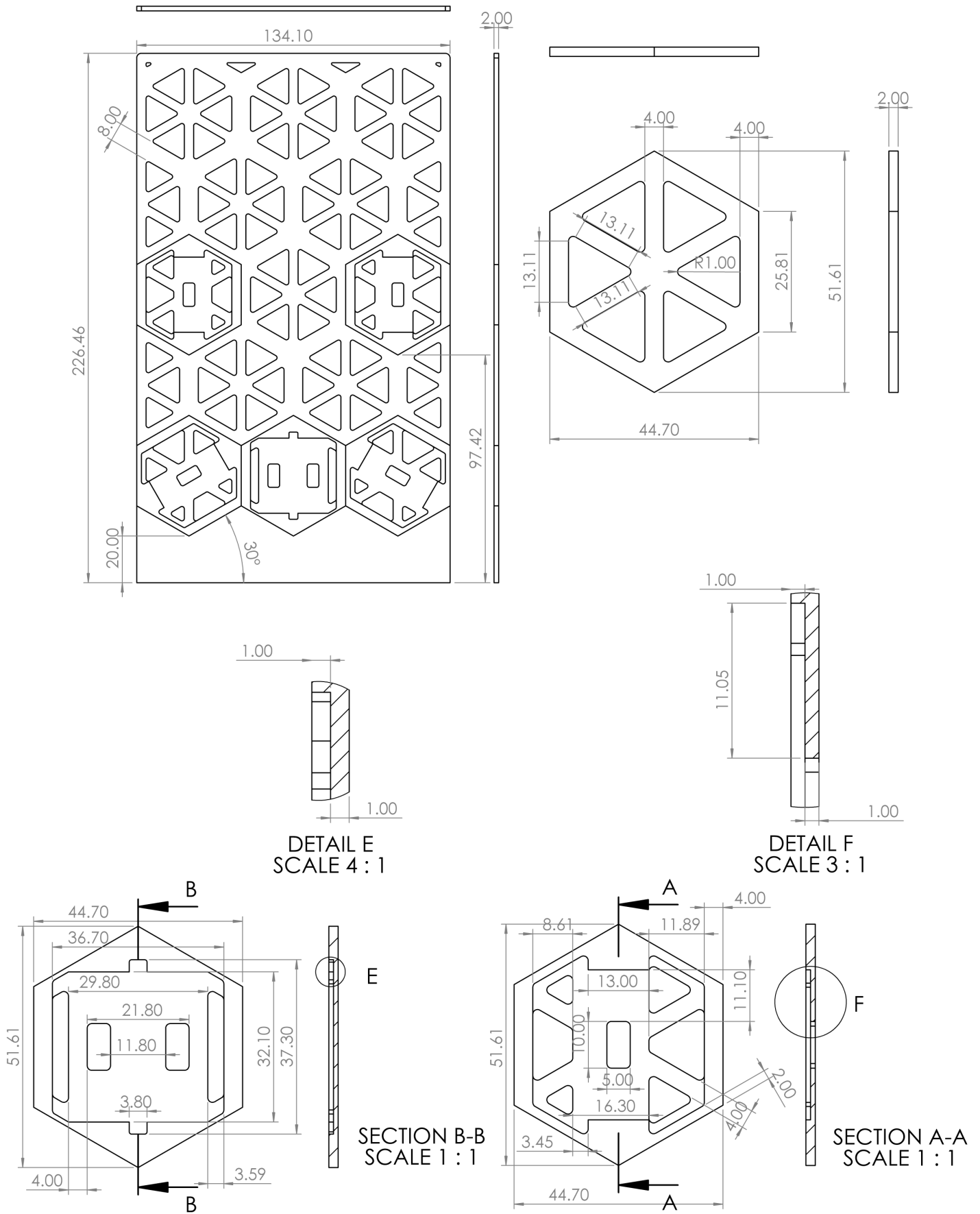


Figure C.24: Part drawing for the UHU Flexure and it's cells

C.7. DP 460 Appendix

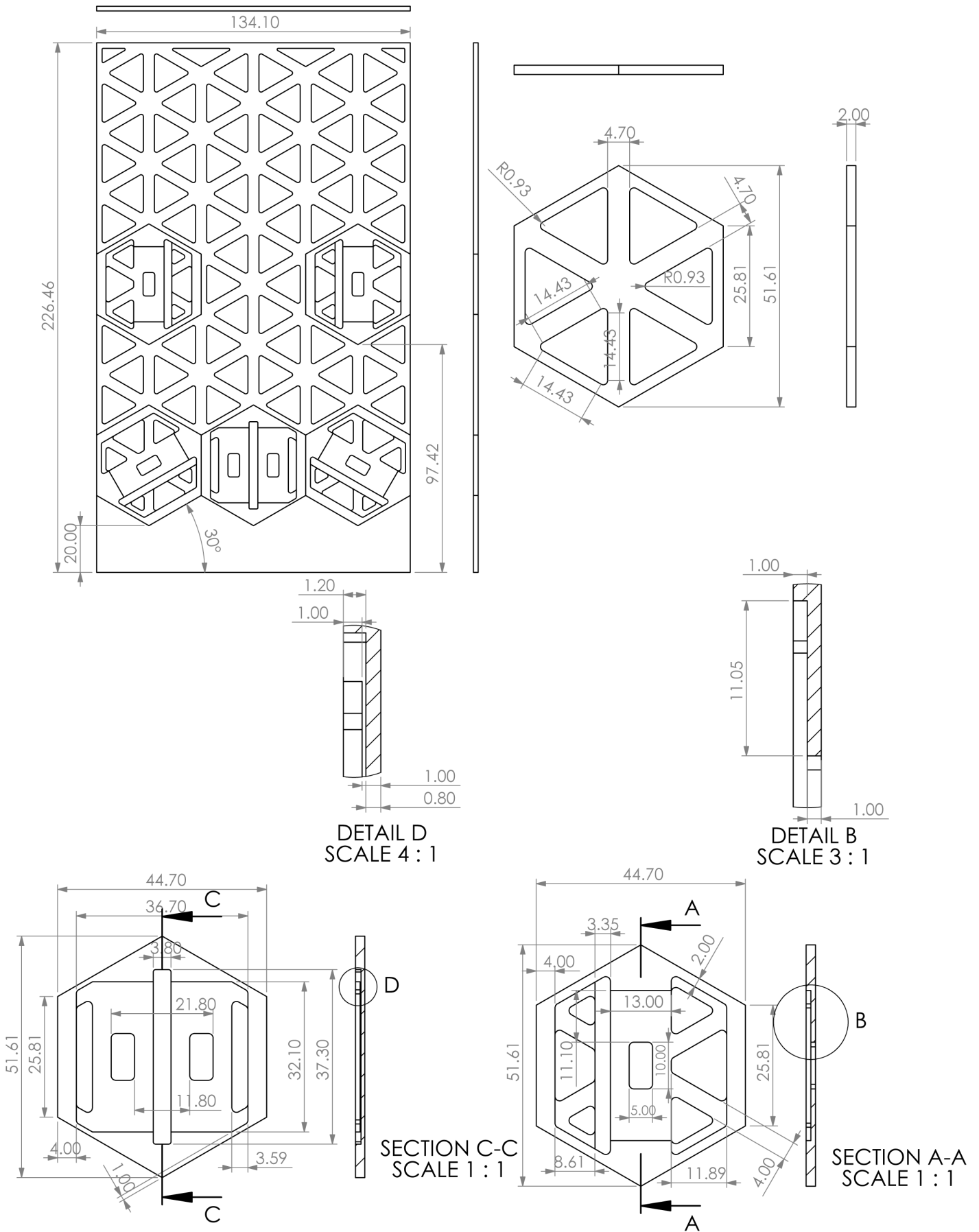


Figure C.25: Part drawing for the DP460 Flexure and its cells

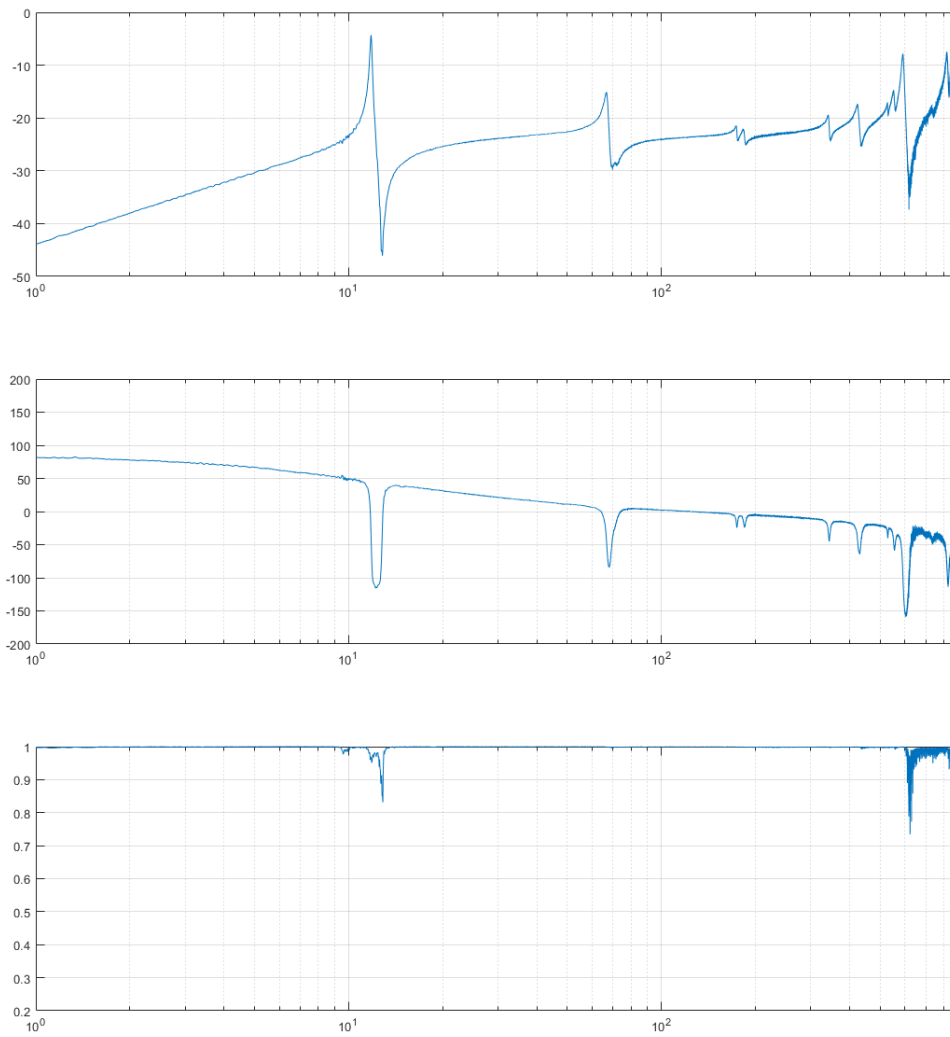


Figure C.26: Bode showing the data from the sensor of P1 when P1 was actuating.

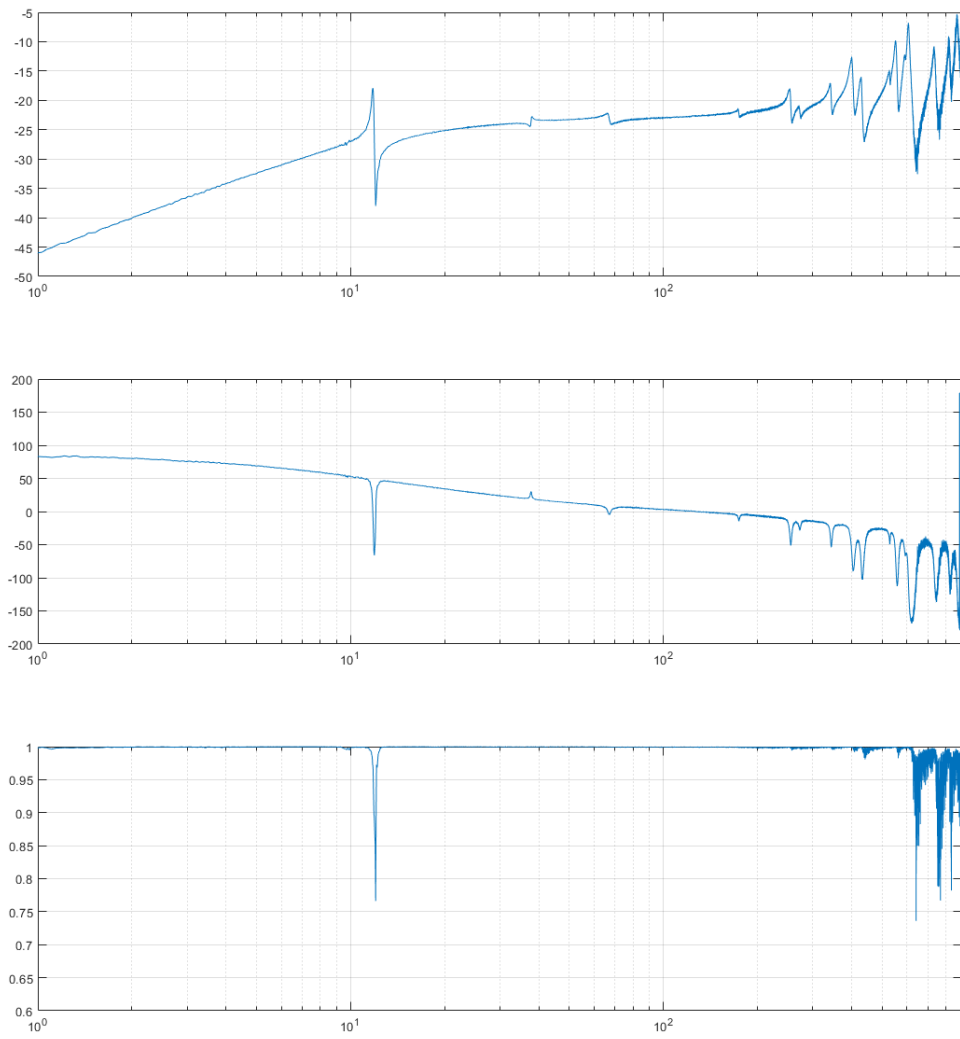


Figure C.27: Bode showing the data from the sensor of P2 when P2 was actuating.

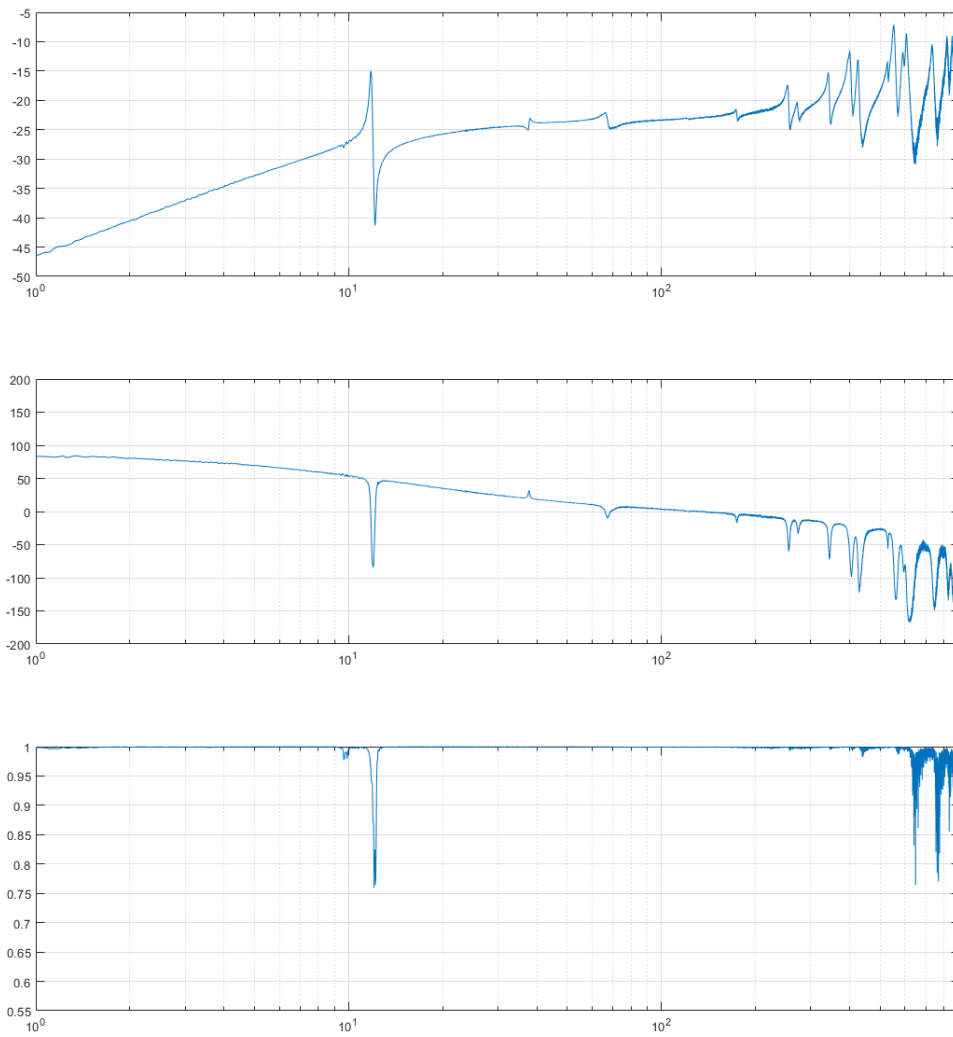


Figure C.28: Bode showing the data from the sensor of P3 when P3 was actuating.

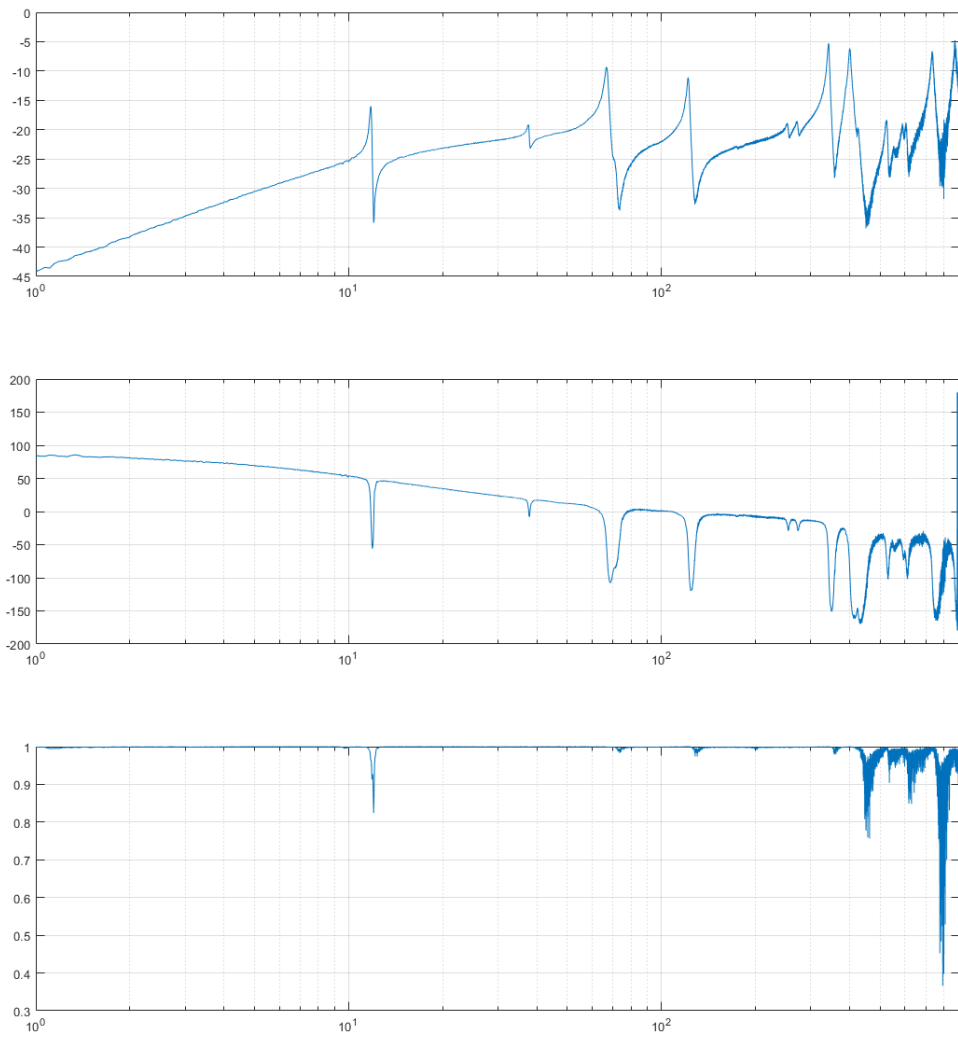


Figure C.29: Bode showing the data from the sensor of P4 when P4 was actuating.

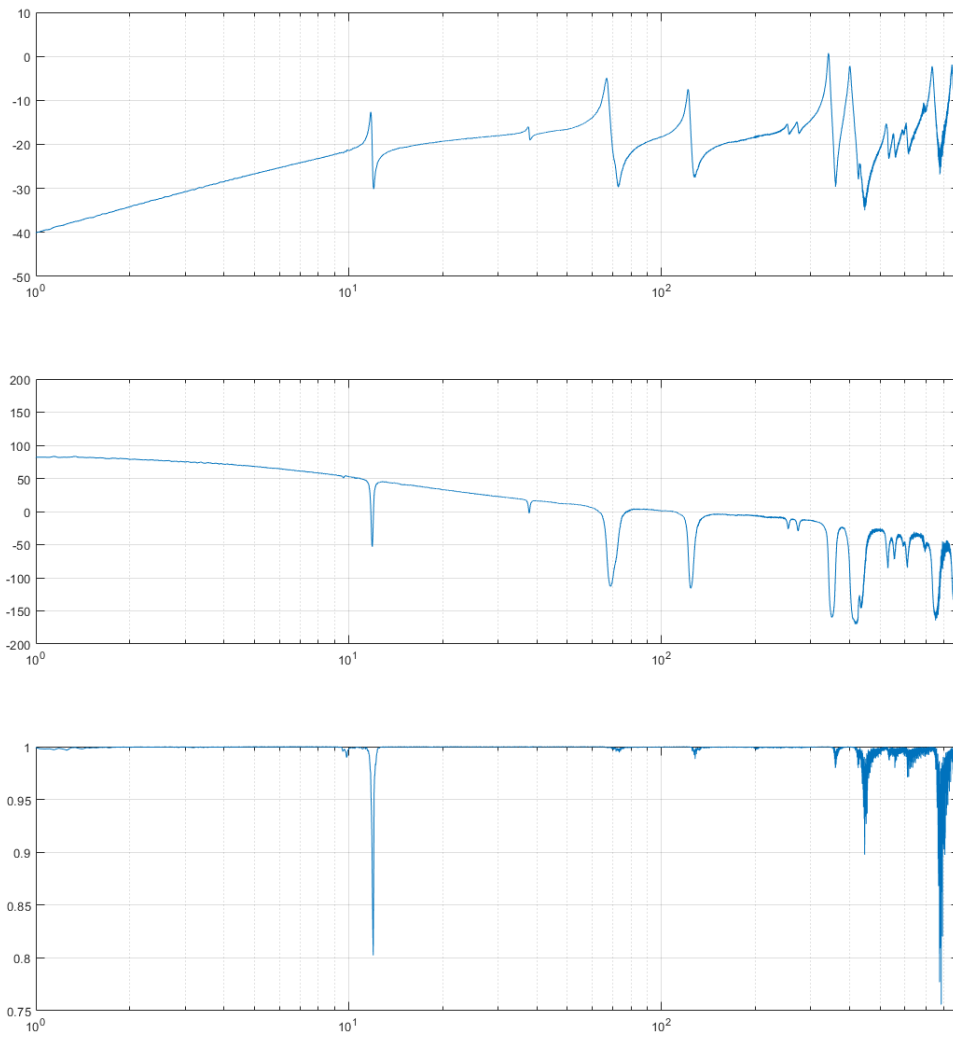


Figure C.30: Bode showing the data from the sensor of P5 when P5 was actuating.

C.8. Bison Appendix

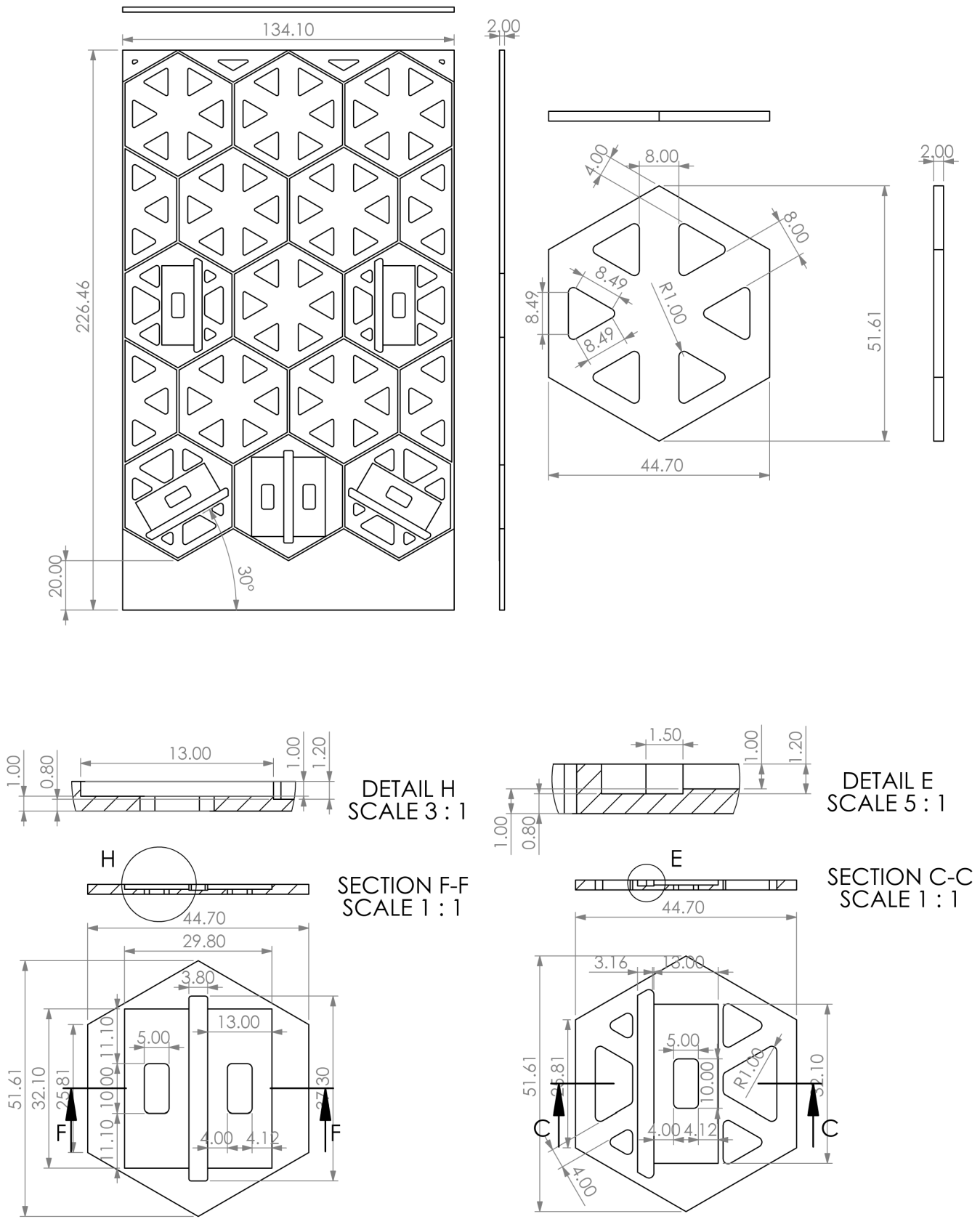


Figure C.31: Part drawing for the Bison Flexure and its cells

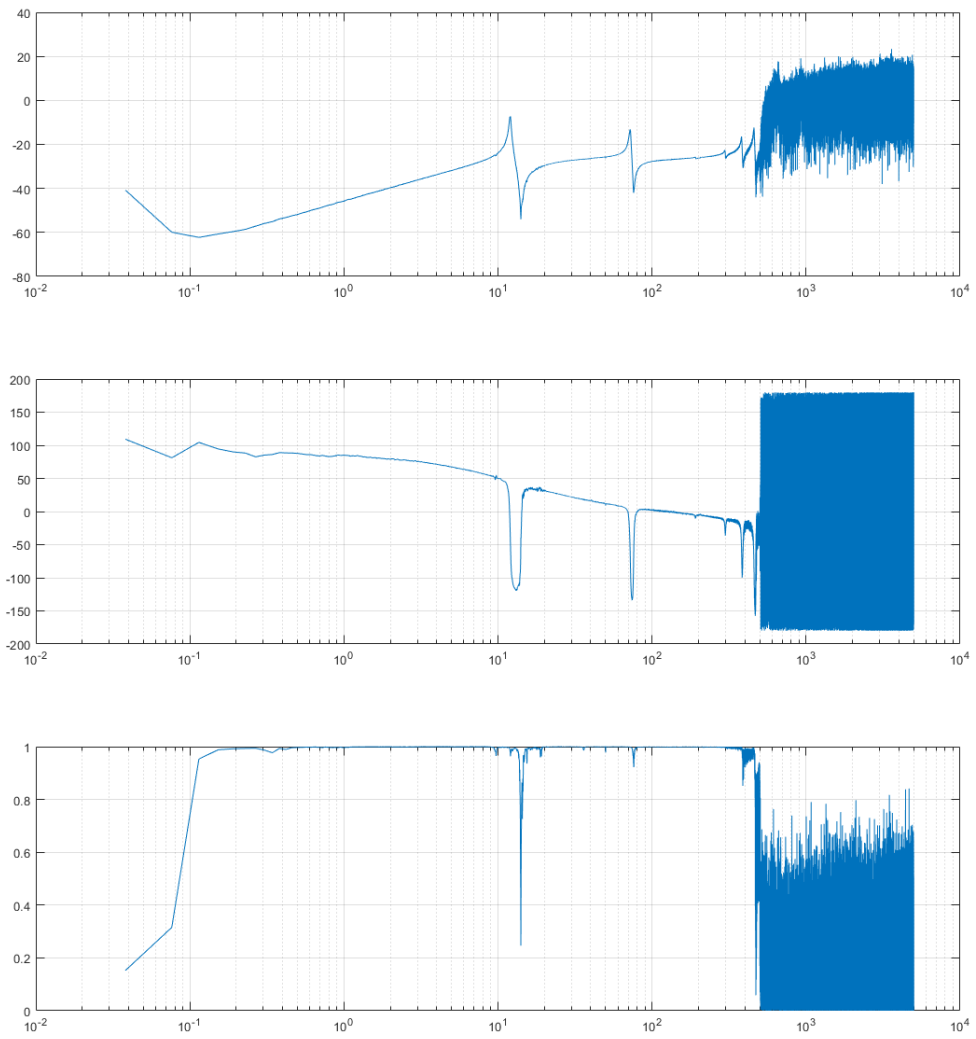


Figure C.32: Bode showing the data from the sensor of P1 when P1 was actuating.

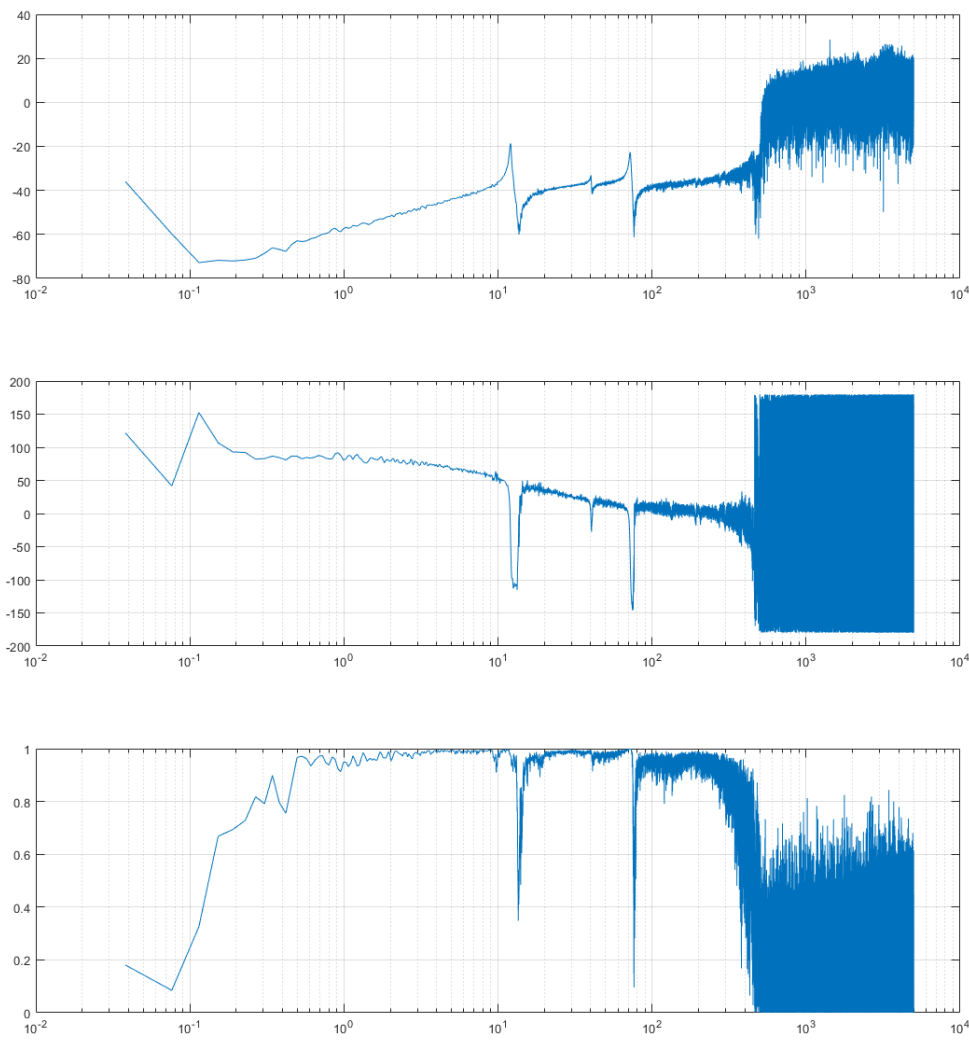


Figure C.33: Bode showing the data from the sensor of P2 when P2 was actuating.

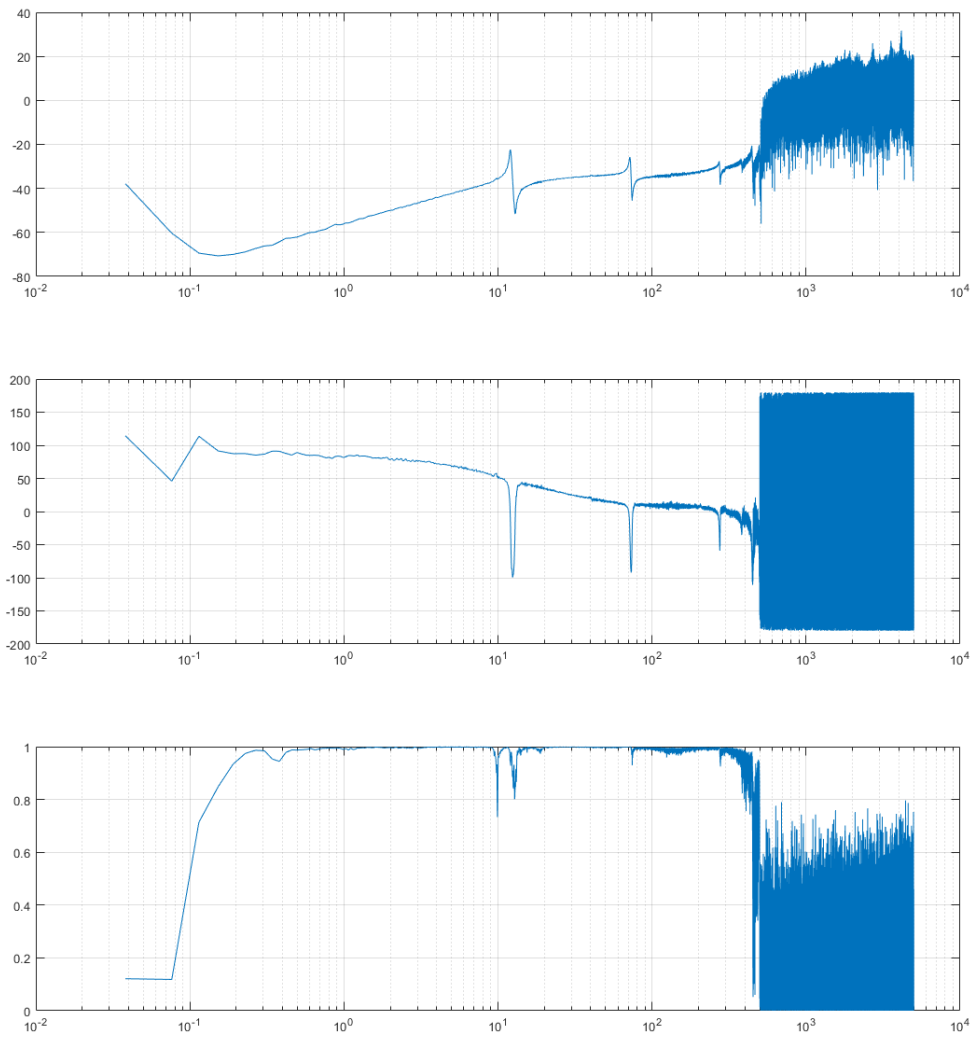


Figure C.34: Bode showing the data from the sensor of P3 when P3 was actuating.

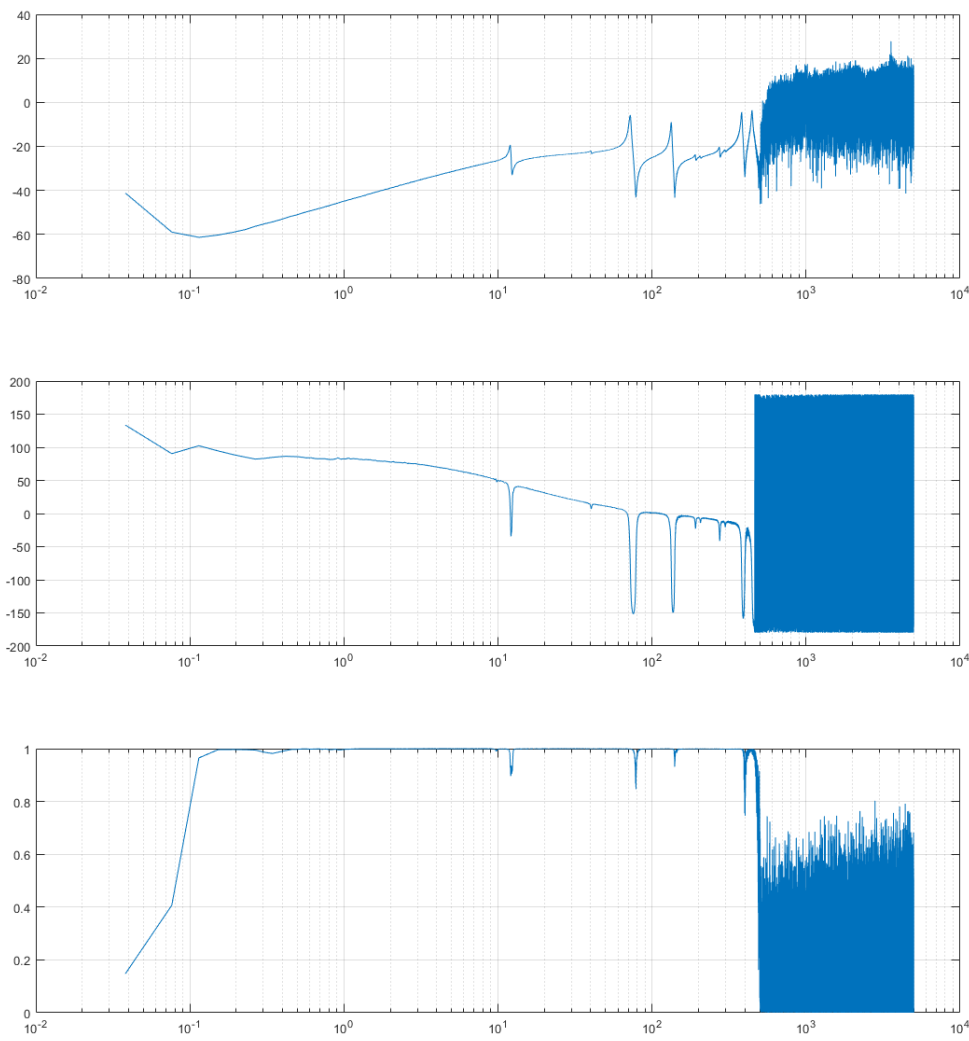


Figure C.35: Bode showing the data from the sensor of P4 when P4 was actuating.

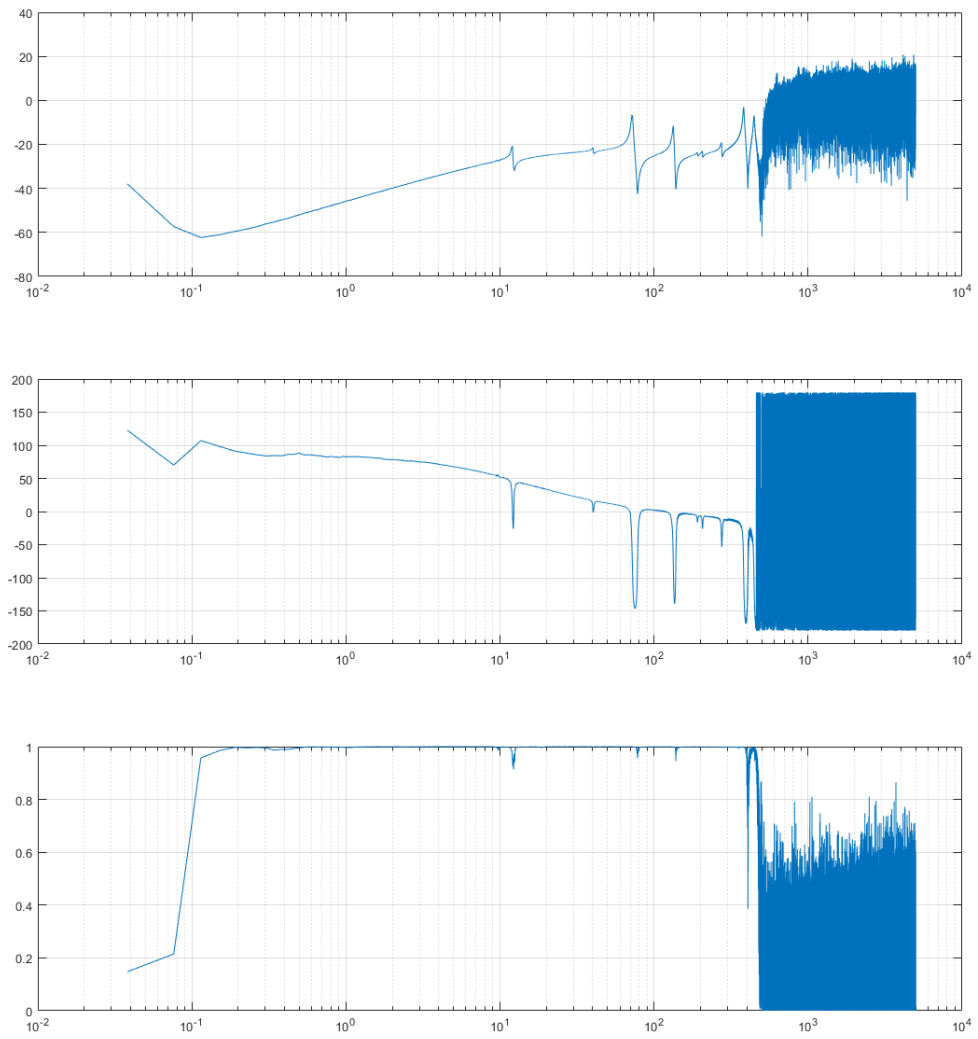


Figure C.36: Bode showing the data from the sensor of P5 when P5 was actuating.